INFORMATION TO USERS

This manuscript has been reproduced from the microfilm master. UMI films the text directly from the original or copy submitted. Thus, some thesis and dissertation copies are in typewriter face, while others may be from any type of computer printer.

The quality of this reproduction is dependent upon the quality of the copy submitted. Broken or indistinct print, colored or poor quality illustrations and photographs, print bleedthrough, substandard margins, and improper alignment can adversely affect reproduction.

In the unlikely event that the author did not send UMI a complete manuscript and there are missing pages, these will be noted. Also, if unauthorized copyright material had to be removed, a note will indicate the deletion.

Oversize materials (e.g., maps, drawings, charts) are reproduced by sectioning the original, beginning at the upper left-hand corner and continuing from left to right in equal sections with small overlaps.

Photographs included in the original manuscript have been reproduced xerographically in this copy. Higher quality 6" x 9" black and white photographic prints are available for any photographs or illustrations appearing in this copy for an additional charge. Contact UMI directly to order.

Bell & Howell Information and Learning
300 North Zeeb Road, Ann Arbor, MI 48106-1346 USA
800-521-0600

UMI®

Downloaded from SHAREOK. Persistent Handle URL: https://hdl.handle.net/11244/283

UNIVERSITY OF OKLAHOMA

GRADUATE COLLEGE

THE VALUE OF POINT-SCALE MEASUREMENTS OF SOIL MOISTURE IN PLANETARY BOUNDARY LAYER SIMULATIONS

A Dissertation

SUBMITTED TO THE GRADUATE FACULTY

in partial fulfillment of the requirements for the

degree of

Doctor of Philosophy

By

JEFFREY BRENT BASARA
Norman, Oklahoma
2001

UMI Number: 3004876



UMI Microform 3004876

Copyright 2001 by Bell & Howell Information and Learning Company.
All rights reserved. This microform edition is protected against unauthorized copying under Title 17, United States Code.

Bell & Howell Information and Learning Company
300 North Zeeb Road
P.O. Box 1346
Ann Arbor, MI 48106-1346

© Copyright by JEFFREY BRENT BASARA 2001
All Rights Reserved.

THE VALUE OF POINT-SCALE MEASUREMENTS OF SOIL MOISTURE IN PLANETARY BOUNDARY LAYER SIMULATIONS

A Dissertation APPROVED FOR THE SCHOOL OF METEOROLOGY

BY

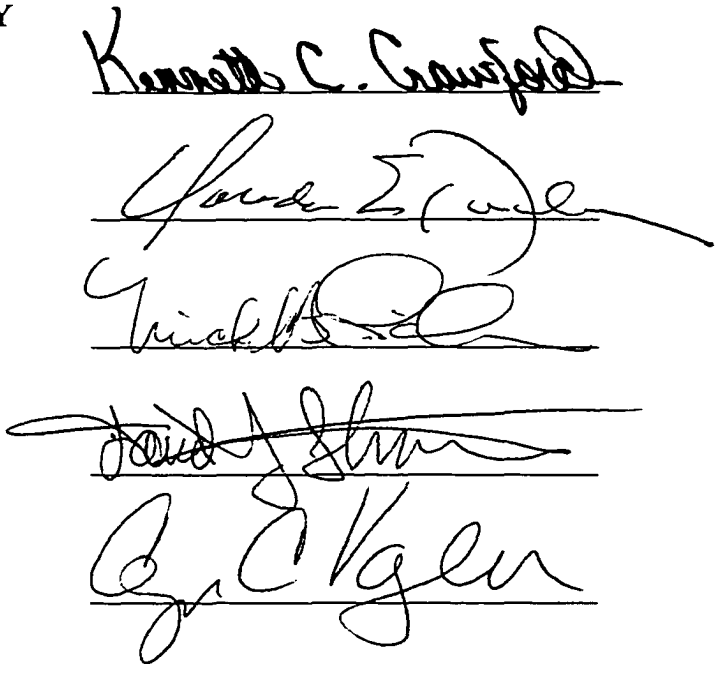

ACKNOWLEDGMENTS

I would first like to thank Dr. Ken Crawford for everything he has done for me. In addition to serving as an outstanding academic mentor and advisor, he has influenced my life in countless ways and is a true role model. I always knew that he had my best interests in mind. To me Dr. Crawford is much more than a professional colleague and there is only one word that captures the essence of his role in my life -- friend.

I would like to thank my committee for their insight and patience. To Dr. Claude Duchon, Dr. Mike Richman, Dr. Caryn Vaughn, and Dr. Dave Stensrud: You have my deepest appreciation.

I must also thank Dr. Karen Humes, Dr. Ron Elliott, and Dr. Ken Fisher for providing insight and knowledge in the disciplines of hydrology and soil physics. Their expertise provided critical understanding needed to complete this dissertation.

A significant portion of this research would not have been accomplished without the aid Dr. Mike Ek and Dr. Ken Mitchell of the National Center for Environmental Prediction. I deeply appreciate their efforts and insight.

I would like to recognize the OCS crew. The Climate Survey is a terrific place to work and interact simply because the organization is filled with tremendous people. It has been an honor to have been part of such a great team.

To Dr. Jerry Brotzge I would like to say thanks for all the good times we shared in the office. I am also really glad that you paved the way for me by graduating a semester ahead of me. I was able to learn a ton from you, and I truly appreciate all that you have done for me. And, let's be real, it was a blast to "he haw" about OU, Purdue, Louisville, Texas or whoever we felt like jabbering about concerning sports.

I would like to acknowledge Dr. Alan Shapiro for his kindness, patience, and instruction during my remedial work. Al, it is scary but true -- you made learning dynamical meteorology an enjoyable experience.

I feel it is important to acknowledge a man who lived thousands of years ago. This man named Jabez uttered a simple prayer which is recorded in I Chronicles 4: 9-10. However, this simple prayer was an inspiration to me and provided a focus well beyond this

dissertation. In return, the efforts to complete this dissertation benefited from a renewed sense of purpose inspired by the Jabez prayer.

Finally, I would like to thank my family for providing the opportunity to pursue a higher level of education. Their support has always been appreciated. Most of all, I would like to thank my dear wife Heather. She has patiently endured the long days and long nights associated with completing this dissertation. And in the times of trial, when I just wanted to quit, she always encouraged me to hang in there and never give up. Without her loving support, I never would have completed this task. Thanks Heather -- I love you.

Table of Contents

Acknowledgements iv
List of Tables vii
Abstract xii

Chapter 1: Introduction 1

Chapter 2: Literature Review 5
2.1 Soil Moisture Variability 5
2.2 Measuring Soil Moisture 10
2.2.1 Methods and Technologies 10
2.2.2 Operational (Near Real-Time) Measurements 12
2.3 Land-Atmosphere Interactions 14
2.3.1 Recent Studies 14
2.3.2 Key Issue 17

Chapter 3: Data 19
3.1 Soil Moisture Observations 19
3.2 Additional Mesonet Observations 23
3.3 Upper Air Observations 27
3.4 Ideal Conditions for Study 28

Chapter 4: 229-L Calibration and Instrument Errors 31
4.1 Initial Calibration and Installation 31
4.2 Field Measurements and Improved Calibration 34
4.3 An Installation Error 38

Chapter 5: Linear Relationships Between Root-Zone Soil Moisture and Atmospheric Processes in the Planetary Boundary Layer 41
5.1. Analysis 41
5.2. Discussion 50

Chapter 6: Sensitivity Analysis of Ground Heat Flux Estimates 59
6.1. Theory 59
6.2 Results 61
6.2.1 Soil Moisture Conditions 61
6.2.2 Ground Heat Flux Estimates Using Field Samples of Soil Moisture and the Original Calibration of the 229-L Sensor 63
6.2.3 Soil Moisture Sensor Calibration and Ground Heat Flux Estimates 67
6.2.4 Closure of the Surface Energy Balance 70
6.3 Discussion 73

Chapter 7: The Sensitivity of Planetary Boundary Layer Simulations to Local Soil Moisture Conditions 75
7.1. Model Description 75
7.2 Simulations Using Data From the Norman Mesonet Site 76
7.3 Results 79
7.3.1 Soil Moisture Variability 79
7.3.1.1 --- 2 July 86

7.3.1.2 --- 15 July 86
7.3.1.3 --- 23 July 91
7.3.1.4 --- 30 July 94
7.3.1.5 --- 7 August 94
7.3.2 Soil Texture Variability 95
7.3.3 The Importance of Sensor Calibration 103
7.3.4 Comparison of Soil Hydraulic Properties with Other Land-Surface Parameters 114
7.3.5 Test for Linearity 115
7.4 Discussion 123

Chapter 8: Summary and Concluding Remarks 129

References 138
Appendix A 146
Appendix B 156
Appendix C 162
Appendix D 173

List of Tables

Table	Page
Table 2.1. Previous small-scale studies of near surface soil moisture (adapted and modified from Famigletti et al. 1998).	8
Table 3.1. Statistical evaluation of volumetric water content, stratified by soil depth, at the Norman Mesonet site (1 June - 12 August 1999).	22
Table 3.2. Examples of the daily coefficient of variation of volumetric water content, stratified by soil depth, at the Norman Mesonet site (1 June - 12 August 1999).	22
Table 3.3. Vertical stratification of soil characteristics at the Norman Mesonet site.	26
Table 3.4. Variability in the vertical stratification of soil characteristics at the Norman Mesonet site.	26
Table 5.1. Linear correlation between soil moisture and atmospheric parameters at the Norman Mesonet site.	58
Table 6.1. Maximum daily ground heat flux computed using soil water content values derived from the 229-L sensor and using the maximum, mean, and minimum values from field samples.	68
Table 6.2. Mean daylight closure of the surface energy balance computed using soil water content from the 229-L sensor and using the maximum, mean, and minimum values from field samples.	71
Table 6.3. Closure of the surface energy balance at the time of maximum ground heat flux computed using soil water content values from the 229-L sensor and using the maximum, mean, and minimum values from field samples.	72
Table 7.1. Vertical stratification of soil characteristics at the Norman Mesonet site.	78
Table 7.2. Soil water content used to initialize the 0-5 and 5-100 cm layers of the OSU model.	80
Table 7.3. Maximum value of the daily-averaged sensible heat flux computed by the OSU model. Soil water content values derived from the maximum, mean, and minimum field sample values as well as the 229-L sensor served as input to the model. The simulations used a clay loam parametrization for soil texture.	81
Table 7.4. Maximum value of the daily-averaged sensible heat flux computed by the OSU model. Soil water content values derived from the maximum, mean, and minimum field sample values as well as the 229-L sensor served as input to the model. The simulations	

used a silt loam parametrization for soil texture. 81

Table 7.5. Maximum value of the daily-averaged latent heat flux computed by the OSU model. Soil water content values derived from the maximum, mean, and minimum field sample values as well as the 229-L sensor served as input to the model. The simulations used a clay loam parametrization for soil texture. 82

Table 7.6. Maximum value of the daily-averaged latent heat flux computed by the OSU model. Soil water content values derived from the maximum, mean, and minimum field sample values as well as the 229-L sensor served as input to the model. The simulations used a silt loam parametrization for soil texture. 82

Table 7.7. Maximum value of the daily-averaged ground heat flux computed by the OSU model. Soil water content values derived from the maximum, mean, and minimum field sample values as well as the 229-L sensor served as input to the model. The simulations used a clay loam parametrization for soil texture. 83

Table 7.8. Maximum value of the daily-averaged ground heat flux computed by the OSU model. Soil water content values derived from the maximum, mean, and minimum field sample values as well as the 229-L sensor served as input to the model. The simulations used a silt loam parametrization for soil texture. 83

Table 7.9. Maximum value of the daily-averaged net radiation computed by the OSU model. Soil water content values derived from the maximum, mean, and minimum field sample values as well as the 229-L sensor served as input to the model. The simulations used a clay loam parametrization for soil texture. 84

Table 7.10. Maximum value of the daily-averaged net radiation computed by the OSU model. Soil water content values derived from the maximum, mean, and minimum field sample values as well as the 229-L sensor served as input to the model. The simulations used a silt loam parametrization for soil texture. 84

Table 7.11. Maximum value of the depth of the PBL computed by the OSU model. Soil water content values derived from the maximum, mean, and minimum field sample values as well as the 229-L sensor served as input to the model. The simulations used a clay loam parametrization for soil texture. 85

Table 7.12. Maximum value of the depth of the PBL computed by the OSU model. Soil water content values derived from the maximum, mean, and minimum field sample values as well as the 229-L sensor served as input to the model. The simulations used a silt loam parametrization for soil texture. 85

Table 7.13. The difference (absolute value) in maximum daily sensible heat flux computed by the OSU Model between the

clay loam parametrization and the silt loam parametrization. Input soil water content values were derived from the maximum, mean, and minimum field sample values as well as from data produced by the 229-L sensor. 106

Table 7.14. The difference (absolute value) in maximum daily latent heat flux computed by the OSU Model between the clay loam parametrization and the silt loam parametrization. Input soil water content values were derived from the maximum, mean, and minimum field sample values as well as from data produced by the 229-L sensor. 106

Table 7.15. The difference (absolute value) in maximum daily ground heat flux computed by the OSU Model between the clay loam parametrization and the silt loam parametrization. Input soil water content values were derived from the maximum, mean, and minimum field sample values as well as from data produced by the 229-L sensor. 107

Table 7.16. The difference (absolute value) in maximum daily net radiation computed by the OSU Model between the clay loam parametrization and the silt loam parametrization. Input soil water content values were derived from the maximum, mean, and minimum field sample values as well as from data produced by the 229-L sensor. 107

Table 7.17. The difference (absolute value) in maximum daily depth of the PBL computed by the OSU Model between the clay loam parametrization and the silt loam parametrization. Input soil water content values were derived from the maximum, mean, and minimum field sample values as well as from data produced by the 229-L sensor. 108

Table 7.18. Soil water content used to initialize the 0-5 and 5-100 cm layers of the OSU model. 112

Table 7.19. The maximum difference between PBL parameters computed using calibrated values of soil water content from the 229-L sensors and values of soil water content determined for the original, improved, and uncalibrated 229-L sensors. 113

Table 7.20. Root mean squared error between PBL parameters computed using calibrated values of soil water content from the 229-L sensors and values of soil water content determined for the original, improved, and uncalibrated 229-L sensors. RMSE was computed using data from the 13 *ideal* study days. 113

Table 7.21. The range (absolute value) of PBL parameters computed using the OSU model with variations in albedo. Soil texture was parameterized as clay loam. 116

Table 7.22. The range (absolute value) of PBL parameters computed using the OSU model with variations in albedo. Soil texture was parameterized as silt loam. 116

Table 7.23. The range (absolute value) of PBL parameters computed using the OSU model with variations in the canopy resistance. Soil texture was parameterized as clay loam. 117

Table 7.24. The range (absolute value) of PBL parameters computed using the OSU model with variations in the canopy resistance. Soil texture was parameterized as silt loam. 117

Table 7.25. The range (absolute value) of PBL parameters computed using the OSU model with variations in the shade factor. Soil texture was parameterized as clay loam. 118

Table 7.26. The range (absolute value) of PBL parameters computed using the OSU model with variations in the shade factor. Soil texture was parameterized as clay loam. 118

Table 7.27. Linear correlation between soil moisture and atmospheric parameters simulated using the OSU model for the silt loam (SL) and clay loam (CL) parameterizations of soil texture. 119

Table 7.28. Root mean squared error (RMSE) between the daily-maximum value of PBL parameters computed using the OSU model and the hourly-averaged daily-maximum values observed at the Norman Mesonet site. RMSE was computed using data from the 13 *ideal* study days. 127

Abstract

A characteristic of the land surface which modulates the partitioning of available solar energy into fluxes of energy (latent, sensible, and ground heat fluxes) is soil moisture. This partitioning occurs directly through evaporation from bare soil and indirectly through vegetation transpiration. In turn, the surface fluxes of energy contribute to the development of the planetary boundary layer (PBL; the greater the partitioning toward sensible heating, the deeper the boundary layer, and vice versa). In order to simulate properly the development of the PBL using numerical models, accurate and representative values of soil moisture must be obtained.

In April 1999, the Norman Mesonet site (NORM) was upgraded to include sensors to measure latent, sensible, and ground heat fluxes, as well as net radiation. In addition, over 2,000 discrete soil samples were collected within a 20 X 20 m enclosure encompassing the Norman Mesonet site between 1 June 1999 and 15 August 1999. These samples were collected to provide point-scale observations of soil-water content for field calibration of in situ (Campbell Scientific model 229-L) soil moisture sensors installed at NORM and to determine the naturally occurring spatial and temporal variability of soil moisture conditions within the outline of the Norman Mesonet site.

One component of this study focuses on the relationship between soil moisture and atmospheric processes at and near NORM using both automated and field samples of hydrologic and atmospheric parameters. The results indicate that, on days with strong radiative forcing and weak shear in the lower troposphere, soil water content in the root-zone was linearly correlated with daily-maximum values of sensible heat flux and latent heat flux.

This study also investigates the sensitivity of ground heat flux estimates at NORM to naturally occurring variability in soil-water content from field samples as well as instrumentation biases associated with the in situ soil moisture sensors. Results indicate that differences in ground heat flux estimates varied by up 20% due to sampling or instrumentation biases. Furthermore, closure of the surface energy budget varied by up to 8% due to these differences in ground heat flux estimates.

Finally, using the Oregon State University one-dimensional, coupled atmospheric-

plant-soil model, PBL conditions were examined at NORM during July 1999. Results indicate that latent and sensible heat fluxes in the model simulations varied by as much as 300 W m^{-2} due to naturally occurring variability of soil-water content determined from field samples and biases occurring in the in situ measurements. Furthermore, ground heat flux values derived by the model varied as much as 50 W m-2.

Chapter 1
Introduction

A characteristic of the land surface which modulates the partitioning of available solar energy into fluxes of energy (latent, sensible, and ground heat fluxes) is soil moisture. This partitioning occurs directly through evaporation and indirectly through vegetation sustenance. In turn, the surface fluxes of energy contribute to the development of the planetary boundary layer (PBL; the greater the partitioning toward sensible heating, the deeper the boundary layer, and vice versa). In order to simulate properly the development of the PBL using numerical models, accurate and representative values of soil moisture must be obtained.

Much of the understanding in recent years concerning the role of soil moisture in near-surface atmospheric processes has been achieved through numerical modeling studies. This accomplishment is due, in large part, to a limited number of field observations of soil moisture. Large field campaigns such as the FIFE experiment in northeast Kansas (1987 and 1989; Sellars et al. 1992) and the Southern Great Plains (SGP) experiments of 1997 and 1999 (Jackson et al. 1999) have provided (and continue to provide) valuable information concerning the spatial and temporal variability of soil-water content, and its relationship with atmospheric processes. Unfortunately, these large field campaigns are limited in time due to the costs associated with maintaining the observing networks.

The need for soil moisture observations has been addressed in recent articles such as Emanuel et al. (1995), who emphasized that improved observations of soil moisture conditions may lead to dramatic forecasting improvements related to the location and timing of the onset of deep convection over land, quantitative precipitation forecasting, and seasonal climate prediction. Furthermore, Entekhabi et al. (1999) stated in the *Bulletin of the American Meteorological Society*:

> *"For a relatively low cost, existing observation networks could be augmented to provide valuable new in situ measurements. Technological advances in instrumentation allow the addition of new variables to the suite of standard measurements available at existing monitoring stations.*

Examples include addition of soil thermistors to measure soil temperature, devices to estimate soil water content, instruments to sense snow properties, and robust devices to measure surface moisture and energy fluxes."

The importance of obtaining these in situ measurements is further emphasized by Entekhabi et al. (1999):

"A final priority for in situ data collection is the development of focused validation datasets that can be used to evaluate new hydrological theories, models, and remote sensing techniques."

Recognizing the need for improved in situ measurements, the Oklahoma Mesonet (Brock et al. 1995), an automated network of 114 remote, meteorological stations across Oklahoma, has integrated additional sensing devices to compliment the standard suite of meteorologic and hydrologic sensors. In addition to providing observations such as air temperature and humidity, station pressure, and wind speed and direction, nearly 100 sites were outfitted with soil thermistors, sensors to measure latent, sensible, and ground heat fluxes, net radiometers, and heat dissipation probes to estimate soil moisture.

More specifically, during 1996, matric potential sensors (the Campbell Scientific 229-L) were installed at 60 sites in the Oklahoma Mesonet. The sensors were installed at depths of 5, 25, 60, and 75 cm. During 1998 and 1999, 229-L sensors were installed at an additional 43 Mesonet sites. The 229-L sensors are unique in that they provide an estimate of both soil-water potential *and* water content every 30 minutes (Basara 1998). As a result, the soil moisture sensors installed at the Mesonet sites provide a continuous record of soil moisture conditions. Additional details concerning the installation and calibration of the 229-L sensors are noted in Chapter 4.

However, simply gathering the observations is not in itself useful. It is important to understand the nature of the observations as well as the limitations. Due to the limited nature of in-situ soil moisture observations in space and time, the utility and application of discrete, point-scale measurements of soil-water content and soil-water potential are unknown. Furthermore, issues such as instrument calibration and naturally occurring variability of soil texture and moisture play a key role in determining the utility of point-

scale observations of soil moisture.

The hypothesis of this study is that point-scale observations of soil moisture conditions, greatly affected by instrumentation errors and naturally occurring variability of soil hydraulic properties, have a limited but quantifiable impact on simulations and computations of atmospheric processes in the PBL. Observations of soil-water content and soil-water potential collected from field and in situ sampling at the Norman Mesonet site (NORM), are used to test the sensitivity of numerical model calculations of soil and atmospheric parameters to perturbations in soil hydraulic properties.

The first objective of this study is to quantify the spatial and temporal variability of soil moisture conditions at the Norman Mesonet site. This objective is achieved by analyzing field observations of soil-water content and soil-water potential collected from 12 locations in the immediate vicinity of the Norman site. In addition, these field observations are used to validate the calibration of the 229-L sensors installed at NORM and to assess the nature of sensor errors inherent in the 229-L. The analysis used to achieve this objective lays the groundwork for two additional objectives of this study.

A basic premise of this study is that the land surface, and more specifically soil moisture conditions, were coupled to the atmosphere at and near the Norman Mesonet site. Thus, the second objective of this study is to document the relationship between atmospheric processes in the PBL with soil moisture conditions at NORM.

The calculation of ground heat flux is a function of soil-water content (de Vries 1975). The third objective of this study seeks to test the sensitivity of ground heat flux measured at NORM to varying soil-water content determined through additional field observations that define the spatial variability of soil-water content. In addition, calibrated and uncalibrated 229-L measurements are used.

The final objective of this study assesses the sensitivity of PBL simulations to spatial and temporal variations of point-scale measurements of soil moisture. This objective is accomplished by using a one-dimensional, coupled atmospheric-plant-soil model developed by Troen and Mahrt (1986) at Oregon State University (OSU), in situ and field observations of soil moisture collected at NORM, atmospheric soundings from the National Weather Service Weather Forecast Office (NWS WFO) in Norman, and atmospheric

observations collected at the NORM site.

Chapter 2 provides the historical background and supporting theory for this study. A synopsis of soil texture and moisture variability and how these soil properties affect PBL development also is included. A description of soil moisture observations collected at the Norman Mesonet site follows in Chapter 3. In particular, the spatial and temporal variability of field samples of soil moisture and texture conditions is examined. The behavior of the 229-L sensors is discussed in Chapter 4.

Chapter 5 investigates land-atmosphere interactions at NORM. Specific emphasis is placed on how atmospheric processes in the PBL are related to the vertical stratification of soil water at the site. The body of Chapter 6 focuses on how natural variability of soil moisture and sensor calibrations affect ground heat flux measurements and the subsequent closure of the surface energy balance. The sensitivity analysis, begun in Chapter 6 using in situ observations, continues in Chapter 7 using numerical simulations of the PBL. An overview of the OSU 1-D PBL model is given prior to simulation examples. Preliminary results are discussed in Chapter 7. In addition Chapter 7 investigates how the results compare when soil moisture conditions are held constant and other land-surface parameters such as canopy resistance, albedo, and plant water content are varied within the model. A summary of important results as well as concluding remarks are presented in Chapter 8.

Chapter 2
Literature Review

Soil moisture is a critical component of a feedback system that conveys meteorological memory to the climate system over land surfaces (Delworth and Manabe 1988 and 1993). On the local scale, soil moisture controls the partitioning of mass and energy between the land surface and the atmosphere through surface fluxes of latent and sensible heat as well as mitigating soil heat flux (Brubaker and Entekhabi 1996).

Soil moisture conditions also contribute to the natural and agricultural productivity of a region by defining the root water that is available for uptake into the vegetation canopy (Hillel 1998). In turn, water is transpired from the vegetated surface to the atmosphere during photosynthesis, thus increasing low level atmospheric moisture on both a local and regional basis.

2.1 Soil Moisture Variability

The spatial and temporal variability of soil moisture conditions (specifically soil water content: the total amount of water contained within a given soil mass or volume) are influenced by a number of competing factors. The factors include soil properties, topography, mean moisture content, depth of the water table, vegetation, meteorological parameters including precipitation and solar radiation, and organic matter within the soil (Famigletti et al. 1998).

On the scale of meters, soil moisture is most directly influenced by a number of microscale physical properties which determine soil composition. These factors include soil texture (size, shape, and mineral composition of the soil particles), soil water potential (the energy state of soil water), and organic matter which directly influence how water moves in soil as well as the magnitude of water contained in any given soil parcel (Miller 1977; Dingman 1994; Hillel 1998). Though the effect of organic matter is usually minimal, soil texture and soil water potential are intricately linked to the actual value of soil water at any given location. This relationship was illustrated by Razumova (1965) who said:

> *"soil is a wetting body. For this reason capillary moisture in the soil has a concave surface and is invariably under supplementary negative pressure [or suction]. Its magnitude is governed by the surface tension of the water and the radii of the curves, which depend on size and shape of the interstices, i.e., in the final analysis on the dispersion of the soil."*

Thus knowledge of two of three soil properties (soil texture, soil water potential, or soil water content) is needed to ascertain the third.

The determination of soil water content at a location is further complicated due to the non-linear relationships (known as soil water release curves) between soil texture, soil water potential, and soil water content. A conceptual example of how the three aforementioned properties interact is shown in Figure 2.1. Note that for a given suction (water potential), different soil textures yield different soil water content values, and vice versa. An additional complication is illustrated in Figure 2.2 using a soil water release curve (for the same soil as in Fig. 2.1) that is influenced by how soil particles are arranged within a given sample. Thus, due to the heterogeneous nature of soil properties, a natural variability of soil water content exists across all spatial and temporal scales.

Many studies using various measurement techniques have attempted to quantify the variability of soil water content over a variety of spatial scales as well as topography, soil texture, and vegetation. A number of studies on either the plot or watershed scale are shown in Table 2.1.

It remains uncertain whether soil moisture conditions are more variable during certain stages of drydown from saturated to dry soils. Hills and Reynolds (1969), Reynolds (1970c), Henniger et al. (1976), Bell et al. (1980), Hawley et al. (1982), and Robinson and Dean (1993) all noted that variability of soil water content decreased during the transition from wet to dry soils. However, Hawley et al. (1982) suggested that variability of soil moisture conditions might increase under extremely dry conditions as well as following precipitation events of different intensity and duration. Because soils dry at different rates, Hills and Reynolds (1969) suggested an additional scenario whereby the

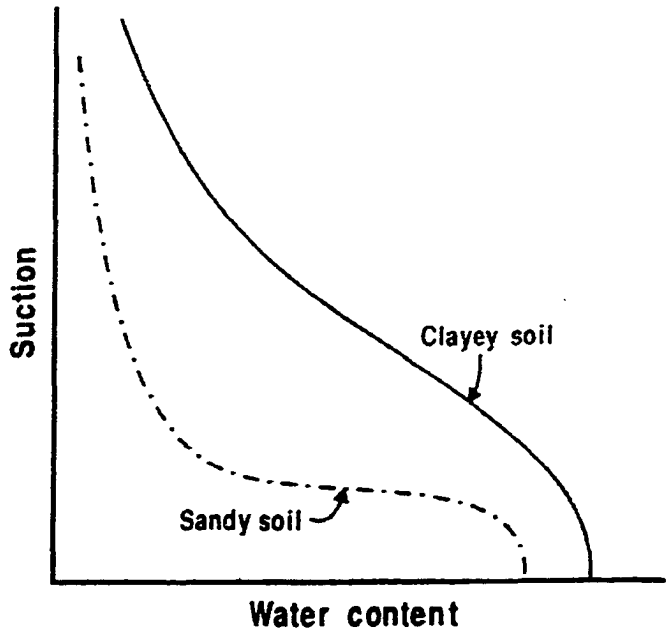

Figure 2.1 The relationship between soil suction (potential) and soil water content for sand and clay (Hillel 1998).

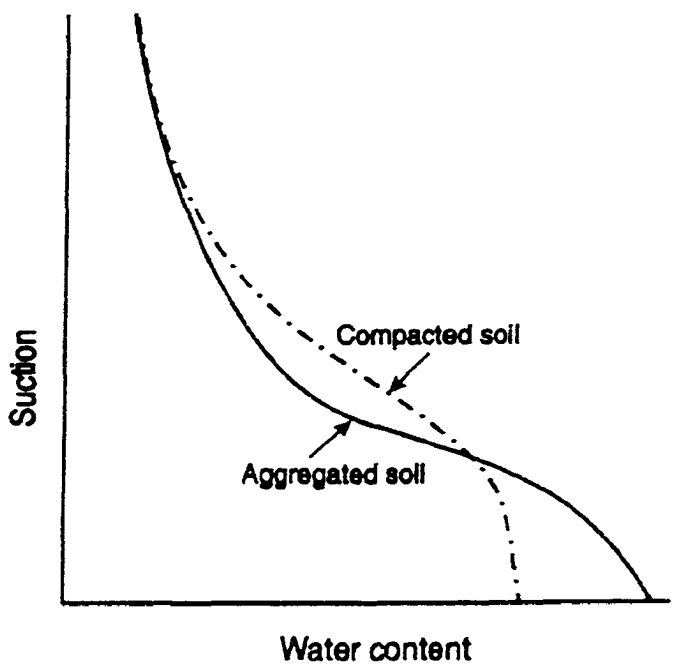

Figure 2.2 The relationship between soil suction (potential) and soil water content for aggregated and compacted soils (Hillel 1998).

Study	Location	Area	Number of Samples	Temporal Frequency	Sampling Depth
Krumbach, 1959	Mississippi, USA	270m^2	120	twice	15-30 cm
Hills and Reynolds, 1969	Chew Stoke, UK	2.4 m^2 to 6 km^2	60 per field/watershed	once	0-8 cm
Reynolds, 1970a; Reynolds, 1970b; Reynolds, 1970c;	Somerset, UK	715 5.9 m^2 plots	10 per plot	monthly for 8 months	0-8 cm
Reid, 1973	Caydell UK	2 10,000 m^2 fields	12 per field	weekly for 1 year	0-32.5 cm
Henninger et al., 1976	Pennsylvania, USA	560 transect	57	weekly for 6 months	0-15 cm
Bell et al., 1980	Arizona, Kansas, and South Dakota, USA	22 160,000 m^2 fields	9-36 per field	1-5 times per field	0-15 cm
Hawley et al., 1982	Maryland, USA	2 m^2 plot	80	3 dates	0-10 cm
Owe et al., 1982	South Dakota, USA	160,000 m^2 fields to 2.6 km^2 fields	42-69 per field	9 dates in 3 years	0-10 cm
Hawley et al., 1983	Oklahoma, USA	8 51,000 m^2 to 179,000 m^2 watersheds	16-92 per watershed	4 dates in 1 month	0-15 cm
Francis et al., 1986	Murcia, Spain	5 transects in 3000 m^2 plot	23-113 per transect	3 dates in 13 months	0-7.5 cm
Moore et al., 1988	New South Wales, Australia	6 190-200 m transects in 7.5 ha watershed	20-21 per transect	twice	0-10 cm
Charpentier and Groffman, 1992	Kansas, USA	2 4356 m^2 plots	49 per plot	twice	0-5 cm
Ladson and Moore, 1992	Kansas, USA	377,000 m^2 watershed	20	9 consecutive days	0-5 cm
Loague, 1992	Oklahoma, USA	100,000 m^2 watershed	4	90 dates in 4 years	0-15 cm
		100,000 m^2 watershed	34	84 dates in 4 years	0-15 cm
		100,000 m^2 watershed	157	once	0-15 cm
		100/250 m^2 transects in 100,000 m^2 watershed	50 per transect	once	0-15 cm
Niemann and Edgell, 1993	British Columbia, Canada	10,000 m^2	31	5 dates in 4 months	0-100 cm
Robinson and Dean, 1993	Oxford, UK	150 m transect	151	4 dates in 15 months	0-10 cm
Whitaker, 1993	Arizona, USA	44,000 m^2	134	4 dates in 2 weeks	0-15 cm
Nyberg, 1996	Gardsjon, Sweden	6,300 m^2	57-73	monthly for 2 months	0-30 cm
Crave and Gascuel-Odoux, 1997	Brittany, France	10 500 m transects	20 per transect	4 dates in 18 months	0-5, 5-10 cm
Famigletti et al., 1998	Texas, USA	200 m transect	21	88 dates in 217 days	0-5 cm
Famigletti et al., 1999	Oklahoma, USA	6 10,000 m^2 grids	27-49	daily for 1 month	0-5 cm

Table 2.1. Previous small-scale studies of near surface soil moisture (adapted and modified from Famigletti et al. 1998).

variability of soil moisture conditions is greatest in the midrange of soil moisture as dry patches are interspersed with wet patches. This behavior was noted by Owe et al. (1982). However, a discernible relationship was not determined by Charpentier and Groffman (1992).

Several studies in Table 2.1 noted that the spatial distribution of soil water content was normal or gaussian (Hills and Reynolds 1969; Bell et al. 1980; Hawley et al. 1983; Loague 1992; Nyberg 1996; and Familgletti et al. 1998). However, results from Familgletti et al. 1999, perhaps the most extensive analysis of near-surface soil water variability to date, noted that soil water content transitioned from nonnormal (negatively skewed) conditions at saturation, to a gaussian distribution during the drydown phase of soil, to nonnormal (positively skewed) during very dry soil conditions. It is quite possible, due to the limited temporal nature of the studies conducted by Hills and Reynolds (1969), Bell et al. (1980), Hawley et al. (1983), Loague (1992), Nyberg (1996), and Familgletti et al. (1998), that nonnormal to normal to nonnormal behavior of soil water content variability was not observed because most soils existed in a state between saturation and dry. It should be noted that Hills and Reynolds (1969), Bell et al. (1980), Familgletti et al. (1998) and Reynolds (1970c) discussed the need for long-term studies to fully determine the spatial and temporal nature of soil-water conditions.

Other characteristics that influence the spatial distribution of soil water content are the physical properties of soil. For example, macropores influence the movement of water within soil which, in turn, creates variable soil water conditions (Niemann and Edgell 1993). In addition, variability in soil water content is strongly influenced by the subtle difference in the number of silt, sand, and clay particles present in soil (Reynolds 1970a,b; Henniger et al. 1976; Crave and Gascuel-Odoux 1997). Hawley et al. (1983) identified the fact that textural variations of soils exert a greater variability in soil water content during wet conditions than during dry conditions.

Another contributing factor to the variability of near-surface soil water content is vegetation (Lull and Reinhart 1955). Lull and Reinhart (1955), Reynolds (1970b,c), Hawley et al. (1983), and Francis et al. (1986) also noted that variability in soil water content was inversely related to vegetation coverage. Furthermore, the magnitude of the

variability is greater during wet episodes than during dry episodes (Hawley et al. 1983).

Finally, topography plays a role in the spatial and temporal variability of soil water conditions. Slope aspect was found to significantly influence the variability of soil water content (Hills and Reynolds 1969; Reid 1973; Moore et al. 1988; Nyberg 1996; and Familgletti et al. 1998). Furthermore, Krumbach (1959), Henniger et al. (1976), Hawley et al. (1983), Robinson and Dean (1993), Nyberg (1996), and Crave and Gascuel-Odoux (1997) noted that soil water content is inversely related to elevation.

Unfortunately, many contradictions appear within the published literature. It is possible that these legitimate variations are clouded due to soil type and texture as well as climate. However, as noted by Famigletti et al. (1999) and by inspection of Table 2.1, the great majority of studies investigating the spatial and temporal behavior of soil moisture variability were limited in time, space, sampling interval below ground, or all the above. Thus, it quite possible that the apparent contradictions are the result of inadequate sampling of soil water conditions.

2.2 Measuring Soil Moisture

2.2.1 Methods and Technologies

The most widely used and accepted technique for measuring soil moisture is known as gravimetric sampling (Hillel 1998). In this method, soil is excavated, weighed, and then placed into an oven for drying purposes. After drying is complete, the soil is weighed again to determine the total water loss from the sample. This water loss (usually measured in grams) is expressed as a ratio with respect to the dry weight of the sample (g_{water}/g_{soil}). The gravimetric measurement technique is very common and the majority of studies discussed in Section 2.1 utilized this method. Even though this technique contains inevitable errors, it is "*the only one that can be generally recommended*" (WMO Technical Note 1968).

To convert the mass ratio of water to soil in a sample to a volume ratio, the gravimetric ratio is divided by the density of water and multiplied by the bulk density of soil (the total mass of soil minerals within a known volume). The result is soil water content

expressed as cm^3_{water}/cm^3_{soil}.

Unfortunately, the gravimetric sampling technique is both destructive and localized. Thus, other sampling techniques have been developed to provide relatively nondestructive measurements of soil moisture over a large spatial domain. One example is the neutron probe method (Holmes 1956; van Bavel 1963). This method utilizes a radioactive element which is lowered into an access tube pre-installed in the soil. Neutrons are released from the radioactive source at a predetermined depth, and the scatter of the neutrons is measured. The amount of neutron scatter is a function of hydrogen atoms in the soil and a direct indication of the soil water content. Still, disadvantages exist to using the neutron scattering method to measure soil moisture. For example, the sensors need to be handled with caution due to the radioactive components of the devices. Moreover, the depth resolution of the sensors are poor, they are inaccurate near the land surface due to the "sensor's sphere of influence", and the sensors cannot be left unattended (Ould Mohamed et al. 1997).

Another device which has been used to assess large area-averaged values of soil moisture is the passive microwave radiometer. When flown at high altitudes either on an aircraft or spacecraft, microwave sensors can observe soil moisture conditions even under moderate levels of vegetation cover. Previous field experiments such as the Southern Great Plains (SGP) experiments of 1997 and 1999 (Jackson et al. 1999) have successfully obtained observations of soil moisture conditions using passive microwave radiometers mounted on aircraft. A major drawback to such a device, though, is its inability to estimate moisture content within the soil below 5 cm (Jackson and Schmugge, 1989). Even so, the Advanced Microwave Scanning Radiometer (AMSR), which is capable of sensing soil moisture within a 50 km x 50 km pixel to a depth of 1 cm, is scheduled to be launched on the Aqua (2001) and ADEOS-II (2001) platforms to provide global measurements of surface soil moisture for the first time in history.

To increase depth resolution of moisture in the soil profile, as well as provide automated observations of soil moisture at regular time intervals, in situ sensors have been developed. One such instrument is the heat dissipation sensor which utilizes a combination of thermocouples and resistors housed within a matrix of porous ceramic (Phene et al. 1971). After installation, and once equilibria with the soil is attained, the thermocouple

measures the ambient soil temperature before an electric current is sent through the resistor. The current heats the moisture contained within the ceramic matrix. After a short period of time, the current is shut off and a second temperature measurement is taken. Because the specific heat and thermal conductivity of water is different from that of the porous ceramic matrix, the amount of heat dissipation will vary with varying contents of soil water.

Heat dissipation sensors provide several distinct advantages in the measurement of soil moisture. First, they can be incorporated easily into remote automated measuring stations and provide estimates of soil water both near the surface and at deep layers. Furthermore, radiation risks, like those associated with neutron scattering probe, are eliminated. Finally, minimal disturbance of the soil is involved during a careful probe installation.

Other in-situ sensors also have been developed which utilize the dielectric constant of water to determine soil moisture conditions. One sensor is the time domain reflectometry (TDR) probe (Topp et al. 1980; Topp and Davis 1985; Petersen et al. 1995). An electric pulse is sent through a closed circuit which consists of two parallel wires. The time it takes for a given pulse to make a round trip is a function of the water content of the soil within the segment being measured. A second type of sensor, which relies on the relationship between soil water content and the dielectric constant of water, is the capacitance probe (Dean et al. 1987; Bell et al. 1987). Various designs of TDR and capacitance sensors have been constructed which include both automated and non-automated varieties.

2.2.2 Operational (Near Real-Time) Measurements

With increased importance being placed on obtaining soil moisture observations for study and assimilation, a number of operational networks have begun either to collect soil samples for gravimetric analysis or obtained soil moisture observations from either a neutron probe or in situ sensors. Robock et al. (2000) describes a number of these world wide data sources.

The longest time series of soil moisture observations available are gravimetric samples collected in Russia. Observations were collected as far back as 1952, although many sites have since been discontinued. Currently, 102 Russian stations are in operation

during the growing season; gravimetric samples are collected approximately 3 times per month. Unfortunately, soil properties and meteorological observations are not collected at these locations. Additional gravimetric samples were once collected every 1-3 weeks in countries such as Mongolia, China, and India. However, these networks also have been discontinued.

In the United States, a number of networks collect soil moisture observations. The most extended data set (1982-present) has been collected by the Illinois Water Survey in their network of 19 stations (Hollinger and Isard 1994). Soil water content is collected from each station approximately twice per month using the neutron probe method. Furthermore, soil properties are available for each site, and 5 soil moisture stations are co-located with meteorological observations.

The Soil Climate Analysis Network (SCAN) operates 49 stations located in 30 states. Observations from these sites are collected hourly using TDR probes manufactured by Vitel (Schaefer 2000).

Three networks currently collect observations of soil moisture in Kansas and Oklahoma. The Agricultural Research Service (ARS) operates a network of 13 sites in Central Oklahoma (Starks 1999). In addition, a network of 23 sites has been installed across Kansas and Oklahoma by the Atmospheric Radiation Measurement (ARM) Program. Finally, the Oklahoma Mesonet (operated by the Oklahoma Climatological Survey) installed soil moisture sensors at 103 locations across the state of Oklahoma (Basara 1998; Basara and Crawford 2000). Details on the Mesonet's soil moisture network is given in Chapter 3. Each network uses heat dissipation sensors manufactured by Campbell Scientific Incorporated (sensor model 229-L) and observations are collected at intervals between 30 and 60 minutes. Furthermore, soil moisture sensors in each network are co-located with instruments to obtain meteorological observations. In addition, soil properties have been documented for each location.

2.3 Land-Atmosphere Interactions

2.3.1 Recent Studies

A process that modulates the exchange of mass and energy between the atmosphere and the land surface involves soil moisture. Differential heating at the earth's surface is the principle forcing mechanism for motion within the atmosphere at all temporal and spatial scales. Heat is dissipated into the atmosphere through turbulent fluxes at the earth's surface; the surface fluxes are strongly controlled by the availability of soil moisture. Furthermore, soil moisture determines the partitioning of the surface fluxes between latent (moist) and sensible (dry).

The input of water vapor into the atmosphere from the land surface results primarily from direct evaporation of moisture from the soil and from transpiration from the vegetative canopy. Transpiration is directly dependent upon the amount of moisture which is contained within the soil. The combined contribution of these two mechanisms is commonly referred to as evapotranspiration (ET).

As a result, soil moisture represents a key contribution to the many processes which occur within the land-atmosphere boundary. Many recent studies have offered valuable insight into the influence of soil moisture upon the atmosphere over variable temporal and spatial scales. Pan and Mahrt (1987) studied interactions between the evolution within the boundary layer and the transport of moisture within the soil. They used an atmospheric boundary-layer model coupled with a two-layer soil moisture model. They concluded that when substantial drying occurs, sensible heat flux becomes much larger than the latent heat flux. As a result, the near-surface atmospheric conditions become warm and dry. However, Mahfouf et al. (1987) demonstrated that, in the presence of vegetation, wet or dry soils can be masked, enabling the canopy to reduce the relative partition between sensible and latent heat flux.

Land atmosphere interactions, with respect to growth in depth of the planetary boundary layer, were studied by Zdunkowski (1975) and Betts and Ball (1995). Betts and Ball (1995) noted how soil moisture could be a major contributor to diurnal variations of both potential and equivalent potential temperature. They also documented how soil

moisture influenced the amount of dry air entrainment which occurred at the top of the boundary layer. Segal et al. (1995) indicated that soil moisture could also impact both dry and precipitating convection, and in general, the formation of clouds.

Brubaker and Entekhabi (1992a-b) illustrated how soil moisture could have a direct influence on the diurnal variation of the thermal state and moisture content of the near surface atmosphere. Furthermore, Brubaker and Entekhabi (1996) revealed that soil moisture control on the magnitude of evaporation is the major mechanism through which the moisture state of the near-surface atmosphere can reinforce thermal anomalies.

Spatial differences between regions of wet and dry soils create large gradients in turbulent heat flux. Segal and Arritt (1992) demonstrated how soil moisture variations could initiate and enhance thermally direct circulations commonly referred to as land-breezes. A study by Enger and Tjernstrom (1991) noted that local precipitation increased due to effects of the local land-breeze, and decreased when a strong synoptic wind was present. Ookouchi et al. (1984) used a numerical model to determine that even a slight moistening of the surface exerted a significant influence on mesoscale flow and that large variations in surface soil moisture lead to circulations which are equivalent in magnitude to sea-breezes.

Local soil moisture variation and variability in ET create variations in latent and sensible heat fluxes. Ultimately, these variations affect the formation of clouds at the top of the boundary layer (Rabin et al. 1990). Furthermore, Lanicci et al. (1987) demonstrated that spatial gradients in soil moisture are an important contributor to severe thunderstorm development in the Great Plains of the United States. Anthes (1984) indicated that precipitation could be enhanced under certain atmospheric conditions in semi-arid regions when dense vegetation occurred in bands about 100 km wide. Furthermore, Zhang and Anthes (1982) concluded that changes in albedo or surface roughness are less significant in their impact than are variations in soil moisture.

Larger spatial phenomena such as squall lines and baroclinic disturbances can also be impacted by spatial variations in soil moisture by influencing pre-storm convergence (Sun and Ogura 1979), by reducing (increasing) the strength of the nocturnal low-level jet over moist (dry) soils (McCorcle 1988), through modification of the boundary layer

structure (Fast and McCorcle 1991), and by influencing evaporation and precipitation patterns (Castelli et al. 1996).

Persistent weather patterns that result from anomalous conditions within the land surface can enhance phenomena such as droughts and floods. Charney (1975) hypothesized that large scale drying of the soil followed by a subsequent loss of vegetation can create a large-scale feedback system which reinforces drought conditions. Namias (1955, 1983, 1988) concluded that features in the underlying terrain had a significant influence on the atmosphere while studying drought conditions over the Great Plains of the United States. Using climate records for the continental United States between 1905 and 1984, Zhao and Kahil (1993) determined that a strong negative correlation existed between precipitation and surface temperature with the strongest correlation in the Central United States and the Great Plains. Huang and van den Dool (1993) included a lag correlation investigation into their analysis which revealed that a negative precipitation anomaly (less than normal rainfall amounts) led to a decrease of near-surface soil moisture and preceded above-average summer temperatures by one month.

Delworth and Manabe (1989) and Manabe and Delworth (1990) used a numerical model to demonstrate that persistent positive anomalies of soil moisture can have a significant impact upon the variability of the lower troposphere. Surface temperature and humidity are significantly altered by persistent wet anomalies due to an increase of latent heat flux and a reduction of sensible heat flux. Delworth and Manabe (1989) further concluded that persistent positive soil moisture anomalies have their greatest impact on the atmosphere across large spatial scales. Furthermore, moisture recycling is a major component in the potential sustenance of wet anomalies and can be a prime source of day-time convection (Zangvil et al. 1993); recycled moisture can account for up to 30% of the annual precipitation over large land areas (Brubaker et al. 1993).

Using simulations from a general circulation model, Koster et al. (2000) studied the seasonal-to-interanual variability and predictability of precipitation in a coupled system. The goal was to assess the relative impact of land surface and ocean boundary conditions. They concluded that the influence of land surface conditions is greatest in regions that are least affected by oceans and that the strength of the land-atmosphere interactions is

controlled by the availability of water and energy from the land surface in those locations. Relying on simulations of the general circulation, Schollser and Milly (2000) concluded that the predictability of soil moisture conditions range from approximately a week in temperate regions to a few months in regions where solar influence is weak.

2.3.2 Key Issue

Unfortunately, observations of soil moisture conditions are limited. In fact, most of the studies and results in Section 2.3.1 derive from numerical modeling studies. Many studies simply use soil moisture as a boundary condition to the atmosphere. In the case of coupled schemes, others use a one-dimensional mode whereby mass and energy are exchanged between the land-surface and the atmosphere. Unfortunately, horizontal movement of water or energy below the land surface does not occur in the model. However, recent studies such as Pielke et al. (1999) have demonstrated that surface characteristics, including soil moisture, must be treated as a dynamically evolving variable instead of a static or prescribed parameter.

Inherently, the lack of information in land-atmosphere studies concerning the spatial and temporal variability of soil moisture creates error within the analyses and results. For example, one might question whether the measurements of soil moisture are calibrated or how representative the measurements are of the surrounding site? Other concerns include how the measurements of soil moisture near the observing tower compare with sensors which measure latent and sensible heat and represent conditions upstream from the atmospheric sensors? These critical questions are generally left unaddressed and the reader can only guess whether the scheme was biased by the point measurements of soil moisture.

It is likely that land-surface schemes are highly sensitive to soil moisture conditions. Other examples such as the diagnostic evaluation by Ek and Cuenca (1994) and by Cuenca et al. (1996) of the 1-D PBL model developed at OSU, noted that surface fluxes of heat and energy are sensitive to the parameterizations of soil texture and soil water content respectively. Wetzel and Chang (1987), Wilson et al. (1987), Entekhabi and Eagleson (1989), and Avissar and Pielke (1989) addressed the sensitivity of the parametrizations of soil properties to land-atmosphere modeling. Yet, even these studies did not use actual field

observations of soil moisture to determine the sensitivity of the numerical model to moisture variability. To the author's knowledge, no study has been published which tests the sensitivity of near-surface atmospheric components on a local scale with the measured variability of soil water content in space and time.

Chapter 3
Data

3.1 Soil Moisture Observations

Between 1996 and 1999, heat dissipation sensors were installed at 103 Mesonet stations (Fig. 3.1) to provide real-time observations of soil moisture (Basara and Crawford 2000) at depths of 5, 25, 60, and 75 cm. These sensors (the Campbell Scientific Model 229-L) utilize thermocouples as temperature sensors and resistors as heating elements housed within a hypodermic needle (Fig 3.2). The hypodermic needle, in turn, is embedded within a ceramic matrix 14 mm in diameter and 60 mm long. During their operation in the soil, the ambient temperature of the sensor is measured by the thermocouple. Then, an electric current is sent through the resistor for 20 seconds. Immediately before the current is terminated, a second temperature is acquired using the thermocouple. The difference between the ambient temperature measured by the sensor and the temperature following the electrical pulse is large (small) in dry (wet) soil, because the heat produced by the resistor is conducted away from the sensor less (more) effectively. This difference (heat dissipation) is directly related to the soil-water potential (Reece 1996; Basara 1998; Starks 1999; Basara and Crawford 2000).

From the measurements of heat dissipation, and subsequently soil-water potential, it is possible to estimate the volumetric water content (cm^3_{water}/cm^3_{soil}) of the soil using the 229-L. These unique measurements are possible because soil samples were acquired at each vertical depth where the 229-Ls were installed. The soil samples were analyzed to determine the soil characteristics (%silt, %sand, %clay). Once characteristics of the soil samples were known, an empirical relationship to estimate volumetric water content from soil-water potential was developed using soil textures (Arya and Paris 1981). It should be noted that the relationship between soil-water potential and volumetric water content is determined specifically for each sensor depth and each site. Additional details concerning the installation and calibration of the 229-L sensors are presented in Chapter 4.

During 1999, field samples of soil water content at Mesonet sites were collected and

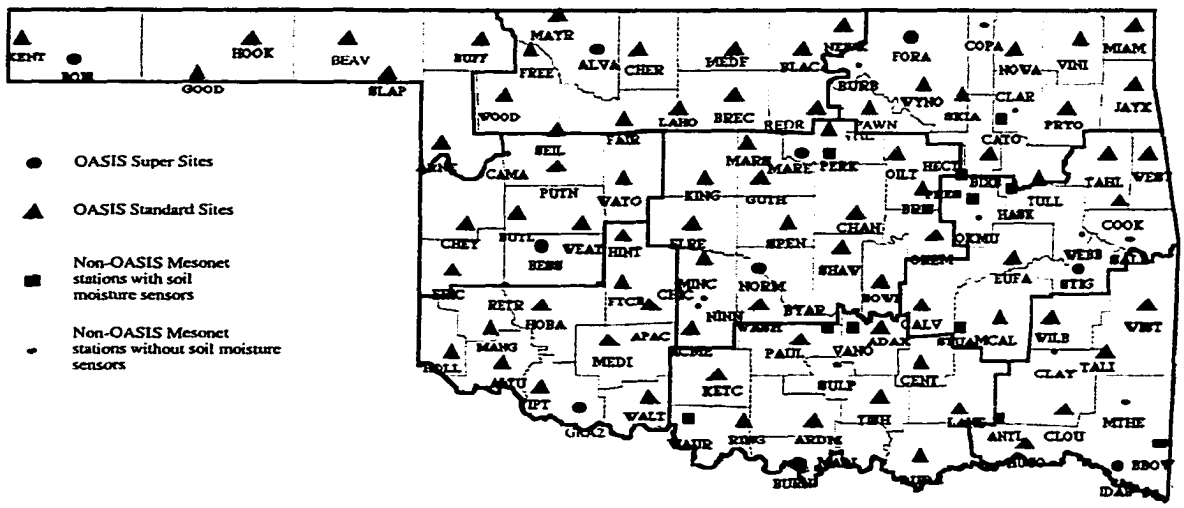

Figure 3.1. The Oklahoma Mesonet.

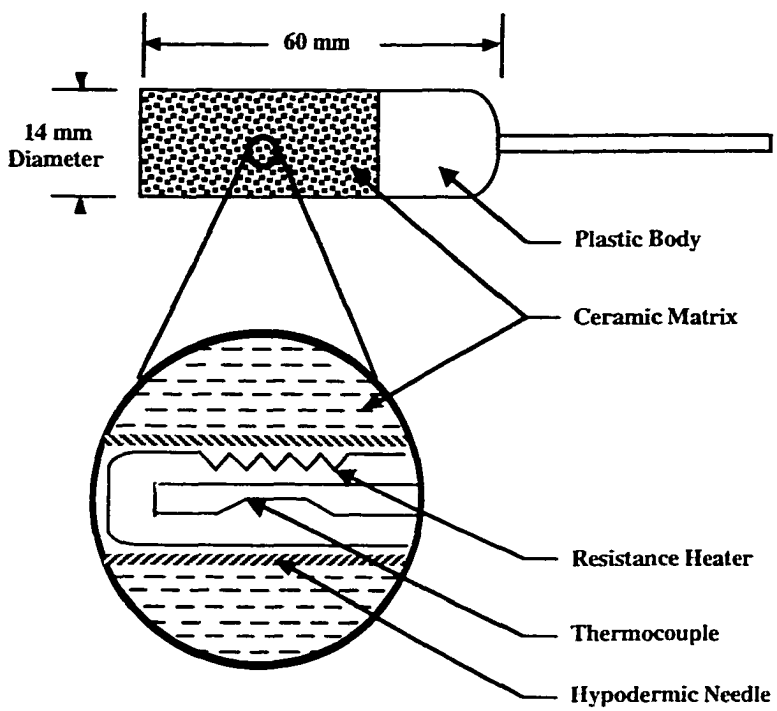

Figure 3.2. The 229-L matric potential sensor (the enlarged diagram represents a cross-section through the ceramic matrix) manufactured by Campbell Scientific.

compared with observations from the 229-L sensors. The purpose was to calibrate the 229-L sensors. Between 1 June 1999 and 31 October 1999, more than 4000 discrete soil samples were collected from 21 Mesonet sites and returned to the laboratory for analysis.

The Norman Mesonet site (NORM) in particular was sampled intensively between 1 June 1999 and 12 August 1999. To provide insight into the spatial and temporal variability of soil moisture both within and immediately surrounding the Norman site, a 20 m x 20 m study plot was created (centered on the 229-L sensors) which enclosed the Norman site and portions of the adjacent landscape. Within the study plot, 12 locations were semi-randomly chosen for sampling (Fig. 3.3). During this period, 2,792 samples were collected from the 12 predetermined locations at depths ranging between 0 and 80 cm. In addition to the field samples, estimates of soil water content were collected at NORM every 30 minutes using the 229-L sensors.

Inspection of Table 3.1 reveals the variability of soil water at the Norman site averaged over the study period. In general, the daily range of volumetric water content (the difference between field sample maximum and field sample minimum) was greatest in the 0-30 cm layer. In addition, strong trends in the vertical variability of soil water was not evident by a simple inspection of the standard deviation or sample variance. However, the mean coefficient of variation (COV) was greater in value near the surface and lesser in value at deeper depths (i.e., below 30 cm).

This trend is confirmed by examining a number of days on which soil samples were collected. Throughout the study period, the greatest values of COV occurred near the surface. Even though the standard deviation of the volumetric water estimate changed little with depth, the magnitude of water content values did change in the vertical. Thus, as soil near the surface became drier, and the magnitude of water content became smaller (with this drying, the standard deviation of soil moisture near the surface versus the mean value of the samples (COV) became greater). One exception was noted on 2 July. In that case, soil conditions were very moist throughout the depth of the soil column. Thus, the COV values were small near the surface due to the increased magnitude of the mean values of soil water content. However as soils dried during the second half of the study period, COV values in the 0-30 cm layer increased relative to depths deeper than 30 cm. This can be attributed to

Soil Depth	Mean Range	Max Range	Min Range	Standard Deviation	Mean Variance	Mean Coefficient of Variation
0 to 5 cm	0.093	0.187	0.048	0.029	0.0010	17.2
5 to 10 cm	0.099	0.285	0.045	0.029	0.0011	18.4
10 to 20 cm	0.148	0.210	0.072	0.046	0.0022	21.8
20 to 30 cm	0.115	0.238	0.063	0.034	0.0013	10.1
30 to 40 cm	0.087	0.196	0.017	0.035	0.0014	10.0
40 to 50 cm	0.090	0.196	0.034	0.036	0.0015	11.1
50 to 60 cm	0.080	0.179	0.031	0.032	0.0012	9.6
60 to 70 cm	0.058	0.116	0.017	0.022	0.0006	7.2
70 to 80 cm	0.068	0.107	0.043	0.028	0.0008	8.3

Table 3.1. Statistical evaluation of volumetric water content, stratified by soil depth, at the Norman Mesonet site (1 June - 12 August 1999).

Soil Depth	6/1/99	6/14/99	7/2/99	7/5/99	7/19/99	8/10/99
0 to 5 cm	22.0	18.7	10.7	20.6	33.2	24.2
5 to 10 cm	24.8	22.2	4.6	10.5	15.5	21.0
10 to 20 cm	28.3	22.1	10.7	12.0	24.7	26.8
20 to 30 cm	11.7	9.2	9.1	5.1	11.6	14.6
30 to 40 cm	9.8	4.9	10.2	8.8	9.4	7.1
40 to 50 cm	8.2	9.7	14.5	7.9	7.3	11.9
50 to 60 cm	8.5	10.7	11.2	4.9	7.5	8.7
60 to 70 cm	5.7	6.3	5.7	6.5	7.1	6.9
70 to 80 cm	6.7	6.2	6.8	10.3	8.4	10.5

Table 3.2. Examples of the daily coefficient of variation of volumetric water content, stratified by soil depth, at the Norman Mesonet site (1 June - 12 August 1999).

the fact that the near-surface soils dried much faster than those at deeper depths. The daily values of soil water content and the variability of the soil water at the Norman site are discussed in Appendix A.

The variability of soil water content at NORM during the study period is illustrated in Table 3.2. One source of variability near the ground surface is precipitation. For near surface soil conditions, the sample range and standard deviation increased dramatically following precipitation events and decreased to a minimum during extended dry periods (Fig. 3.4a). However, this trend was not observed at depths greater than 20 cm (Figs. 3.4b-c)

In addition, the daily variability in soil moisture at NORM noted in Table 3.2 can be attributed, in part, to differences in soil texture at each of the 12 sample locations (Tables 3.3 and 3.4). Soil samples were collected at each of the 12 locations for the purpose of soil classification. The samples were analyzed in the laboratory and soil texture was determined using the Bouyoucos Hydrometer method (Hillel 1998). For example, though the general classification of soil within the study plot between the depths of 0 and 5 cm is silty clay loam, slight differences exist in the percentages of sand, silt, and clay at each location. As a result, textural differences created differential values of wetting and drying within the soil layers at NORM.

3.2 Additional Mesonet Observations

The Norman Mesonet site is equipped with instruments to measure air temperature and relative humidity at 1.5 m, wind speed and direction at 10 m, pressure, solar radiation, rainfall, air temperature at 9 m, wind speed at 2 m, and bare and vegetated soil temperatures at 10 cm below ground level. Other parameters measured include temperature at 5 cm under bare and vegetated soil, and at 30 cm under vegetated soil. Observations from NORM are acquired at intervals of between 5 and 30 minutes and are subjected to rigorous QA procedures (Shafer et al. 2000).

During 1999, sensors at the Norman Mesonet site were upgraded as part of the OASIS Project (Brotzge et al. 1999; Brotzge 2000). The primary addition of new sensors

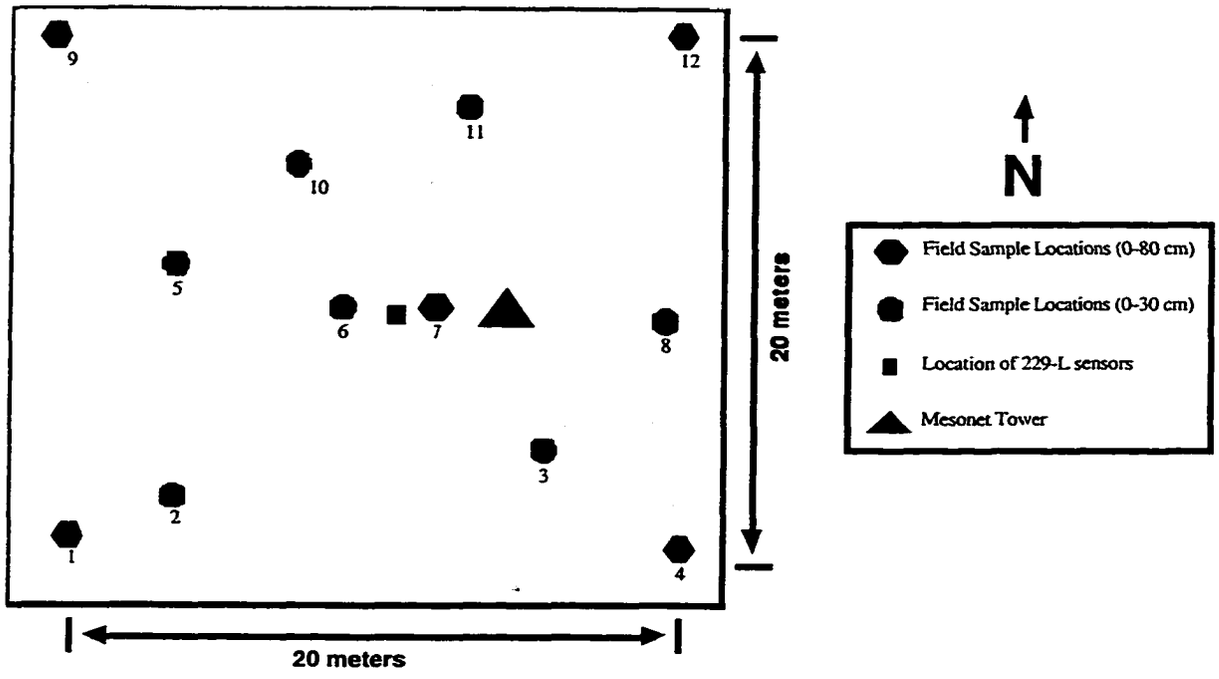

Figure 3.3. Locations at the Norman Mesonet site where soil moisture and soil texture were sampled.

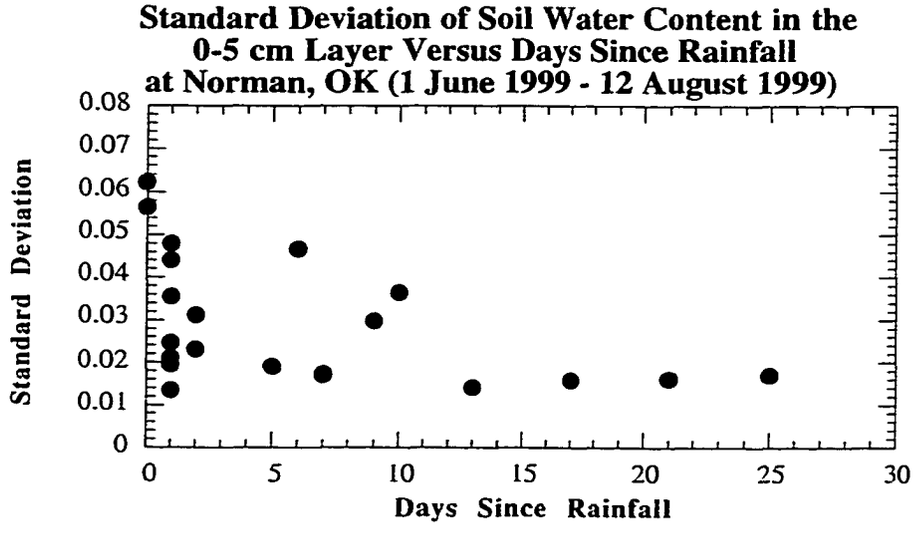

Figure 3.4a. The variability of soil moisture (0-5 cm) at the Norman site versus days after precipitation.

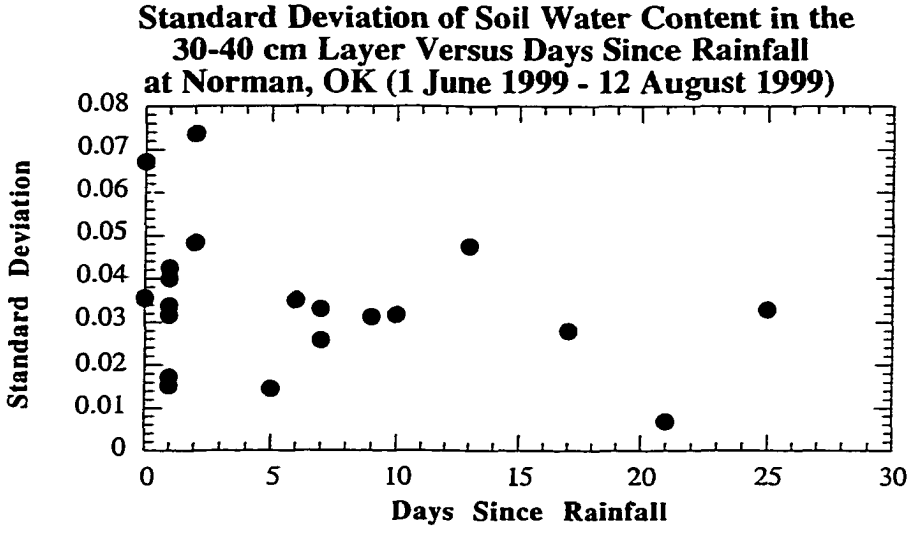

Figure 3.4b. The variability of soil moisture (30-40 cm) at the Norman site versus days after precipitation.

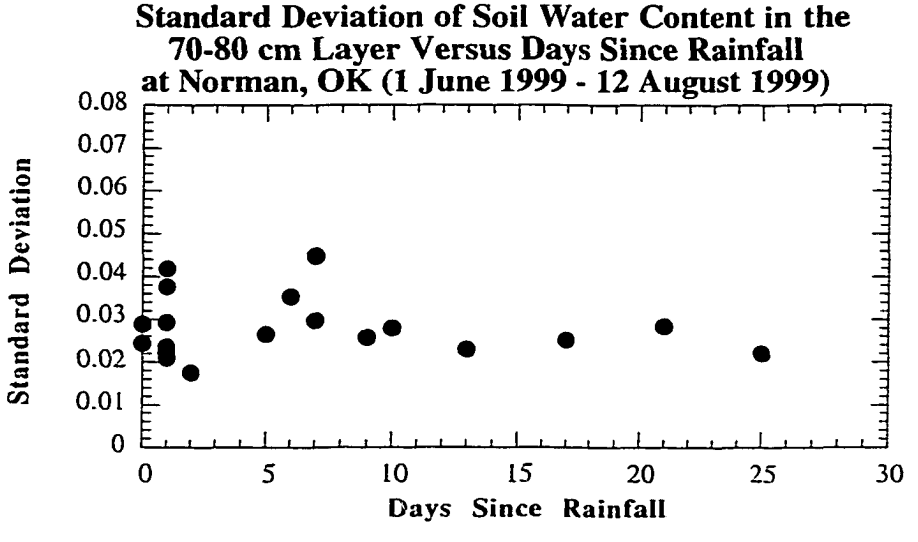

Figure 3.4c. The variability of soil moisture (70-80 cm) at the Norman site versus days after precipitation.

Depth	Mean % Gravel	Mean % Sand	Mean % Silt	Mean % Clay	Soil Classification
0-5 cm	0.2	34.7	51.0	14.1	Silt Loam
5-10 cm	0.0	35.4	47.9	16.7	Loam
10-20 cm	0.2	30.9	43.6	25.3	Loam
20-30 cm	0.0	26.8	33.8	39.4	Clay Loam
30-40 cm	0.0	27.0	34.3	38.7	Clay Loam
40-50 cm	0.8	31.8	30.0	37.3	Clay Loam
50-60 cm	1.8	28.9	33.5	35.8	Clay Loam
60-70 cm	3.2	30.8	30.0	36.0	Clay Loam
70-80 cm	2.3	31.6	32.0	34.1	Clay Loam

Table 3.3. The mean vertical stratification of soil characteristics at the Norman Mesonet site.

Depth	Standard Deviation % Gravel	Standard Deviation % Sand	Standard Deviation % Silt	Standard Deviation % Clay
0-5 cm	0.6	7.7	9.1	4.6
5-10 cm	0.1	6.0	6.6	3.3
10-20 cm	0.4	5.3	4.8	6.1
20-30 cm	0.0	7.5	8.0	5.9
30-40 cm	0.1	4.5	3.9	3.4
40-50 cm	1.2	4.1	5.0	3.5
50-60 cm	1.7	4.5	3.6	2.6
60-70 cm	1.4	8.2	9.1	3.5
70-80 cm	1.5	6.8	5.7	3.8

Table 3.4. Variability in the vertical stratification of soil characteristics at the Norman Mesonet site.

included a sonic anemometer and krypton hygrometer (4.5 m above ground), a four-component net radiometer (1.5 m), a domeless net radiometer (1.5 m), and heat flux plates at 5 cm. Sensible and latent heat fluxes (SH and LH) were computed using the eddy correlation approach (Brotzge 2000).

Sensible heat flux was also estimated using the profile approach. Vertical gradients in air temperature were measured using sensors at 1.5 and 9 meters. Similarly, the vertical gradient in wind speed was measured using anemometers at 2 and 10 meters. Sensible heat flux was estimated by applying Monin-Obukov similarity theory to observed gradients in wind speed and temperature (Brotzge and Crawford 2000). Furthermore, because net radiation (Rn) and ground heat flux (GH) are measured at the site (Brotzge 2000), latent heat flux was estimated as the residual in the surface energy budget:

$$Rn = SH + LH + GH \tag{3.1}$$

which becomes,

$$LH = Rn - SH - GH \tag{3.2}$$

Net radiation, ground heat flux, sensible heat flux, and latent heat flux were collected at 15 minute intervals and processed through QA routines.

3.3 Upper Air Observations

The Norman Mesonet site is approximately 3.03 km (1.08 miles) from the OUN upper air station. Weather balloons are launched twice daily at 0000 and 1200 UTC which provide information pertaining to the vertical profile of the atmosphere (temperature, moisture, wind speed, and wind direction). The close proximity of the sounding location to the Norman Mesonet site provides an excellent opportunity to study the boundary layer near and above the NORM site.

Balloons were launched twice daily during the study period. On any given day, the early morning sounding represents the atmosphere before the boundary layer has begun its daytime oscillation. On the other hand, the evening sounding represents the boundary layer near the end of its daily oscillation. Thus, the sounding data provides *endpoints* of the daily

evolution of the atmospheric boundary layer near the NORM site. This sounding information is critical to initialize the PBL model, and to verify model predictions regarding the depth, temperature, and moisture profiles of the PBL.

3.4 Ideal Conditions for Study

Ideal conditions during the study period refer to days when solar radiation was at or near its theoretical maximum (no cloud cover) and shear in the lower troposphere was weak. A detailed analysis of the four components in the surface energy budget is easier to interpret during ideal conditions. A visual inspection of observations from the summer of 1999 yielded 13 days which could be classified as ideal. In addition, this 13-day data set is thought to have limited contamination by the horizontal advection of temperature or moisture into the PBL.

An example of *ideal* conditions for study occurred on 2 July (Figs. 3.5 and 3.6). Soil conditions at NORM on 2 July were extremely moist throughout the measured soil profile. Thus, it was not surprising that latent heat flux was nearly double the magnitude of sensible heat flux (Fig. 3.5). Additionally, the vertical profile of the lower troposphere (Fig. 3.6) revealed a well mixed PBL at 0000 UTC which extended to a depth of 1470 meters above ground level.

A second data set associated with *ideal* atmospheric conditions is shown in Figures 3.7 and 3.8 (25 July). In this case, an extended dry period was underway. As a result, near-surface soil conditions were quite dry. However, soil moisture below 20 cm was still quite moist. The result was decreased latent heat flux at the site (versus that observed on 2 July) as well as increased sensible heat flux. In fact, the magnitude of both fluxes was nearly identical on 25 July (Fig. 3.7). Since the partitioning of available energy was greater toward sensible heat flux when compared with 2 July, the PBL extended to greater depth on 25 July (2386 m; Fig. 3.8).

The examples noted in Figures 3.5 through 3.8 offer insight into the atmospheric conditions used for this study. Additional plots of net radiation as well as sensible and latent heat flux for other *ideal* conditions are shown in Appendix B.

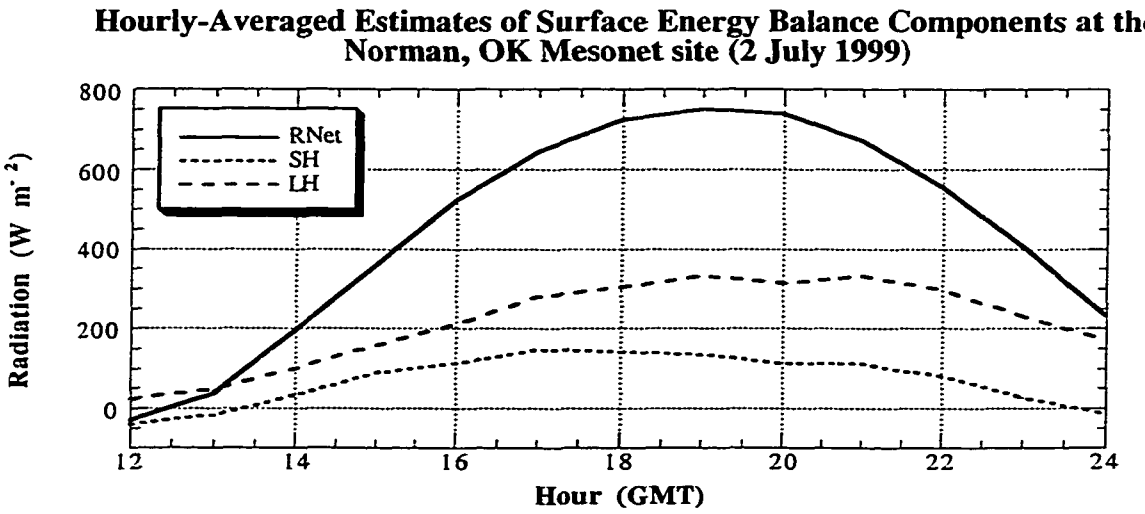

Figure 3.5. Hourly-averaged values of net radiation, sensible heat flux, and latent heat flux on 2 July 1999 at the Norman Mesonet site.

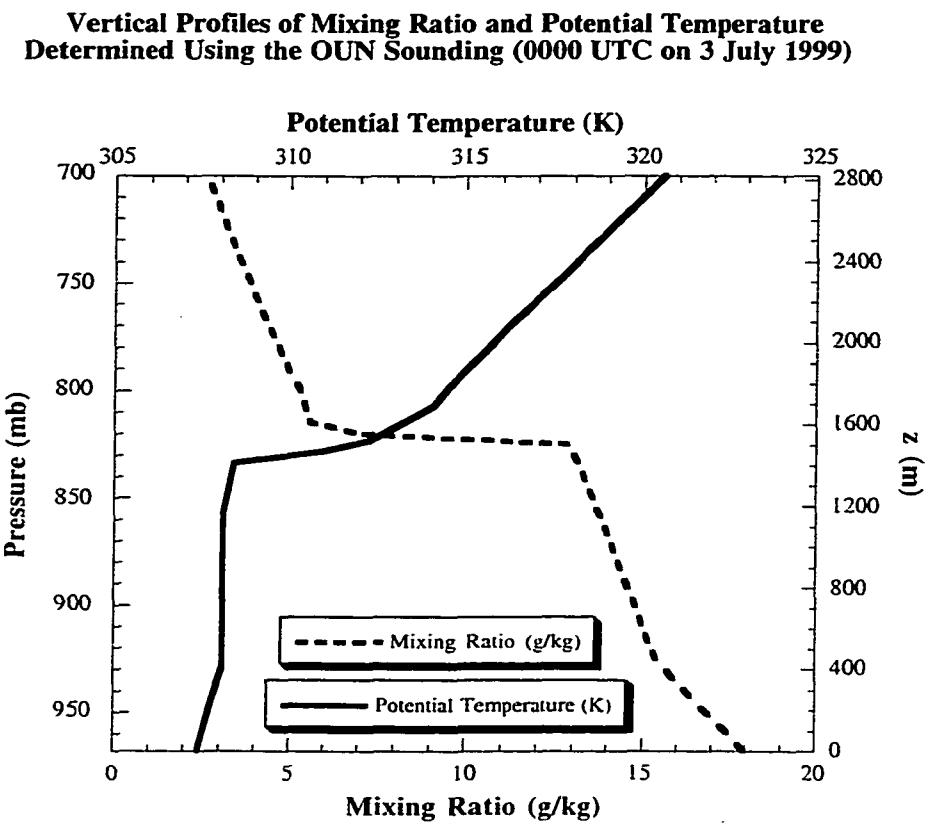

Figure 3.6. Vertical profiles of mixing ratio and potential temperature determined using the OUN sounding (0000 UTC on 3 July 1999).

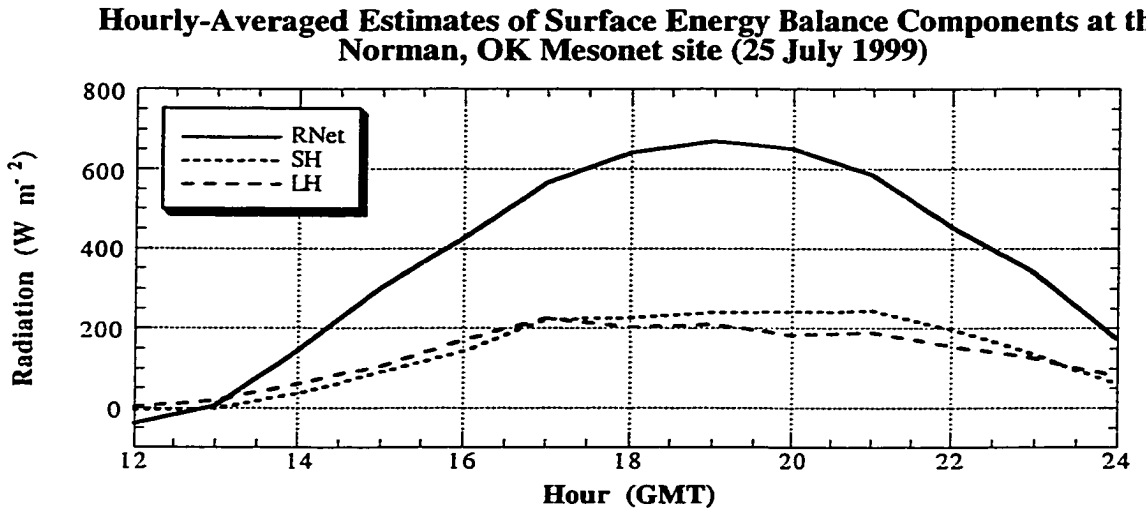

Figure 3.7. Hourly-averaged values of net radiation, sensible heat flux, and latent heat flux on 25 July 1999 at the Norman Mesonet site.

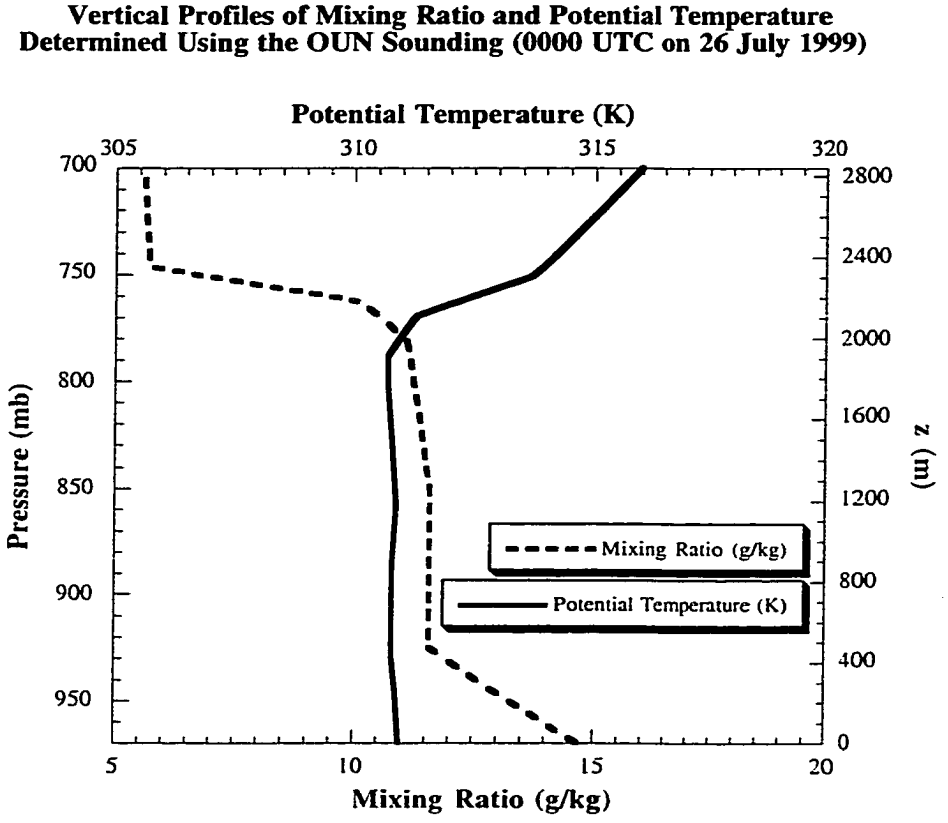

Figure 3.8. Vertical profiles of mixing ratio and potential temperature determined using the OUN sounding (0000 UTC on 26 July 1999).

Chapter 4

229-L Calibration and Instrument Errors

4.1 Initial Calibration and Installation

The amount of water in the soil is commonly expressed in terms of potential. Soil-water potential is defined as the amount of work needed to transfer a unit mass of water from the soil to a reference pool at the same elevation. Established convention dictates that these values are negative; thus, larger absolute values of potential represent drier soils. Typically, the work per unit mass of water (J kg^{-1}) is multiplied by the density of water (approximately 1000 kg m^{-3}) to determine soil-water potential expressed in terms of pressure (kPa; Marshall et al. 1996). Determining the soil-water potential is crucial when considering the availability of water for the sustenance of vegetation. It is widely accepted that vegetation has great difficulty in extracting water from soils when the potential is less than about -1500 kPa (Dingman 1994). Thus, an estimate of soil-water potential is a valuable resource to help understand both the flow of moisture within the soil and its impact on both the atmosphere and the biosphere.

Using a device that consists of a temperature sensor and a heating unit placed directly into the soil, Shaw and Baver (1939) demonstrated that the rate at which heat is dissipated in the soil can be an indicator of the matric potential (water potential) of the soil. Phene et al. (1971) developed a sensor using a Germanium P-N diode as the temperature sensor; when the sensor was wrapped with 40-gauge copper wire, it acted as the heating coil. The apparatus was then embedded in a porous block. Various materials such as gypsum, ceramics, and mixtures of ceramic and castone were tested as potential porous materials that could be used in the block. They determined that the ceramic block provided a stable solid matrix due to the linear response exhibited by the material during testing. Sensors based on the design of Phene et al. (1971) have been successfully utilized in sandy loam (Phene and Howell 1984), clay loam (Phene et al. 1989), silt (Fredlund 1992), and clay (Fredlund 1992).

The 229-L sensor, manufactured by Campbell Scientific Inc., incorporates this

design (Fig. 3.2). A thermocouple and a resistor are housed within a hypodermic needle. The hypodermic needle, in turn, is embedded within a ceramic matrix 14 mm in diameter and 60 mm long. Once the sensor is buried within the soil, the matrix must be permitted to come into equilibrium with the surrounding soil (typically 2-3 months). Once equilibrium is attained, the thermocouple measures the soil temperature both before and after an electric current of 50 mA is passed through a 33 W resistor for 20 seconds. After the current pulse, the temperature difference is larger (smaller) in drier (wetter) soil, because the heat produced by the resistor is conducted away from the sensor less (more) effectively. This difference is directly related to the soil water potential.

The 229-L sensors were subjected to a two-step laboratory calibration before they were installed at remote sites. First, the sensors underwent an endpoint test, whereby heat dissipation (temperature rise of the sensor) was measured under both dry and saturated conditions. To accomplish this, the sensors were subjected to a dry air environment using dessicant bags. The temperature rise for each sensor was calculated over a twelve hour period. Once the sensors temperature increase in an extreme dry environment was established, the sensors were immersed in distilled water and a similar set of measurements were performed over a twelve hour period. Finally, a set of calibration coefficients was created using the endpoint data, and applied to each sensor's response to remove the inherent sensor-to-sensor variability:

$$\Delta T_{ref} = m^{*}\Delta T_{sensor} + b \qquad (4.1)$$

where ΔT_{ref} is the response of a "reference" sensor, ΔT_{sensor} is the observed response of an individual sensor ($T_{after\ heating} - T_{before\ heating}$), and m and b are empirical coefficients unique to each sensor.

Sensor response also was compared with known potentials created in the laboratory. Subsequently, an equation was developed by Dr. Daniel K. Fisher (a consultant to the Oklahoma Mesonet) to convert temperature changes generated by a sensor into values of matric potential:

$$\psi = \frac{1}{a}\left(\frac{\Delta T_w - \Delta T_d}{\Delta T_{ref} - \Delta T_d} - 0.9\right)^{\frac{1}{n}} \tag{4.2}$$

where ψ is the matric potential (kPa), ΔT_d is the standard temperature difference for dry soil (4.0°C), ΔT_w is the standard temperature difference for saturated soil (1.45°C), and *a* and *n* are empirical coefficients (-0.01 kPa^{-1} and 0.77, respectively). An independent study by Reece (1996) indicated that the methodology described above is a reliable method for calculating the water potential of the soil.

It is also desirable to estimate the volumetric water content (cm^3_{water}/cm^3_{soil}) of the soil using the 229-L. During installation, soil samples from each site were acquired at each vertical depth at which the 229-Ls were installed. These samples were sent to Oklahoma State University to determine the soil characteristics of each sample. Once characteristics of the soil samples were known (%silt, %sand, %clay), an empirical relationship to estimate volumetric water content was developed using soil textures (Arya and Paris 1981). Thus, an estimate of volumetric water content is determined using estimated values of water potential from Equation 4.2:

$$\theta_{soil} = \theta_r + \frac{\theta_s - \theta_r}{\left[1 + \left(\alpha(-\psi/100)\right)^h\right]^{1 - 1/h}} \tag{4.3}$$

where θ_{soil} is volumetric soil water content, θ_r and θ_s are the residual water content and saturated water content respectively (values unique to soil texture), and α and h are empirical constants (values unique to soil texture). It should be noted that organic matter was not sampled or considered in developing this empirical relationship to determine soil water content.

Once calibrated in the laboratory, the sensors were installed at each of 60 Mesonet site locations. The same installation procedure was used for each soil moisture probe. First, a shallow trench 3.7 m long was dug westward from the base of the Mesonet tower. A second shallow trench 0.61 m long was dug south from the endpoint of the first trench. The purpose of these trenches was for a protective conduit to house the wiring of each 229-

L sensor.

At the end of the second conduit trench, three holes approximately 10 cm in diameter were created using a post-hole digger. The first hole, located east of the endpoint of the second trench, was dug to a depth of 5 cm. A second hole (25 cm deep) was dug at the endpoint of the second trench. Just west of the endpoint of the second trench, a hole 70 cm deep was dug. As the soil was excavated from each hole, great care was taken to preserve the original stratification of the soil. This excavation placed each layer of soil in separate piles upon a tarp; each pile maintained the vertical stratification of the soil except laid out in a horizontal manner.

The sensors at the 5 and 25 cm depths were installed horizontally while the sensors at the 60 and 75 cm depths were installed at a 45° angle (Fig. 4.1). The actual sensor was inserted 10 cm into a small hole that was the width of the sensor (14 mm). Once inserted, a mixture of water and soil removed from the sensor hole were combined into a slurry. The slurry was subsequently squirted into the sensor hole to backfill the sensor hole to promote complete contact between the sensor and the soil, and to remove preferential pathways for water flow. Extreme care was taken when backfilling the installation holes to replace the soil in a manner consistent with the soil stratification prior to installation. Once the installation holes were filled, the trench containing the sensor wires inside the conduit was also filled, thus burying the conduit.

4.2 Field Measurements and Improved Calibration

Beginning in June 1999, field samples of soil water content were collected from 21 Mesonet sites to validate and calibrate the soil water content values derived from the in situ 299-L sensors. Between the dates of 1 June and 31 October of 1999, 4002 discrete soil samples were collected using a coring device approximately 1.5 cm in diameter; the samples were acquired from the following layers: 0-5, 5-10, 10-20, 20-30, 30-40, 40-50, 50-60, 60-70, and 70-80 cm. With the exception of the Norman Mesonet site and during each visit to the other sites, 3 cores to a depth of 80 cm were collected within 3 m of the 229-L sensors. At NORM, 5 cores were collected to a depth of 80 (locations 1, 4, 7, 9, and 12 in Fig. 3.3)

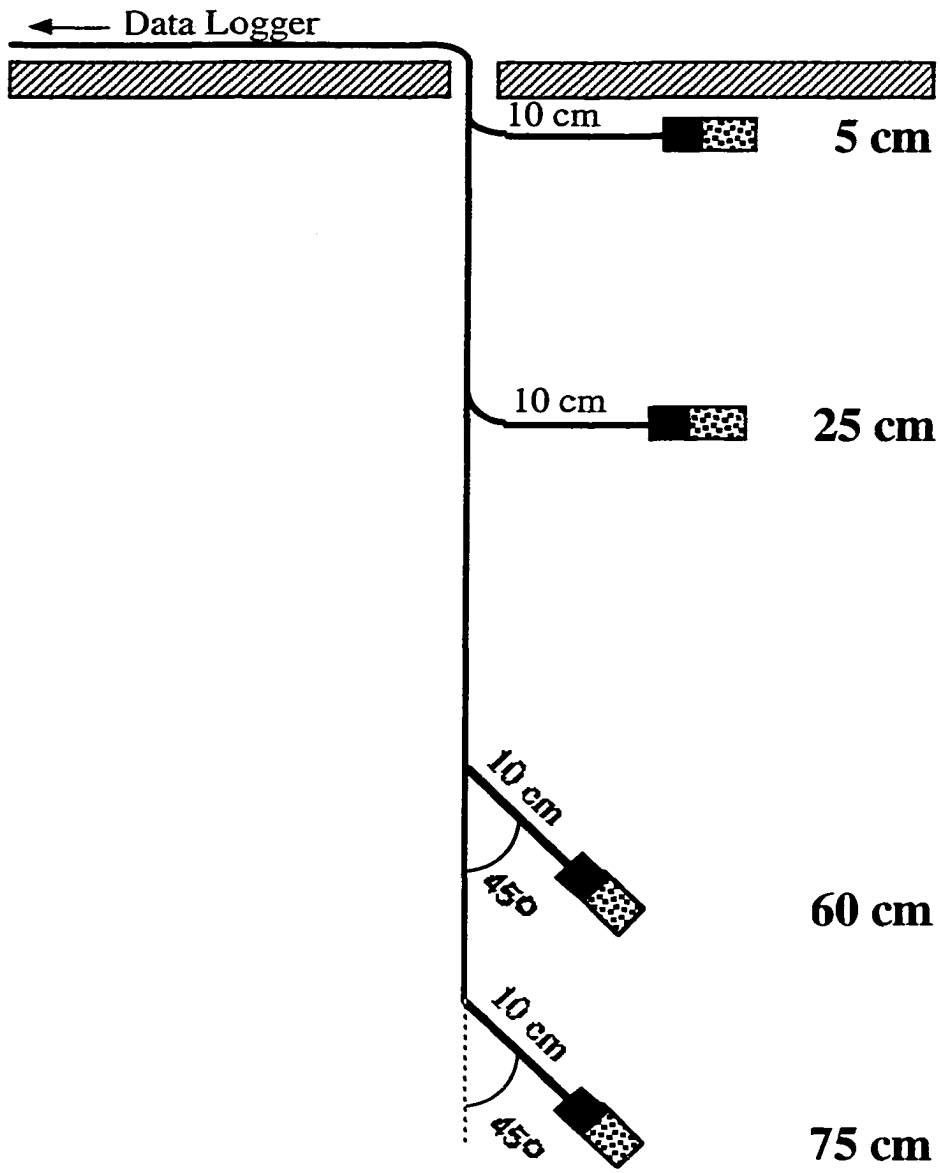

Figure 4.1. The vertical profile (planar view) of 229-L sensors installed at Oklahoma Mesonet stations.

and 7 cores were collected to a depth of 30 cm (locations 2, 3, 5, 6, 8, 10, and 11 in Fig. 3.3). Volumetric water content was obtained for each sample at each site and depth using the product of the gravimetric sample with the bulk density of the soil (known for each site and depth) and dividing by the density of water.

The field samples values of soil water content were compared with observations from the 229-L sensors. Some sensors, such as the 5 cm sensor at NORM compared well in both magnitude and trend with the field samples. However, a majority of sensors revealed a significant dry bias in soil water content derived using the 229-L.

Comparison between field samples of soil water content and soil water estimated using the 229-L sensors revealed that improvements were necessary to the derived soil water content from the sensors. Initial improvements focused on the relationship between ΔT_{ref} and ψ in Equation 4.2 (the first step in converting 229-L output to water content estimates). Laboratory tests were performed by Dr. Daniel K. Fisher to improve the relationship between ΔT_{ref} and ψ.

In the first test, a tensiometer and several 229-L sensors were buried in soil within a container (closed on the bottom and sides but exposed to air at the top; a bucket). The soil, sensors, and tensiometer were subsequently saturated with water and allowed to dry via evaporation. Tensiometer measurements were collected concurrently along with 229-L measurements using a datalogger and a multiplexor.

The second test involved the same container, soil, and 229-L sensors. In this case, however, the tensiometer was replaced by a vacuum tube which was inserted into the soil. Once again, the soil and sensors were saturated within the bucket. A vacuum pump was connected to the vacuum tube which allowed the tension (negative soil water potential) within the soil to be set at a specific level while an electronic pressure transducer, attached to the vacuum tube, measured the tension. The 229-Ls were allowed to equilibrate with the soil, and measurements were made before tension was increased with the vacuum pump.

In the final test, several 229-L sensors were placed in a soil sample on a large ceramic plate within a pressure chamber. The soil, sensors, and ceramic plate were saturated. The wire for the 229-L sensors was passed through a hole in the chamber and attached to the multiplexor. Then, as the chamber was under pressure, continuous

measurements by the 229-L sensors were collected

Unfortunately, the dry bias occurred at tensions that could not be attained in the controlled laboratory setting. However, an exponential equation converting ΔT_{ref} to ψ compared well with tensions obtained in the laboratory and produced a more gradual drying trend at higher tension values. Because field analyses of water content indicated a more gradual transition from wet to dry, the exponential form of ΔT_{ref} was adopted as the preferred means in estimating soil water potential using 229-L data. The improved relationship between ΔT_{ref} and ψ is given by:

$$\psi = -c * \exp(d * \Delta T_{ref}) \tag{4.4}$$

where c and d are empirical coefficients (1.788 $^{o}C^{-1}$ and 0.717, kPa respectively). Thus, equation 4.4 replaces equation 4.2 as the preferred method for computing soil water potential using ΔT_{ref} data.

Unfortunately improvements in the relationship between ΔT_{ref} and ψ did not eliminate the dry bias in 229-L soil water content. Thus, the empirical relationship used to convert ψ to volumetric water content in Equation 4.3 was investigated. The goal was to improve the estimates of empirical coefficients θ_r, θ_s, α, and h derived using the methodology described by Arya and Paris (1981).

First, a correction noted in the literature (Arya and Dierolf 1992) was applied to the methodology of Arya and Paris (1981) to rederive appropriate coefficients. Even after the correction was applied, water content values derived from 229-L measurements still revealed a dry bias. Thus, linear regression, applied to the empirically derived water regression curves, was compared with laboratory measured water regression curves. The results improved the performance of water content values derived from 229-L data when compared to field measurements at Mesonet sites.

Consider the examples shown in Figures 4.2-4.4 which represent 229-L sensors at depths of 25, 60, and 75 cm compared with field samples of soil water content at the Norman Mesonet site. In each case the improved calibration outperforms the original

calibration in terms of magnitude and trend of soil water content. Unfortunately, the improved calibration performed worse at the 5 cm depth when compared with the original calibration and field samples of soil water content (Fig. 4.5). However, this result was noted only at the Norman site, and was not conclusively demonstrated at other validation sites.

4.3 An Installation Error

The method used to install the matric potential sensors in the Oklahoma Mesonet at depths of 60 and 75 cm was determined to have a fundamental flaw. Unfortunately, this flaw can lead to significant errors in soil moisture observations under certain conditions (Basara and Crawford 2000). By installing the sensors at a 45° angle with respect to vertical, water can flow down the instrument wire via the paths of disturbed soil created during installation. The preferential path allows water to moisten the sensor without impacting the rest of the soil layer. However, it should be noted that no evidence has been found (at any Mesonet site location) to indicate that the 5 or 25 cm sensors are contaminated via preferential pathways. Thus, sensors should be installed horizontally (at all levels) to minimize the possibility of measurement error.

It should be noted that this installation procedure represents an anomaly in the operation of soil moisture sensors across Oklahoma. More than three million observations of soil moisture conditions were observed between 1996 and 1999; yet the number of observations affected by this installation error account for less than one percent of the data archives. In addition, the errant deep-layer values of soil moisture, detected following extended dry periods, occur in soils of mainly silt and clay particles. In most cases and at most sites, measurement errors do not occur.

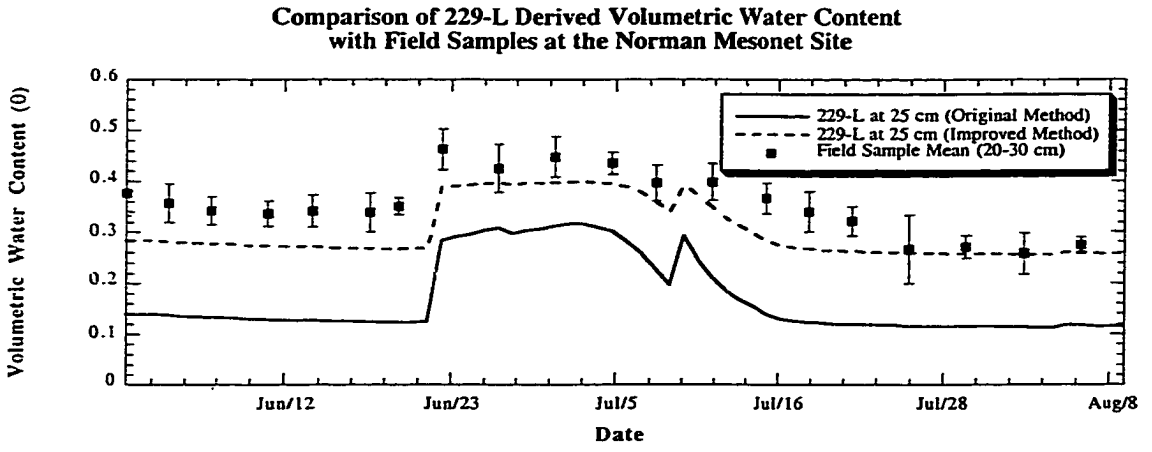

Figure 4.2. Comparison of original and improved methods for estimating volumetric water content of the soil using the 229-L sensor (25 cm) versus field samples of soil water content (20-30 cm) at the Norman Mesonet site (1 June - 10 August 1999).

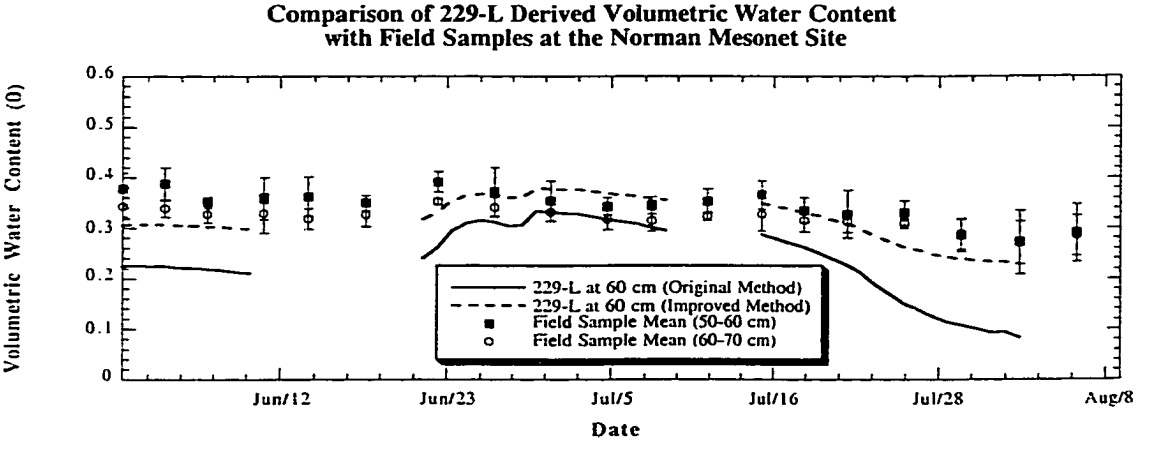

Figure 4.3. Comparison of original and improved methods for estimating volumetric water content of the soil using the 229-L sensor (60 cm) versus field samples of soil water content (50-60 and 60-70 cm) at the Norman Mesonet site (1 June - 10 August 1999).

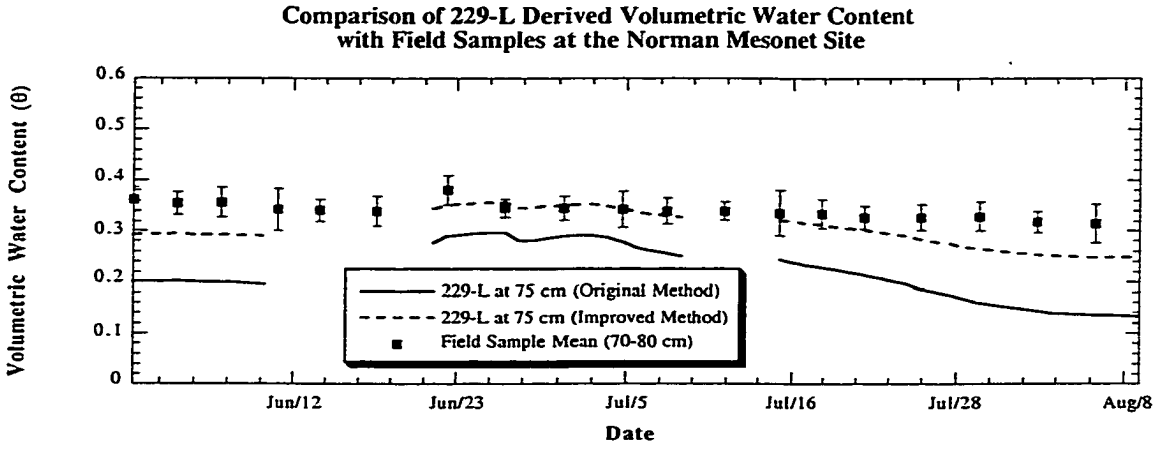

Figure 4.4. Comparison of original and improved methods for estimating volumetric water content of the soil using the 229-L sensor (75 cm) versus field samples of soil water content (70-80 cm) at the Norman Mesonet site (1 June - 10 August 1999).

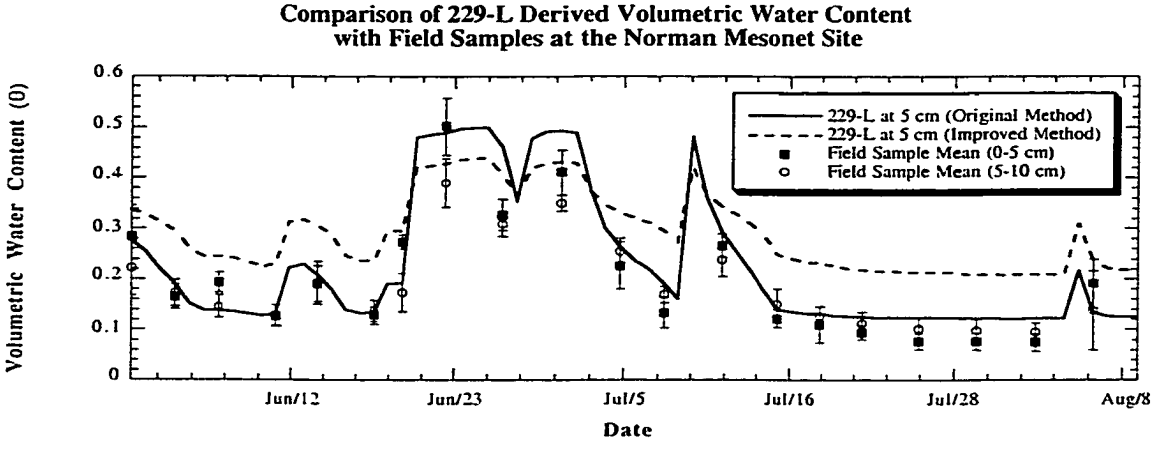

Figure 4.5. Comparison of original and improved methods for estimating volumetric water content of the soil using the 229-L sensor (5 cm) versus field samples of soil water content (0-5 and 5-10 cm) at the Norman Mesonet site (1 June - 10 August 1999).

Chapter 5

Linear Relationships Between Root-Zone Soil Moisture and Atmospheric Processes in the Planetary Boundary Layer

The results presented in this study are based on the assumption that land-atmosphere interactions occurred at the Norman Mesonet site during the study period. In particular, the focus is on 13 days characterized by strong radiative forcing was and weak shear in the lower troposphere. On these days considered *ideal* for PBL studies, soil water clearly modulated atmospheric processes at the Norman Mesonet site.

5.1. Analysis

While diurnal trends of sensible and latent heat flux are driven by incoming solar radiation, the magnitude of sensible and latent heating is contingent upon a number of localized features including soil moisture. On days which met the *ideal* criterion, the daily-maximum of hourly-averaged values of latent and sensible heat flux, measured using the eddy correlation technique, were compared with soil moisture conditions. This comparison method was chosen because the land surface was determined to have its most evident impact upon the peak values of sensible and latent heat fluxes. Use of hourly-averaged values also was determined to diminish the highly variable nature of flux measurements.

To provide consistent comparisons of field conditions of soil water content throughout the study period, the observed mean values of the field samples were interpolated to those dates when manual samples were not collected. First, a linear interpolation was performed between observations. Next, a 3-day running mean was applied to the time series of data points to eliminate high frequency features that resulted from the linear interpolation. An example of results from this interpolation technique is shown in Figure 5.1. Thus, this study used the mean volumetric water content, interpolated from field samples, as representative values of soil water content at each soil layer on each day. In addition to the field samples, estimates of soil water content were

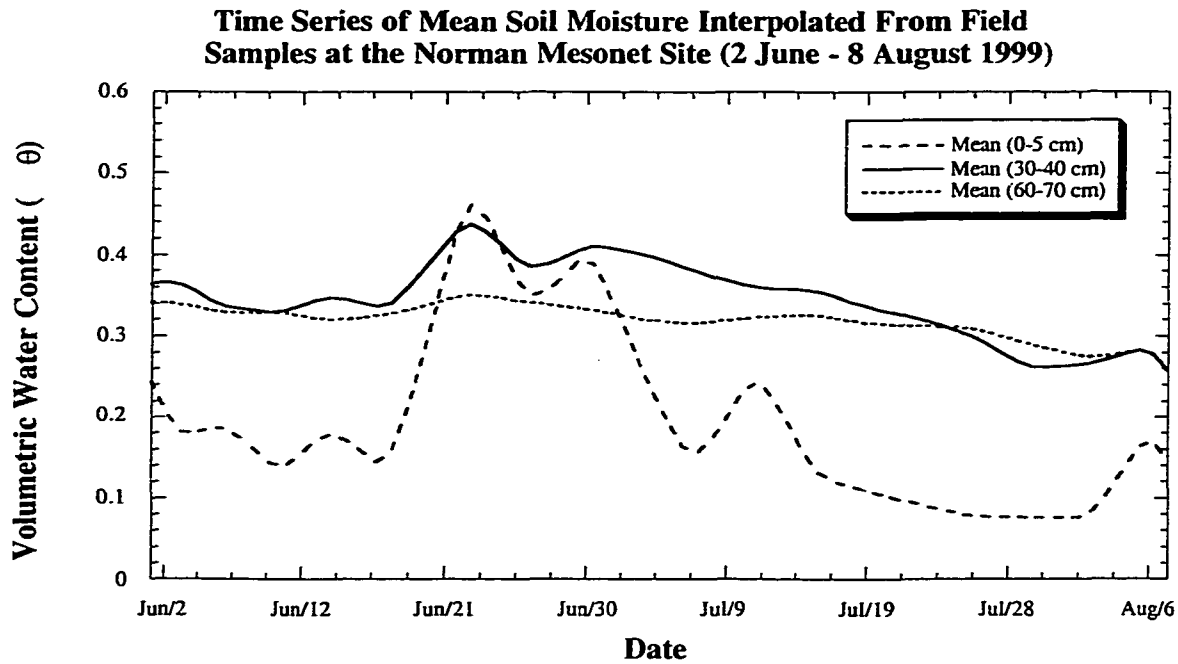

Figure 5.1. Mean soil water content interpolated from field samples at layer depths of 0-5, 30-40, and 60-70 cm (2 June -8 August 1999).

collected for this study using the 229-L sensors at NORM.

Figures 5.2a-b reveal a significant relationship between daily-maximum values of sensible and latent heat flux and mean soil water content near the surface (in the 0-5 cm layer). The data values compared were either interpolated from field samples or observed with the 229-L sensor at 5 cm. A nonlinear relationship was uncovered. In each comparison, an empirical "best fit" curve to the observations was a second-order polynomial.

However, strong but unexpected linear relationships were discovered when values of heat flux were compared to soil moisture at deeper depths. For example, daily-maximum values of sensible and latent heat flux were plotted as a function of soil water content sampled between 30-40 cm (Fig. 5.3a). When a deeper layer of soil moisture is used, the relationship between soil moisture conditions and sensible and latent fluxes appeared linear. The linear variance value is 0.902 between soil water in the 30-40 cm layer and sensible heat

flux measured at 4.5 meters. Equally as strong, the variance value between latent heat flux and soil water conditions in the 30–40 cm depth is 0.854. Similar results were noted when peak values of sensible and latent heat flux were compared with volumetric water content determined using the 229-L sensor at 60 cm (Fig. 5.3b). Even when automated soil moisture observations are used, the linear correlations between soil water at 60 cm and sensible and latent heat fluxes were 0.963 and 0.947 respectively.

A more indepth inspection of these data indicated that the relationship between the land surface and the atmosphere (using proxies of soil water and heat fluxes in the near-surface atmosphere) were nonlinear. More importantly, that relationship quickly becomes linear when data from the 20-60 cm layer (Fig. 5.4) are used. Because soil moisture conditions at depths greater than 60 cm were nearly constant throughout the study period, the impact of deeper layer soil moisture upon the atmosphere becomes decoupled and the linear relationships gradually decreased. Similar results were obtained when data from the automated 229-L sensors were compared with sensible and latent heat fluxes (Fig. 5.5). Thus, the relationships were highly nonlinear when data from shallow soil depths were used. That relationship became increasingly linear with depth but linearity peaked at 60 cm. The linearity with surface processes decreased when deep-layer soil moisture was used

Since linear relationships between root-zone soil moisture and both sensible and latent heat fluxes were observed at NORM, closure of the surface energy balance was investigated to determine if similar relationships existed. The surface energy balance is defined as:

$$RN - GH = SH + LH \tag{5.1}$$

where SH is the sensible heat flux (W m^{-2}), LH is the latent heat flux (W m^{-2}), RN is the Net Radiation (W m^{-2}), and GH is the ground heat flux (W m^{-2}). Closure of the surface energy balance is defined as:

$$Cl = \frac{SH + LH}{RN - GH} * 100 \tag{5.2}$$

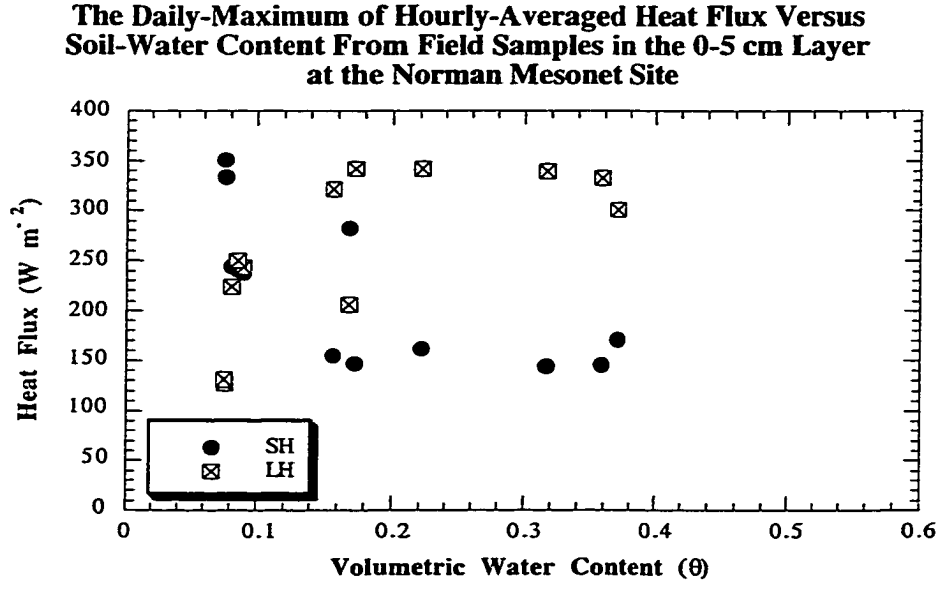

Figure 5.2a. The daily-maximum of hourly-averaged values of sensible and latent heat flux versus soil water content estimated from field samples in the 0-5 cm layer at the Norman Mesonet Site.

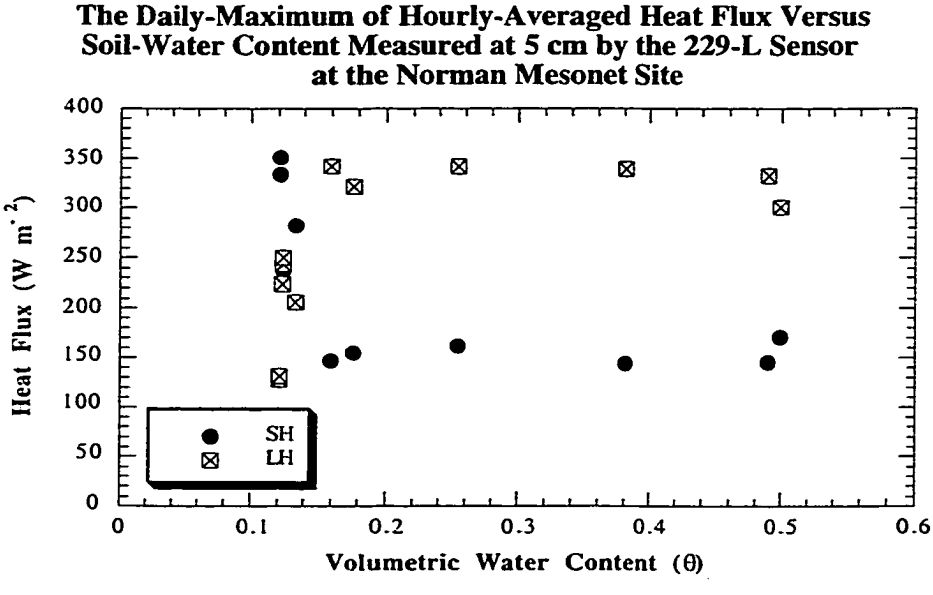

Figure 5.2b. The daily-maximum of hourly-averaged values of sensible and latent heat flux versus soil water content measured at 5 cm by using the 229-L sensor at the Norman Mesonet Site.

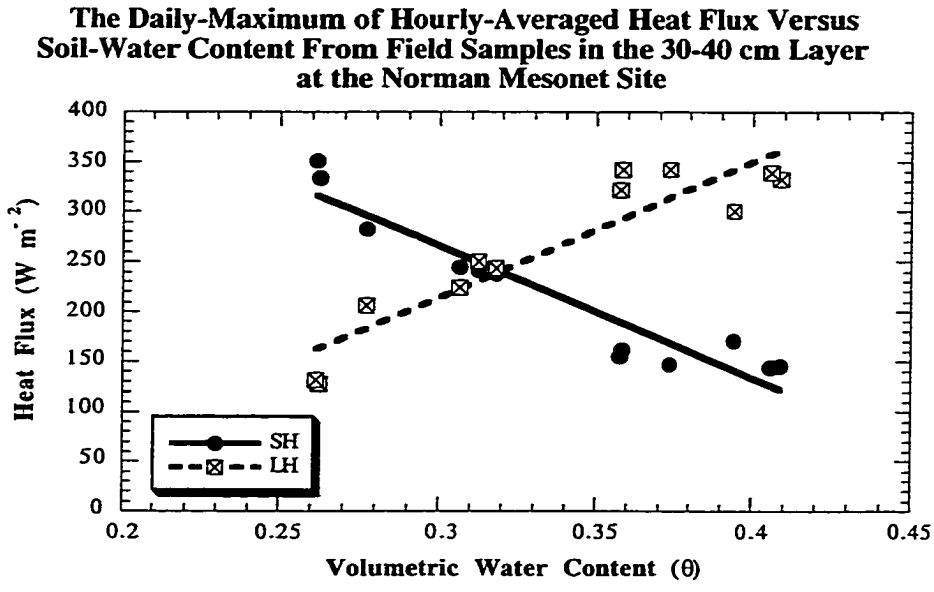

Figure 5.3a. The daily-maximum of hourly-averaged values of sensible and latent heat flux versus soil water content estimated from field samples in the 30-40 cm layer at the Norman Mesonet Site.

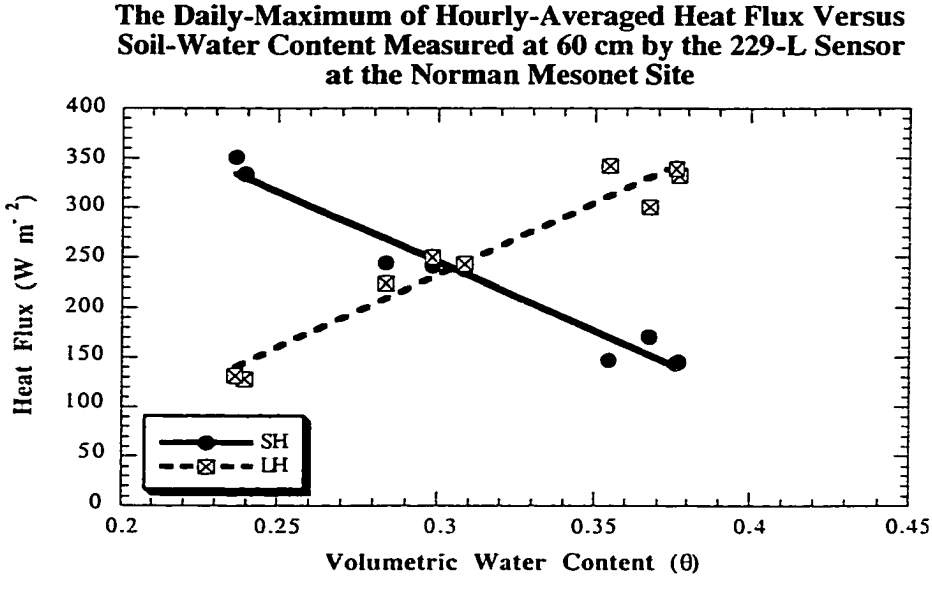

Figure 5.3b. The daily-maximum of hourly-averaged values of sensible and latent heat flux versus soil water content measured at 60 cm by using the 229-L sensor at the Norman Mesonet.

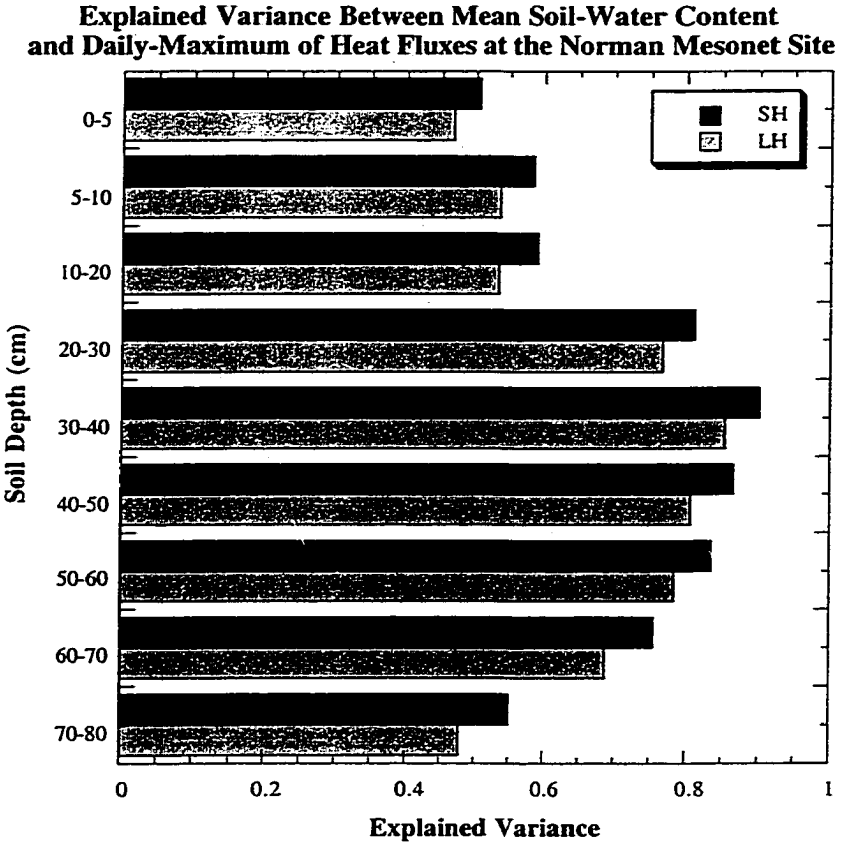

Figure 5.4. Explained variance stratified by soil depth between mean soil water content estimated from field samples and the daily-maximum of heat fluxes at the Norman Mesonet site.

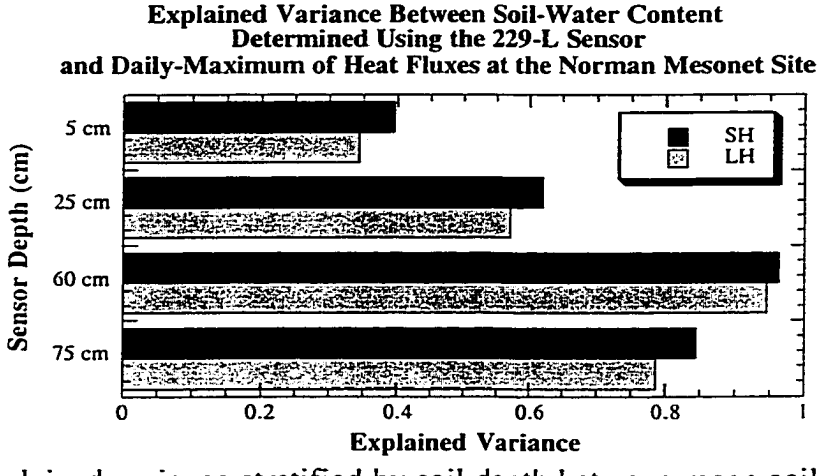

Figure 5.5. Explained variance stratified by soil depth between mean soil water content estimated from the 229-L sensor and the daily-maximum of heat fluxes at the Norman Mesonet site.

where Cl represents the degree of closure of the surface energy balance (%).

Closure, plotted versus estimates of soil water determined from field samples at depths of 0-5 and 30-40 cm (Fig. 5.6), reveals the relationship is nonlinear with significant scatter when soil water from the 0-5 cm layer is used. However, a linear trend becomes obvious when closure is compared with soil water from the 30-40 cm layer. Similar results are noted in Figure 5.7. In this case, closure is plotted versus soil water content derived using the 229-L sensor at depths of 5 and 60 cm. Thus, closure of the surface energy balance was linearly related to soil water in the root-zone but nonlinearly related to soil water in surface layer.

This discovery is further emphasized by the results presented in Figures 5.8 and 5.9. As with latent and sensible heat flux, the linear correlation between closure and soil water increases dramatically within the root-zone before decreasing at soil depths deeper than 60 cm. Furthermore, the results are similar regardless of whether soil water was determined from fields samples estimated using the 229-L sensors.

It should be noted that linear relationships between soil water content and atmospheric properties were not limited to sensible and latent heat fluxes. Thermal parameters such as the daily-maximum air temperature at 1.5 meters (Figs. 5.10a-b) and mean potential temperature in the 925-850 mb layer at 0000 UTC also revealed strong linear relationships to soil water in the 20-60 cm depths (Figs. 5.11a-b). Surface moisture parameters such as mixing ratio at 1.5 meters (averaged between 1800 and 0000 UTC; Figs. 5.12a-b) and mean mixing ratio in the 925-850 mb layer at 0000 UTC (Figs. 5.13a-b) revealed a great degree of scatter when compared with soil moisture from field samples or 229-L sensors. Linear relationships were noted at shallower soil depths (10-30 cm). PBL depth at 0000 UTC also was linearly related to soil water content in the 20-30 cm layer (Figs. 5.14a-b). The positive correlation between PBL depth and soil water was stronger than atmospheric moisture parameters but was weaker than the atmospheric thermal parameters. Linear relationships were not observed between soil moisture in the 0-10 cm layer and any other atmospheric parameter. In fact, the relationship between soil moisture in the 0-10 cm layer and all atmospheric parameters was highly nonlinear. Table 5.1

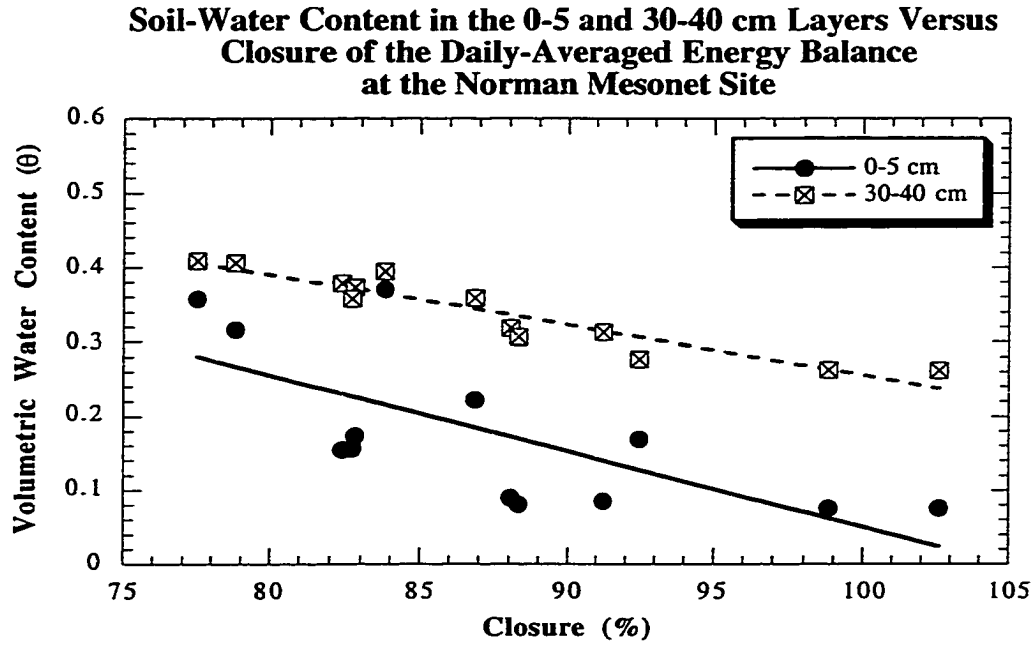

Figure 5.6. Soil water content estimated from field samples in the 0-5 and 30-40 cm layers versus closure of the daily-averaged energy balance at the Norman Mesonet Site.

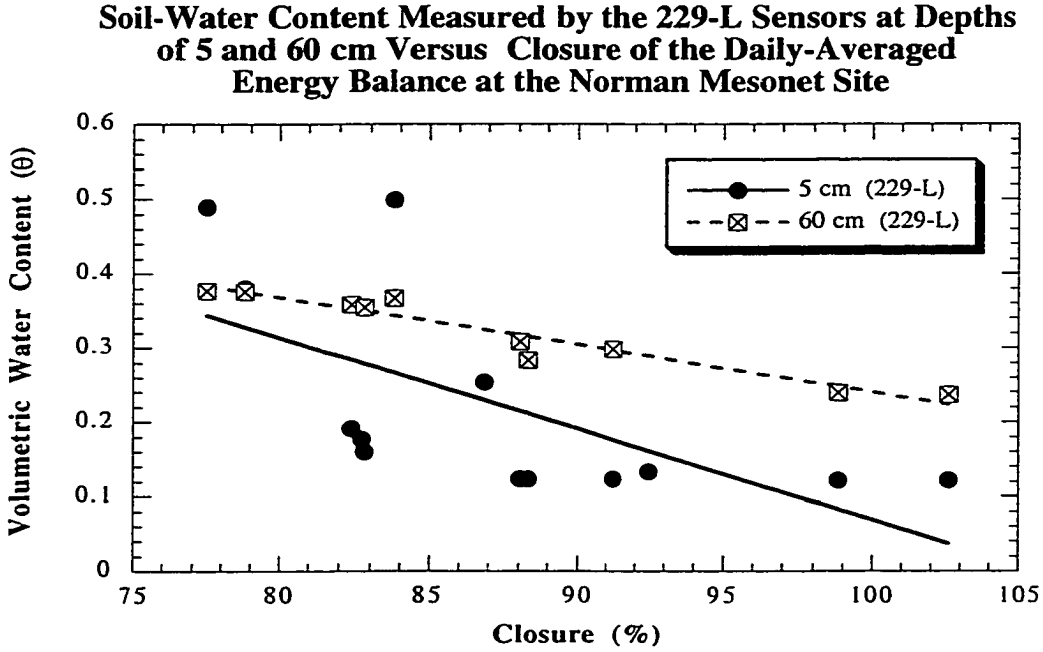

Figure 5.7. Soil water content measured using the 229-L sensors at depths of 5 and 60 cm versus closure of the daily-averaged energy balance at the Norman Mesonet Site.

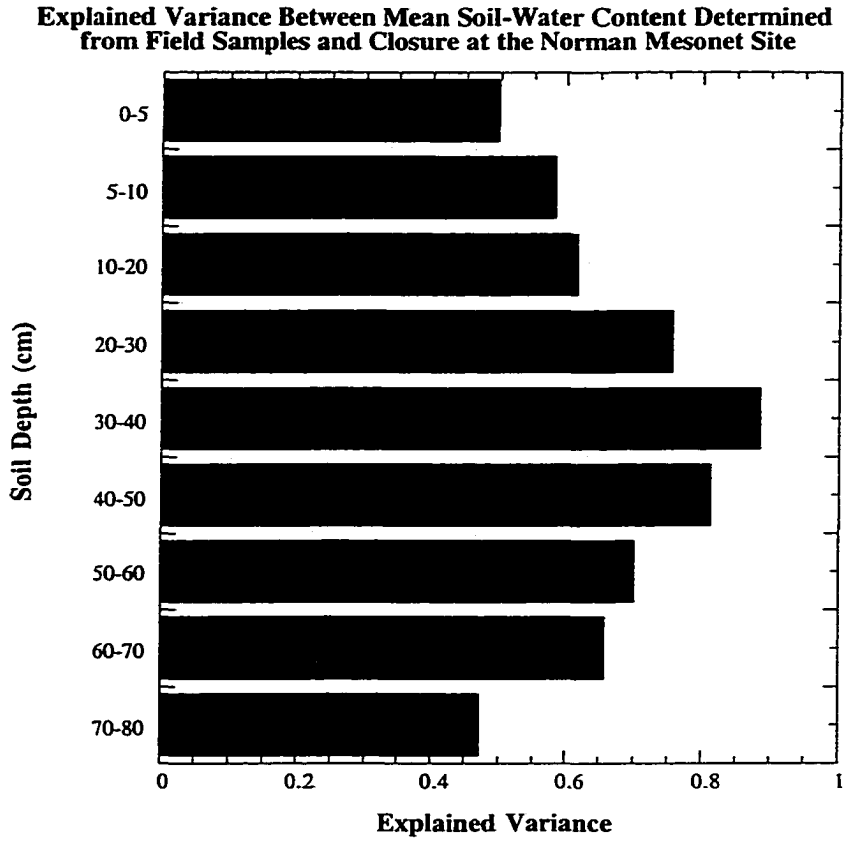

Figure 5.8. Explained variance between mean soil water content estimated from field samples and closure of the daily-averaged surface energy balance at the Norman Mesonet site.

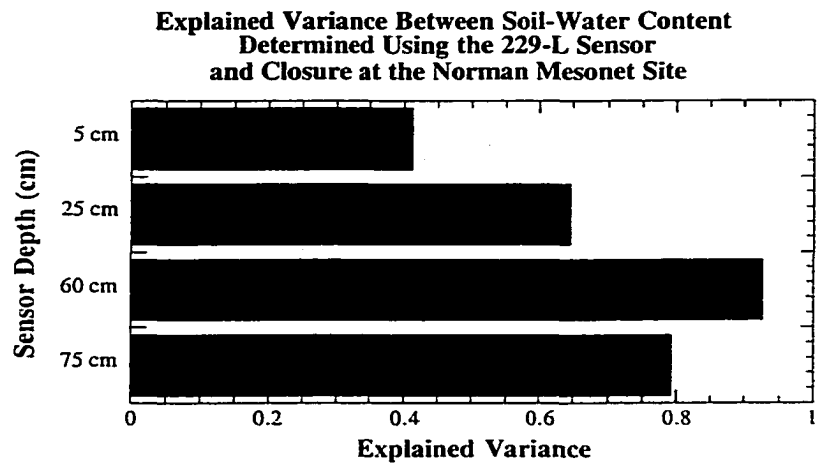

Figure 5.9. Explained variance between mean soil water content estimated using the 229-L sensor and closure of the daily-averaged surface energy balance at the Norman Mesonet site.

summarizes the linear correlation between soil water and atmospheric parameters at the Norman Mesonet site.

5.2. Discussion

The mechanism by which soil water at depths well below the surface influences and modulates atmospheric processes is transpiration through the vegetated canopy. In turn, transpiration impacts the partitioning of latent and sensible heat flux near the surface (Rabin et al. 1990; Chang and Wetzel 1991; Collins and Avissar 1994; and Beljaars et al. 1996). Results from the current study are consistent with previous investigations. Most important, the current results reveal that the relationship between *root-zone soil water* and most atmospheric parameters is linear at the Norman site.

Vegetation at the Norman site ranged between 15-30 cm in height during the study period and consisted primarily of short grasses. Although the tap root of grasses may extend several meters below the soil surface, grasses have fibrous and branched root systems; the greatest biomass is found within the first meter below ground (Salisbury and Ross 1992). Furthermore, soil characteristics play a pivotal role in determining the density of root structures (Klepper 1987). For example, if the topsoil is relatively thin and situated on top of clay or rock, rooting structures are inhibited from drawing water from deep layer soil. This latter situation occurs at the Norman site. Soil in the upper 30 cm is a mixture of silt and sand particles; it is classified as silt loam. Below 30 cm, the clay fraction of the soil increases greatly, and the soil is classified as a clay loam. A visual inspection of many soil cores at depths below 60 cm failed to reveal much root biomass. The visual observations also indicated that the greatest density of roots at NORM existed in the soil layer spanning 0-60 cm.

Another issue in this study concerned sensors that measure latent and sensible heat fluxes which are mounted 4.5 m above the land surface. The flux measurements appear to represent flux conditions upstream of the site on the order of tens of meters. Yet, atmospheric observations at NORM were strongly correlated with soil moisture observations collected at the site; the soil moisture clearly represented a smaller scale. This apparent complication is unraveled by examining the spatial and temporal variability of soil

water at the site. The greatest variability in soil water content (as measured via field samples) occurred in the 0-5 cm layer. However, as soil depth increased, the spatial and temporal variability of soil water decreased substantially (determined using the COV analysis in Chapter 3). Furthermore, soil cores collected at the site also revealed that variability in soil texture (which strongly influences soil water content) also decreased with depth. Thus, soil moisture observations collected at depths below 20 cm likely were more representative of the surrounding area (including those regions upstream from the site) than were surface-based values of soil water content.

The results of this study are important for several reasons. First, two independent soil moisture data sets revealed virtually the same linear relationships between variability in soil water content in the 20-60 cm depths and variability of atmospheric properties. The two soil moisture datasets also consistently demonstrated that atmospheric parameters measured at or near the Norman Mesonet site were nonlinearly related to the near-surface soil water content. Minor variations in these discoveries, derived from different soil moisture datasets, were thought to result from the fact that field samples of soil water content are integrated measurements while the 229-L sensors are point-scale measurements.

In addition, measurements of sensible and latent heat flux (determined using the eddy correlation method) were verified using the profile method to estimate sensible heat flux, and calculating latent heat flux as a residual. Though profile measurements are generally not as accurate as heat flux values determined using the eddy correlation technique, a linear relationship existed between soil moisture and either set of flux data. Thus, it appears possible to investigate linear/nonlinear relationships between soil moisture and atmospheric processes using instruments installed at standard OASIS sites (80 locations across Oklahoma). The standard sites provide estimates of sensible heat flux using the profile method and calculate latent heat flux as a residual.

Another key result of this study concerns the relationship between closure of the surface energy balance and root-zone soil moisture. Brotzge (2000) noted that one explanation for the consistent underestimate of closure of the energy balance was the inability to measure latent heat flux as accurately as the other parameters in the energy balance equation (net radiation, sensible and ground heat flux). He concluded that

vegetation, rather than soil moisture, likely contributed to large errors in the measurement of latent heat flux, and thus to closure. The findings of this study support those conclusions. Figures 5.6-9 clearly show a strong linear relationship between closure and soil water in the root-zone. However, the relationship between soil moisture near the surface and closure of the surface energy balanced was weak and nonlinear. Thus, it appeared that at the Norman site, soil moisture in the root-zone had a much greater controlling influence on closure of the surface energy balance than did the near-surface soil moisture. This influence on the latent heat flux effect can only be accomplished through the influence of vegetation and evapotranspiration.

Because the impact of soil moisture upon the atmosphere extends to the synoptic and climate scales, this study provides insight into the complex issue of partitioning available energy at the earth's surface. Furthermore, determining when and where linear relationships exist between land and atmospheric properties could lead to better parameterizations and, thereby, to significant improvements in numerical models which couple the land surface to the atmosphere.

Finally, this study notes some of the limitations of using soil water near the surface to mirror atmospheric parameters. Nonlinear processes are much more difficult to simulate than are linear ones. Thus, this study suggests that it is more advantageous to numerical weather prediction to have accurate, representative observations of soil moisture at deeper depths rather than from shallower depths. Because, techniques which remotely sense soil moisture do not extend below a depth of 5 cm, soil moisture at deeper depths must be obtained via in situ measurements or through accurate simulations of soil moisture conditions.

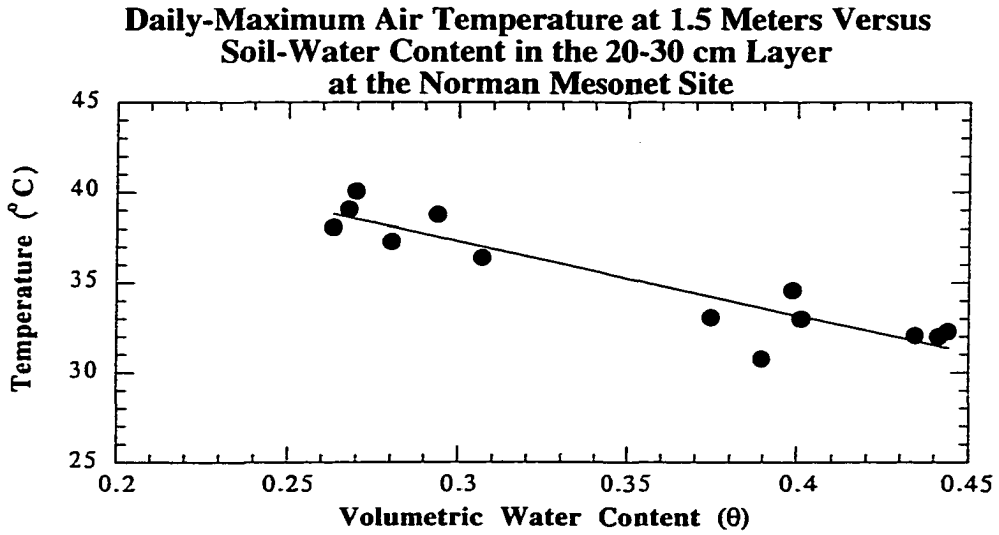

Figure 5.10a. The daily-maximum of hourly-averaged air temperature at 1.5 m versus soil water content estimated from field samples in the 20-30 cm depth at the Norman Mesonet Site.

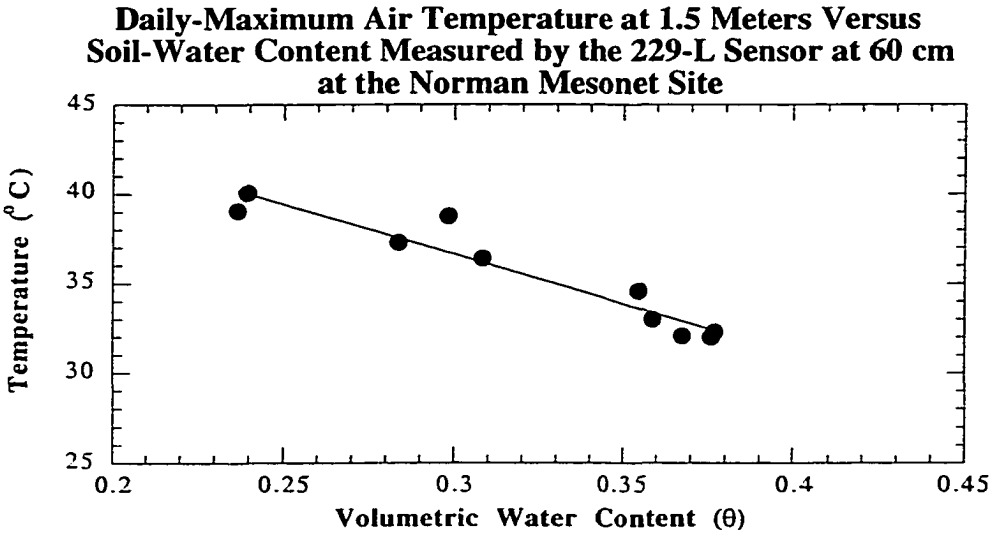

Figure 5.10b. The daily-maximum of hourly-averaged air temperature at 1.5 m versus soil water content measured by the 229-L at 60 cm sensor at the Norman Mesonet Site.

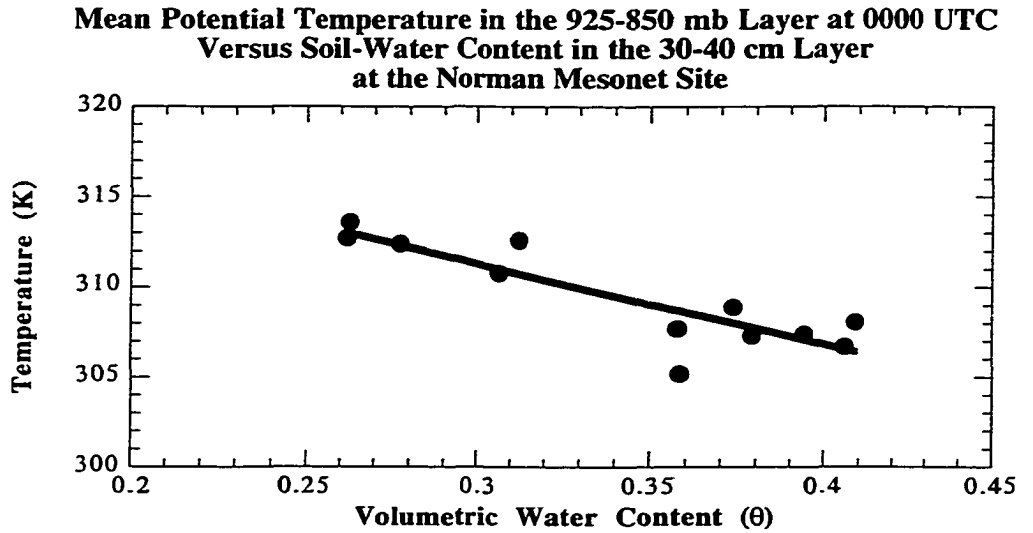

Figure 5.11a. The mean potential temperature in the 925-850 mb layer (0000 UTC) versus soil water content estimated from field samples in the 30-40 cm layer at the Norman Mesonet Site.

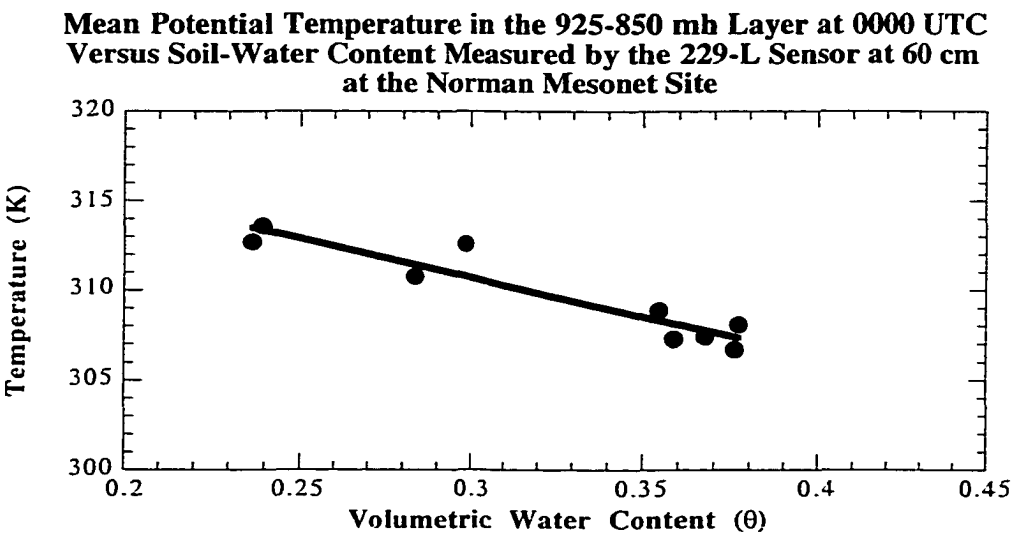

Figure 5.11b. The mean potential temperature in the 925-850 mb layer (0000 UTC) versus soil water content measured by the 229-L at 60 cm sensor at the Norman Mesonet Site.

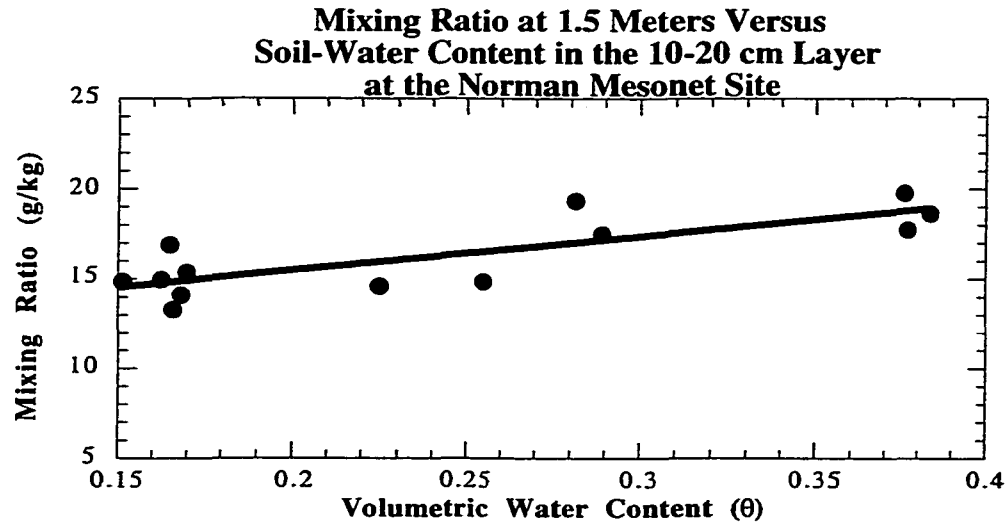

Figure 5.12a. Mixing ratio at 1.5 m (averaged between 1800-0000 UTC) versus soil water content estimated from field samples in the 10-20 cm layer at the Norman Mesonet Site.

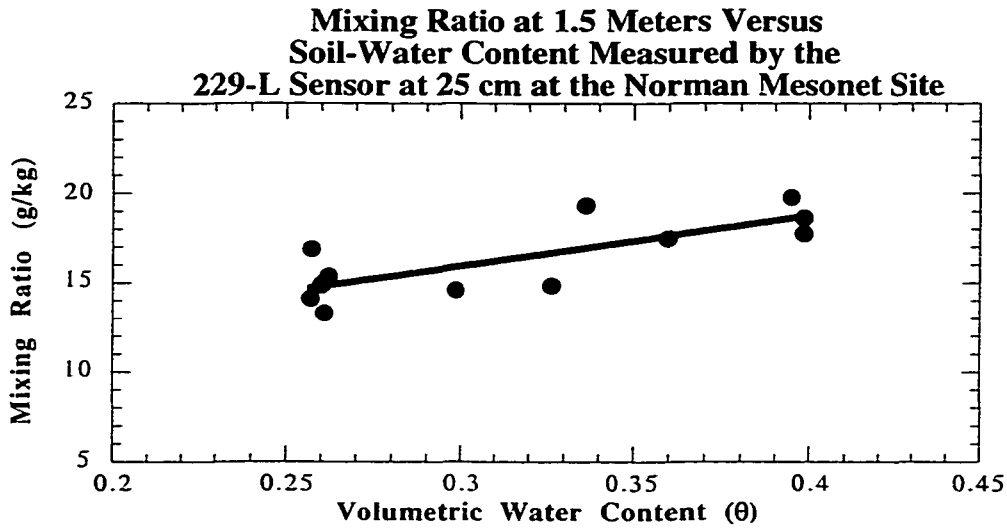

Figure 5.12b. Mixing ratio at 1.5 m (averaged between 1800-0000 UTC) versus soil water content measured by the 229-L at 25 cm sensor at the Norman Mesonet Site.

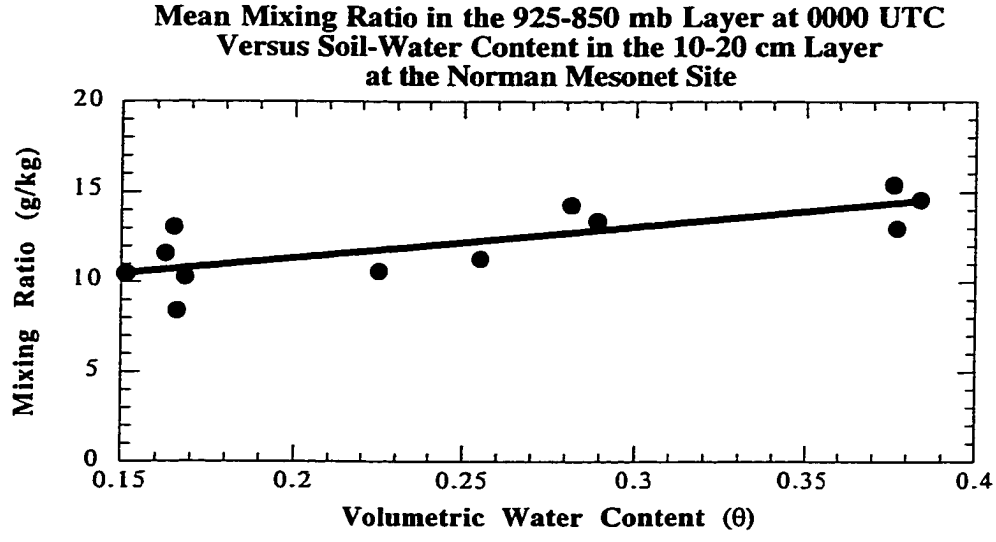

Figure 5.13a. The mean mixing ratio in the 925-850 mb layer (0000 UTC) versus soil water content estimated from field samples in the 10-20 cm layer at the Norman Mesonet Site.

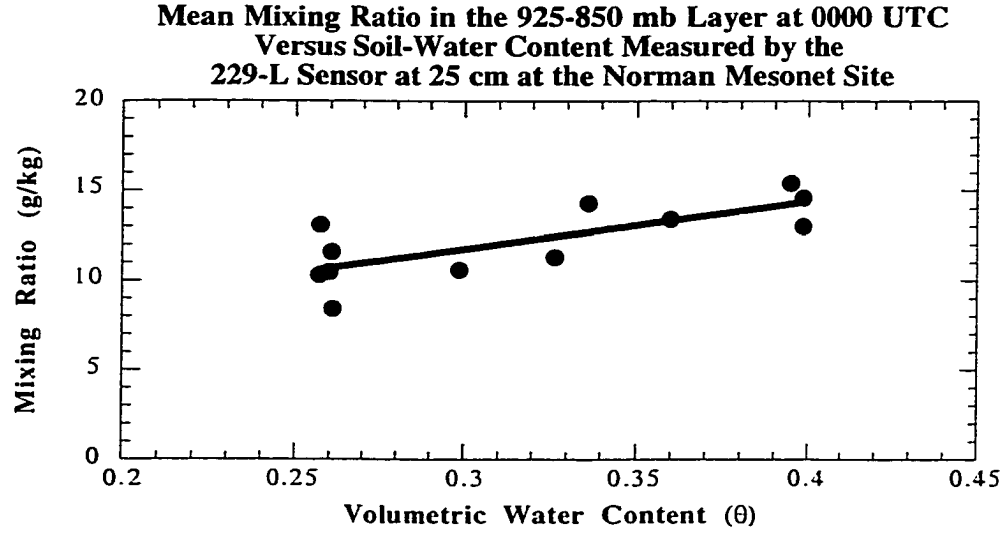

Figure 5.13b. The mean mixing ratio in the 925-850 mb layer (0000 UTC) versus soil water content measured by the 229-L at 25 cm sensor at the Norman Mesonet Site.

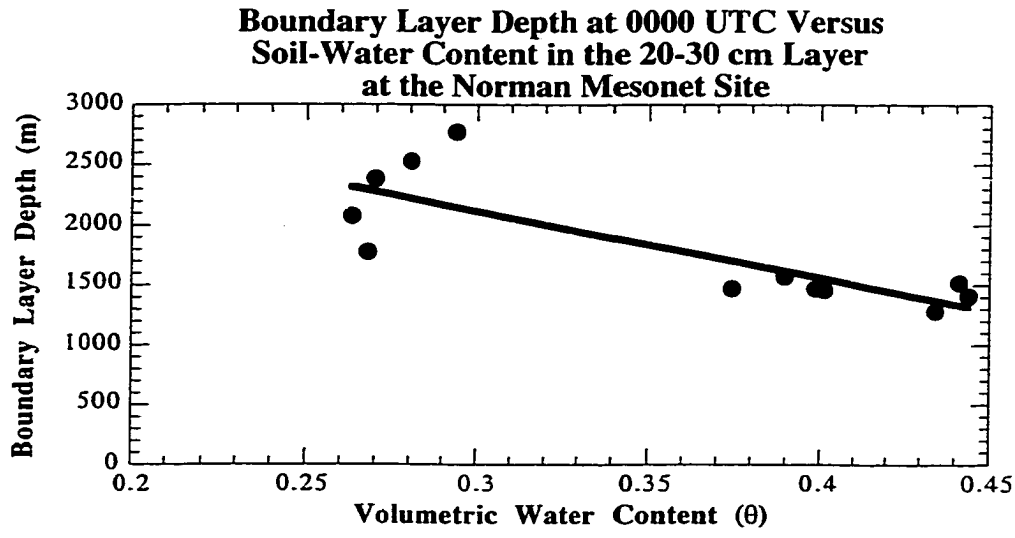

Figure 5.14a. Boundary layer depth at 0000 UTC versus soil water content estimated from field samples in the 20-30 cm layer at the Norman Mesonet Site.

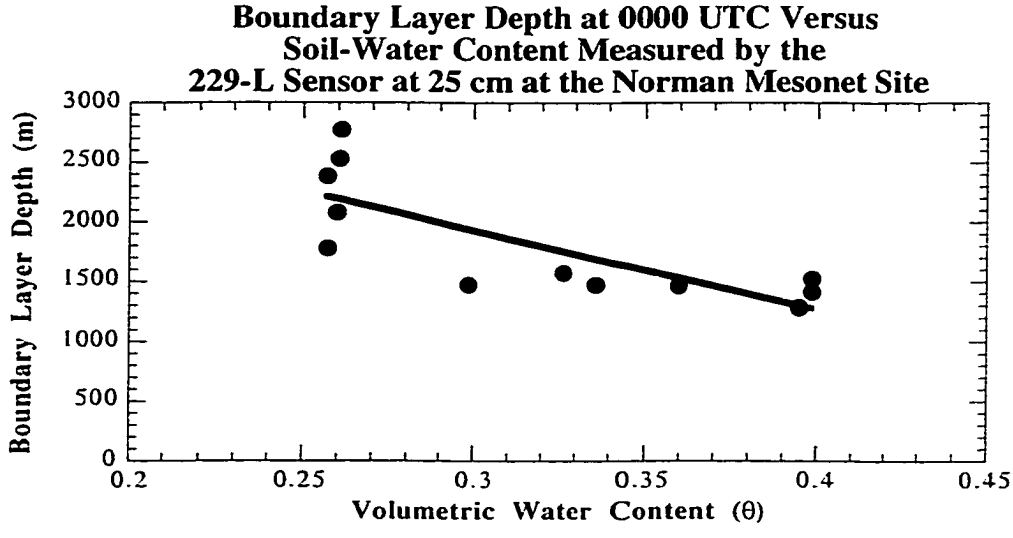

Figure 5.14b. Boundary layer depth at 0000 UTC versus soil water content measured by the 229-L at 25 cm sensor at the Norman Mesonet Site.

Soil Moisture	Sensible Heat Flux (EC)	Latent Heat Flux (EC)	Sensible Heat Flux (Profile)	Daily Maximum Air Temperature (1.5 m)	Mixing Ratio (1.5 m)	Potential Temperature (925-850 mb)	Mixing Ratio (925-850 mb)	Boundary Layer Depth	Energy Balance Closure
0-5 cm	0.505	0.468	0.545	0.608	0.469	0.473	0.432	0.498	0.497
5-10 cm	0.585	0.536	0.616	0.690	0.534	0.568	0.496	0.560	0.583
10-20 cm	0.591	0.533	0.64	0.679	0.629	0.579	0.578	0.593	0.616
20-30 cm	0.812	0.767	0.816	0.854	0.507	0.780	0.451	0.659	0.756
30-40 cm	0.902	0.854	0.846	0.833	0.438	0.759	0.373	0.522	0.885
40-50 cm	0.866	0.807	0.733	0.766	0.314	0.728	0.276	0.356	0.812
50-60 cm	0.836	0.784	0.686	0.749	0.204	0.737	0.187	0.340	0.701
60-70 cm	0.756	0.688	0.573	0.690	0.234	0.662	0.223	0.308	0.658
70-80 cm	0.552	0.479	0.500	0.628	0.464	0.589	0.453	0.469	0.471
229-L at 5 cm	0.397	0.344	0.389	0.517	0.452	0.384	0.449	0.400	0.412
229-L at 25 cm	0.621	0.571	0.702	0.722	0.614	0.634	0.567	0.613	0.645
229-L at 60 cm	0.963	0.947	0.935	0.917	0.505	0.884	0.376	0.484	0.927
229-L at 75 cm	0.845	0.787	0.721	0.882	0.569	0.864	0.484	0.468	0.792

Table 5.1. Linear correlation between soil moisture and atmospheric parameters at the Norman Mesonet site.

Chapter 6

Sensitivity Analysis of Ground Heat Flux Estimates

Soil heat flux is estimated using two HFT3.1 heat flux plates manufactured by Radiation & Energy Balance Systems, Inc. (REBS). The soil heat storage term in the energy balance equation is estimated using two REBS platinum resistance temperature detectors (PRTDs); the latter estimate includes soil moisture measured at 5 cm (using the Campbell Scientific Inc. model 229-L) and knowledge of soil properties at each site.

6.1 Theory

A combination method is used to measure the total ground heat flux (Tanner 1960). The combination approach includes separate estimates for the ground heat flux and storage terms:

$$GH = -\lambda\left(\frac{dT}{dz}\right) - C\rho z_2\left(\frac{d\overline{T}}{dt}\right) \tag{6.1}$$

where λ is the thermal conductivity, dT is the temperature difference across the plate thickness, C is the soil heat capacity, ρ is air density, z_2 is the depth of the soil layer, and $d\overline{T}/dt$ is the temporal rate of change in the soil temperature between 0 and 5 cm (Fritschen and Gay 1979).

The first term in Equation (6.1; i.e., $\lambda[dT/dz]$) is estimated using soil heat flux plates. The temperature difference measured across the depth of the plate is equivalent to the vertical movement of heat within the soil. Standard OASIS sites (80 of the 90 OASIS sites; Brotzge et al. 1999) have two REBS HFT 3.1 heat flux plates installed at a depth of 5 cm. Thus, the arithmetic mean of measurements from the two sensors is used. Each plate has an individual calibration which is applied during post-processing.

The second term in Equation (6.1; i.e., $C\rho z_2[d\overline{T}/dt]$) is the storage term and includes measurements of the soil temperature within the top 5 cm of soil. Like the heat

flux plates, two REBS PRTDs are installed at each site and the mean value of observations from the two sensors is used. Each PRTD has an individual calibration which is applied during post-processing. The ground heat flux storage term also is a function of the soil heat capacity (C), defined by de Vries (1975) as:

$$C = X_s C_s + X_w C_w + X_a C_a \tag{6.2}$$

where the X is the volume fractions of solid components (s), water components (w), and air (a) components of the soil. The contribution to C from the individual components is the product of the density of the component and the specific heat of the component (i.e., $C_w = \rho_w c_w$). Equation (6.2) can be expanded to:

$$C = X_m C_m + X_o C_o + X_w C_w + X_a C_a \tag{6.3}$$

where the solid phase of soil includes mineral (m) and organic (o) components (Fritschen and Gay 1979). Because the density of air is approximately 1/1000 that of water, Equation (6.3) can be simplified to:

$$C = X_m C_m + X_o C_o + X_w C_w \tag{6.4}$$

Substituting the appropriate values for C_m, C_o, and C_w, and noting that X_w is equivalent to the volumetric water content (θ) of the soil, Equation (6.4) becomes:

$$C = X_m * 1.93 + X_o * 2.51 + \theta * 4.19 \tag{6.5}$$

The heat capacity of minerals and organic material are set at 0.528 MJ $(m^3K)^{-1}$ and 0.030 MJ $(m^3K)^{-1}$ respectively. The final form of C thus becomes:

$$C = 1.094 + \theta * 4.19 \tag{6.6}$$

where C varies with varying values of volumetric water content. The volumetric water content of the soil is calculated using soil moisture sensors installed at the site (the 229-L).

6.2 Results

6.2.1 Soil Moisture Conditions

Because estimates of ground heat flux only utilize the soil water to a depth of 5 cm, field samples of soil water content collected between 0 - 5 cm are compared in this study (Fig. 6.1) with observations from the 229-L sensor at 5 cm. Some discrepancies exist in the analysis; however, the overall trends and magnitudes compare quite well. For example, comparison of the daily-averaged 229-L measurement and the arithmetic mean of field samples yield an R^2 of 0.85 and an RMSE value of 0.051. In addition, some discrepancies result from the comparison of a point-scale measurement (229-L) with an integrated measurement (field samples).

Note the difference between the mean sample value and the 229-L value which occurred on 7 June 1999 (Fig. 6.1). On 6 June 1999, a rainfall event produced 5.3 mm of precipitation at the Norman site (Fig. 6.2). During soil excavation the following day, the wetting front was still clearly visible in the soil. However, the penetration of water did not extend beyond 4 cm at any of the 12 sample locations. Thus, the 229-L sensor buried at 5 cm was not impacted by the precipitation event (shown in Fig. 6.1) which *did* influence the field samples.

The analysis in Figure 6.1 also reveals the variability of soil water content at the Norman Mesonet site during the study period. In general, the sample range (the difference between field sample maximum (FSMax) and field sample minimum (FSMin)) and standard deviation increased following precipitation events and decreased to a minimum during the study period (Fig. 3.4a).

Unfortunately, it was not feasible to collect field samples of soil water content on each day of the study period. Furthermore, atmospheric conditions were not always ideal with respect to surface energy balance conditions on days when samples were collected. Thus, to provide accurate and consistent estimates of field conditions of soil water content throughout the study period (i.e., maximum, minimum, and mean), the observed sample values were interpolated for those dates on which samples were not collected (Fig. 6.3). As

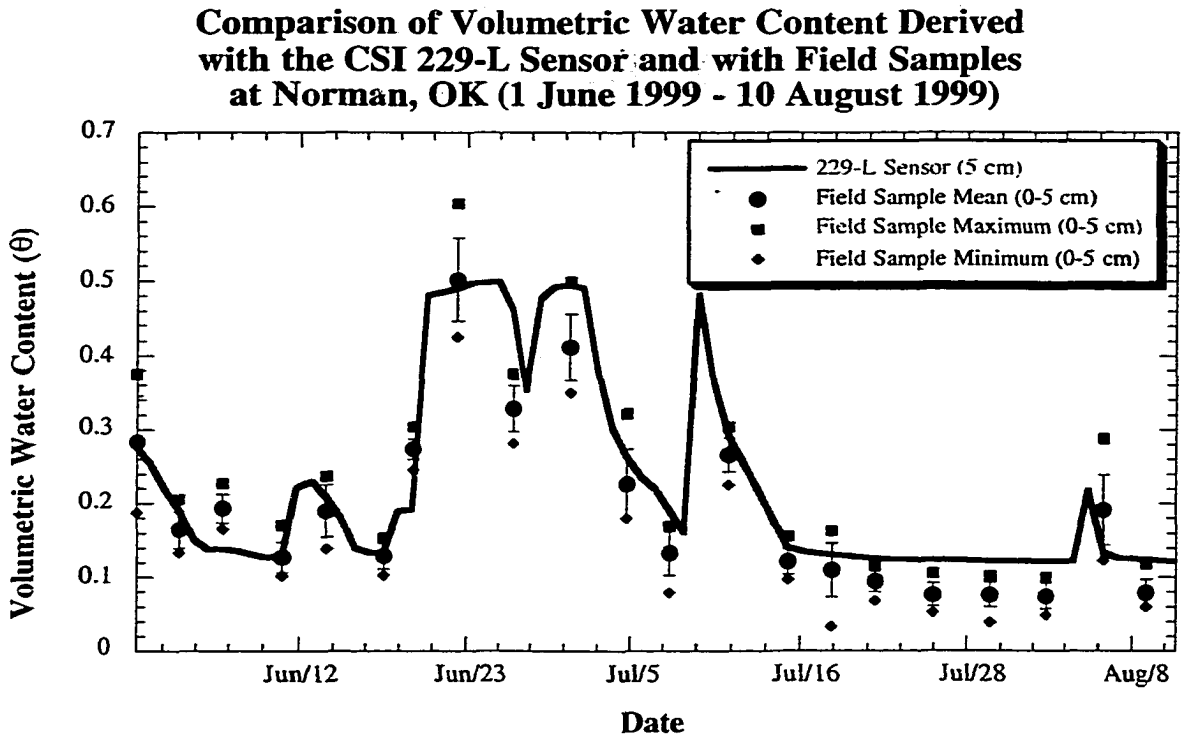

Figure 6.1. Soil water content derived from the 229-L sensor and determined from field samples at the Norman Mesonet site (1 June - 10 August 1999).

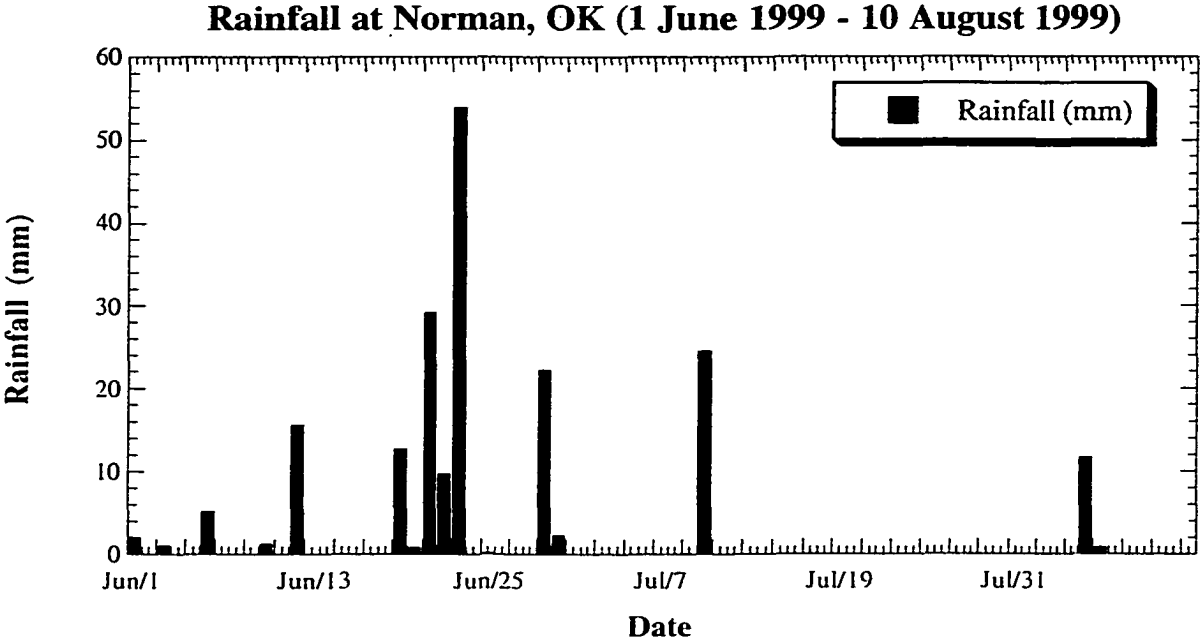

Figure 6.2. Rainfall at the Norman Mesonet site (1 June - 10 August 1999).

in Section 5.1, a linear interpolation was performed between observations. Next, a 3-day running mean was applied to the time series of data points to eliminate high frequency artifacts resulting from the linear interpolation. The results of the final interpolated time series provide an envelope which likely bound the range of soil water conditions within the study plot at NORM for any given date during the study period (Fig. 6.3).

6.2.2 Ground Heat Flux Estimates Using Field Samples of Soil Moisture and the Original Calibration of the 229-L Sensor

Many sensors involved in the ground heat flux estimate (e.g., REBS HFT3.1) are averaged spatially (data from 2 ground heat flux plates are averaged) and temporally (5 minute time average). However, soil moisture observations (229-L) provide a point measurement in space (one sensor) and time (1 observation every 30 minutes). Thus, the storage term represented by Equation 6.6 is susceptible to spatial and temporal variability of water content; the variability is not detected by a single 229-L sensor.

The results in Section 6.2.1 provide an envelope around possible values of soil water content at the Norman site which can be used to test the sensitivity of ground heat flux to the variability of soil water content. To begin this sensitivity testing, ground heat flux was computed using the standard operating procedure to estimate soil water content (229-L; original calibration). Next, the same procedure was utilized but field samples (either observed or interpolated) were used instead of the 229-L estimates. Thus, each daily analysis consisted of ground heat flux computed using water content values from the 229-L and from field sample values (maximum, mean, and minimum).

An example from 2 July 1999 consisted of wet soil conditions (Fig. 6.1) with a range between maximum and minimum sample values of 0.1452 cm^3/cm^3. The hourly-averaged ground heat flux at NORM is shown for the daylight hours on 2 July (Fig. 6.4a). Note that near sunrise (approximately 1200 GMT), the ground heat flux for values of soil moisture was identical. However, as incoming solar and net radiation increased throughout the day, significant discrepancies were noted between the four estimates; the maximum difference of 23.97 W m^{-2} (Table 6.2) occurred when maximum ground heat flux was observed. In addition, the ground heat flux produced using the 229-L sensor is greater than

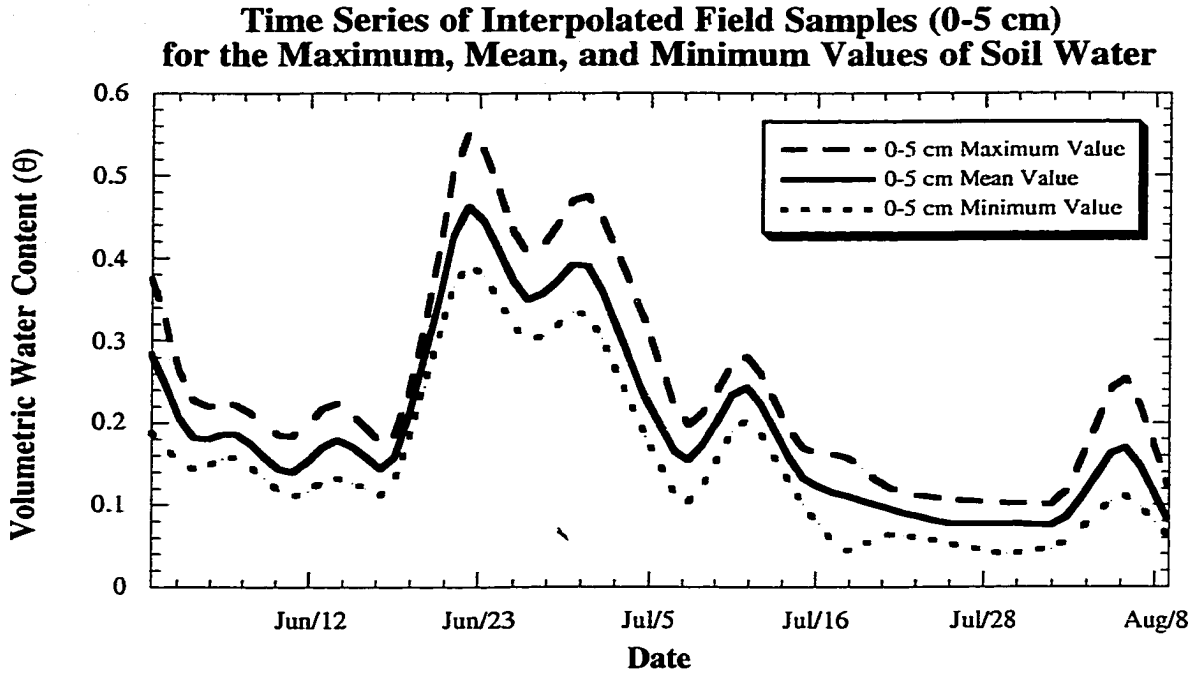

Figure 6.3. Interpolated time series of maximum, mean, and minimum values of soil water content at the Norman Mesonet site (1 June - 10 August 1999).

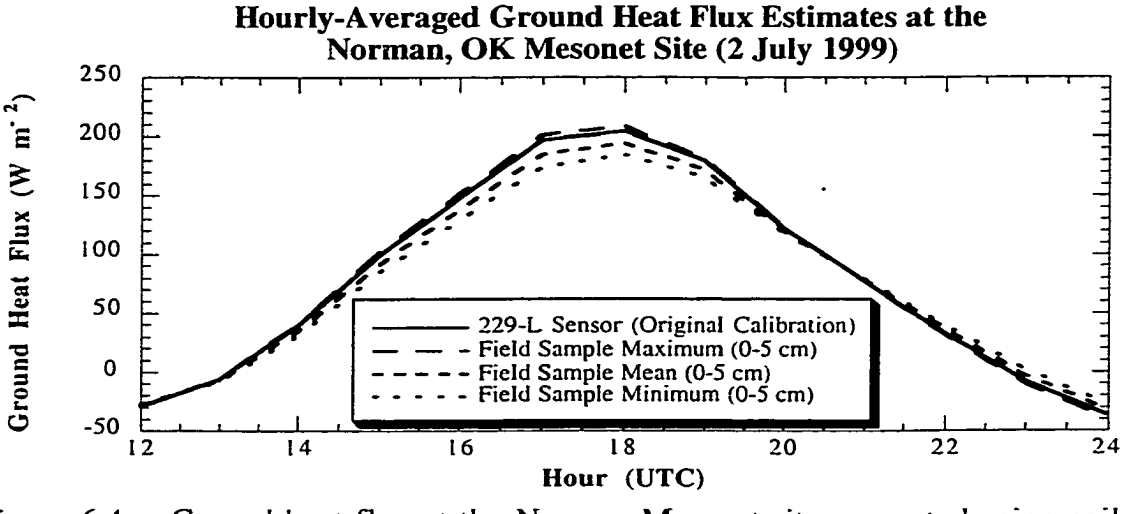

Figure 6.4a. Ground heat flux at the Norman Mesonet site computed using soil water content derived from the 229-L sensor (5 cm) as well as maximum, mean, and minimum values of soil water content (0-5 cm) determined from field samples on 2 July 1999.

the estimate produced using the mean of the field samples (FSMean). However, because the estimate produced by the 229-L lies within the bounds of ground heat flux based upon the FSMax and FSMin values, a representative measurement resulted.

A second example on 13 July 1999 (Fig. 6.4b) was based upon moderate values of soil water content. The range of values differed by only 0.073 cm^3/cm^3. While the ground heat flux estimates were identical at sunrise, they diverged to a maximum difference of 14.2 W m^{-2}. Throughout the day, the 229-L sensor produced an estimate of ground heat flux which were equal to other estimates created by using three field values of soil moisture.

A final example in Figure 6.4c revealed the sensitivity of ground heat flux to the variability of soil water content during extremely dry soil conditions. In this case, water content only varied across a range of 0.062 cm^3/cm^3. Note that the magnitude of ground heat flux estimates on 30 July were less than in the examples from 2 and 13 July; these smaller values resulted from limited water content on 30 July. Second, the maximum difference in ground heat flux of 14.5 W m^{-2} was the difference between the estimate using the 229-L sensor and the ground heat flux based upon the minimum water content from a field sample. This small difference resulted from the fact that the 229-L installed at 5 cm had a slight wet bias compared with field samples on 30 July (Fig. 6.1). In this case, the ground heat flux computed using standard procedures was not considered representative of the ground heat flux determined using field samples of water content primarily because 229-L values were beyond the range of maximum and minimum values of ground heat flux.

Estimates of ground heat flux were computed for the 10 remaining days of the study period. Peak values of ground heat flux are shown in Table 6.1 while the daylight behavior of ground heat flux are demonstrated in Appendix C. In general, ground heat flux decreased as the soil transitioned from wet to dry. As the variability (or envelope) of soil moisture conditions at NORM decreased with extended drying, the range of flux values at the time of peak flux decreased as well. However, the range of ground heat flux using field samples of soil water always exceeded 11 W m^{-2} at the time of maximum ground heat flux.

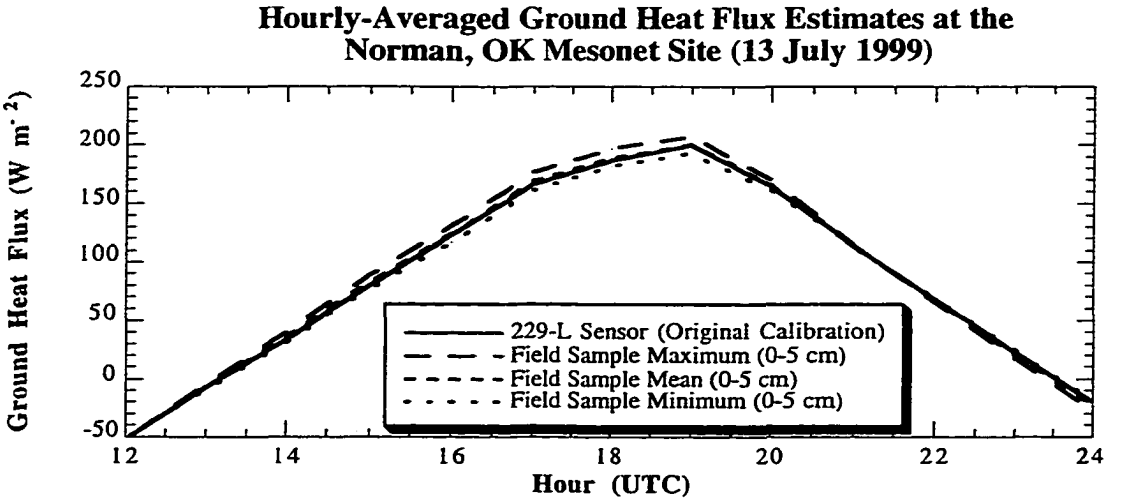

Figure 6.4b. Ground heat flux at the Norman Mesonet site computed using soil water content derived from the 229-L sensor (5 cm) as well as maximum, mean, and minimum values of soil water content (0-5 cm) determined from field samples on 13 July 1999.

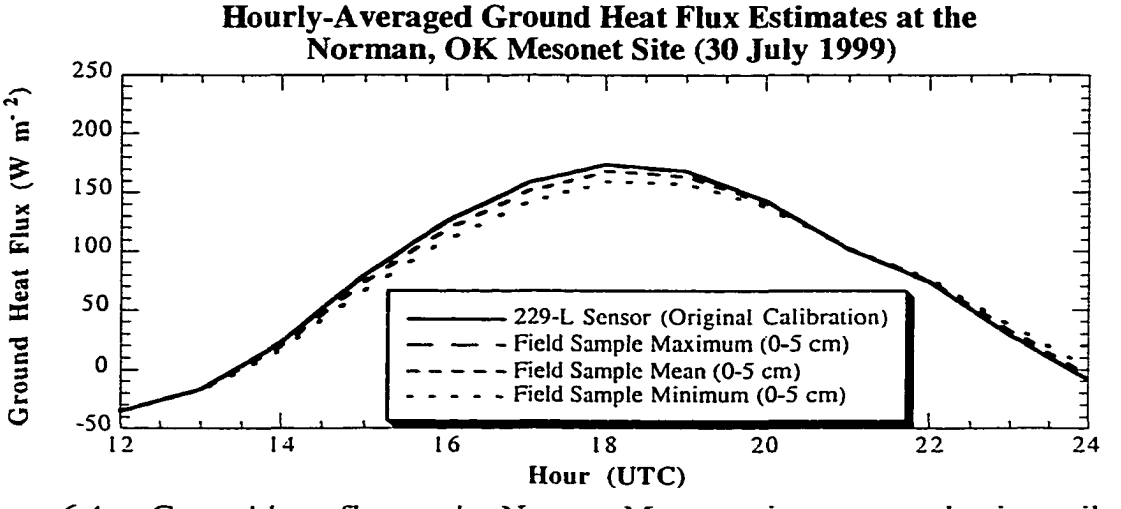

Figure 6.4c. Ground heat flux at the Norman Mesonet site computed using soil water content derived from the 229-L sensor (5 cm) as well as maximum, mean, and minimum values of soil water content (0-5 cm) determined from field samples on 30 July 1999.

6.2.3 Soil Moisture Sensor Calibration and Ground Heat Flux Estimates

Another source of variability in ground heat flux estimates resulted from soil moisture sensors which were not properly calibrated. Chapter 4 discussed improvements which were made to the calibration of soil moisture senors across the Mesonet. Though the improved calibration procedures applied *across the Mesonet* were determined to be more accurate than the original calibration, the 229-L sensor at the 5 cm depth at NORM produced estimates which were worse than those produced using the original calibration for that sensor. The following text documents how ground heat flux estimates at NORM were affected by improper sensor calibration.

Consider the case shown in Figure 6.5a in which ground heat flux was estimated on 2 July using the original and improved calibration procedures for the 229-L sensor. The estimates of ground heat flux using the two sets of calibration coefficients produced little discernible difference during the day as well as at the time of the daily-maximum value of ground heat flux (3.6 W m^{-2}; Table 6.1). Similar results occurred on days with very moist soil conditions (e.g., 26 June and 3 July; Table 6.1). Thus, when soil conditions were sufficiently moist, calibration errors in the soil moisture sensors contributed little to the overall error in the ground heat flux estimate.

However, as soil conditions dried, the difference between the calibration methods of the soil moisture became more evident in estimates of the ground heat flux as shown by the values of ground heat flux on 13 July and 30 July (Figs. 6.5b-c). Furthermore, note that at the time of the daily-maximum of ground heat flux, the differences in soil moisture calibration created flux differences that approached or exceed 20 W m^{-2} (Table 6.1).

The largest deviation in ground heat flux occurred on 8 July and resulted from different techniques for soil moisture calibration (Table 6.1). In days preceding 8 July, soil in the 0-5 cm layer at NORM underwent a drying trend. Values of daily-averaged soil water content derived using the 229-L sensor were 0.191 and 0.295 cm^3/cm^3 for the original and improved calibration methods, respectively; field samples collected on 8 July in the 0-5 cm layer yielded a mean soil water content value of 0.133 cm^3/cm^3. Thus, the large range of

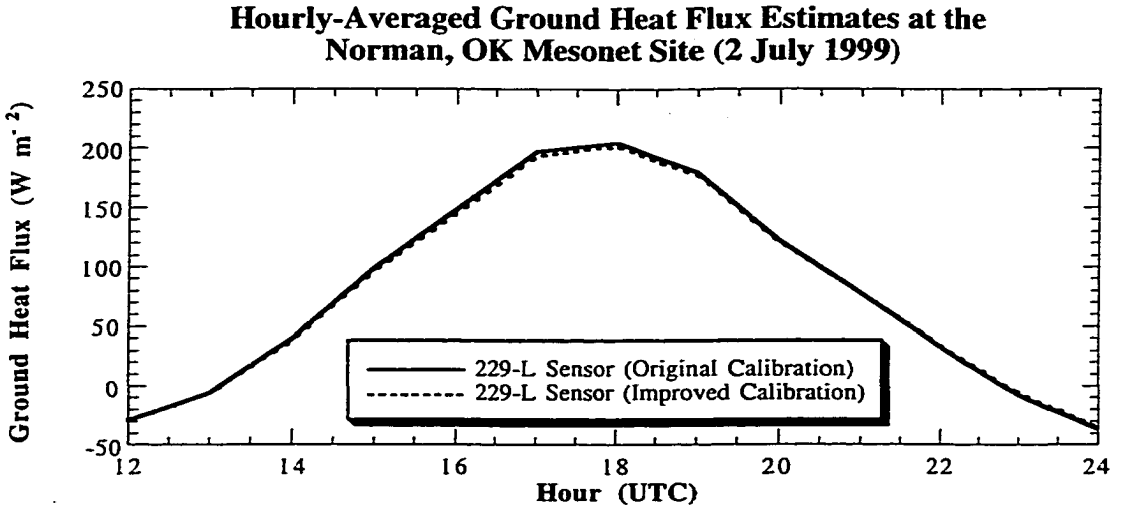

Figure 6.5a. Ground heat flux at the Norman Mesonet site computed using soil water content derived from data obtained via a 229-L sensor at 5 cm (original calibration and improved calibration) on 2 July 1999.

				Range of			Range of	
				Ground			Ground	
				Heat Flux	Ground	Ground	Heat Flux	*Maximum*
				Determined	Heat Flux	Heat Flux	Determined	Range of
	Ground	Ground	Ground	Using	229-L	229-L	Using	Ground
	Heat Flux	Heat Flux	Heat Flux	*Field*	*Original*	*Improved*	*229-L*	Heat Flux
Date	*FSMax*	*FSMean*	*FSMin*	*Samples*	*Calibration*	*Calibration*	*Sensors*	Values
6/26/99	225.83	213.81	203.13	22.71	220.41	216.14	4.27	22.71
7/2/99	208.46	193.83	184.49	23.97	204.48	200.90	3.59	23.97
7/3/99	215.06	197.83	187.77	27.29	201.53	206.63	5.09	27.29
7/8/99	225.59	214.07	200.33	25.26	214.87	247.32	32.45	46.98
7/9/99	210.83	201.58	189.83	21.00	192.83	221.47	28.64	31.64
7/13/99	207.15	200.03	192.95	14.20	199.57	218.46	18.89	25.51
7/15/99	164.63	158.54	153.60	11.03	159.27	180.11	20.83	26.50
7/23/99	178.33	172.81	166.63	11.70	176.15	190.06	13.91	23.44
7/24/99	184.91	178.75	172.54	12.37	183.36	197.76	14.41	25.22
7/25/99	169.77	163.93	158.60	11.18	168.92	181.10	12.18	22.51
7/30/99	173.96	167.82	159.45	14.51	174.20	182.94	8.74	23.49
7/31/99	194.17	188.80	181.77	12.40	194.76	206.84	12.08	25.07
8/7/99	174.25	159.63	149.47	24.78	155.60	174.94	19.33	25.47

Table 6.1. Maximum daily ground heat flux computed using soil water content values derived from the 229-L sensor and using the maximum, mean, and minimum values from field samples.

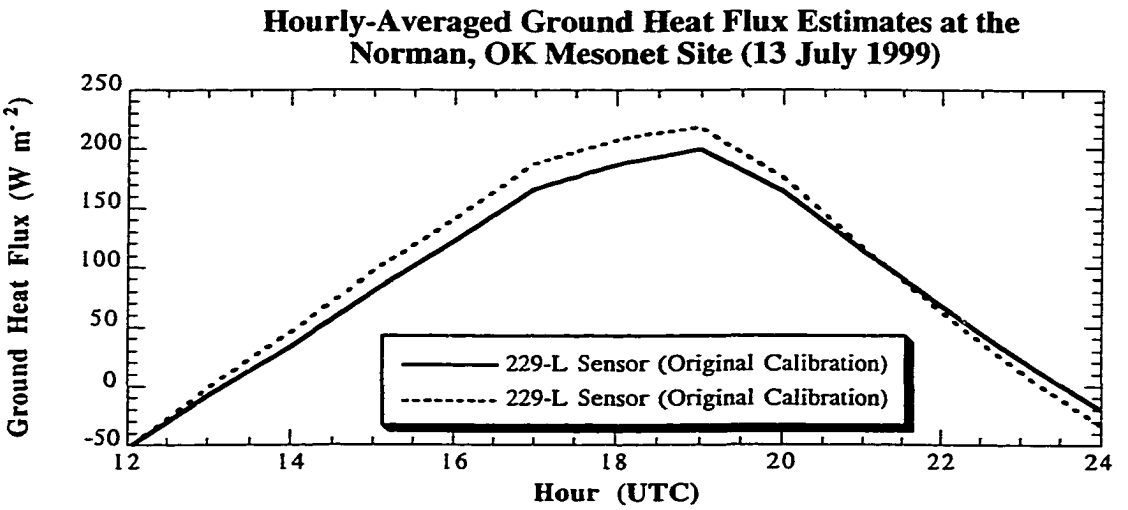

Figure 6.5b. Ground heat flux at the Norman Mesonet site computed using soil water content derived from data obtained via a 229-L sensor at 5 cm (original calibration and improved calibration) on 13 July 1999.

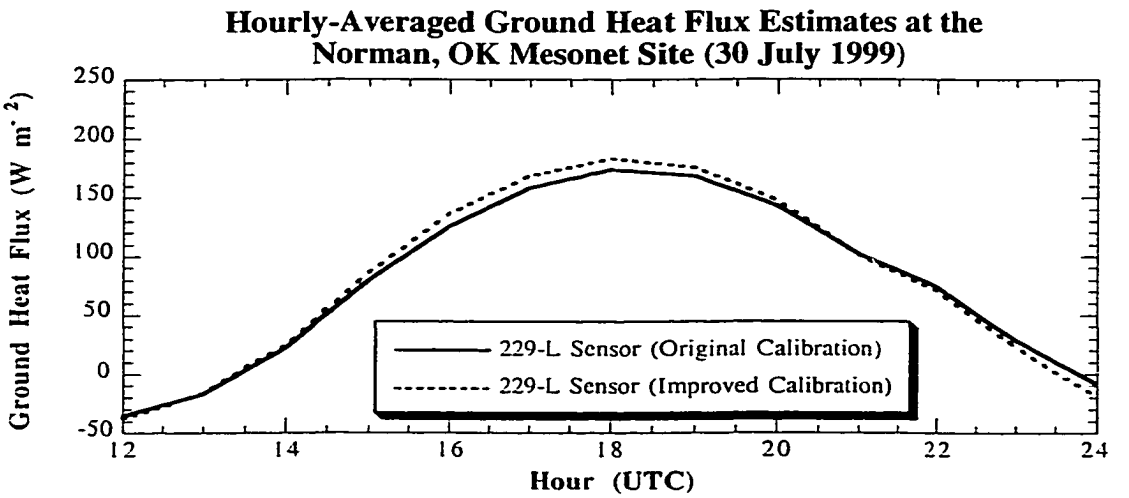

Figure 6.5c. Ground heat flux at the Norman Mesonet site computed using soil water content derived from data obtained via a 229-L sensor at 5 cm (original calibration and improved calibration) on 30 July 1999.

water content values produced by the soil moisture sensors created a dissimilarity of 32.5 W m^{-2} at the time of the daily-maximum ground heat flux. Similar results were noted for 9 July and 15 July which also experienced a drying trend. Thus, the results indicate that ground heat flux estimates were more susceptible to errors associated with soil moisture calibration during drydown periods than during extended wet or dry periods.

6.2.4 Closure of the Surface Energy Balance

The results have shown that significant spatial and temporal variability existed in surface soil water content at and near the Norman Mesonet site during the study period. This variability, when incorporated into computations of ground heat flux at the site, created significant differences between heat flux estimates at or near the time of the maximum daily ground heat flux. This section investigates the effect of variability in soil moisture conditions and the associated sensitivity of the ground heat flux estimate on the closure of the surface energy balance.

Closure was calculated using mean daylight values (i.e., an average of all observations during daylight; Table 6.2) and using those associated with peak values of ground heat flux (Table 6.3) determined from hourly averages. In the case of mean daylight closure, slight differences were noted. In general, during daylight, the variability of ground heat flux created by varying soil moisture conditions produced closure differences of ~5% or less for those days studied. However, when closure is determined at the time of maximum ground heat flux, the range of closure differences increased to and even exceed 7%. Thus, closure of the surface energy balance equation is much more sensitive to variability in ground heat flux during times when the ground heat flux is at its maximum value versus other times of the day. In addition, when closure is analyzed on time scales greater than a few hours, the sensitivity of closure to variation in ground heat flux is greatly reduced.

				Energy	Energy	
				Balance	Balance	
	Energy	Energy	Energy	Closure	Closure	
	Balance	Balance	Balance	229-L	229-L	
	Closure	Closure	Closure	*Original*	*Improved*	
	FSMax	*FSMean*	*FSMin*	*Calibration*	*Calibration*	*Range*
Date	%	%	%	%	%	%
6/26/99	85.52	83.82	82.58	85.06	84.69	2.94
7/2/99	78.73	77.49	76.77	78.44	78.59	1.96
7/3/99	80.14	78.80	78.08	79.37	80.04	2.06
7/8/99	83.32	82.37	81.30	82.41	85.27	3.97
7/9/99	83.52	82.82	82.00	82.25	84.87	2.87
7/13/99	88.09	86.87	85.74	86.45	90.46	4.72
7/15/99	83.36	82.73	82.24	82.68	85.49	3.25
7/23/99	88.59	88.05	87.47	88.38	90.22	2.75
7/24/99	91.91	91.24	90.60	91.73	93.72	3.12
7/25/99	89.00	88.32	87.75	88.89	90.65	2.91
7/30/99	99.60	98.84	97.89	99.62	100.78	2.89
7/31/99	103.52	102.62	101.56	103.56	104.76	3.20
8/1/99	95.08	92.46	90.90	91.62	95.46	4.56

Table 6.2. Mean daylight closure of the surface energy balance computed using soil water content from the 229-L sensor and using the maximum, mean, and minimum values from field samples.

				Energy	Energy	
				Balance	Balance	
	Energy	Energy	Energy	Closure	Closure	
	Balance	Balance	Balance	229-L	229-L	
	Closure	Closure	Closure	*Original*	*Improved*	
	FSMax	*FSMean*	*FSMin*	*Calibration*	*Calibration*	*Range*
Date	%	%	%	%	%	%
6/26/99	85.10	82.70	80.68	84.00	83.16	4.42
7/2/99	85.88	83.51	82.06	85.22	84.64	3.82
7/3/99	97.43	94.01	92.13	94.73	95.73	5.30
7/8/99	NA	NA	NA	NA	NA	NA
7/9/99	89.55	87.81	85.7	86.23	91.63	5.94
7/13/99	89.53	88.31	87.14	88.24	91.53	4.40
7/15/99	82.56	81.67	80.96	81.77	84.92	3.96
7/23/99	96.04	94.92	93.70	95.59	98.49	4.79
7/24/99	97.39	96.09	94.81	97.06	100.23	5.42
7/25/99	91.50	90.38	89.38	91.34	93.76	4.38
7/30/99	106.27	104.65	102.51	106.34	108.74	6.24
7/31/99	116.63	115.11	113.18	116.80	120.39	7.21
8/7/99	113.01	109.31	106.88	108.33	113.18	6.30

Table 6.3. Closure of the surface energy balance at the time of maximum ground heat flux computed using soil water content values from the 229-L sensor and using the maximum, mean, and minimum values from field samples.

6.3 Discussion

The results of Section 6.2 highlight the importance of determining the variability of soil moisture measurements at any particular location, assessing the representativeness of the measurements collected, and determining how those observations affect other computations. First, significant variability existed in soil moisture conditions between the surface and 5 cm at NORM during the study period. Even though variability in water content (determined from field samples) decreased to a minimum value during extended dry periods, the standard deviation of field samples following precipitation events ranged between approximately 0.012 to 0.062. In addition, slight variations in soil texture led to different thresholds for wetting and drying. Thus, as the soil dried during a 20 day period, the range of soil water content values was ~0.05 cm^3/cm^3 in the field samples collected. Differences in soil texture created differences in residual water content. Furthermore, the variability of soil water content was impacted by the variability in soil texture especially after heavy precipitation. The differences in particle size distribution yielded variable values of saturated water content which, in turn, influenced surface infiltration.

Even though soil water content varied significantly at NORM (especially considering the study plot was 20 m X 20 m), the 229-L sensor using the original calibration performed well. Thus, with a few minor deviations, the 5 cm water content estimates from the properly calibrated 229-L were considered representative of the site during the study period. The majority of unrepresentative values occurred during extremely dry periods. It is likely that the discrepancies resulted from comparing an integrated sample versus a point measurement. Even so, the majority of cases revealed that ground heat flux derived using the 229-L data lay within the bounds defined by the range of field sample estimates.

Ground heat flux differences exceeded 30 W m^{-2} when the sensor was not properly calibrated at the time of the daily-maximum. The natural variability in soil water content combined with sensor biases in measuring soil moisture is a critical combination. The final column of Table 6.1 illustrates the range of daily-maximum ground heat flux estimates when sensor calibration and sample variability are considered. For each day in the study,

the range of ground heat flux at the time of the daily-maximum always exceeded 22 W m^{-2} and was a maximum on 8 July at ~47 W m^{-2}. This provides a quantitative estimate of the uncertainty in the ground heat flux due to difficulties in measuring soil moisture at the Norman site.

The range of ground heat flux at the time of the daily-maximum did influence closure of the surface energy balance. At this time of day, closure ranged between 3.8 and 7.3 percent. However, the range of closure dropped to less than 4% when closure was averaged across all daylight hours. Thus, even though variability in soil moisture influenced closure at the time of the daily-maximum of ground heat flux, the impact on closure of the surface energy budget was small.

However, the variability of ground heat flux obtained from varying soil water at NORM should not be dismissed. The range of ground heat flux estimates always exceed 11 W m^{-2}, even under the best of circumstances. Unfortunately, this variability cannot be captured using a single point measurement of soil water, such as those obtained using the 229-L sensors at Mesonet sites. The highly variable nature of soil water and its impact on ground heat flux is significant. Because latent heat flux can be calculated as a residual of other measured components of the surface energy balance, bias in the ground heat flux due to sensor errors or spatial variability *will be transferred into the estimate of latent heat flux.*

Chapter 7

The Sensitivity of Planetary Boundary Layer Simulations to Local Soil Moisture Conditions

The local variability in soil moisture can lead to variability in the measurement of ground heat flux. Because latent heat flux can be estimated as a residual in the surface energy budget, biases within the estimate of ground heat flux are incorporated into the estimate of latent heat flux.

The analyses in Chapter 6 offer intriguing insights into the value of *point-scale* measurements of soil moisture in the study of surface energy budgets. However, additional analyses of feedback processes within the land-atmosphere continuum are required to fully assess the value of point-scale measurements of soil moisture to the simulation of the PBL. Thus, the one-dimensional, coupled atmospheric-plant-soil model from Oregon State University is used to assess the influence of the spatial and temporal variability of soil moisture. In addition, the impact on simulations of the PBL from calibration and operational errors in estimates of soil moisture is assessed. Finally, the sensitivity of model simulations to the variability of other parameters in land surface portion of the model (e.g., albedo, canopy resistance, and the shading factor) is evaluated.

7.1 Model Description

The one-dimensional PBL model from Oregon State University is a coupled atmospheric-plant-soil model developed by Troen and Mahrt (1986). Their boundary layer model is coupled to a two-layer soil model (Mahrt and Pan 1994) and a simple plant model (Pan and Mahrt 1987). In addition, the vegetation submodel has been modified to include the interactive effects of vegetation noted by Noilhan and Planton (1989) and Jacquemin and Noilhan (1990).

The decision to use the OSU model was based on three facts. First, the model is designed such that the comprehensive algebraic equations simulate processes within the land-atmosphere system; yet, this model is simple enough for high resolution diurnal

simulations that require limited computer resources. Second, the model is robust in terms of its simulation of atmospheric stability over a wide variety of global conditions. Finally, the PBL model used in this study is identical to the operational three-dimensional forecast models used by the National Weather Service (i.e., the Medium Range Forecast Model; MRF) and is similar to modified versions such as the NOAH scheme used in the ETA model.

The component critical to this study is the soil portion of the OSU 1-D model. In the OSU model, the soil portion is divided into two soil layers that represent surface layer (0-5 cm) and deep-layer (5-100 cm) processes. In addition, soil texture is specified throughout the 0-100 cm layer as a single texture composed of either sand, loamy sand, sandy loam, silt loam, loam, sandy clay loam, silty clay loam, clay loam, sandy clay, silty clay, or clay. In other words, a vertical stratification of soil texture is not permitted. Studies by Ek and Cuenca (1994) and Cuenca et al. (1996) noted that surface fluxes of heat and energy are sensitive to the parametrization of soil texture and soil water content respectively. Unfortunately, these studies did not use field observations of soil texture and soil moisture to determine the model sensitivity to this variability. Instead, the model was initialized with hypothetical values of soil water content and soil texture. Features in the PBL were compared for different perturbations in soil texture and water content. This current study seeks to determine the sensitivity of PBL simulations to *known* variabilities in soil water content and soil texture. The objective is to determine biases observed in the model's surface fluxes of heat and moisture and growth of the PBL.

7.2 Simulations Using Data From the Norman Mesonet Site

Numerous challenges exist in numerical simulations that use data at or near the Norman site. First, the measured variability in soil water content at the site must be converted to input data for the model. On days when field observations were not collected, interpolation of the field data was required. To represent the upper layer in the model, the field sample maximum (FSMax), the field sample mean (FSMean), and the field sample minimum (FSMin) of soil water content within the 0-5 cm layer were used (Fig. 6.3). Data from the 229-L sensor at 5 cm also were used to approximate soil water in the 0-5 cm

depth.

A similar approach was used to approximate the 5-100 cm layer in the OSU model. Unfortunately, field samples were only collected to a depth of 80 cm while 229-L sensors are buried only to a depth of 75 cm. Thus, it was necessary to estimate the deep-layer soil moisture conditions required by the model.

Because bulk density at the Norman Mesonet varied with depth, the volumetric water content was computed for discrete samples from each depth and location. Then, for each depth, FSMax, FSMean, and FSMin were computed on each sampling date. When field samples were collected, the maximum value of volumetric water content (FSMax) for the 5-80 cm layer was determined by averaging the individual FSMax values at depths between 5 and 80 cm (i.e., 5-10, 10-20, 20-30 cm, etc.). Similar analyses were conducted to determine the values of FSMean and FSMin for the 0-80 cm layer. Finally, values for FSMax, FSMean, and FSMin for the 5-80 cm layer were estimated on days when field observations were not collected. The results provide an envelope of soil water conditions that likely occurred within the study plot in the 5-80 cm layer on any day during the study period (Fig 7.1). The 5-100 cm model layer was initialized using an analysis of the 5-80 cm layer. In simulations when water content was estimated via the 229-L sensors, the 5-100 cm layer in the model was initialized with the mean volumetric water content based on point observations from 25, 60, and 75 cm.

A second challenge concerned the parametrization of the actual soil texture at the site because vertical stratification of soil texture is not permitted in the model. Yet, soil texture at the Norman site varied *both* vertically (Table 7.1) and horizontally. Because silt loam is the predominant soil texture in the 0-5 cm layer, the first simulations used a parametrization based on silt loam with a wilting point value of 0.10 cm3/cm^3 (Fetter 1988). In addition, clay loam was observed as the dominant soil texture below 5 cm. Thus, a second set of simulations were conducted using the texture parametrization of clay loam and a wilting point value of 0.21 cm^3/cm^3 (Fetter 1988).

The initialization of upper air features used the 1200 UTC sounding located 3.03 km southeast of the Norman Mesonet site. Surface atmospheric parameters were initialized

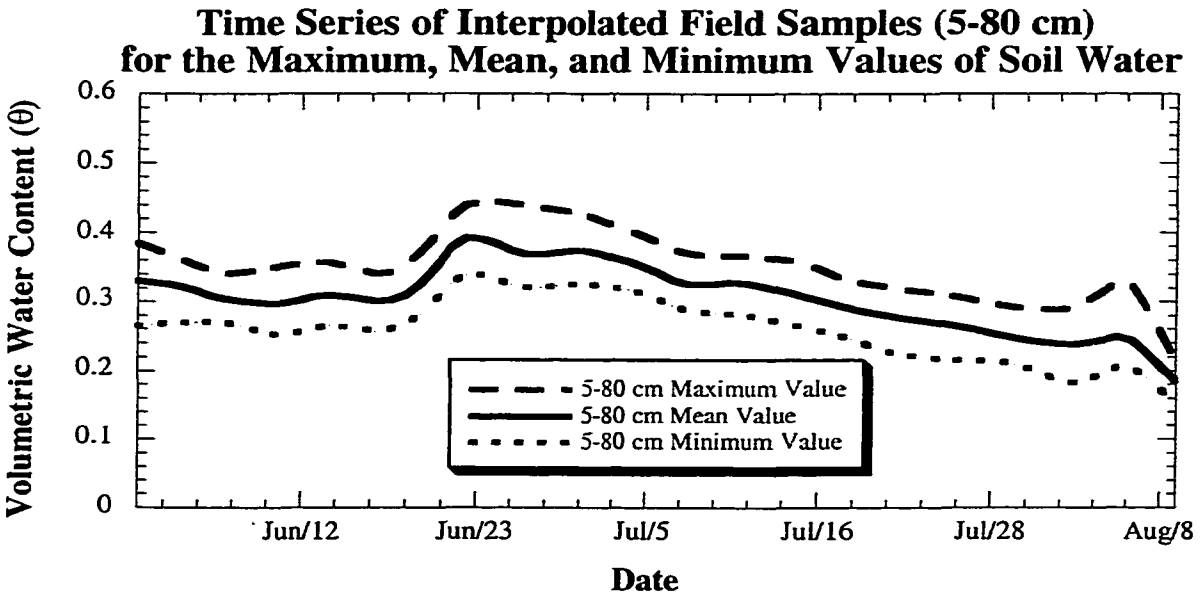

Figure 7.1. Interpolated time series of maximum, mean, and minimum values of soil water content in the 5-80 cm layer at the Norman Mesonet site (1 June - 10 August 1999).

Depth	Mean % Gravel	Mean % Sand	Mean % Silt	Mean % Clay	Soil Classification
0-5 cm	0.2	34.7	51.0	14.1	Silt Loam
5-10 cm	0.0	35.4	47.9	16.7	Loam
10-20 cm	0.2	30.9	43.6	25.3	Loam
20-30 cm	0.0	26.8	33.8	39.4	Clay Loam
30-40 cm	0.0	27.0	34.3	38.7	Clay Loam
40-50 cm	0.8	31.8	30.0	37.3	Clay Loam
50-60 cm	1.8	28.9	33.5	35.8	Clay Loam
60-70 cm	3.2	30.8	30.0	36.0	Clay Loam
70-80 cm	2.3	31.6	32.0	34.1	Clay Loam
5-80 cm	1.0	30.4	35.6	32.9	Clay Loam

Table 7.1. Vertical stratification of soil characteristics at the Norman Mesonet site.

using 1200 UTC observations from NORM.

Finally, knowledge of other parameters was required to test the model sensitivity to variable soil moisture conditions. Thus, the roughness lengths for momentum (z_o) and heat (z_{oh}) were set at 0.1 and 0.01 m respectively (Brotzge 2000); the albedo was fixed at 0.2 (Crawford 1998). In addition, the vegetation canopy was given a canopy resistance of -50 (Crawford 1998). The shade factor was set at 0.5 because vegetation at the site was 15-30 cm tall, yet exposed soil was visually noted at the site during the study.

7.3 Results

Model simulations were conducted for days with high solar insolation and weak shear in the lower troposphere. Each simulation was initialized at 1200 UTC (approximately sunrise) and integrated for 12 hours.

7.3.1 Soil Moisture Variability

To test the sensitivity of the model to variable soil moisture conditions, input files used soil water content determined from field samples (FSMax, FSMean, and FSMin) and from calibrated 229-L measurements (Table 7.2). Input files also were created to account for the two main soil textures: clay loam and silt loam.

To assess the sensitivity of the 1-D model to varying soil conditions, this portion of the study focused on the maximum value (i.e., the magnitude) of flux values, net radiation, and depth of the PBL. Representative values of soil water content observed at the Norman Mesonet site were used. Of particular interest is the range of values (e.g., sensible heat flux) produced by the model during varying soil moisture conditions. The magnitude and range of sensible heat flux, latent heat flux, ground heat flux, net radiation, and depth of the PBL for days with *ideal* atmospheric conditions is shown in Tables 7.3 through 7.12.

To highlight important soil moisture conditions which existed at the Norman site during the study, 5 cases-study days are presented in detail. The first case, 2 July, represents a day at the site when extremely moist soil existed throughout the depth of the soil profile. The second case, 15 July, occurred during a drying trend. Thus, soil conditions at the surface were in a stage of moderate soil wetness while soil in the 5-100 cm

	Maximum	Mean	Minimum	Maximum	Mean	Minimum	229-L	229-L
Date	0-5 cm	0-5	0-5	5-80	5-80	5-80	5 cm	25-75 cm
6/26/99	0.431	0.37	0.316	0.441	0.374	0.325	0.499	0.372
7/2/99	0.446	0.358	0.301	0.417	0.369	0.323	0.49	0.376
7/3/99	0.408	0.317	0.263	0.41	0.364	0.321	0.381	0.375
7/8/99	0.197	0.154	0.103	0.369	0.326	0.287	0.191	0.349
7/9/99	0.212	0.173	0.124	0.367	0.325	0.284	0.16	0.339
7/13/99	0.259	0.222	0.186	0.364	0.323	0.276	0.254	0.326
7/15/99	0.192	0.157	0.128	0.36	0.313	0.267	0.177	0.299
7/23/99	0.114	0.09	0.062	0.316	0.274	0.221	0.124	0.286
7/24/99	0.111	0.085	0.059	0.313	0.271	0.219	0.124	0.279
7/25/99	0.108	0.081	0.056	0.31	0.268	0.217	0.123	0.274
7/30/99	0.102	0.076	0.041	0.291	0.247	0.209	0.121	0.254
7/31/99	0.102	0.076	0.042	0.29	0.244	0.202	0.121	0.252
8/7/99	0.254	0.169	0.11	0.323	0.244	0.204	0.134	0.254

Table 7.2. Soil water content used to initialize the 0-5 and 5-100 cm layers of the OSU model.

layer was still quite moist. Very dry soil conditions at the surface overlying moderate soil moisture below is shown in the third case (23 July). A fourth case, 30 July, had extremely dry soil throughout the entire soil profile. The final case (7 August) focused on a day following a light precipitation event at the Norman site. On 7 August, soil moisture at the surface varied greatly, however, soil in the 5-100 layer remained quite dry. Even though the focus of this portion of the study involved 5 of the 13 study days, plots of sensible, latent, and ground heat flux as well as depth of the PBL are plotted for all study days in Appendix D.

Date	FSMax	FSMean	FSMin	229-L	Range
6/26/99	98.5	106	110.9	105.2	12.3
7/2/99	115.5	121	126.6	119.7	11.1
7/3/99	110.9	116	225.9	114.6	115
7/8/99	100.4	299.7	320.3	172.1	219.9
7/9/99	98.8	339.9	366.3	315.2	267.4
7/13/99	100.8	308.9	382.6	253.2	281.8
7/15/99	98.9	358.1	375.3	358.9	276.4
7/23/99	306.3	320	379.5	310.9	73.2
7/24/99	294	310.6	376.9	300.4	82.9
7/25/99	306.3	325.6	391.6	316.9	85.3
7/30/99	321.1	356.1	409.9	344.8	88.7
7/31/99	321.1	359.3	421.3	346.7	100.2
8/7/99	234.1	361.5	419.5	354.2	185.4

Table 7.3. Maximum value of the daily-averaged sensible heat flux computed by the OSU model. Soil water content values derived from the maximum, mean, and minimum field sample values as well as the 229-L sensor served as input to the model. The simulations used a clay loam parametrization for soil texture.

Date	FSMax	FSMean	FSMin	229-L	Range
6/26/99	99.9	103.3	106.9	103	7
7/2/99	115.9	118.8	122.1	112.6	9.5
7/3/99	110.7	113.5	116.4	112.6	5.8
7/8/99	95.8	101	139.5	98.1	43.7
7/9/99	95.8	99.3	132.1	98.2	36.3
7/13/99	97.4	100.3	104.9	100	7.5
7/15/99	99.5	103.1	268.4	103.9	168.8
7/23/99	97	243.4	315	98.5	218
7/24/99	99.4	235.8	302.5	128.7	203.1
7/25/99	76.1	272.4	314.6	182.9	238.4
7/30/99	119.1	315.4	327.5	288.6	208.5
7/31/99	118.9	318.7	328.2	292.7	209.3
8/7/99	85.7	260.4	332.2	282	246.4

Table 7.4. Maximum value of the daily-averaged sensible heat flux computed by the OSU model. Soil water content values derived from the maximum, mean, and minimum field sample values as well as the 229-L sensor served as input to the model. The simulations used a silt loam parametrization for soil texture.

Date	FSMax	FSMean	FSMin	229-L	Range
6/26/99	461	481	494.4	478.5	33.4
7/2/99	421.4	437	451.5	432.9	30.1
7/3/99	435.8	451	304.2	446.1	146.9
7/8/99	429.2	168.8	170	405	260.3
7/9/99	479.6	173.5	160.9	249.7	318.7
7/13/99	482.3	217.4	141.5	290.8	340.8
7/15/99	480.2	161.4	148.6	161.8	331.6
7/23/99	175	170.2	101.5	176.4	74.9
7/24/99	184.3	175.6	101.7	182.6	82.6
7/25/99	181.9	169.6	94.6	175.2	87.3
7/30/99	178.7	140.3	75.7	148.6	102.9
7/31/99	178.6	136.1	60	146	118.6
8/7/99	267.9	129.5	61.4	143	206.4

Table 7.5. Maximum value of the daily-averaged latent heat flux computed by the OSU model. Soil water content values derived from the maximum, mean, and minimum field sample values as well as the 229-L sensor served as input to the model. The simulations used a clay loam parametrization for soil texture.

Date	FSMax	FSMean	FSMin	229-L	Range
6/26/99	464.7	473.9	483.5	473.1	18.8
7/2/99	422.9	431.2	440.7	441	18.1
7/3/99	435.4	443.6	452.7	441	17.3
7/8/99	423.2	432.2	457.2	427.2	34.1
7/9/99	471	480.1	469.7	477.3	10.5
7/13/99	469.1	479.6	494	478.2	24.9
7/15/99	465.1	475.1	321.8	478.3	156.5
7/23/99	469.6	350.4	177.9	496.4	318.5
7/24/99	492.3	316.2	186.8	459	305.5
7/25/99	515.9	274.2	184.3	398.9	331.6
7/30/99	525.7	178.5	180.6	225.1	347.2
7/31/99	525.1	178.9	180.8	214.2	346.3
8/7/99	471.5	251.5	174.3	242.2	297.2

Table 7.6. Maximum value of the daily-averaged latent heat flux computed by the OSU model. Soil water content values derived from the maximum, mean, and minimum field sample values as well as the 229-L sensor served as input to the model. The simulations used a silt loam parametrization for soil texture.

Date	FSMax	FSMean	FSMin	229-L	Range
6/26/99	84.6	84.6	69.2	69.2	20.9
7/2/99	89.8	89.8	69.6	69.6	26
7/3/99	86.3	86.3	94.2	94.2	8.3
7/8/99	100.1	100.1	72.8	72.8	44.4
7/9/99	92.4	92.4	64.8	64.8	38.2
7/13/99	109.2	109.2	76.2	76.2	33.1
7/15/99	69.3	69.3	63.6	63.6	5.7
7/23/99	65.7	65.7	62.8	62.8	7.4
7/24/99	73.9	73.9	70	70	8.6
7/25/99	63.3	63.3	61.9	61.9	6.1
7/30/99	61.1	61.1	56.6	56.6	9.7
7/31/99	61.3	61.3	57.4	57.4	9.2
8/7/99	67.9	67.9	64.8	64.8	3.9

Table 7.7. Maximum value of the daily-averaged ground heat flux computed by the OSU model. Soil water content values derived from the maximum, mean, and minimum field sample values as well as the 229-L sensor served as input to the model. The simulations used a clay loam parametrization for soil texture.

Date	FSMax	FSMean	FSMin	229-L	Range
6/26/99	103.7	91	78.2	78.2	25.5
7/2/99	108.4	97	84.1	84.1	24.3
7/3/99	107.1	96.3	84	84	23.1
7/8/99	113.8	97.5	95.2	95.2	18.6
7/9/99	94.9	80.3	71	71	23.9
7/13/99	130.2	112.6	85.2	85.2	45
7/15/99	90.8	73.9	88.1	88.1	22
7/23/99	86.3	98.8	63.2	63.2	35.6
7/24/99	97.6	109.8	70.9	70.9	38.9
7/25/99	80.6	95.9	60.4	60.4	35.5
7/30/99	81.1	70.3	56.4	56.4	32.9
7/31/99	81.4	66.5	56	56	32.5
8/7/99	84.1	89.7	60.2	60.2	29.5

Table 7.8. Maximum value of the daily-averaged ground heat flux computed by the OSU model. Soil water content values derived from the maximum, mean, and minimum field sample values as well as the 229-L sensor served as input to the model. The simulations used a silt loam parametrization for soil texture.

Date	FSMax	FSMean	FSMin	229-L	Range
6/26/99	652.2	650.5	649.3	650.7	2.9
7/2/99	637.2	635.3	633.5	635.8	3.7
7/3/99	638.8	637.2	609.6	637.7	29.3
7/8/99	620.6	551.2	545.3	597.6	75.3
7/9/99	646	583.4	577.5	589.5	68.5
7/13/99	644.2	595.8	580.3	612.7	64
7/15/99	636.6	572.5	568.6	572.3	68
7/23/99	545.2	541	521.1	544	24.1
7/24/99	535.6	530.6	510.1	533.7	25.5
7/25/99	546.5	540.7	520.6	543.6	25.9
7/30/99	553.4	542.5	525.3	546	28.1
7/31/99	553.5	541.6	521.7	545.5	31.8
8/7/99	582.9	547.1	531.4	549.1	51.5

Table 7.9. Maximum value of the daily-averaged net radiation computed by the OSU model. Soil water content values derived from the maximum, mean, and minimum field sample values as well as the 229-L sensor served as input to the model. The simulations used a clay loam parametrization for soil texture.

Date	FSMax	FSMean	FSMin	229-L	Range
6/26/99	651.9	651.1	650.3	651.2	1.6
7/2/99	637.1	636.1	634.9	638.3	3.4
7/3/99	638.9	638.1	637.1	638.3	1.8
7/8/99	622.6	620.6	614.1	621.8	8.5
7/9/99	647.1	646.1	636.8	646.4	10.4
7/13/99	645.3	644.5	643	644.6	2.3
7/15/99	638.1	637.1	596.4	636.9	41.7
7/23/99	625.6	572.5	542.4	625.3	83.2
7/24/99	614	555.4	533.1	598.7	81
7/25/99	632.2	558.4	543.9	592.3	88.3
7/30/99	629.3	554.8	551.4	563	77.9
7/31/99	629.3	554	551.3	561.9	78.1
8/7/99	623.2	575	554.9	567.5	68.3

Table 7.10. Maximum value of the daily-averaged net radiation computed by the OSU model. Soil water content values derived from the maximum, mean, and minimum field sample values as well as the 229-L sensor served as input to the model. The simulations used a silt loam parametrization for soil texture.

Date	FSMax	FSMean	FSMin	229-L	Range
6/26/99	1338	1383.8	1410.7	1378	72.7
7/2/99	883.9	922.1	973.2	907.8	89.3
7/3/99	1111.3	1131.7	1675	1128.4	563.7
7/8/99	1404.5	2649.2	2721.3	1906.3	1316.8
7/9/99	1436.2	2428.5	2685.9	2186.7	1249.7
7/13/99	1866.5	2190.5	2277.7	2062.1	411.2
7/15/99	1667.5	2739.8	2866.1	2746	1198.6
7/23/99	3063.4	3092.4	3262.2	3070.4	198.8
7/24/99	2956.9	3074.8	3245.3	3034.9	288.4
7/25/99	3288.6	3296	3472.3	3292.7	183.7
7/30/99	3291.8	3314.9	3451.3	3309.3	159.5
7/31/99	3291.5	3316.6	3457.8	3310.1	166.3
8/7/99	2383.9	3148.4	3428.5	3082.4	1044.6

Table 7.11. Maximum value of the depth of the PBL computed by the OSU model. Soil water content values derived from the maximum, mean, and minimum field sample values as well as the 229-L sensor served as input to the model. The simulations used a clay loam parametrization for soil texture.

Date	FSMax	FSMean	FSMin	229-L	Range
6/26/99	1359.7	1342.7	1364	1387.9	45.2
7/2/99	1125.3	885.6	902.5	928.3	239.7
7/3/99	1125.3	1099.1	1127.1	1132.8	33.7
7/8/99	1390.2	1368.8	1407.6	1660.7	291.9
7/9/99	1408.9	1389	1428.5	1647	258
7/13/99	1860.5	1851.2	1862.4	1888.3	37.1
7/15/99	1635.4	1606.6	1629.4	2325.3	718.7
7/23/99	1841.4	1656.6	2704.9	3082.3	1425.7
7/24/99	2258.4	1462.9	2724.7	3047.4	1584.5
7/25/99	3057	1723.5	3263.2	3292.1	1568.6
7/30/99	3194	1840.7	3290.3	3299.1	1458.4
7/31/99	3252.8	1838.5	3290	3299.7	1461.2
8/7/99	2740.5	1390.4	2597.8	2993.4	1603

Table 7.12. Maximum value of the depth of the PBL computed by the OSU model. Soil water content values derived from the maximum, mean, and minimum field sample values as well as the 229-L sensor served as input to the model. The simulations used a silt loam parametrization for soil texture.

7.3.1.1 --- 2 July

Simulations of sensible heat flux during very wet soil conditions (2 July 1999) are shown in Figure 7.2a-b. The model simulations are very similar in magnitude and trend, regardless of soil water content or soil texture. Similar results were obtained for latent heat flux, ground heat flux, net radiation, and depth of the PBL (Tables 7.3 through 7.12). Thus, under very wet conditions in the soil profile, little variability resulted in model derived parameters even though soil water content and soil texture varied considerably .

7.3.1.2 --- 15 July

However, as soil dried at the site, increased variability occurred in the model parameters needed as input to the model. For example, near-surface (0-5 cm) values of soil water content on 15 July were greatly reduced compared to 2 July. However, soil moisture initialized in the 5-100 cm soil layer was only slightly drier than observed on 2 July. As a result of drier soil moisture conditions near the surface, simulations of sensible heat flux (daily maximum) were quite variable (Figs. 7.3a-b). On this day, the range of sensible heat flux produced by the model exceeded 276.4 W m^{-2} in the clay loam simulations and 168 W m^{-2} for the simulations using the silt loam parametrization (Tables 7.3 and 7.4).

Simulations of latent heat flux were equally as variable (Figs. 7.4a-b); peak values ranged between 331 W m^{-2} and 157 W m^{-2} for soil textures parametrized as clay loam and silt loam respectively (Tables 7.5 and 7.6). Variability in the simulation of ground heat flux ranged 10 W m^{-2} - 27 W m^{-2} at the time of daily-maximum ground heat flux (Tables 7.7 and 7.8). At the same time, net radiation ranged 68 W m^{-2} - 42 W m^{-2} at the time of daily-maximum net radiation (Tables 7.9 and 7.10). Both were significantly less than the values of latent and sensible heat flux. The combined influences of the aforementioned components of the surface energy balance created substantial differences in the depth of the PBL after 12 hours (Fig. 7.5a-b). Inspection of Tables 7.11 and 7.12 revealed that the depth of the PBL varied approximately 1200 meters in the clay loam simulations and nearly 720 meters in the silt loam simulations.

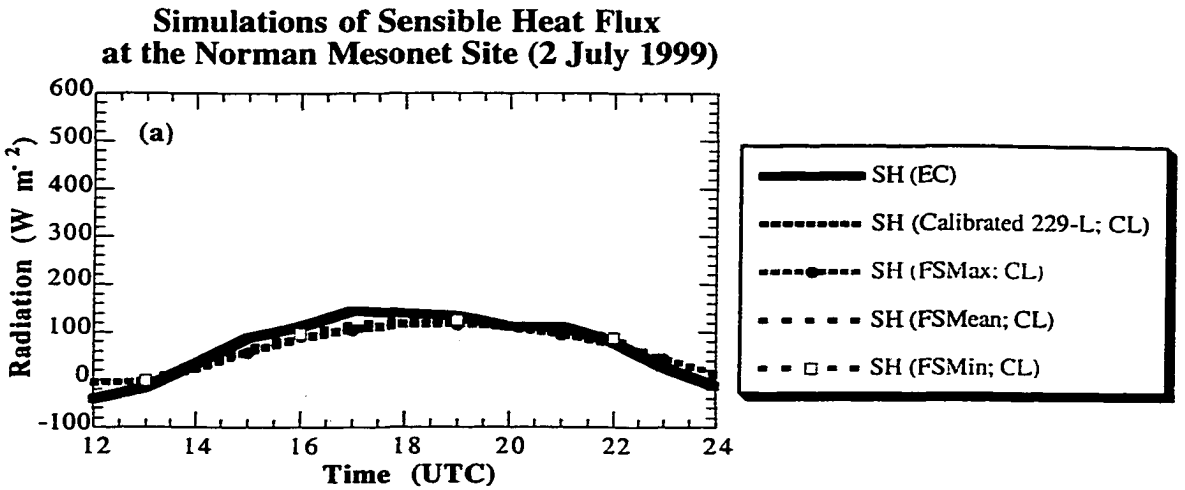

Figure 7.2a. Simulations of sensible heat flux at the Norman Mesonet site on 2 July 1999 using the clay loam soil parameterization (CL). Calibrated measurements of 229-L soil water content, and soil water determined from field samples were used as input. Hourly-averaged observations from the Norman site are plotted for reference (black curve).

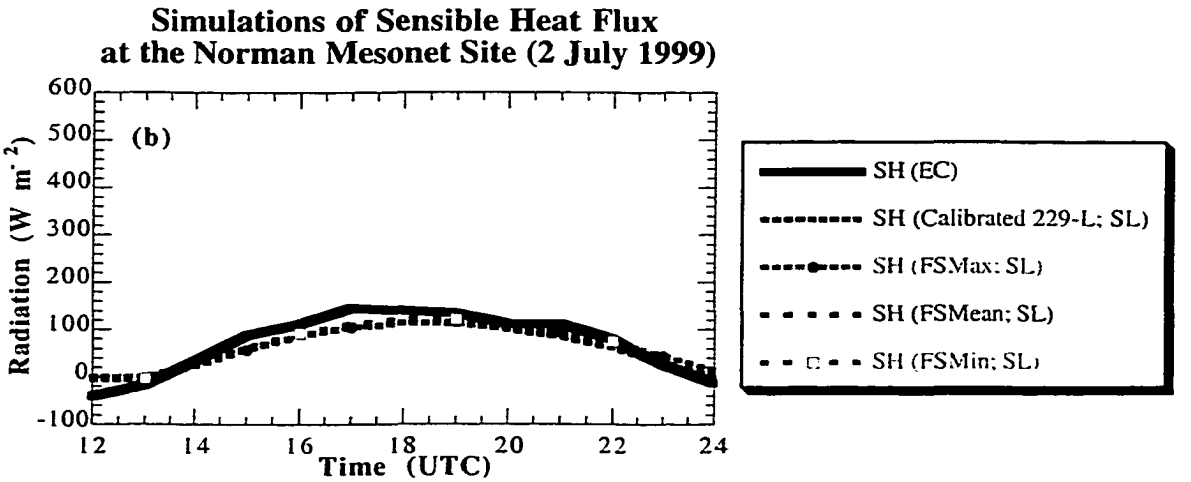

Figure 7.2b. Simulations of sensible heat flux at the Norman Mesonet site on 2 July 1999 using the silt loam soil parameterization (SL). Calibrated measurements of 229-L soil water content, and soil water determined from field samples were used as input. Hourly-averaged observations from the Norman site are plotted for reference (black curve).

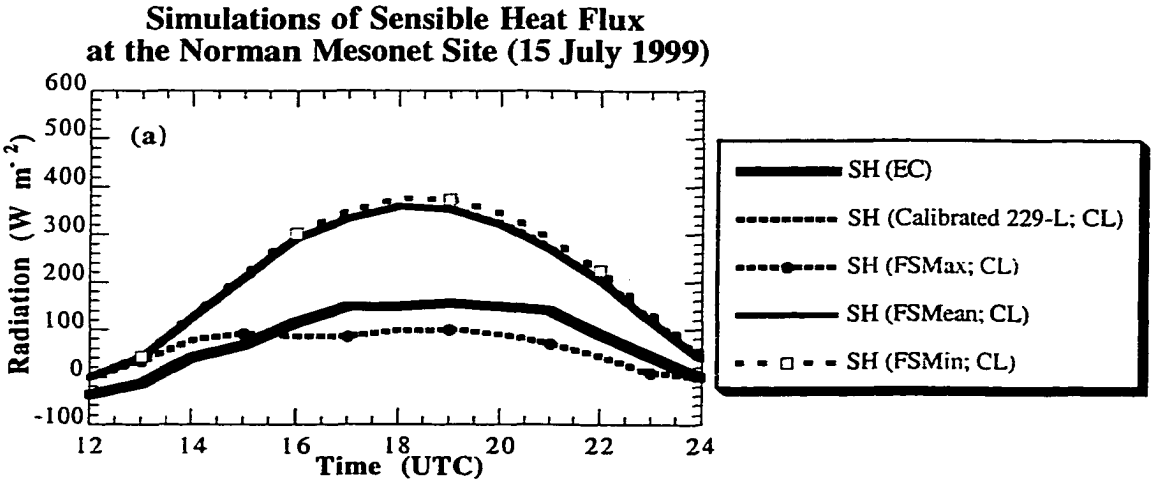

Figure 7.3a. Simulations of sensible heat flux at the Norman Mesonet site on 15 July 1999 using the clay loam soil parameterization (CL). Calibrated measurements of 229-L soil water content, and soil water determined from field samples were used as input. Hourly-averaged observations from the Norman site are plotted for reference (black curve).

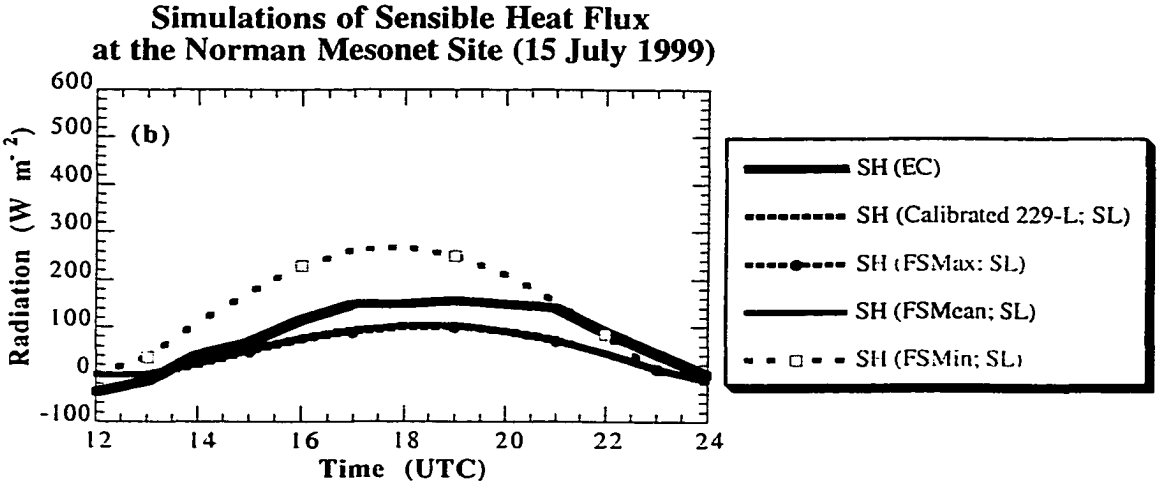

Figure 7.3b. Simulations of sensible heat flux at the Norman Mesonet site on 15 July 1999 using the silt loam soil parameterization (SL). Calibrated measurements of 229-L soil water content, and soil water determined from field samples were used as input. Hourly-averaged observations from the Norman site are plotted for reference (black curve).

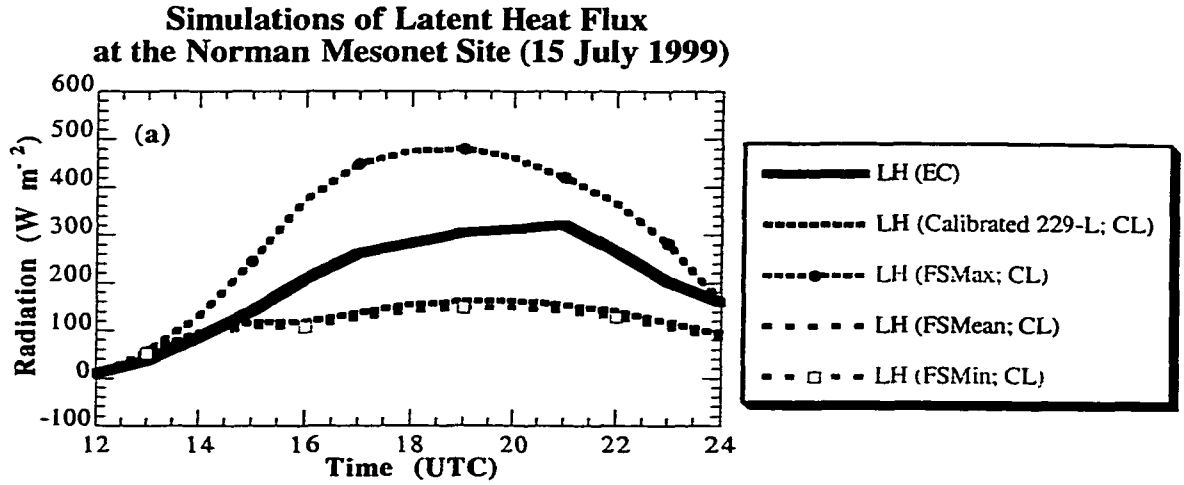

Figure 7.4a. Simulations of latent heat flux at the Norman Mesonet site on 15 July 1999 using the clay loam soil parameterization (CL). Calibrated measurements of 229-L soil water content, and soil water determined from field samples were used as input. Hourly-averaged observations from the Norman site are plotted for reference (black curve).

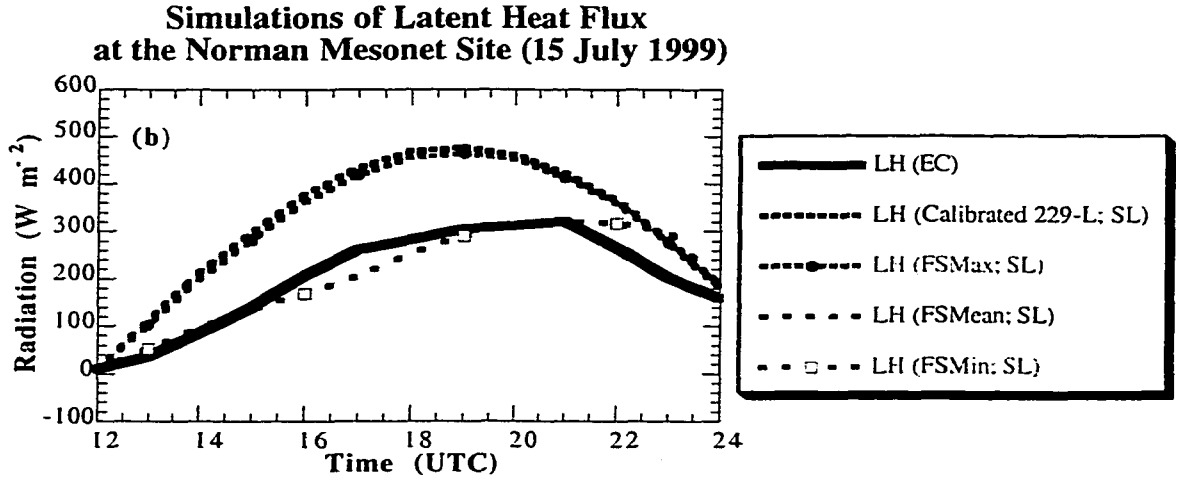

Figure 7.4b. Simulations of latent heat flux at the Norman Mesonet site on 15 July 1999 using the silt loam soil parameterization (SL). Calibrated measurements of 229-L soil water content, and soil water determined from field samples were used as input. Hourly-averaged observations from the Norman site are plotted for reference (black curve).

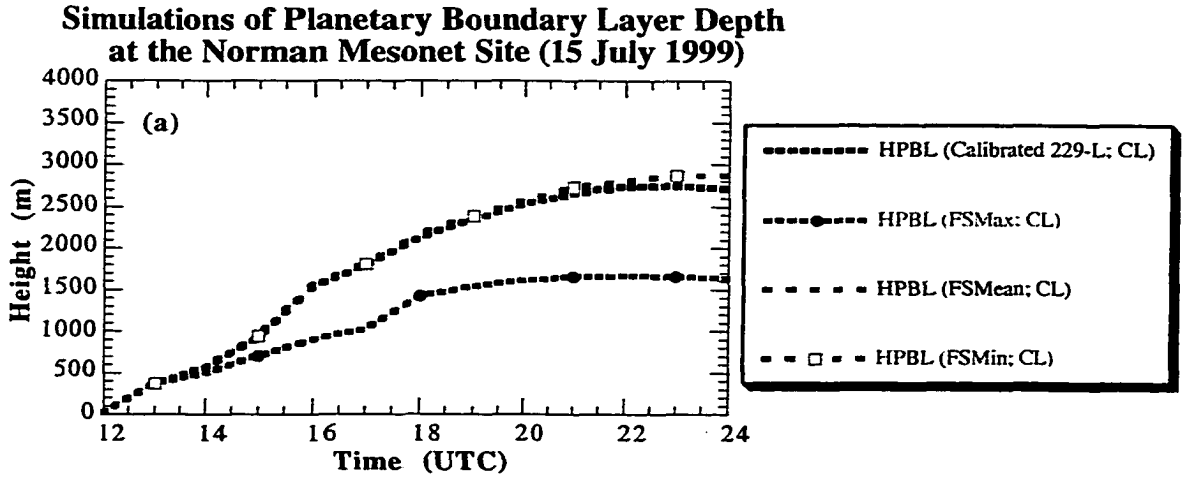

Figure 7.5a. Simulated height of the PBL at the Norman Mesonet site on 15 July 1999 using the clay loam soil parameterization (CL). Calibrated measurements of 229-L soil water content, and soil water determined from field samples were used as input.

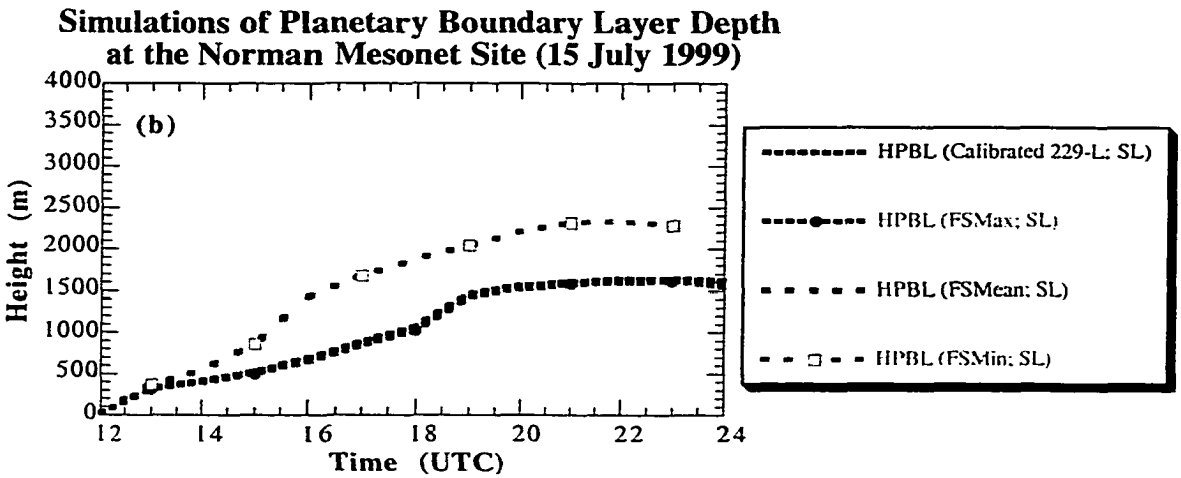

Figure 7.5b. Simulated height of the PBL at the Norman Mesonet site on 15 July 1999 using the silt loam soil parameterization (SL). Calibrated measurements of 229-L soil water content, and soil water determined from field samples were used as input.

7.3.1.2 --- 23 July

Conditions in the soil profile continued to dry through 23 July at the Norman site. In the near surface layer, input soil moisture for all simulations had dried below the wilting point for clay loam (0.18) and was approaching or beyond the threshold of the wilting point for clay loam (0.10). However, deep layer soil moisture used to initialize the OSU model remained moderately moist .

The influence of the soil moisture variability is evident in the model simulations of sensible heat flux (Fig7.6a-b). The simulations of sensible heat flux using the clay loam parametrization produced less variability than occurred on 15 July (range of 73 W m^{-2}; Table 7.3). However, simulations which used the silt loam parametrization revealed an increased variability when compared with similar simulations on 15 July (range of 218 W m^{-2}; Table 7.4).

Latent heat flux was also greatly impacted by the variability of soil moisture used to initialize the model (not shown). For example, the range of latent heat flux values (daily maximum) spanned approximately 75 W m^{-2} (Table 7.5) in the clay loam simulations and 320 W m^{-2} (Table 7.6) in the silt loam simulations. However, as with 15 July, ground heat flux and net radiation were not as sensitive to the soil moisture variability as were the fluxes of sensible and latent heat (Table 7.7 through 7.10). Even so, the variability in ground heat flux exceeded 36 W m^{-2} and exceeded 24 W m^{-2} for the net radiation simulations.

The combined variability in components of the surface energy balance created a significant variability in the depth of the PBL (Figs 7.7a-b). Because some simulations produced more turbulent energy transfer (sensible heating) than did others, the depth of the PBL produced by the model grew at different rates. This trend is especially notable in the simulations which used the silt loam parametrization. In those cases, the range of PBL depth produced by the model due to soil moisture variability exceeded 1425 meters (Table 7.12). However, using the clay loam parametrization, less variability was observed in the simulated values of sensible, latent, and ground heat fluxes as well as net radiation. As a result, PBL depth only varied approximately 200 meters.

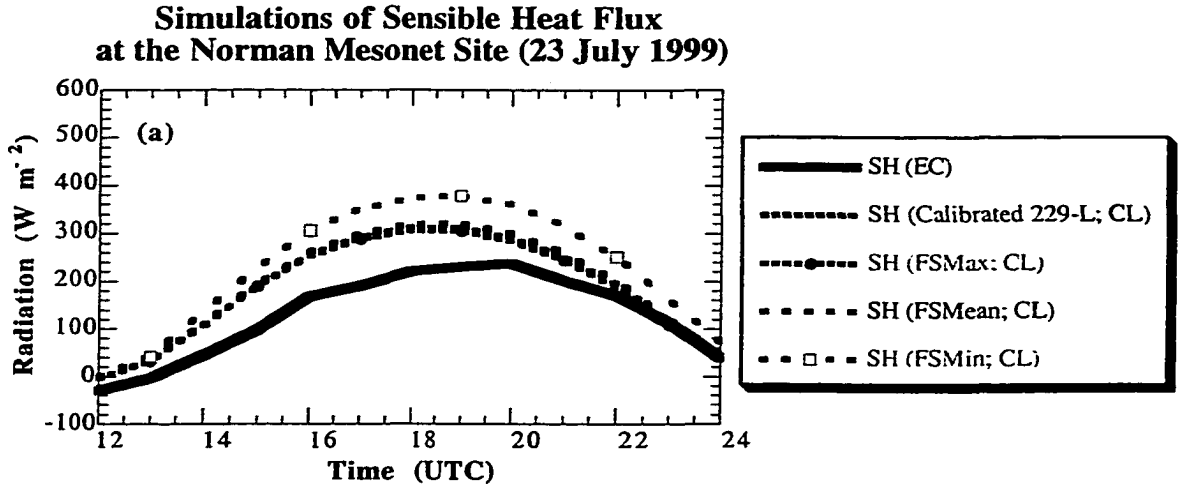

Figure 7.6a. Simulations of sensible heat flux at the Norman Mesonet site on 23 July 1999 using the clay loam soil parameterization (CL). Calibrated measurements of 229-L soil water content, and soil water determined from field samples were used as input. Hourly-averaged observations from the Norman site are plotted for reference (black curve).

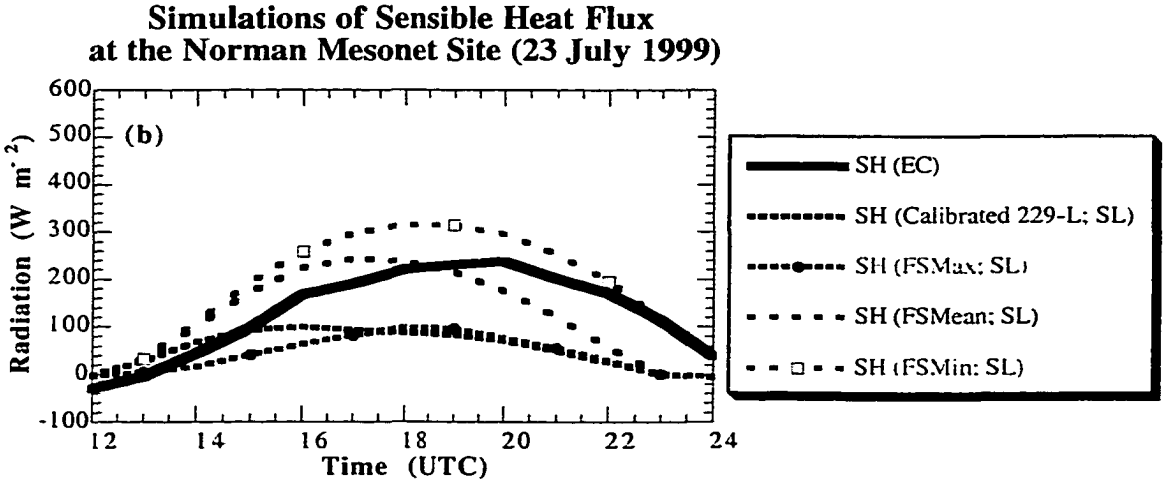

Figure 7.6b. Simulations of sensible heat flux at the Norman Mesonet site on 23 July 1999 using the silt loam soil parameterization (SL). Calibrated measurements of 229-L soil water content, and soil water determined from field samples were used as input. Hourly-averaged observations from the Norman site are plotted for reference (black curve).

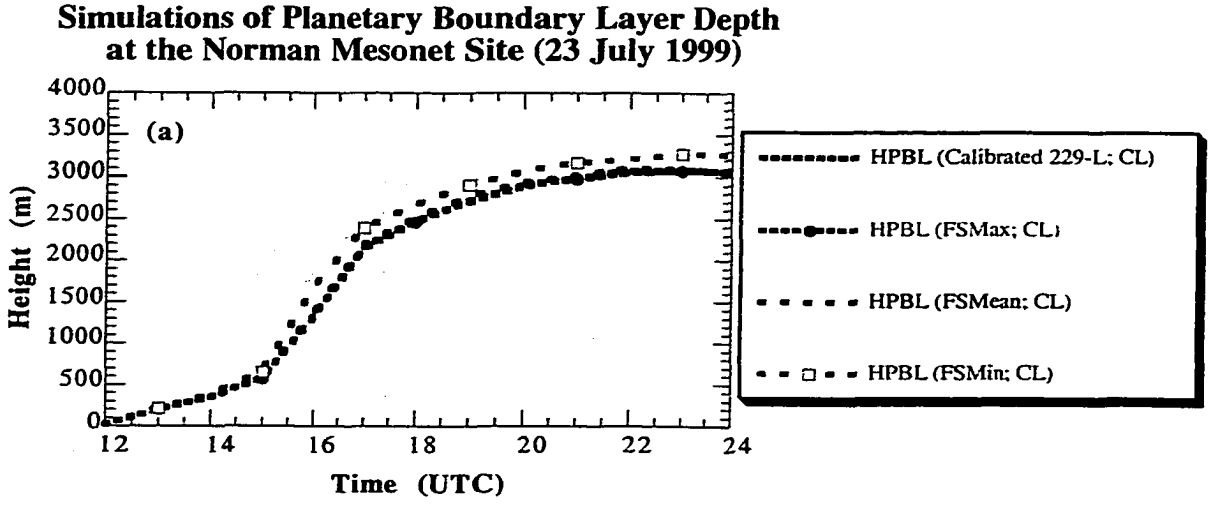

Figure 7.7a. Simulated height of the PBL at the Norman Mesonet site on 23 July 1999 using the clay loam soil parameterization (CL). Calibrated measurements of 229-L soil water content, and soil water determined from field samples were used as input.

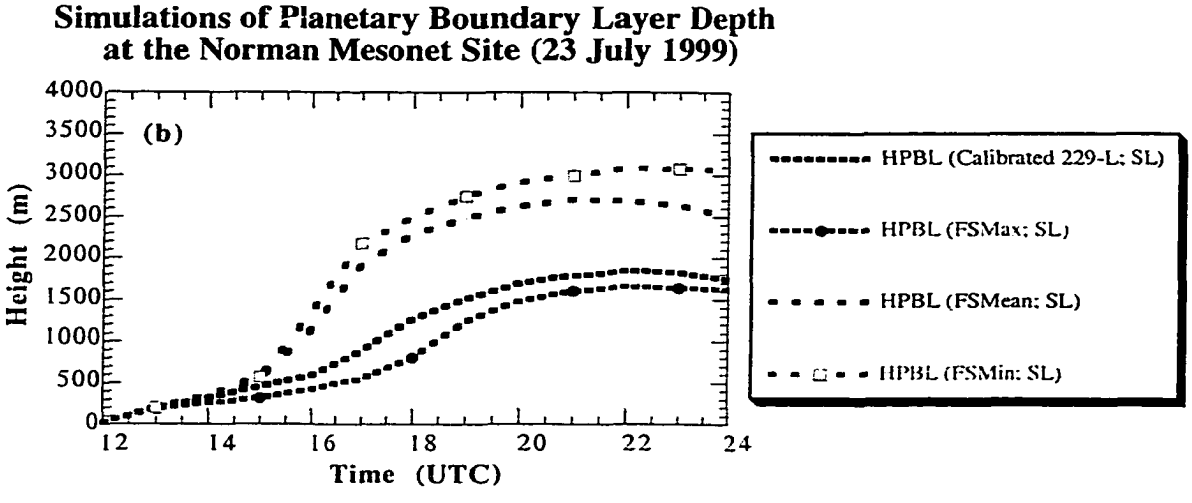

Figure 7.7b. Simulated height of the PBL at the Norman Mesonet site on 23 July 1999 using the silt loam soil parameterization (SL). Calibrated measurements of 229-L soil water content, and soil water determined from field samples were used as input.

7.3.1.2 --- 30 July

Soil moisture conditions used to initialize the model were quite dry on 30 July (Table 7.2). In general, reduced variability occurred in the model derived values of sensible heat flux (Figs. 7.8a-b) and latent heat flux (Figs. 7.9a-b) when compared with output from 15 and 23 July. This reduced variability was evident for both the clay loam and silt loam simulations. However, the simulation using silt loam initialized with the maximum value of soil water content determined from field samples behaved quite differently than the other simulations. Sensible heat flux in this simulations was nearly 160 W m^{-2} less than any other simulation. In addition, latent heat flux was greater than 300 W m^{-2} compared to other simulations for 30 July.

Variability in the simulations of ground heat flux and net radiation was small (with the exception of the silt loam simulation initialized with FSMax values; Tables 7.7 through 7.10). Thus, the outlier in simulations of PBL depth compared to other simulations (Figs. 7.10a-b) was attributed to the reduced partitioning of sensible heat flux and increased latent heat flux. As a result, PBL depth initialized with FSMax values was ~ 1150 meters less than any of the other simulations on 30 July.

7.3.1.2 --- 7 August

During late July and early August, the soil profile at NORM began a continuous drying trend due to an extended period of no precipitation. However, during the overnight hours on 5-6 August, approximately 13 mm of precipitation was recorded. Soil cores collected on 7 August revealed significant variability in soil water content both horizontally and vertically. This variability is attributed to differential infiltration of water into the soil. Thus, one profile experienced a significant moistening while limited infiltration at another location resulted in a drier soil profile.

When the increased variability of soil moisture was used to represent the spectrum of initial conditions in the OSU model, the surface fluxes of sensible and latent heat were dramatically impacted. For example, consider the simulation of sensible heat flux for both the clay loam and silt loam soil parameterizations (Figs. 7.11a-b). The range of sensible

heat flux at the time of maximum heating is approximately 185 W m^{-2} and 246 W m^{-2} (Tables 7.5 and 7.6) for simulations using clay loam and silt loam textured soils respectively. Similar results were noted for simulations of latent heat flux (Figs. 7.12a-b). The results (Tables 7.5 and 7.6) reveal that the range of simulated values for latent heat flux using the clay loam soil texture exceed 206 W m^{-2}. In addition, simulations using the silt loam parametrization produced a range of latent heat flux values that exceed 297 W m^{-2}.

Though soil moisture conditions varied significantly in the input files used to initialize the model, ground heat flux and net radiation were less impacted than were sensible and latent heat flux. In fact, the variability of ground heat flux computed by the model was quite small compared to the fluxes of sensible and latent heat (30 W m^{-2} for the clay loam simulation and 4 W m^{-2} for the silt loam simulations; Table 7.7 and 7.8). Likewise, simulations of net radiation produced much less variability than did sensible and latent heat flux (52 W m^{-2} for the clay loam simulation and 68 W m^{-2} for the silt loam simulations; Table 7.9 and 7.10).

The large variability in the partitioning of available energy into sensible and latent heat did impact the growth of the PBL in the model simulations (Figs. 7.13a-b). The model simulated PBL depth ranged across ~1045 meters when the clay loam soil texture was used. Even greater variability was noted for the model simulations which used the silt loam parametrization. When PBL depth was simulated using variable soil moisture conditions and the silt loam soil texture, the range of values exceeded 1600 meters!

7.3.2 Soil Texture Variability

The results in Section 7.3.1 clearly established how the OSU model is sensitive to soil moisture conditions. However, close inspection of the plots and data also indicate that, in some cases, simulations of PBL processes using the model are highly dependent upon soil texture. To test the sensitivity of the model to variation in soil texture, simulations based upon soil water content determined from field samples (FSMax, FSMean, and FSMin) and calibrated 229-L measurements were analyzed. For each set of input values of

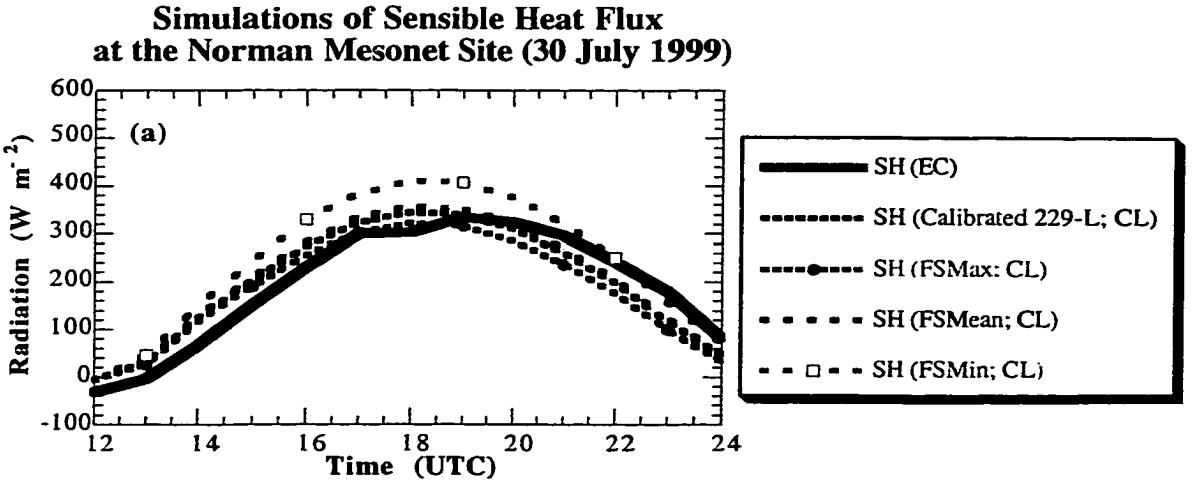

Figure 7.8a. Simulations of sensible heat flux at the Norman Mesonet site on 30 July 1999 using the clay loam soil parameterization (CL). Calibrated measurements of 229-L soil water content, and soil water determined from field samples were used as input. Hourly-averaged observations from the Norman site are plotted for reference (black curve).

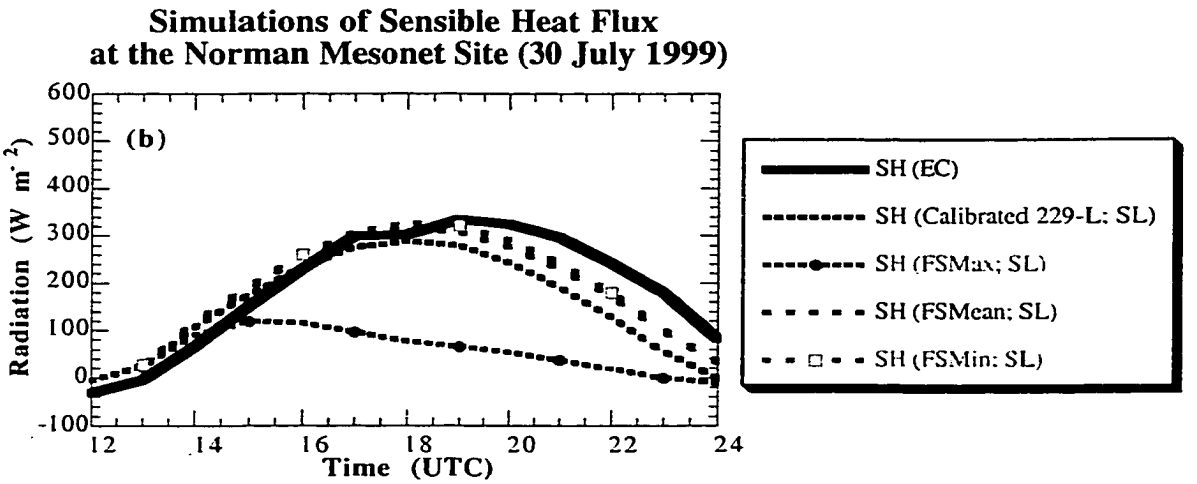

Figure 7.8b. Simulations of sensible heat flux at the Norman Mesonet site on 30 July 1999 using the silt loam soil parameterization (SL). Calibrated measurements of 229-L soil water content, and soil water determined from field samples were used as input. Hourly-averaged observations from the Norman site are plotted for reference (black curve).

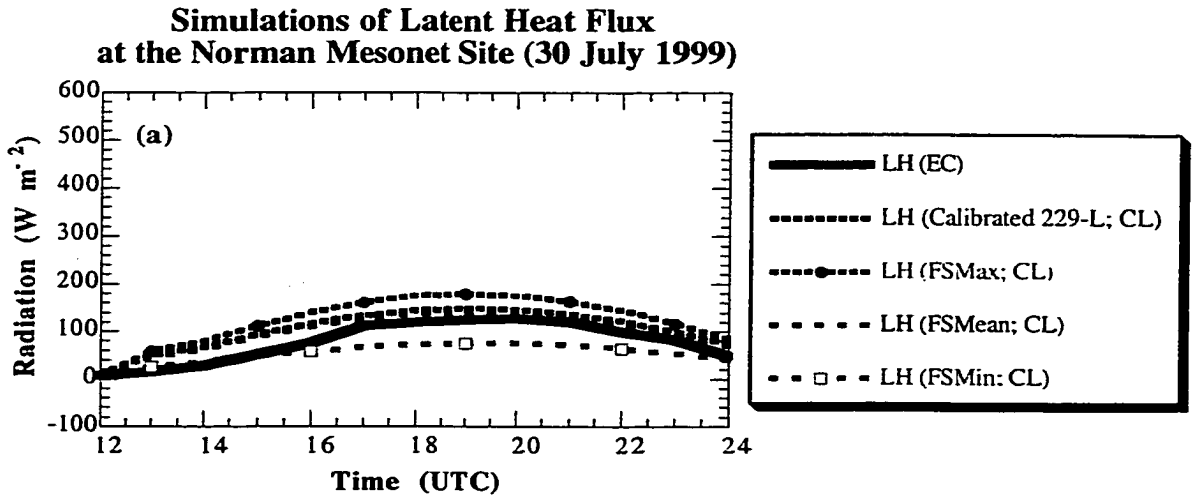

Figure 7.9a. Simulations of latent heat flux at the Norman Mesonet site on 30 July 1999 using the clay loam soil parameterization (CL). Calibrated measurements of 229-L soil water content, and soil water determined from field samples were used as input. Hourly-averaged observations from the Norman site are plotted for reference (black curve).

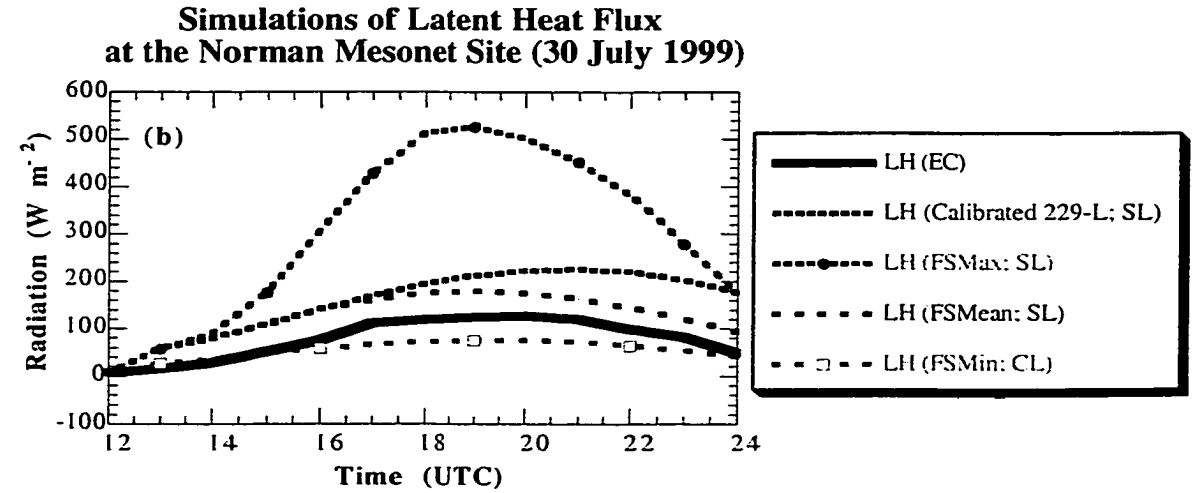

Figure 7.9b. Simulations of latent heat flux at the Norman Mesonet site on 30 July 1999 using the silt loam soil parameterization (SL). Calibrated measurements of 229-L soil water content, and soil water determined from field samples were used as input. Hourly-averaged observations from the Norman site are plotted for reference (black curve).

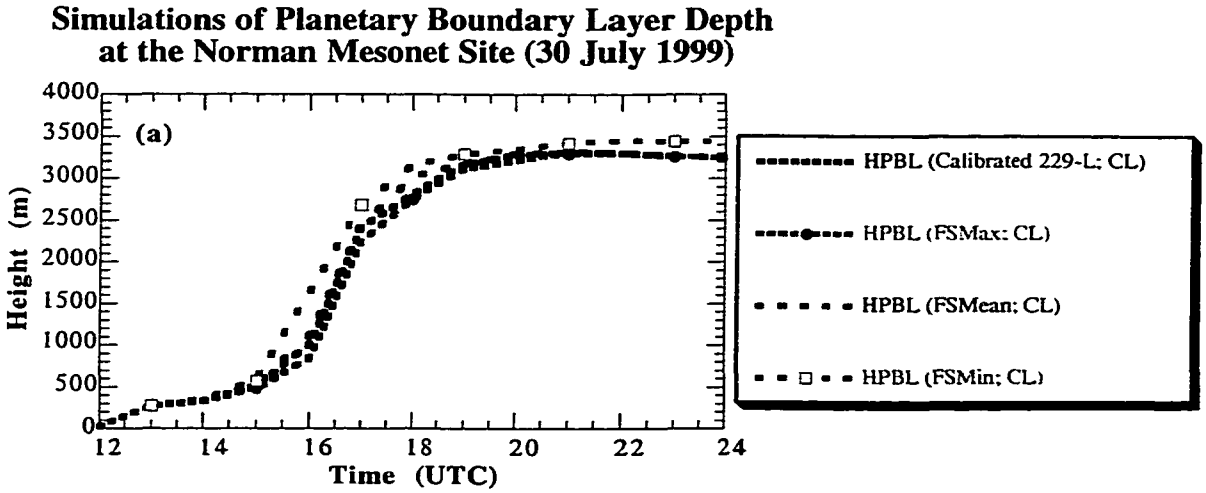

Figure 7.10a. Simulated height of the PBL at the Norman Mesonet site on 30 July 1999 using the clay loam soil parameterization (CL). Calibrated measurements of 229-L soil water content, and soil water determined from field samples were used as input.

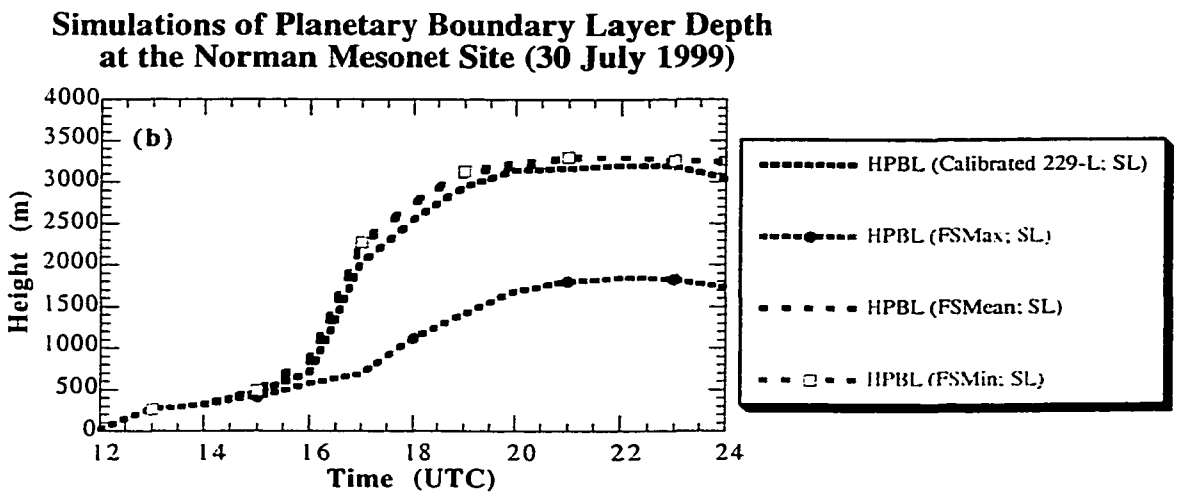

Figure 7.10b. Simulated height of the PBL at the Norman Mesonet site on 30 July 1999 using the silt loam soil parameterization (SL). Calibrated measurements of 229-L soil water content, and soil water determined from field samples were used as input.

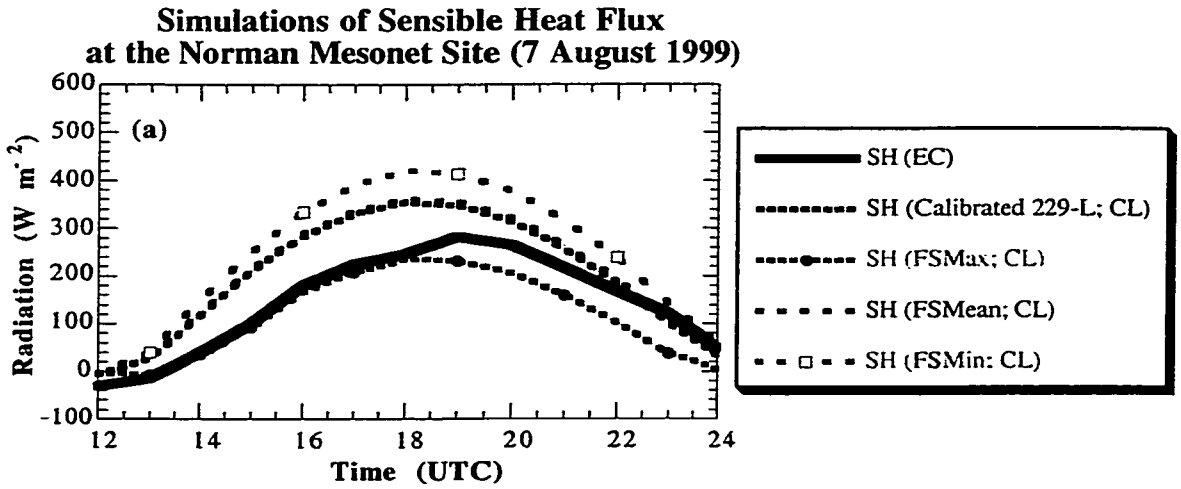

Figure 7.11a. Simulations of sensible heat flux at the Norman Mesonet site on 7 August 1999 using the clay loam soil parameterization (CL). Calibrated measurements of 229-L soil water content, and soil water determined from field samples were used as input. Hourly-averaged observations from the Norman site are plotted for reference (black curve).

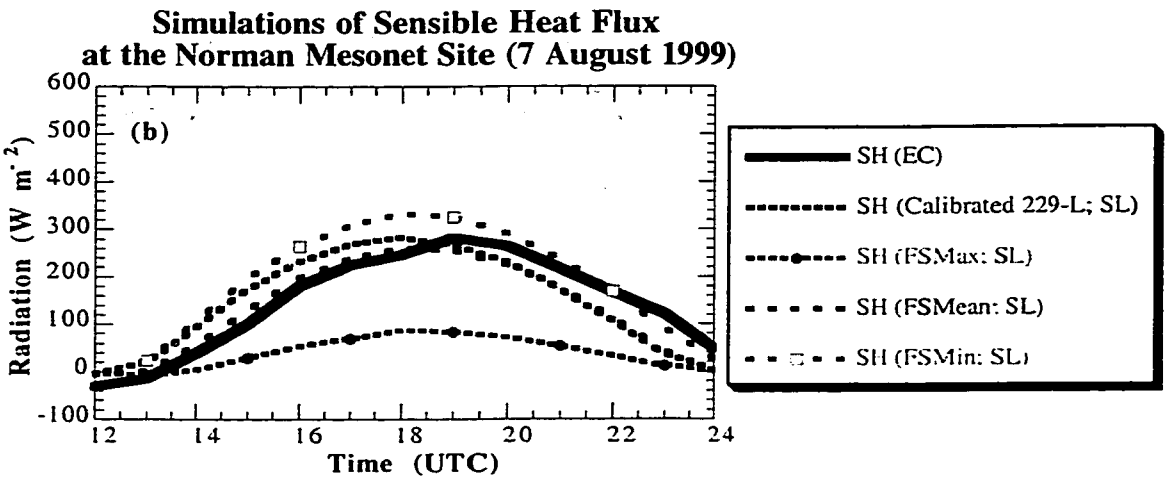

Figure 7.11b. Simulations of sensible heat flux at the Norman Mesonet site on 7 August 1999 using the silt loam soil parameterization (SL). Calibrated measurements of 229-L soil water content, and soil water determined from field samples were used as input. Hourly-averaged observations from the Norman site are plotted for reference (black curve).

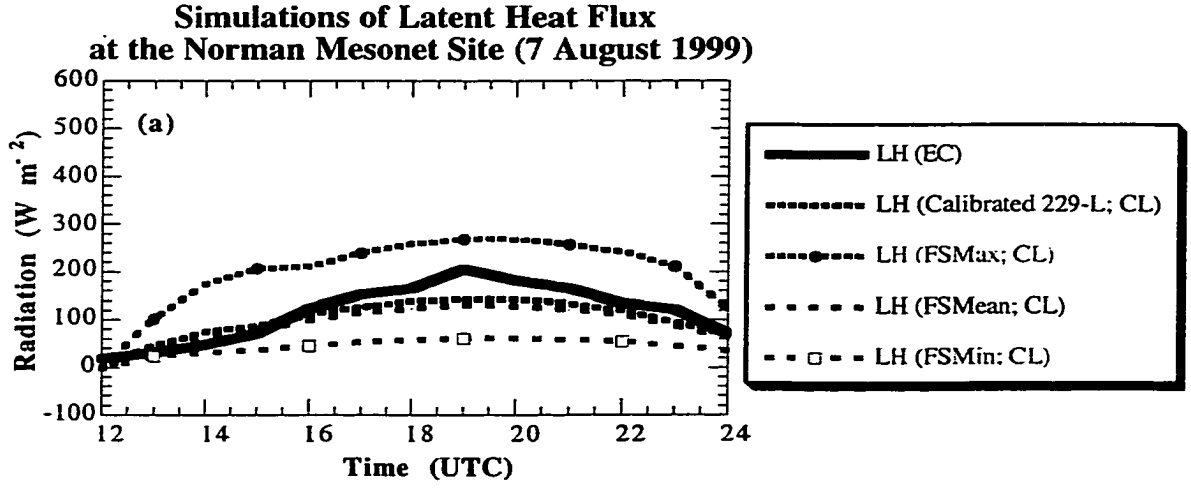

Figure 7.12a. Simulations of latent heat flux at the Norman Mesonet site on 7 August 1999 using the clay loam soil parameterization (CL). Calibrated measurements of 229-L soil water content, and soil water determined from field samples were used as input. Hourly-averaged observations from the Norman site are plotted for reference (black curve).

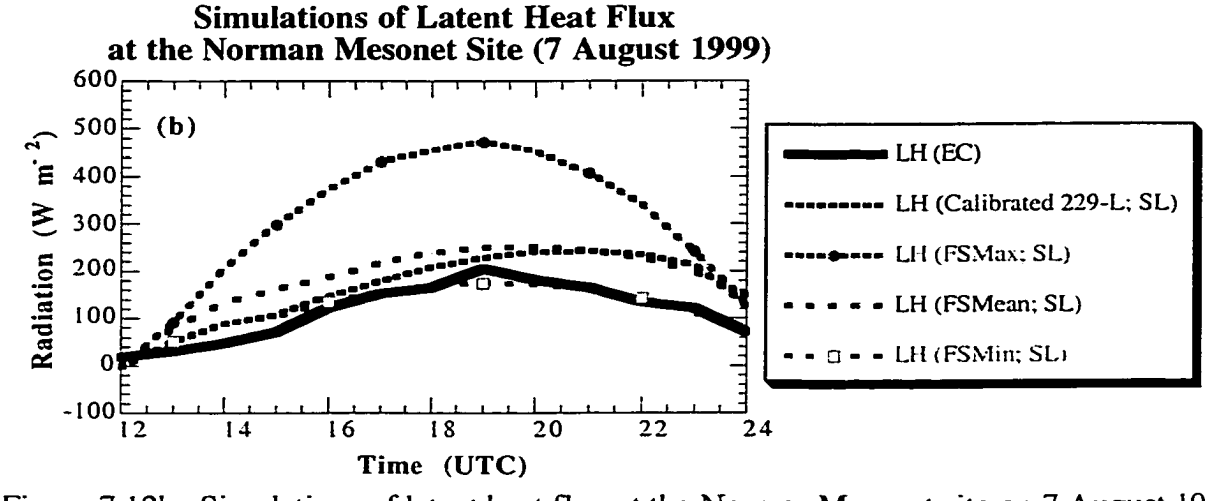

Figure 7.12b. Simulations of latent heat flux at the Norman Mesonet site on 7 August 1999 using the silt loam soil parameterization (SL). Calibrated measurements of 229-L soil water content, and soil water determined from field samples were used as input. Hourly-averaged observations from the Norman site are plotted for reference (black curve).

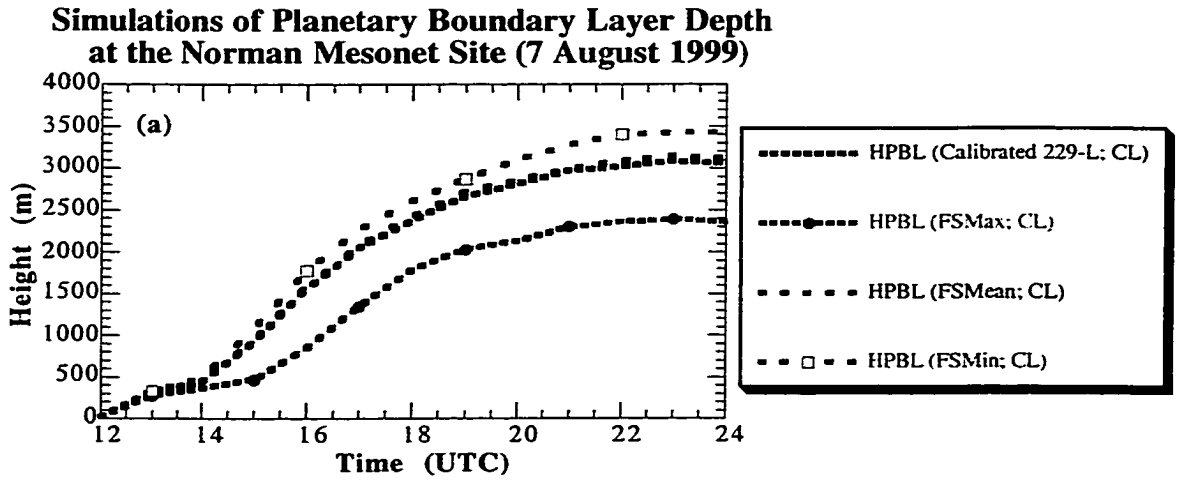

Figure 7.13a. Simulated height of the PBL at the Norman Mesonet site on 7 August 1999 using the clay loam soil parameterization (CL). Calibrated measurements of 229-L soil water content, and soil water determined from field samples were used as input.

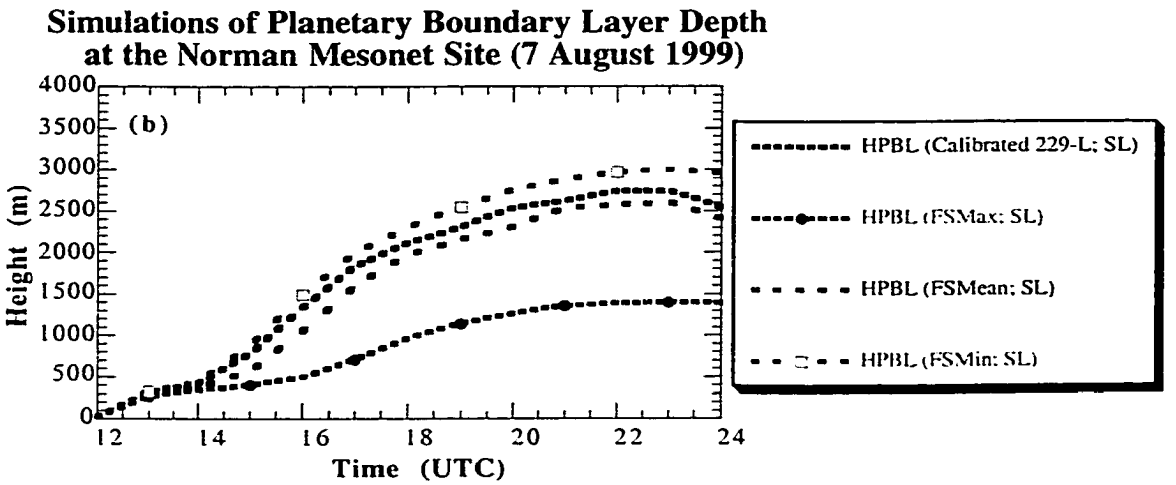

Figure 7.13b. Simulated height of the PBL at the Norman Mesonet site on 7 August 1999 using the silt loam soil parameterization (SL). Calibrated measurements of 229-L soil water content, and soil water determined from field samples were used as input.

soil moisture, simulations were run for the two dominant soil textures at the Norman site: clay loam and silt loam. Next, the simulated values of sensible heat flux, latent heat flux, ground heat flux, net radiation, and PBL depth were compared to quantify the sensitivity of model generated processes with *known* soil texture variability. Once values for each component of the energy balance were obtained, the daily maximum value was determined. Finally, results from the simulation using silt loam was subtracted from the clay loam simulation to assess the maximum variability.

An example of when a minimal difference occurred between simulations due to soil texture variability is minimal is presented in Figure 7.14. In this case (the FSMean value of water content initialized the model), little difference was noted in the magnitude or trend of sensible heat flux produced by the model. In fact, the maximum difference between the 2 simulations was 2.2 W m^{-2} (Table 7.13).

Further inspection of Table 7.13 reveals that the largest difference in sensible heat flux due to soil texture variations occurred in the FSMin simulations on 13 July (Fig 7.15). Thus, the subtle change of soil texture in the model resulted in sensible heat flux values which varied by 278 W m^{-2}. This dramatic event is not an isolated case. Of the 52 simulations of sensible heat flux computed using soil moisture initialized with values of FSMax, FSMean, and FSMin values as well as calibrated 229-L values, 12 cases (or 23%) varied by over 200 W m^{-2}. Furthermore 22 (or 42%) of the sensible heat flux simulations varied by over 100 W m^{-2}. This surprisingly large variability resulted from the change in soil texture within the model.

Even greater variability was noted for simulations of latent heat flux (Table 7.14). The largest difference in latent heat flux occurred on 30 July when the model was initialized with FSMax values (Fig. 7.16). By changing the parametrization from clay loam to silt loam, the maximum value of latent heat flux exceeded 500 W m^{-2}. This increase was a change of 347 W m^{-2} from the clay loam simulation. As with with sensible heat flux, this significant impact on latent heat flux was not an isolated case. Of the 52 simulations conducted for latent heat flux, 10 cases (or 19%) had differences in excess of 300 W m^{-2},

18 (or 35%) had differences larger than 200 W m^{-2}, and 27 (an astounding 52%) had differences greater than 100 W m^{-2}. In contrast, only 18 simulations (35%) had differences less than 50 W m^{-2}.

The change from a clay loam soil texture to silt loam did not produced the same magnitude of variability in the ground heat flux simulations as it did for sensible or latent heat flux. In fact, Table 7.15 reveals that the largest difference in the magnitude of ground heat flux was 36 W m^{-2} on 24 July. Furthermore 35 out of a possible 52 simulations (67%) had differences that were less than 20 W m^{-2}. Variability in the magnitude of net radiation was also much less than sensible or latent heat flux. The largest difference occurred on 25 July when the model was initialized with FSMax values of soil water content (Table 7.16). In addition, 32 of the 52 simulations (62%) resulted in simulation differences of less than 30 W m^{-2}.

Because PBL development was strongly related to the magnitude of sensible and latent heat flux, the depth of the PBL was strongly impacted by the change from clay loam soil to silt loam. Consider the example shown in Figure 7.17 where PBL depth varied by more than 1550 meters due to the simple change between clay loam and silt loam. In addition, Table 7.17 reveals that 12 of 52 simulations (23%) resulted in a change of PBL depth by more than 1000 meters simply by changing from clay loam to silt loam.

7.3.3 The Importance of Sensor Calibration

The results summarized in sections 7.3.1 and 7.3.2 dramatically show that, under certain conditions, the model is extremely sensitive to *natural* variability in soil moisture and soil texture. However, the results from Chapter 4 note that accurate, reliable estimates of soil water content using the 229-L sensor is a daunting task. Thus, this narrative will document how sensor calibration (in reference to soil water content) impacted simulations of the PBL.

Chapter 4 summarizes the effort to acquire the best possible observations of soil water content using the 229-L sensor. At the Norman site, the most accurate observations at

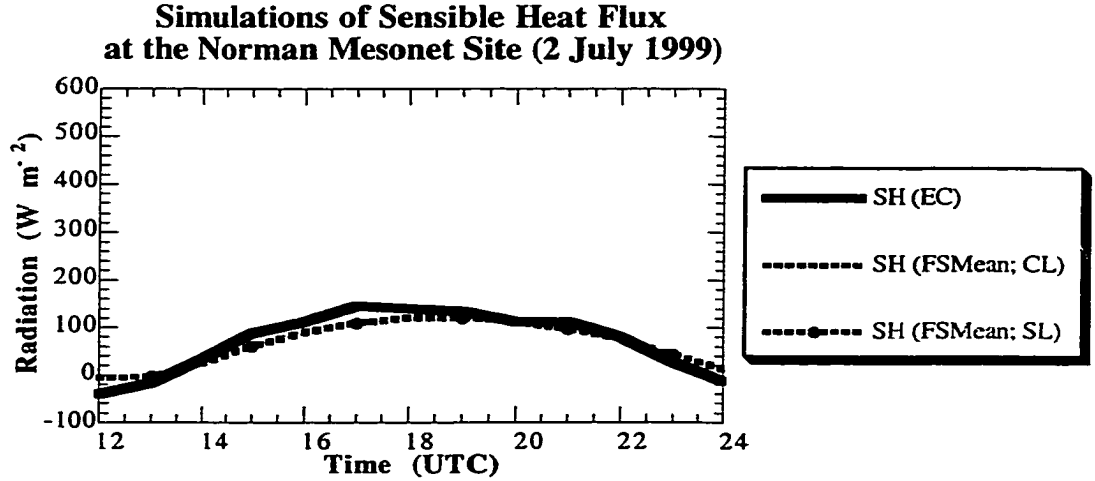

Figure 7.14. Simulations of sensible heat flux at the Norman Mesonet site on 2 July 1999 using the clay loam soil parameterization (CL), the silt loam soil parameterization (SL), and soil water determined from field samples (FSMean). Hourly-averaged observations from the Norman site are plotted for reference (black curve).

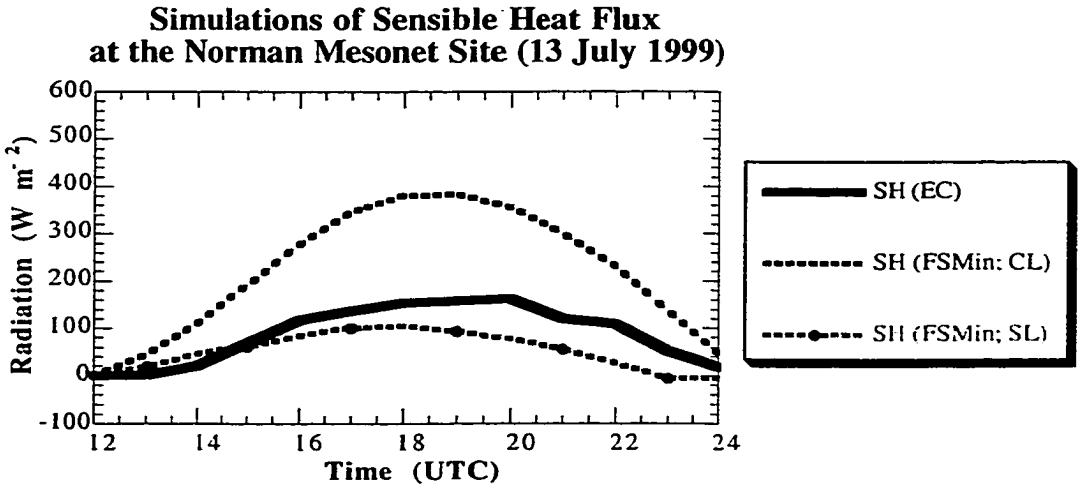

Figure 7.15. Simulations of sensible heat flux at the Norman Mesonet site on 13 July 1999 using the clay loam soil parameterization (CL), the silt loam soil parameterization (SL), and soil water determined from field samples (FSMin). Hourly-averaged observations from the Norman site are plotted for reference (black curve).

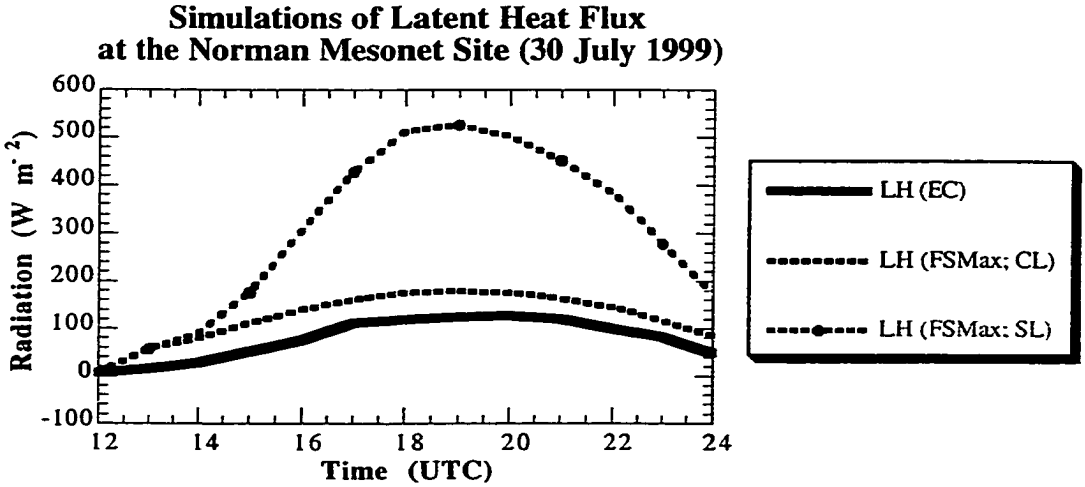

Figure 7.16. Simulations of latent heat flux at the Norman Mesonet site on 30 July 1999 using the clay loam soil parameterization (CL), the silt loam soil parameterization (SL), and soil water determined from field samples (FSMax). Hourly-averaged observations from the Norman site are plotted for reference (black curve).

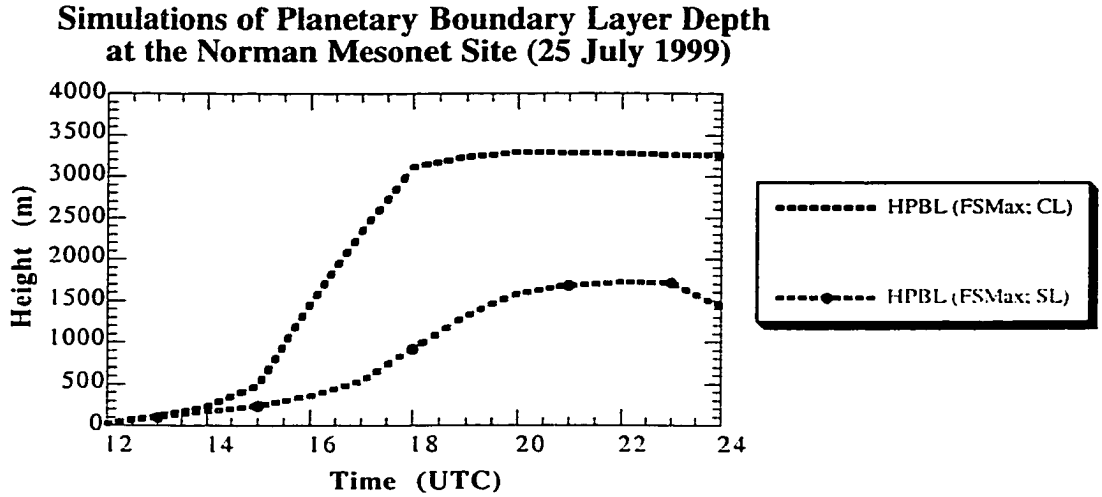

Figure 7.17. Simulated height of the PBL at the Norman Mesonet site on 25 July 1999 using the clay loam soil parameterization (CL), the silt loam soil parameterization (SL), and soil water determined from field samples (FSMax).

Date	FSMax	FSMean	FSMin	229-L
6/26/99	1.3	2.8	4	2.2
7/2/99	0.4	2.2	4.5	7.1
7/3/99	0.3	2.5	109.5	2
7/8/99	4.6	198.7	180.8	74
7/9/99	3	240.5	234.2	217
7/13/99	3.4	208.7	277.7	153.2
7/15/99	0.7	255.1	106.9	255
7/23/99	209.3	76.6	64.5	212.3
7/24/99	194.7	74.9	74.4	171.7
7/25/99	230.2	53.2	77.1	134
7/30/99	202.1	40.7	82.3	56.1
7/31/99	202.2	40.7	93.1	54
8/7/99	148.3	101.1	87.3	72.3

Table 7.13. The difference (absolute value) in maximum daily sensible heat flux computed by the OSU Model between the clay loam parametrization and the silt loam parametrization. Input soil water content values were derived from the maximum, mean, and minimum field sample values as well as from data produced by the 229-L sensor.

Date	FSMax	FSMean	FSMin	229-L
6/26/99	3.7	7.1	10.9	5.4
7/2/99	1.5	5.8	10.8	8.1
7/3/99	0.4	7.5	148.5	5.1
7/8/99	6	263.3	287.3	22.2
7/9/99	8.6	306.7	308.8	227.7
7/13/99	13.2	262.2	352.5	187.4
7/15/99	15.2	313.7	173.2	316.5
7/23/99	294.6	180.2	76.3	319.9
7/24/99	308	140.6	85.1	276.3
7/25/99	334	104.6	89.7	223.8
7/30/99	347.1	38.2	104.9	76.5
7/31/99	346.5	42.8	120.8	68.2
8/7/99	203.6	122	112.8	99.3

Table 7.14. The difference (absolute value) in maximum daily latent heat flux computed by the OSU Model between the clay loam parametrization and the silt loam parametrization. Input soil water content values were derived from the maximum, mean, and minimum field sample values as well as from data produced by the 229-L sensor.

Date	FSMax	FSMean	FSMin	229-L
6/26/99	19.1	6.3	9	2
7/2/99	18.5	7.2	14.5	4.1
7/3/99	20.8	10	10.2	5.1
7/8/99	13.6	2.7	22.3	10.3
7/9/99	2.4	12.1	6.2	17.8
7/13/99	21	3.4	9.1	16.4
7/15/99	21.6	4.6	24.5	0.1
7/23/99	20.6	33	0.4	5.8
7/24/99	23.7	36	0.9	17.7
7/25/99	17.3	32.6	1.5	23.7
7/30/99	20	9.2	0.3	22.9
7/31/99	20.1	5.2	1.4	22
8/7/99	16.2	21.8	4.6	23.2

Table 7.15. The difference (absolute value) in maximum daily ground heat flux computed by the OSU Model between the clay loam parametrization and the silt loam parametrization. Input soil water content values were derived from the maximum, mean, and minimum field sample values as well as from data produced by the 229-L sensor.

Date	FSMax	FSMean	FSMin	229-L
6/26/99	0.3	0.6	1	0.5
7/2/99	0.1	0.8	1.4	2.5
7/3/99	0.1	0.8	27.6	0.6
7/8/99	2	69.4	68.8	24.2
7/9/99	1.1	62.7	59.2	57
7/13/99	1.1	48.7	62.8	32
7/15/99	1.5	64.7	27.8	64.5
7/23/99	80.4	31.5	21.3	81.3
7/24/99	78.4	24.8	22.9	64.9
7/25/99	85.7	17.7	23.3	48.7
7/30/99	75.9	12.3	26.1	17
7/31/99	75.9	12.5	29.6	16.4
8/7/99	40.3	27.9	23.5	18.4

Table 7.16. The difference (absolute value) in maximum daily net radiation computed by the OSU Model between the clay loam parametrization and the silt loam parametrization. Input soil water content values were derived from the maximum, mean, and minimum field sample values as well as from data produced by the 229-L sensor.

Date	FSMax	FSMean	FSMin	229-L
6/26/99	4.7	19.8	22.8	18.3
7/2/99	1.7	19.7	44.9	217.5
7/3/99	12.2	4.6	542.2	3.1
7/8/99	35.7	1241.6	1060.6	516.1
7/9/99	47.2	1000	1038.9	777.8
7/13/99	15.3	328.1	389.4	201.6
7/15/99	60.9	1110.4	540.8	1110.6
7/23/99	1406.8	387.5	179.9	1229
7/24/99	1494	350.1	197.9	776.5
7/25/99	1565.1	32.8	180.2	235.7
7/30/99	1451.1	24.6	152.2	115.3
7/31/99	1453	26.6	158.1	57.3
8/7/99	993.5	550.6	435.1	341.9

Table 7.17. The difference (absolute value) in maximum daily depth of the PBL computed by the OSU Model between the clay loam parametrization and the silt loam parametrization. Input soil water content values were derived from the maximum, mean, and minimum field sample values as well as from data produced by the 229-L sensor.

5 cm were obtained when the "original" calibration coefficients were used. On the contrary, at depths of 25 cm, 60 cm, and 75 cm, the "improved" calibration coefficients provided the most accurate observations when compared with field samples evaluated using traditional methods. Thus, "calibrated" values of 229-L observations refer to the original calibration at the 5 cm depth, and the improved calibration at the deeper depths (25, 60, and 75 cm).

Because many calibration relationships exist among raw observations, soil texture, and individual sensors, an excellent opportunity was available to test the sensitivity of the OSU model to biases in soil moisture observations resulting from measurement uncertainty. For example, the "original" calibration provided accurate observations of soil water at the depth of 5 cm at the Norman site. However, at deeper depths, the original calibration had a significant dry bias. Conversely, the "improved" calibration provided more accurate observations at the deeper depths, but proved to be too moist at 5 cm (especially during extended dry periods). Thus, by using these different calibration relationships, it was possible to test the impact of sensor bias at different layers in the model. Finally, "uncalibrated" sensor output was defined as the improved relationship at 5 cm (generally

too moist) and the original relationship at 25, 65, and 75 cm (generally too dry). A summary of soil moisture conditions used to initialize the PBL model (with respect to varying sensor calibration) appear in Table 7.18.

Simulations initialized with soil moisture from the calibrated sensor values were compared with simulations initialized with soil moisture determined using the original, improved and uncalibrated sensor values. The results of the comparisons revealed large differences in PBL depth, sensible and latent fluxes which were further accentuated by soil texture. Consider the example shown in Figure 7.18 which depicts sensible heat flux initialized with the clay loam soil texture. Because the original sensor calibration produced the driest soil conditions (Table 7.18), the model responded by producing large values of sensible heat flux. Conversely, the model simulation initialized with soil moisture determined using the the least amount of sensible heat flux: the improved sensor calibration produced soil moisture conditions which were wetter than the other calibration relationships (Table 7.18). The range of sensible heat flux using the clay loam parameterization was approximately 354 W m^{-2}.

Similar results were noted for simulations involving latent heat flux (Fig. 7.19). The largest values of latent heat flux were produced by the simulations initialized with the improved sensor calibration and were due to the wetter soil conditions initialized into the model (Table 7.18). In addition, simulations initialized with soil moisture determined from the original calibration were associated reduced values of latent heat flux.

Model simulations involving the biased values of soil moisture were compared with simulations involving calibrated values soil moisture (Tables 7.19 and 7.20). The largest errors were noted when the original calibration was used; the error for the sensible and latent heat fluxes exceeded 230 W m^{-2} for clay loam soil and 270 W m^{-2} for silt loam. In addition, the root mean squared error (RMSE) for sensible and latent heat flux at the time of the daily-maximum values exceeded 136 W m^{-2} for both the clay loam and silt loam simulations.

Inspection of Tables 7.19 and and 7.20. reveals that the simulations initialized with the uncalibrated values of soil water content had smaller errors than those simulations using

soil moisture data computed with the original or improved calibration coefficients. Because the original calibration resulted in a dry bias at the deeper depths, the combination of actual dry conditions at the surface and the dry bias at deeper depths lead to an entire soil profile which was drier than profiles computed using the calibrated, improved, or uncalibrated coefficients. Conversely, the improved calibration resulted in values of soil water which were too moist at the surface. Consequently, the soil profile using the values of soil water determined via the improved calibration was more moist than the other profiles. Recall that the uncalibrated values of soil moisture were too moist near the surface and too dry at deeper depths. However, this resulted in a moderate soil wetness throughout the soil profile and results which were closer in comparison to the simulations initialized with calibrated values of soil water.

The most dramatic results were noted when biased soil moisture values were coupled with changes in soil texture. Consider the example where the soil moisture values computed using the original calibration were used to initialize the OSU model on 15 July (Fig. 7.20). Because the original calibration produced very dry soil moisture values, simulations of latent heat were limited. Even so, the simulation using the silt loam soil texture produced latent heat flux which peaked at 137 W m^{-2}. However, when the soil texture was changed to clay loam, latent heat flux was not produced during the entire 12 hour simulation (a peak value of 0 W m^{-2})! Inspection of Table 7.18 reveals the reason why latent heat flux was not produced for the clay loam simulation. Recall that the wilting point for clay loam was 0.18 cm^3/cm^3 (Fetter 1988). However, the original sensor calibration produced water content values of 0.177 and 0.155 cm^3/cm^3 as input for the 0-5 and 5-100 cm layers of the model. Thus soil moisture conditions in the entire model profile were below the wilting point. As a result, there was no available water in the soil profile for evaporation or transpiration. Thus, the model did not produce any values of latent heat flux. Conversely, the wilting point of silt loam was 0.10 cm^3/cm^3. Thus, the limited amount of available water allowed the model to produce values of latent heat flux throughout the simulation.

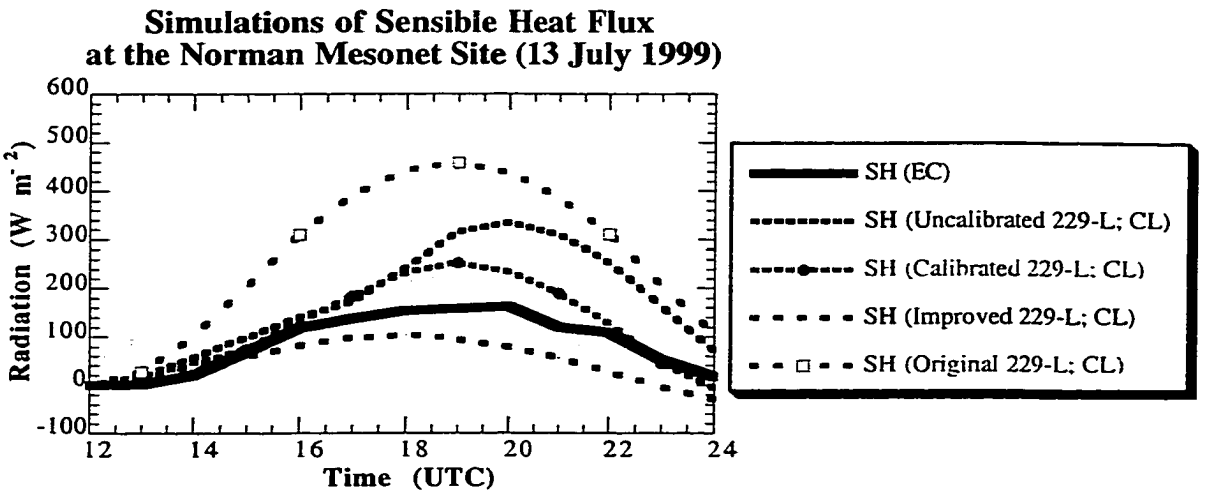

Figure 7.18. Simulations of sensible heat flux at the Norman Mesonet site on 13 July 1999 using the clay loam soil parameterization (CL). Soil water content was determined using various calibrations applied to the 229-L sensor. Hourly-averaged observations from the Norman site are plotted for reference (black curve).

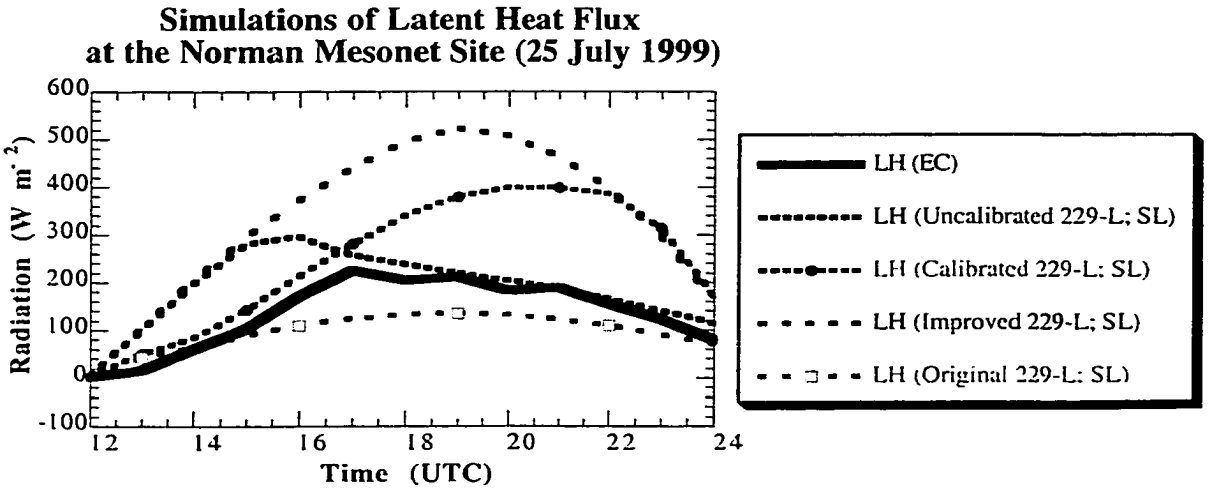

Figure 7.19. Simulations of latent heat flux at the Norman Mesonet site on 25 July 1999 using the silt loam soil parameterization (SL). Soil water content was determined using various calibrations applied to the 229-L sensor. Hourly-averaged observations from the Norman site are plotted for reference (black curve).

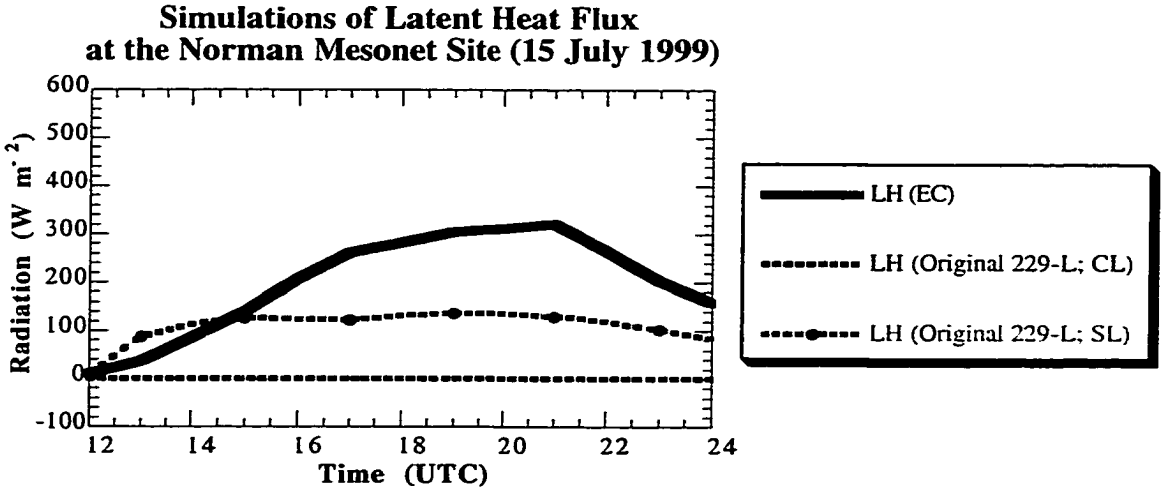

Figure 7.20. Simulations of latent heat flux at the Norman Mesonet site on 15 July 1999 using the clay loam soil parameterization (CL) and the silt loam soil parameterization (SL). Soil water content was determined using "original" calibration coefficients applied to the 229-L sensor. Hourly-averaged observations from the Norman site are plotted for reference (black curve).

	Calibrated	Calibrated	Original	Original	Improved	Improved	Uncalibrated	Uncalibrated
	229-L	229-L	229-L	229-L	229-L	229-L	229-L	229-L
Date	5 cm	25-75 cm	5 cm	25-75 cm	5 cm	25-75 cm	5 cm	25-75 cm
6/26/99	0.499	0.372	0.499	0.305	0.439	0.372	0.439	0.305
7/2/99	0.49	0.376	0.49	0.312	0.428	0.376	0.428	0.312
7/3/99	0.381	0.375	0.381	0.312	0.374	0.375	0.374	0.312
7/8/99	0.191	0.349	0.191	0.261	0.295	0.349	0.295	0.261
7/9/99	0.16	0.339	0.16	0.247	0.271	0.339	0.271	0.247
7/13/99	0.254	0.326	0.254	0.184	0.328	0.326	0.328	0.184
7/15/99	0.177	0.299	0.177	0.155	0.285	0.299	0.285	0.155
7/23/99	0.124	0.286	0.124	0.179	0.215	0.286	0.215	0.179
7/24/99	0.124	0.279	0.124	0.169	0.215	0.279	0.215	0.169
7/25/99	0.123	0.274	0.123	0.16	0.214	0.274	0.214	0.16
7/30/99	0.121	0.254	0.121	0.127	0.208	0.254	0.208	0.127
7/31/99	0.121	0.252	0.121	0.123	0.208	0.252	0.208	0.123
8/7/99	0.134	0.254	0.134	0.127	0.237	0.254	0.237	0.127

Table 7.18. Soil water content used to initialize the 0-5 and 5-100 cm layers of the OSU model.

	Range	Range	Range	Range	Range
Clay Loam	SH	LH	GH	Rnet	HPBL
Improved	187.4	231.3	33.6	54.9	645.1
Original	236.9	254.3	35.8	54.9	1159.9
Uncalibrated	194.4	181	44.1	40.4	1238.4
Silt Loam					
Improved	189.9	245.3	23.6	54.4	1312.5
Original	274.8	341.6	22.2	73.8	1162.4
Uncalibrated	158.9	131.1	25.8	42.6	864.7

Table 7.19. The maximum difference between PBL parameters computed using calibrated values of soil water content from the 229-L sensors and values of soil water content determined for the original, improved, and uncalibrated 229-L sensors.

	RMSE	RMSE	RMSE	RMSE	RMSE
Clay Loam	SH	LH	GH	Rnet	HPBL
Improved	76.2	104.8	20.4	21.8	289.4
Original	136.2	166.4	17.5	37.6	521.8
Uncalibrated	96.1	117.5	27	24.7	396.4
Silt Loam					
Improved	74.4	111.9	9.3	25.7	669.9
Original	136.7	178.5	16.6	39.2	513
Uncalibrated	76.9	64.4	16.4	17.4	311.1

Table 7.20. Root mean squared error between PBL parameters computed using calibrated values of soil water content from the 229-L sensors and values of soil water content determined for the original, improved, and uncalibrated 229-L sensors. RMSE was computed using data from the 13 *ideal* study days.

7.3.4 Comparison of Soil Hydraulic Properties with Other Land-Surface Parameters

To assess the importance of soil hydraulic properties in the sensitivity of the model, additional land-surface properties were varied within the model. First, it was assumed that the mean value of soil water content determined from field samples were the "most representative" values of soil water at the site. Crawford (1998) demonstrated that albedo varied between 0.18 and 0.22 at the Norman Mesonet site during the summer months. Thus a set of simulations were conducted which used the aforementioned range in albedo. A second set of simulations varied the canopy resistance, which, in the original simulations, was held at a value of -50. However, to provide reasonable variability in this model parameter, canopy resistance was decreased by a factor of 2 (-100) to simulate the the minimum resistance and increased by a factor of to (-25) to simulate the maximum value of resistance. Finally, a parameter which impacts bare soil evaporation in the model is the shade factor; the shade factor varies from 0 (no vegetation) to 1 (fully vegetated conditions and no exposed soil). To represent extreme conditions at the Norman site (such as in an extended drought), the shade factor was decreased to 0.2. Conversely, a second set of simulations involved a shade factor of 0.8 which represented lush and vibrant vegetation. For each set of surface variations (albedo, canopy resistance, and shade factor) model simulations were performed for both clay loam and silt loam soil textures soils.

The variation in surface albedo had limited impacts on the simulation of surface fluxes and PBL depth (Tables 7.21 and 7.22). The impact of varying the albedo resulted in a range of sensible heat flux (at the daily maximum) which was less than 25 W m^{-2}. Similarly, the range of latent heat flux was less than 25 W m^{-2}, ground heat flux values were less than 5 W m^{-2}, and net radiation was less than 36 W m^{-2}. The results combined to produce model simulations of PBL depth (at the daily maximum) which ranged less than 177 meters.

When canopy resistance was varied in the model, the range of values associated with PBL parameters (daily maximum) increased relative to those simulations which used variations in albedo (Tables 7.23 and 7.24). In the case of canopy resistance, sensible heat flux varied between 31 and 97 W m^{-2} and the range of values for latent heat flux varied

between 55 and 131 W m^{-2}. However, the range of ground heat flux values (6 to 20 W m^{-2}) and net radiation values (10 to 31 W m^{-2}) were much reduced compared to the fluxes of sensible or latent heat. The combined impact of the variability in heat fluxes and net radiation resulted in PBL depth which ranged from 67 to 595 meters.

The greatest variation of atmospheric processes simulated by the OSU model (aside from soil moisture or texture) was caused by the shade factor (Tables 7.25 and 7.26). For example, sensible heat flux varied between 37 and 156 W m^{-2} at the time of the daily-maximum values. Similarly, latent heat flux varied between 40 and 210 W m^{-2}. However, the variability in ground heat flux and net radiation was less than 35 and 50 W m^{-2} respectively. Due the variability of the surface fluxes, the depth of the PBL varied between 165 and 810 meters.

7.3.5 Test for Linearity

When soil moisture conditions were compared with observations of atmospheric processes in Chapter 5, nonlinear relationships were found at very shallow soil depths (0-10 cm). However, the relationship between soil water content in the root zone and atmospheric processes in the PBL was linear. This portion of the narrative will focus on the ability of the model to produce the aforementioned linear/nonlinear relationships.

As in Chapter 5, the mean soil water determined from field samples and observations from the 229-L sensors were compared with atmospheric processes. However, because deep-layer soil in the model was represented by a layer spanning 5-100 cm, the layer averages of calibrated 229-L observations and FSMean values were used (Table 7.2). Once the values of soil water content were used to initialize the OSU model the fluxes of sensible and latent heat as well as PBL depth were computed. The peak values of these parameters were compared with the input soil moisture values to assess the ability of the model to generate the observed linear processes. The simulations were duplicated for clay loam and silt loam textures soils.

Table 7.27 displays the linear correlation values when model generated fluxes and PBL depth were compared with soil water values used as input. The results reveal a number

Date	SH	GH	LH	Rnet	HPBL
6/26/99	8.7	3.4	24.6	35.3	49.3
7/2/99	8	3.5	24.3	34.8	52.8
7/3/99	7.7	3.3	24.9	35	50
7/8/99	20.9	3.4	7.4	30.8	110.9
7/9/99	22.2	3.4	6.6	31.7	176.2
7/13/99	24	4	5.7	32.3	109.4
7/15/99	22.8	2.4	7.2	31.8	87.7
7/23/99	21.5	3	6.8	29.1	41
7/24/99	23	2.2	6.3	29.9	99.1
7/25/99	23	2.5	6	29.3	10.3
7/30/99	22.9	1.6	5	29.3	14.3
7/31/99	23.1	1.6	4.8	29.2	15.5
8/7/99	23.5	2.4	4.8	30	169.3

Table 7.21. The range (absolute value) of PBL parameters computed using the OSU model with variations in albedo. Soil texture was parameterized as clay loam.

Date	SH	GH	LH	Rnet	HPBL
6/26/99	8.7	3.6	24.4	35.4	50.5
7/2/99	7.7	3.9	23.9	34.9	52.7
7/3/99	7.6	3.8	24.7	35	52.3
7/8/99	9.8	3.3	20.8	33.8	91.4
7/9/99	8.8	2.7	24.1	34.9	71.7
7/13/99	8.5	3.9	24.6	35	28.9
7/15/99	8.6	2.6	24.9	34.7	52.1
7/23/99	17.3	3.4	5.1	29.5	83.2
7/24/99	19.2	4.2	4.7	30.1	101.4
7/25/99	19.5	4	4.7	29.9	15
7/30/99	21.1	2.9	6.7	29.8	7.6
7/31/99	21.2	2.8	6.7	29.8	8.9
8/7/99	21.5	3	6.5	30.7	41

Table 7.22. The range (absolute value) of PBL parameters computed using the OSU model with variations in albedo. Soil texture was parameterized as silt loam.

Date	SH	GH	LH	Rnet	HPBL
6/26/99	49.5	15.4	80	13.1	229
7/2/99	32.6	15.2	56	11.3	169.3
7/3/99	36.7	15.4	66.3	12.1	170.1
7/8/99	72.3	13.4	101.8	22.4	253.5
7/9/99	82.2	13.9	105.9	20.6	594.7
7/13/99	81.7	16.4	103.8	17.7	168.2
7/15/99	87.9	8.9	121.1	21.3	415
7/23/99	85.3	11.5	120.7	29.9	232.9
7/24/99	94.5	9.1	128.1	29.7	251.3
7/25/99	96.3	10.6	130.6	30.8	181.5
7/30/99	87.8	6.9	122.8	28	146
7/31/99	86.6	6.7	121.2	27.7	146.5
8/7/99	85.8	8.9	117.1	23.1	399.2

Table 7.23. The range (absolute value) of PBL parameters computed using the OSU model with variations in the canopy resistance. Soil texture was parameterized as clay loam.

Date	SH	GH	LH	Rnet	HPBL
6/26/99	47.8	19.3	78.7	12.5	201.7
7/2/99	31.3	16.2	55.7	10.9	154.7
7/3/99	35.2	16.8	64.9	11.5	180.2
7/8/99	51.4	18.7	90.2	18.1	354.7
7/9/99	52.7	16.1	86.1	14.9	315
7/13/99	47.8	9.1	80.5	13.5	116.1
7/15/99	54.2	15.2	85.6	16	211.1
7/23/99	65.5	14.6	83.2	27	341.6
7/24/99	73.1	14.7	90.7	26.8	256.2
7/25/99	81.3	17	85.8	28.8	67.5
7/30/99	91.1	13.3	130.3	29	162.6
7/31/99	92	12.7	130.7	29.2	163.4
8/7/99	85.9	12.6	116	22.1	424.8

Table 7.24. The range (absolute value) of PBL parameters computed using the OSU model with variations in the canopy resistance. Soil texture was parameterized as silt loam.

Date	SH	GH	LH	Rnet	HPBL
6/26/99	81	25.3	133.8	20.2	332.7
7/2/99	37.6	21.6	67.5	13.3	195.4
7/3/99	46.1	23.9	89.5	15.2	258.1
7/8/99	127.6	23.1	168.2	40.3	549.7
7/9/99	117.1	18.4	135.6	30.5	809.6
7/13/99	78.2	17.9	88.1	17.7	168.5
7/15/99	130.4	11	181.4	32.3	596.7
7/23/99	138.5	15.9	199.6	49.5	417.6
7/24/99	155.3	14.3	210	49.2	467.4
7/25/99	147.6	14.9	201.3	47.7	214.2
7/30/99	115.7	8.5	165.8	37.3	168.1
7/31/99	112.3	8.1	161	36.2	165.4
8/7/99	107.9	10.1	151.8	29.5	572

Table 7.25. The range (absolute value) of PBL parameters computed using the OSU model with variations in the shade factor. Soil texture was parameterized as clay loam.

Date	SH	GH	LH	Rnet	HPBL
6/26/99	77.9	28.7	128.7	19.6	319.4
7/2/99	36.9	20.1	65.2	13.2	183.7
7/3/99	44.4	22.2	84.4	14.6	246.3
7/8/99	73.9	34.1	132.3	25.2	499.9
7/9/99	91.4	26.3	138.2	22	485.5
7/13/99	86.6	11.2	151.9	23.8	199
7/15/99	93.1	26.1	136.9	23.2	367.9
7/23/99	80.7	16.7	40.8	27.1	363.2
7/24/99	104.3	23	61	34.6	306.9
7/25/99	122.3	25.6	72.8	40.7	182.7
7/30/99	142.5	21	212	46.1	282.9
7/31/99	143.7	19.8	212.3	46.4	281
8/7/99	95.1	7.9	139.5	24.2	450.5

Table 7.26. The range (absolute value) of PBL parameters computed using the OSU model with variations in the shade factor. Soil texture was parameterized as silt loam.

(Input Soil Water Content; Soil Texture)	Model 0-5 cm	Model 5-100 cm
SH (FSMean Water Content, CL)	0.798	0.688
SH (FSMean Water Content, SL)	0.506	0.801
LH (FSMean Water Content, CL)	0.849	0.714
LH (FSMean Water Content, SL)	0.438	0.753
HPBL (FSMean Water Content, CL)	0.928	0.876
HPBL (FSMean Water Content, SL)	0.693	0.872
SH (Calibrated 229-L Water Content, CL)	0.721	0.801
SH (Calibrated 229-L Water Content, SL)	0.198	0.563
LH (Calibrated 229-L Water Content, CL)	0.705	0.878
LH (Calibrated 229-L Water Content, SL)	0.141	0.42
HPBL (Calibrated 229-L Water Content, CL)	0.794	0.96
HPBL (Calibrated 229-L Water Content, SL)	0.459	0.831

Table 7.27. Linear correlation between soil moisture and atmospheric parameters simulated using the OSU model for the silt loam (SL) and clay loam (CL) parameterizations of soil texture.

of interesting patterns. For example, the relationship between sensible heat flux at the time of the daily-maximum values simulated using the clay loam soil texture and water content determined from field samples at 5 cm appeared to be linear (variance of 0.798; Fig. 7.21). The linear relationship decreased when soil water in the 5-100 cm layer (FSMean) is compared with the daily-maximum values of sensible heat flux (Fig. 7.22; variance of 0.688)). However, the opposite occurred when the soil texture is changed from silt loam to clay loam. In that case, the relationship between soil moisture (FSMean values) and sensible heat flux at the daily-maximum is nonlinear near the surface (0-5 cm; Fig. 7.21) and linear at deeper depths (5-100 cm; 7.22). Similar results were observed for simulated values of latent heat flux (Figs. 7.23 and 7.24) and PBL depth (Figs. 7.25 and 7.26).

A different pattern was observed when calibrated values of soil water (the 229-L sensors) used to initialize the model were compared with PBL depth and surface fluxes. First, the correlation increased from the shallow soil depths to the deeper soil depths for every simulation regardless of soil texture. Thus, linearity increased with depth for these simulations. However, the simulations involving the silt loam soil texture had smaller

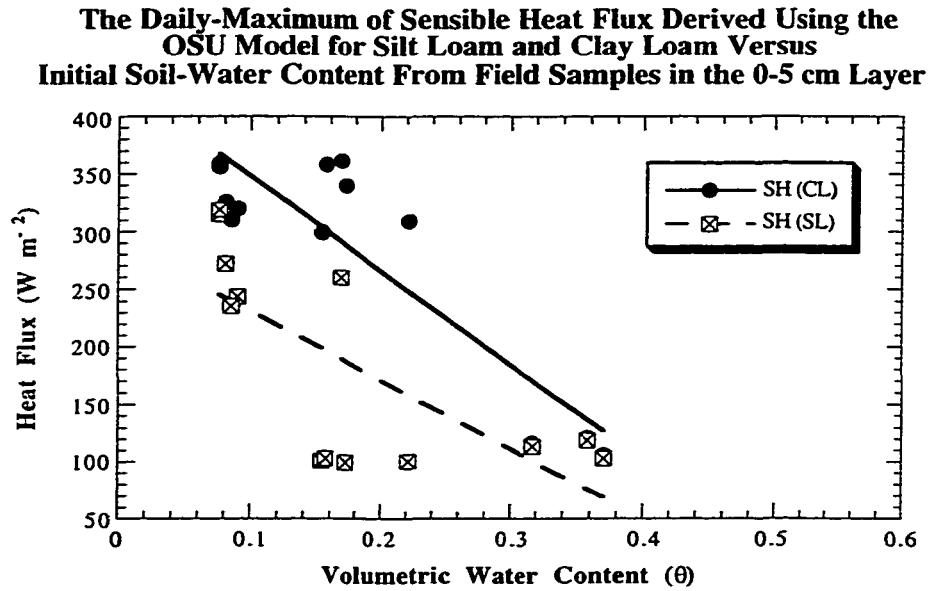

Figure 7.21. The daily-maximum values of sensible heat flux determined using the OSU model for the clay loam (CL) and silt loam (SL) parameterizations of soil texture versus initial soil water content estimated from field samples in the 0-5 cm layer.

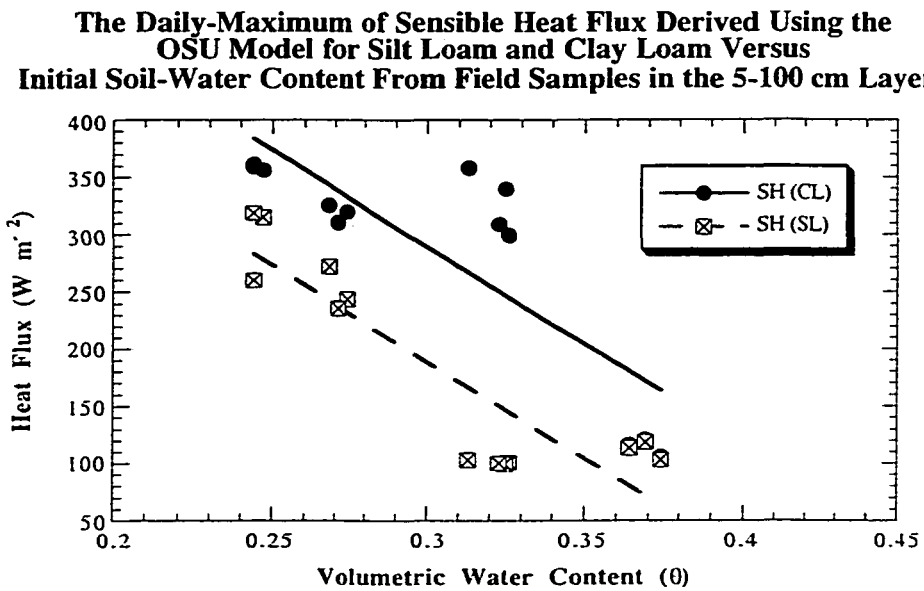

Figure 7.22. The daily-maximum values of sensible heat flux determined using the OSU model for the clay loam (CL) and silt loam (SL) parameterizations of soil texture versus initial soil water content estimated from field samples in the 5-100 cm layer.

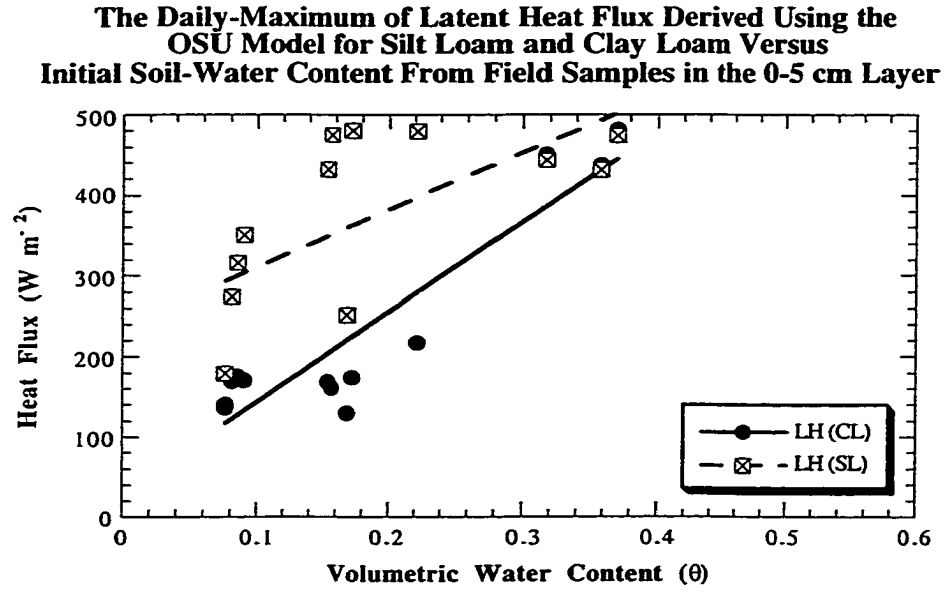

Figure 7.23. The daily-maximum values of latent heat flux determined using the OSU model for the clay loam (CL) and silt loam (SL) parameterizations of soil texture versus initial soil water content estimated from field samples in the 0-5 cm layer.

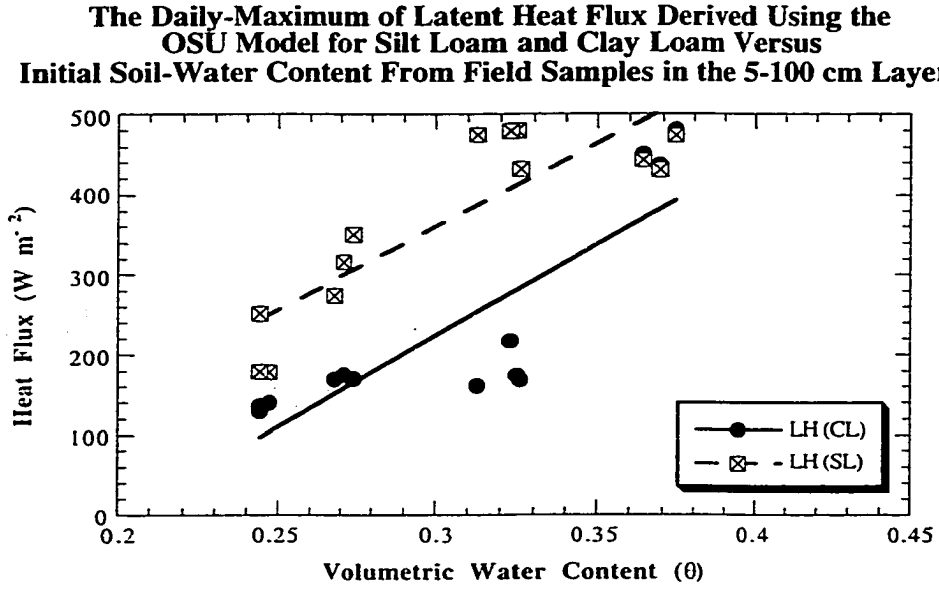

Figure 7.24. The daily-maximum values of latent heat flux determined using the OSU model for the clay loam (CL) and silt loam (SL) parameterizations of soil texture versus initial soil water content estimated from field samples in the 5-100 cm layer.

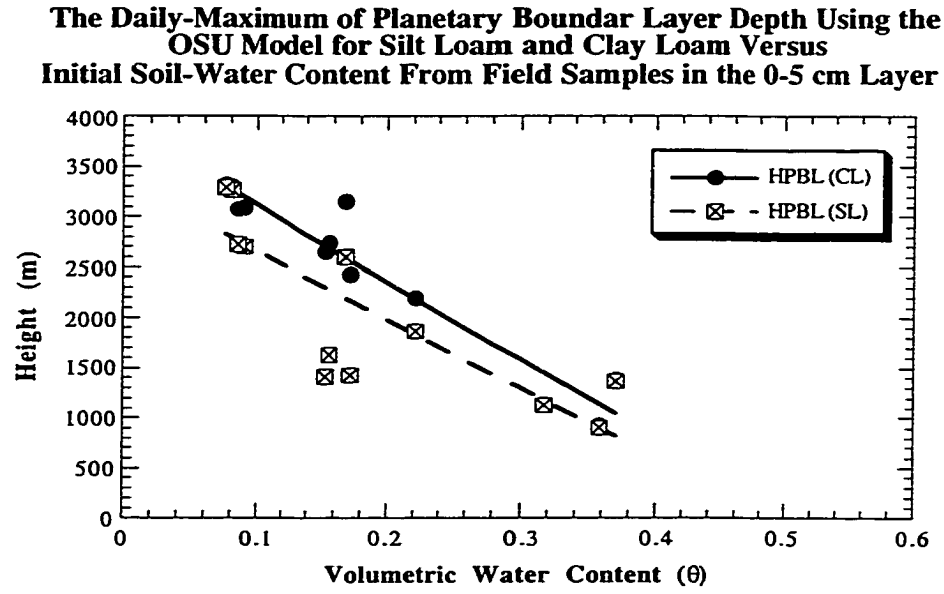

Figure 7.25. The daily-maximum values of PBL depth determined using the OSU model for the clay loam (CL) and silt loam (SL) parameterizations of soil texture versus initial soil water content estimated from field samples in the 0-5 cm layer.

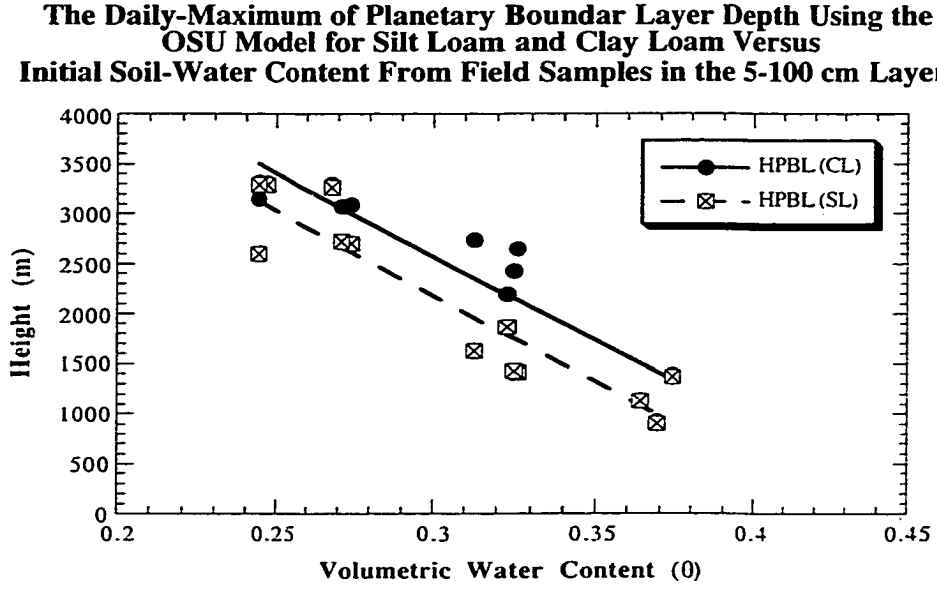

Figure 7.26. The daily-maximum values of PBL depth determined using the OSU model for the clay loam (CL) and silt loam (SL) parameterizations of soil texture versus initial soil water content estimated from field samples in the 5-100 cm layer.

correlations when compared with clay loam. This implies that the change from clay loam to silt loam greatly reduced the linearity between the atmospheric processes simulated in the model, and initial values of soil moisture.

A final trend worth noting concerns the model simulated values of PBL depth. Inspection of Table 7.27 revealed that the strongest linear relationship between atmospheric processes and initial soil water occurred with respect to PBL depth. For example, the variance of sensible heat flux initialized with FSMean values of soil water and a clay loam soil texture at 5 cm was 0.798. Latent heat flux had a value of 0.849 for the same initial conditions. However, PBL depth had an variance of 0.928. Thus, the linear relationship between PBL depth and soil water content was stronger than either sensible or latent heat flux.

7.4 Discussion

The results of Section 7.3 clearly establish that the OSU PBL model was sensitive to natural variability in *both* soil texture and soil moisture. In many of the cases studied, significant variability was noted in the surface fluxes and the growth of the PBL. Most if not all of the variability associated with atmospheric processes simulated by the OSU model can be explained by examining Figure 7.27. In the OSU model, the complex relationship between soil water, texture and pressure (potential) is parametrized with empirical soil water release curves developed by Clapp and Hornberger (1978). The soil water release curves for the two soil textures used in this study (clay loam and silt loam) are plotted in Figure 7.27.

Consider the hypothetical case where the FSMax, FSMean, and FSMin values of soil water content are 0.3, 0.25, and 0.2 cm^3/cm^3 respectively. Those values of soil water are plotted on the release curves for silt loam and clay loam (Fig. 7.27). Though the degree of soil "wetness" is determined by the soil water content, the energetics of water in the soil is related to potential. Thus, as potential decreases (toward the right of the plot), the surface tension between soil particles and the water in the soil increases. This increase in tension limits the movement of water in the soil.

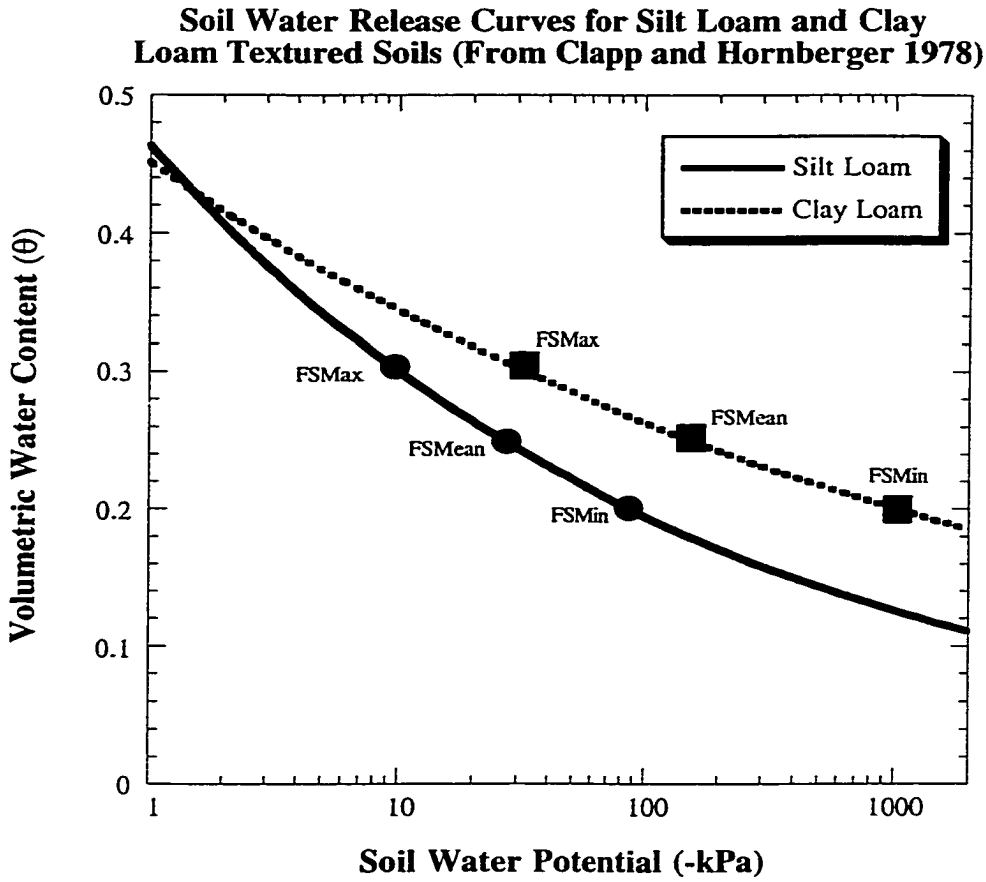

Figure 7.27. Soil water release curves in the OSU model for silt loam and clay loam textured soils (determined from Clapp and Hornberger 1978).

In moving from the FSMax, to FSMean, and to FSMin on the release curve for silt loam not only decreases the soil water content, but increases the soil water pressure (potential). In fact, the soil water pressure increases by an order of magnitude between values of soil water content at the FSMax value versus the FSMin value. The resulting difference between these 2 points results different amounts of water available for evaporation or transpiration. Thus, there is less available water at the FSMin value than the FSMax value which results in a greater partitioning of available energy to sensible heat flux versus latent heat flux in the model. Furthermore, since the value of FSMax represents soil water which is unstressed, the available water is much greater and latent heat flux dominates the partitioning of available energy in the model. The results of Section 7.3.1 support this

analysis. In all simulations conducted using field sample values of soil water content, sensible heat flux was greatest in simulations initialized with FSMin values while latent heat flux was greatest in simulations initialized with FSMax values.

The model simulations are complicated by multiple soil layers. Even so, the controlling factor on available water for evaporation in the model is controlled by both the water content and the water potential. When the water potential is between 0 and 30 kPa, the soil is unstressed. In Figure 7.27, this represents water contents greater than 0.25 cm^3/cm^3 for the silt loam soil texture. If, for example, the soil water content varied between 0.45 and 0.35 cm^3/cm^3, the available water would still be virtually the same and the model fluxes would not vary a great deal. This was evident in the simulations on 2 July. Conversely, as the soil dries, the soil wetness decreases as the soil water pressure increases. Thus, even though water content may vary 0.10 cm^3/cm^3 the limited amount of water combined with the large tensions results in limited variability of sensible or latent heat fluxes (such as 30 July).

The largest range of heat fluxes occurred when one set of input values in the soil profile were at unstressed values while another profile of soil used soil water at stressed values. This occurred for simulations on 15 and 23 July as well as 7 August. The soil profiles which were at relatively unstressed (stressed) values of soil water content produced much larger values of latent (sensible) heat flux than did those which were at greater (lesser) values of soil water pressure. The difference between the July cases and the 7 August case was that the variability of soil moisture in July was due to differential drying rates of the soil profile during an extended dry period However, the variability in soil water content observed on 7 August was due to a precipitation event.

A further sensitivity observed in the model simulations was the differential soil texture. Inspection of Figure 7.27 reveals that the same values of soil water content were at a different values of soil water pressure for the 2 soils. Thus, when soil texture was changed from clay loam to silt loam in the simulations, the soil water pressure decreased. As a result, more soil water was available for evapotranspiration in the model, and latent heat flux increased. Conversely, the change from clay loam to silt loam resulted in less sensible heat flux being produced by the model. This explains why simulations using the clay loam

parametrization always produced more sensible heat (at a given water content) than those using silt loam. However, as seen in Section 7.3.2, the range of simulated PBL parameters was greater during certain soil conditions than others. Again, this can be explained by considering Figure 7.27. Note that the FSMean value of soil water content along the clay loam curve is in a stressed environment. However, a change to silt loam results in the FSMean value of water content being unstressed. Just as in the variability of soil water content, the largest range of heat fluxes occurred when one input value (or set of values in the soil profile) of soil water was unstressed value while another was stressed. In this case, the change from stressed to unstressed soil water conditions (or vice versa) was due to soil texture variability.

Unfortunately, the relationships between soil water content and texture also apply to input values of soil water computed using the 229-L sensor. Since different calibration techniques resulted in different values of soil water initialized into the model, atmospheric processes were impacted. The greatest impact on PBL processes occurred when one soil profile was under stressed water conditions while another was unstressed. This was particularly evident between the improved calibration (wet soil profile; unstressed) and the original calibration (stressed). The results clearly show that the original calibration continuously produced more sensible heat flux than the improved calibration. Conversely, model simulations initialized with soil water (improved calibration) produced greater values of latent heat flux than the original calibration.

Alternative model simulations were conducted to assess the variability of the model to other land surface features such as albedo, canopy resistance, and the shade factor. However, the variability in atmospheric processes simulated using the OSU model caused by variability in soil moisture, soil texture, and sensor calibration were greater than those caused by albedo, canopy resistance, or the shade factor. In the case of alibied, the natural variability resulted in limited variability in surface fluxes. Changes to canopy resistance produced sensible and latent heat fluxes which consistently varied ~100 W m^{-2}. This was still quite small compared to the range of sensible and latent heat flux (each in excess of 250 W m^{-2}) caused by variability in soil moisture and soil texture. The only land surface

Simulation	RMSE SH	RMSE LH	RMSE GH	RMSE Rnet	RMSE HPBL
Calibrated 229-L; CL	89.1	90.2	105.5	108.7	776.7
Improved 229-L; CL	47.7	92.7	98.7	95	652.1
Original 229-L; CL	195.4	203.8	106.6	142.5	1111.7
Uncalibrated 229-L; CL	155.3	156.4	90.2	127	935.6
Calibrated 229-L; SL	66.1	143.9	97.2	75.2	566.8
Improved 229-L; SL	114.3	209.3	99.3	70.3	508
Original 229-L; SL	105.4	127.4	106.6	105.1	845.5
Uncalibrated 229-L; SL	37.7	116.2	100.1	86.1	600.5
Simulation	**RMSE SH**	**RMSE LH**	**RMSE GH**	**RMSE Rnet**	**RMSE HPBL**
FSMax; CL	48.9	98.5	110.2	92.6	581.5
FSMean; CL	100.2	105.8	99.6	116.1	866.4
FSMin; CL	137.4	136.8	121.4	128.7	984.8

Table 7.28. Root mean squared error (RMSE) between the daily-maximum value of PBL parameters computed using the OSU model and the hourly-averaged daily-maximum values observed at the Norman Mesonet site. RMSE was computed using data from the 13 *ideal* study days.

property which compared in magnitude with the simulations involving soil moisture and soil texture was the shade factor. Unfortunately, the variability in shade factor was extreme and would not occur naturally on the time scale of days. Rather, the variability in shade factor would take place over a course of weeks or months.

Finally, the model was examined to determine if it produced linear relationships between atmospheric processes in the PBL and root-zone soil moisture similar to those documented in Chapter 5. Though some simulations produced linear relationships between root-zone soil moisture and atmospheric processes (e.g., FSMax and silt loam), a simple change of soil texture produced nonlinear results (FSMax and clay loam). In the case of model simulations initialized with the calibrated 229-L observations and clay loam textured soils, the relationships appeared linear at both model depths (slightly stronger relationships in the 5-100 cm layer). However, the same soil moisture observations initialized with the silt loam soil parametrization resulted in nonlinear relationships throughout the soil column. Furthermore, the strongest relationships between soil moisture and atmospheric processes were with the depth of the PBL. This is opposite to what was noted in Chapter 5. Thus, the

model did accurately simulate the linear relationships between root-zone soil moisture and PBL parameters.

Overall the OSU model proved to be very useful in determining the sensitivity of PBL simulations to variability in soil moisture, texture, and sensor calibration. However, a number of consistent biases were noted in the model simulations. First, the model consistently underestimated ground heat flux. In fact, the daily-maximum values of ground heat flux observed at the site were nearly 100 W m^{-2} greater than those produced by the model regardless of soil texture. In addition, the model consistently underestimated net radiation by approximately 80 W m^{-2} while it consistently overestimated PBL depth.

No single simulation technique proved to be affective when compared with the hourly-averaged values of heat flux, net radiation (daily maximum), or PBL depth (Table 7.28). However, simulations initialized with the "original" calibration values of soil moisture from the 229-L sensor and the clay loam soil texture had the largest RMSE errors (at the time of daily-maximum values) when compared with hourly-averaged observations at the time of the daily-maximum values at the Norman site.

Chapter 8

Summary and Concluding Remarks

The hypothesis of this dissertation was that *point-scale observations of soil moisture conditions, greatly affected by instrumentation errors and naturally occurring variability of soil hydraulic properties, have a limited but quantifiable impact on simulations and computations of atmospheric processes in the PBL.* To investigate the validity of this hypothesis, over 2,000 soil samples were collected from the Norman Mesonet site. Using these field samples, the spatial and temporal variability of soil moisture was quantified to a depth of 80 cm between the dates of 1 June and 7 August 1999. Then, the nature of land-atmosphere interactions using field and in situ observations at and near NORM was investigated. Next, the sensitivity of ground heat flux measurements at NORM was tested using observed spatial variability in soil water. Finally, the observed spatial variability in soil moisture and texture permitted a unique examination of the sensitivity of the OSU model to variability in soil hydraulic parameters.

Due to the limited number of soil moisture observations, soil moisture remains a critical scientific issue in determining the impact of land surface conditions on atmospheric processes. Many studies have sought to quantify the variability of soil moisture (e.g., Hills and Reynolds 1969; Bell et al. 1980; Hawley et al. 1983; Loague 1992; Nyberg 1996; and Famigletti et al. 1998) while others have used complex numerical models to simulate land atmosphere interactions (e.g., Troen and Mahrt 1986; Pan and Mahrt 1987; Delworth and Manabe 1989; Koster et al. 2000). However, little effort has been made to coordinate these types of field observations (especially deep-layer samples of soil moisture) and observed atmospheric conditions with current models that couple the land surface to the atmosphere. In fact, many studies simply use soil moisture as a boundary condition to the atmosphere. In the case of coupled schemes, others use a one-dimensional mode whereby mass and energy are exchanged between the land-surface and the atmosphere. Few studies, if any, have been published which test the sensitivity of near-surface atmospheric components simulated by a numerical model (on a local scale) with the *measured* variability of soil water content in space and time. Thus, this dissertation is among the first studies to quantify the

variability in soil hydraulic conditions at a location able to measure energy balance components and then use those observations to test the sensitivity of a coupled land-atmosphere model.

To complete the examination of the OSU model, observations of soil and atmospheric parameters were collected at the Norman Mesonet site. In situ observations collected at the site were processed through automated QA routines (Shafer et al. 2000). In addition, field samples of soil were analyzed in the laboratory to determine mineral composition and water content. Intercomparisons were conducted between automated soil moisture sensors (229-L) and field samples to calibrate and validate the in situ observations of soil water content. The key results include:

1. At the Norman site, 2,792 soil samples were collected from 12 predetermined locations at depths ranging between 0 and 80 cm. The samples quantified the spatial and temporal variability of soil water content and soil texture at the site.

2. The greatest variability in soil water content followed precipitation events. However, this increased variability was limited to near-surface soil (0-20 cm) and decreased during extended dry periods.

3. Over the course of the 73-day study period, the mean standard deviation of soil water was nearly uniform with depth. Nevertheless, since values of water content tended to be less near the surface, the coefficient of variation was greatest in the near-surface (0-20 cm) soil layer and decreased with depth.

4. The performance of the automated soil moisture sensors (229-L) was investigated using field samples of soil water content and several algorithms used to compute soil water. It was determined that, at the Norman site, the original calibration provided the best measurements of soil water content for the 5 cm depth. Conversely, the improved calibration performed best at the depths of 25, 60, and 75 cm.

5. An error in soil water measured by sensors at depths of 60 and 75 cm was detected. Errant output from the sensor was due to the manner in which the sensors were installed (Basara and Crawford 2000).

Once the observations were collected, soil samples were analyzed, and the 229-L sensors were calibrated and validated, the relationship between soil water and atmospheric processes was examined. First, 13 days were classified as *ideal* since solar radiation was at or near its theoretical maximum (no cloud cover) and shear in the lower troposphere was weak. Second, the field samples of soil water content were interpolated to those dates when manual samples were not collected. Finally, the mean value of soil water determined from field samples (FSMean) and observations from the 229-L sensors were compared with measurements of energy fluxes and other atmospheric parameters measured at or near the site. Key results include:

1. The relationship between soil water near the surface (0-10 cm) was nonlinearly related to PBL processes. However, soil water in the root-zone (20-60 cm) was linearly related to PBL processes. Furthermore, the aforementioned nonlinear/linear relationships were discovered and verified using 2 independent soil moisture data sets and atmospheric observations which were measured at the site as well as from balloon observations which spanned the depth of the PBL.

2. It was discovered that closure of the surface energy balance was linearly related to root-zone soil moisture while near-surface soil water and closure were nonlinearly related. Thus, soil water in the root-zone has a much stronger controlling influence on closure than does surface soil moisture.

3. The relationship between root-zone soil water and thermal parameters such as air temperature at 1.5 meters or potential temperature in the PBL, was stronger than the relationship between root-zone soil moisture and moisture in the near surface

atmosphere (mixing ratio at 1.5 meters or in the PBL).

4. It was concluded that the media responsible for the linear relationships between root-zone soil moisture and atmospheric processes in the PBL was vegetation at the site.

After quantifying the relationship between soil moisture and atmospheric parameters, the focus of the study shifted to measurements of ground heat flux at the Norman site. Since ground heat flux is directly related to the soil water content in the first few centimeters of soil, the measurements were tested to diagnose the sensitivity of ground heat flux to the spatial and temporal variability of soil moisture. Furthermore, it was necessary to determine how sensor biases in the 229-L impact the measurement of ground heat flux. Thus, the daylight behavior of ground heat flux was scrutinized for the 13 *ideal* days during the study. The key results are listed below.

1. The spatial variability of soil water conditions can lead to ground heat flux measurements which differ by up to 25 W m^{-2} at the time of the daily-maximum values.

2. Ground heat flux decreased as the soil transitioned from wet to dry. Also, as the variability (or envelope) of soil moisture conditions at NORM decreased with extended drying, the range of flux values at the time of peak flux decreased as well. However, the range of ground heat flux using field samples of soil water always exceeded 11 W m^{-2} at the time of maximum ground heat flux.

3. Sensor calibration is important. In some cases, errors produced when the sensor was not properly calibrated (the improved method) exceeded 30 W m^{-2} at the time of daily-maximum ground heat flux.

4. Of greater importance is the combination of natural variability in soil water content and sensor biases in measuring soil moisture. The final column of Table 6.1 illustrates the range of daily-maximum ground heat flux measurements when both sensor calibration and sample variability are considered. Note that for each day in the study, the range at daily-maximum ground heat flux always exceeded 22 W m^{-2} and was a maximum on 8 July at nearly 47 W m^{-2}. This provides a quantitative estimate of uncertainty in the ground heat flux estimate due to difficulties in measuring soil moisture at the Norman site.

5. Even though variability in soil moisture measurements influenced closure at the daily-maximum of ground heat flux, the overall affect on closure of the surface energy balance was small.

Finally, the spatial variability in soil water and texture at the site was used to test the sensitivity of the OSU model to *known* variability in soil hydraulic properties. In addition, biases in sensor output produced by the 229-L were initialized into the model. The simulations of energy balance components were compared with other variations of land surface parameters including albedo, canopy resistance, and shade factor. The key results include:

1. Model simulations of sensible and latent heat flux were very sensitive to input values of soil water content observed at the site. Due to the variability of soil water, latent and sensible heat fluxes varied as much as 300 W m^{-2} at the time of daily-maximum values and PBL depth varied as much as 1500 meters. However, the variability was greatly reduced during extremely wet or dry soil conditions.

2. The simple change of soil texture between clay loam and silt loam (the 2 predominant textures in the soil profile at NORM) resulted in simulations of sensible and latent heat flux that varied as much as 300 W m^{-2}. Furthermore, in

some cases, PBL depth had a range of over 1500 meters at the time of daily maximum. Thus, the variability of sensible and latent heat flux due to soil texture was equal in magnitude to variability caused by variable soil moisture.

3. Sensor calibration is important. The range of simulated values of PBL parameters was greatly impacted by soil moisture conditions initialized with sensor biases.

4. The principle reason explaining how simulations of PBL parameters initialized with soil moisture and texture vary greatly in some cases, but do not in others is related to how soil moisture is parametrized in the model. Inspection of the soil water release curves for silt loam and clay loam (Clapp and Hornberger 1978) verified that small changes in the soil water content due to natural or sensor variability result in large differences in the soil water pressure. Similarly, a change from silt loam to clay loam resulted in an increase of soil water pressure for the same value of soil water content. Thus, the change from one value of soil water pressure to another dramatically altered the water available for evapotranspiration. The impacts were then manifest in the PBL parameters studied.

5. Albedo, canopy resistance, and the shade factor did not produce the range of simulated values of PBL processes when compared with variable soil water or texture in this model.

6. The model did not consistently produce the same linear/nonlinear results noted in Chapter 5.

The results of this dissertation provide a number of critical insights related to soil moisture and the study of land-atmosphere interactions. First, the *critical layer* of soil which impacts atmospheric processes was not the surface layer at the Norman site. Furthermore, even when soil water content was measured correctly, the spatial and temporal variability impacted the ground heat flux measurement as well as simulations of PBL

parameters using the OSU model. These impacts were further compounded due to soil texture variability and biases in the 229-L observations. Thus, recommendations for future studies include the following:

1. To account for the spatial variability of soil water content, automated sensors should be installed in no less than 3 replicate profiles at each observing site. The information gathered by replicate sensors per soil depth would quantify the variability of soil moisture under a number of atmospheric and hydraulic conditions. This increased knowledge of the variability of soil water would improve the measurements in ground heat flux collected using observations of soil moisture.

2. Soil moisture sensors should be strategically installed to maximize their effectiveness in sampling *root-zone* soil moisture. This would entail a detailed survey of the site before sensor installation to characterize the vegetation conditions. Furthermore, soil cores should be collected from multiple locations to determine rooting depth and root density. Once this has has been accomplished, sensors should be installed within the root-zone.

3. Multiple soil cores should be collected from each site to a depth of a least 1 meter to quantify the horizontal and vertical variability of soil texture. As seen in Chapter 7, the simple change of soil texture in the model produced results which were equal in magnitude to variability of soil water. Thus, to improve model simulations and better understand the variability of soil water, the *variability* in soil texture must be quantified at any location where soil moisture observations are being collected.

4. Continuous soil sampling should be conducted at sites containing soil moisture sensors. As seen in Chapters 6 and 7, sensor biases in soil water manifest themselves in other measurements or simulations. Some of the sensor biases can produce extremely errant values of PBL parameters when initialized into numerical

models. Thus, repetitious sampling should be conducted at sites containing soil moisture sensors and should be performed under a number of atmospheric and hydraulic conditions (e.g., after precipitation events or during extended dry periods).

5. Resolution in the soil model should be increased. Again however, this increase should be strategically designed to better simulate root-zone processes and their impacts on atmospheric conditions. In addition, future operational models should permit the parametrization of multiple soil types. In fact, each vertical layer in the soil model should contain an independent soil texture.

6. As witnessed in Chapter 7, the interaction between the soil portion of the model and the atmosphere is very dependent upon the initial conditions. Thus, future studies should explore this sensitivity. One approach is to run the model in an ensemble mode whereby soil conditions such as moisture and texture are varied. Since other land-surface parameters also result in the variable PBL values, ensemble simulations should also consider variability in those parameters.

The results of this dissertation have highlighted the importance of accurate, representative measurements of soil moisture. The hypothesis of this dissertation is that *point-scale observations of soil moisture conditions, greatly affected by instrumentation errors and naturally occurring variability of soil hydraulic properties, have a limited but quantifiable impact on simulations and computations of atmospheric processes in the PBL.* This hypothesis must be rejected based on the results described in this dissertation. The impact of soil moisture observations on ground heat flux measurements was indeed limited. Conversely, the impact of soil moisture observations on simulations of atmospheric processes was, at times, *dramatic*. By simply replacing the initial soil water content with other values determined to be representative of the site, surface fluxes of latent and sensible heat increased or decreased by as much as 300 W m^{-2}. Furthermore, PBL depth simulated in the model was also severely altered under certain conditions and varied by as much as 1500 meters. These impacts cannot be described as *limited*.

This study uncovered how observed soil moisture in the root zone was linearly related to atmospheric processes in the PBL at the Norman Mesonet site Because soil moisture and atmospheric conditions are linked at nearly all spatial and temporal scales, the discoveries from this limited study should be validated at other sites and during other atmospheric conditions. The critical depth at which soil moisture most impacts atmospheric processes likely varies with the degree of biomass, the vertical stratification of soil texture, seasonality, and annual precipitation. Thus, more comprehensive experiments should be conducted across a wide range of vegetation and climate conditions and should incorporate observations of soil, vegetation, and atmospheric properties to quantify when and where linear relationships between soil water and the atmosphere are present.

This dissertation also notes limitations of using soil water near the surface to mirror atmospheric parameters. Nonlinear processes are much more difficult to simulate than are linear one. Thus, this study suggests that it is more advantageous to numerical weather prediction to have accurate, representative observations of soil moisture at deeper depths rather than from shallower depths. Because, techniques which remotely sense soil moisture do not extend below a depth of 5 cm, soil moisture at deeper depths must be obtained via in situ measurements or through accurate simulations of soil moisture conditions. Of course, the modeling framework must also advance to capture the true nature of processes which occur within the land-vegetation-atmosphere continuum. Thus, renewed effort must be undertaken by the scientific community to improve the current parameterizations used in the land portion of coupled atmosphere-biosphere-soil models.

It is also no longer sufficient to simply have observations of soil moisture and soil texture. The variability of these soil properties are extremely critical to processes which occur in the PBL and to those who wish to simulate these phenomena on a local scale. Hopefully, the results of this work will prompt a greater awareness to the need for increased observations of soil moisture which provide much more than a single, point measurement. Future studies which use soil moisture will only benefit from the additional information.

References

Anthes, R. A., 1984: Enhancement of convective precipitation by mesoscale variation in vegetative covering in semiarid regions. *J. Clim. Appl. Meteor.*, **23**, 541-554.

Arya, L. M., and J. F. Paris, 1981: A physioempirical model to predict the soil moisture characteristic from particle-size distribution and bulk density data. *Soil Sci. Soc. Am. J.*, **45**, 1023-1030.

Arya, L.M. and T.S. Dierolf, 1992: Predicting soil moisture characteristics from particle-size distributions: an improved method to calculate pore radii from particle radii. In *Indirect Methods for Estimating the Hydraulic Properties of Unsaturated Soils*, edited by van Genuchten et al., U.S. Salinity Laboratory, Riverside, CA, 115-124.

Avissar, R., and R. A. Pielke, 1989: A parametrization of heterogeneous land surfaces for atmospheric numerical models and its impact on regional meteorology. *Mon. Wea. Rev.*, **117**, 2113-2136.

Basara, J. B., 1998: The relationship between soil moisture variation across Oklahoma and the Physical State of the near-surface atmosphere during the spring of 1997. M.S. thesis, School of Meteorology, University of Oklahoma, 192 pp.

Basara, J. B. and T. M. Crawford, 2000: Improved installation procedures for deep layer soil moisture measurements. *J. Atmos. Oceanic Technology*, **17**, 879-884.

Beljaars, A. C. M., P. Viterbo, M. J. Miller, and A. K. Betts, 1996: The Anomalous Rainfall over the United States during July 1993: Sensitivity to Land Surface Parameterization and Soil Moisture Anomalies. *Mon. Wea. Rev.*, **124**, 362-383.

Bell, J. P., T. J. Dean, and M. G. Hodnett, 1987: Soil moisture measurement by an improved capacitance technique, Part II. Field techniques, evaluation, and calibration. *J. Hydrol.*, **93**, 79-90.

Bell, K. R., B. J. Blanchard, T. J. Schmugge, and M.W. Witczak, 1980: Analysis of surface moisture variations within large field sites. *Water Resour. Res.*, **16**, 796-810.

Betts, A. K., and J. H. Ball, 1994: Coupling between the land-surface, boundary layer parameterizations and rainfall on local and regional scales: Lessons from the wet summer of 1993. *Fifth Symp. on Global Change Studies*, January 23-28, Nashville, Tennessee, American Meteorological Society, 174-181.

Betts, A. K., and J. H. Ball, 1995: The FIFE surface diurnal cycle climate. *J. Geophys. Res.*, **101**, 25674-25693.

Brubaker, K. L., and D. Entekhabi, 1992a: Soil moisture and near-surface atmospheric variability in a statistical-dynamical model of land surface-atmosphere interaction. *Eos Trans. AGU*, **73**, Fall Meeting suppl., 236.

Brubaker, K. L., and D. Entekhabi, 1992b: A statistical-dynamical model of land surface hydrothermal balance. *Eos Trans. AGU*, **73**, Spring Meeting suppl., 49.

Brubaker, K. L., D. Entekhabi, P. S. Eagleson, 1993: Estimation of continental precipitation

recycling. *J. Clim.*, **6**, 1077-1089.

Brubaker, K. L., and D. Entekhabi, 1996: Analysis of feedback mechanisms in land-atmosphere interaction. *Water Resour. Res.*, **5**, 1343-1357.

Brock, F. V., K. C. Crawford, R. L. Elliott, G. W. Cuperus, S. J. Stadler, H. L. Johnson, and M. D. Eilts, 1995: The Oklahoma Mesonet: A technical overview. *J. Atmos. Oceanic Technology*, **12**, 5-19.

Brotzge, J. A., S. J. Richardson, K. C. Crawford, T. W. Horst, F. V. Brock, K. S. Humes, Z. Sorbjan, and R. L. Elliott, 1999: The Oklahoma Atmospheric Surface-layer Instrumentation System (OASIS) project. *Thirteenth Symposium on Boundary Layers and Turbulence*, Dallas, TX, Amer. Meteor. Soc., 612-615.

Brotzge, J. A., 2000: Closure of the surface energy budget. Ph.D. dissertation, School of Meteorology, University of Oklahoma, 149 pp.

Brubaker, K. L., and D. Entekhabi, 1996: Analysis of feedback mechanisms in land-atmosphere interaction. *Water Resour. Res.*, **5**, 1343-1357.

Castelli, R., I. Rodriguez-Iturbe, and D. Entekhabi, 1996: An analytic framework for the modeling of the spatial interaction between the soil moisture and the atmosphere. *J. Hydrol.*, **184**, 19-34.

Chang, J. T., and P. J. Wetzel, 1991: Effects of Spatial Variations of Soil Moisture and Vegetation on the Evolution of a Prestorm Environment: A Numerical Case Study. *Mon. Wea. Rev.*, **119**, 1368-1390.

Charney, J. G., 1975: Dynamics of deserts and droughts in the Sahel. *Quar. J. Royal Meteor. Soc.*, **101**, 193-202.

Charpentier, M. A., and P. M. Groffman, 1992: Soil moisture variability within remote sensing pixels. *J. Geophys. Res.*, **97**, 18987-18995.

Collins, Dan C., and R. Avissar, 1994: An evaluation with the Fourier Amplitude Sensitivity Test (FAST) of which land-surface parameters are of greatest importance in atmospheric modeling. *J. Clim.*, **7**, 681-703.

Crave, A., and C. Gascuel-Odoux, 1997: The influence of topography on time and space distribution of soil surface water content. *Hydrological Processes*, **11**, 203-210.

Crawford, T. M., 1998: Development of a diagnostic surface energy budget model using Oklahoma Mesonet and ARM data. Ph.D. dissertation, School of Meteorology, University of Oklahoma, 149 pp.

Cuenca, R. H., M. Ek, L. Mahrt, 1996: Impact of soil water property parameterization on atmospheric boundary layer simulation. *J. Geophys. Res.*, **101**, 7269-7277.

Dean, T. J, J. P. Bell, and A. J. B. Baty, 1987: Soil moisture measurement by an improved capacitance technique. Part I. Sensor design and performance. *J. Hydrol.*, **93**, 67-78.

Delworth, T., and S. Manabe, 1988: The influence of potential evaporation on the

variabilities of simulated soil wetness and climate. *J. Clim.*, **1**, 523-547.

Delworth, T., and S. Manabe, 1989: The influence of soil wetness on near-surface atmospheric variability. *J. Clim.*, **2**, 1147-1462.

Delworth, T., and S. Manabe, 1993: Climate variability and land surface processes. *Adv. Water Resour.*, **16**, 3-20.

de Vries, D. A., 1975: Heat Transfer in Soils. *Heat and Mass Transfer in the Biosphere*, D. A. de Vries and N. H. Afgan, Eds., Scripta Book Co., Washington, DC, 5-28.

Dingman, S. L., 1994: *Physical Hydrology*. Prentice Hall, 575 pp.

Ek, M., and R. H. Cuenca, 1994: Variation in soil parameters: implications for modeling surface fluxes and atmospheric boundary-layer development. *Bound.-Layer Meteor.*, **70**, 369-383.

Elliott, R. L., F. V. Brock, M. L. Stone, and S. L. Harp, 1994: Configuration decisions for an automated weather station network. *Appl. Eng. Agric.*, **10**, 45-51.

Emmanuel, K., D. Raymond, A. Betts, L. Bosart, C. Bretherton, K. Droegemeier, B. Farrell, J. M. Fritsch, R. Houze, M. Le Mone, D. Lilly, R. Rotunno, M. Shapiro, R. Smith, and A. Thorpe, 1995: Report of the first prospectus development team of the U.S. Weather Research Program to NOAA and the NSF. *Bull. Amer. Meteor. Soc.*, **76**, 1194-1208.

Enger, L., and M. Tjernstrom, 1991: Estimating the effects on regional precipitation climate in semiarid regions caused by an artificial lake using a mesoscale model. *J. Appl. Meteor.*, **30**, 227-250.

Entekhabi, D., and P. S. Eagleson, 1989: Land-surface hydrology parameterization for atmospheric general circulation models including subgrid-scale spatial variability. *J. Clim.*, **2**, 816-831.

Entekhabi, D., G. R. Asrar, A. K. Betts, K. J. Beven, R. L. Bras, C. J. Duffy, T. Dunne, R. D. Koster, D. P. Lattenmaier, D. B. McLaughlin, W. J. Shuttleworth, M. T. van Genuchten, M. Wei, and E. F. Wood, 1999: An agenda for land surface hydrology research and a call for the Second International Hydrological Decade. *Bull. Amer. Meteor. Soc.*, **80**, 2043-2058.

Famigletti, J. S., J. W. Rudnicki, and M. Rodell, 1998: Variability in surface moisture content along a hillslope transect: Rattlesnake Hill, Texas. *J. Hydrol.*, **210**, 259-281.

Famigletti, J. S., J. A. Devereaux, C. A. Laymon, T. Tsegaye, P. R. Houser, T. J. Jackson, S. T. Graham, M. Rodell, and P. J. van Oevelen, 1999: Ground-based investigation of soil moisture variability within remote sensing footprints during the Southern Great Plains 1997 (SGP97) Hydrology Experiment. *Water Resour. Res.*, **35**, 1839-1851.

Fast, J. D., and M. D. McCorcle, 1991: The effect of heterogeneous soil moisture on a summer baroclinic circulation in the United States. *Mon. Wea. Rev.*, **119**, 2140-2167.

Francis, C. F., J. B. Thornes, A. Diaz Romero, F. Lopez Bermuda, and G. C. Fisher, 1986: Topographic control of soil moisture, vegetation cover and land degradation in a moisture stressed Mediterranean environment. *Catena*, **13**, 211-225.

Fredlund D. G., 1992: Background, theory, and research related to the use of thermal conductivity sensors for matric suction measurement. *Advances in Measurement of Soil Physical Properties: Bringing Theory into Practice*, Soil Science Society of America, SSSA Special Publication no. 30, 249-261.

Fritschen, L. J., and L. W. Gay, 1979: *Environmental Instrumentation*. Springer-Verlag, 216 pp.

Hawley, M. E., R. H. McCuen, and T. J. Jackson, 1982: Volume-accuracy relationships in soil moisture sampling. *J. Irrig. Drain. Div. Proc. Am. Soc. Civ. Eng.*, **108**, 1-11.

Hawley, M. E., T. J. Jackson, and R. H. McCuen, 1983: Surface soil moisture variation on small agricultural watersheds. *J. Hydrol.*, **62**, 179-200.

Henninger, D. L., G. W. Peterson, and E. T. Engman, 1976: Surface soil moisture within a watershed: Variations, factors influencing, and relationships to surface runoff. *Soil Sci. Soc. Am. J.*, **40**, 773-776.

Hillel, D., 1998: *Environmental Soil Physics*. Academic Press, 771 pp.

Hills, T. C., and S. G. Renyolds, 1969: Illustrations of soil moisture variability in selected areas and plots of different sizes. *J. Hydrol.*, **8**, 27-47.

Hollinger, S. E., and S. A. Isard, 1994: A soil moisture climatology of Illinois. *J. Clim.*, **7**, 822-833.

Holmes, J. W., 1956: Calibration and field use of the neutron scattering method of measuring soil water content. *Aust. J. Appl. Sci.*, **7**, 45-58.

Huang, J., and van den Dool, H. M., 1993: Monthly precipitation temperature relations and temperature prediction over the United States. *J. Clim.*, **6**, 1111-1132.

Jackson, T. J., and T. J. Schmugge, 1989: Passive microwave remote sensing system for soil moisture: some supporting research. *IEEE Trans. on Geo. Remote Sensing*, **27**, 225-235.

Jackson, T.J., D. M. Le Vine, A. Y. Hsu, A. Oldak, P. J. Starks, C. T. Swift, J. D. Isham, and M. Haken, 1999: Soil moisture mapping at regional scales using microwave radiometry: The Southern Great Plains Hydrology Experiment. *IEEE Trans. on Geo. and Remote Sensing*, **37**, 2136-2151.

Jacquemin, B., and J. Noilhan, 1990: Sensitivity study and validation of a land surface parameterization using the HAPEX-MOBILHY data set. *Bound.-Layer Meteor.*, **52**, 93-134.

Klepper, B., 1987: Origin, branching, and distribution of root systems. In: P. J. Gregory, J. V. Lake, and D. A. Rose, eds., *Root Development and Function - Effects of the*

Physical Environment, Cambridge University Press, Cambridge.

Koster, R., M. suarez, and M. Heiser, 2000: Variance and predictability of precipitation at seasonal-to-interannual timescales. *J. Hydromet.*, **1**, 26-46.

Krumbach, A. W. Jr., 1959: Effects of Microrelief on distribution of soil moisture and bulk density, *J. Geophys. Res.*, **64**, 1587-1590.

Lanicci, J. M., T. B. Carlson, and T. T. Warner, 1987: Sensitivity of the Great Plains severe-storm environment to soil moisture distribution. *Mon. Wea. Rev.*, **115**, 2660-2673.

Laogue, K., 1992: Soil water content at R-5. Part 1. Spatial and temporal variability. *J. Hydrol.*, **139**, 233-251.

LeMone, M. A., R. L. Grossman, R. L. Coulter, M. L. Wesley, G. E. Klazura, G. S. Poulos, W. Blumen, J. K. Lundquist, R. H. Cuenca, S. F. Kelly, E. A. Brandes, S. P. Oncley, R. T. McMillen, and B. B. Hicks, 2000: Land-atmosphere interaction research, early results, and opportunities in the Walnut River Watershed in southeast Kansas: CASES and ABLE. *Bull. Amer. Meteor. Soc.*, **81**, 757-779.

Lull, H. W., K. G. Reinhart, 1955: Soil moisture measurement. USDA Southern For. Exp. Sta., New Orleans, La., Occas. Paper No 140.

Mahrt, L. and H. L. Pan, 1984: A two-layer model of soil hydrology. *Bound.-Layer Meteor.*, **29**, 1-20.

Manabe, S., and T. Delworth, 1990: The temporal variability of soil wetness and its impact on climate. *Mon. Wea. Rev.*, **116**, 1705-1720.

Marshall, T. J., J. W. Holmes, and C. W. Rose, 1996: *Soil Physics*, third edition. Cambridge University Press, 453 pp.

McCorcle, M. D., 1988: Simulation of surface soil moisture effects on the Great Plains low-level jet. *Mon. Wea. Rev.*, **116**, 1705-1720.

Miller, D. H., 1977: *Water at the Surface of the Earth*, Academic Press, 557 pp.

Moore, I. D., G. J. Burch, and D. H. Mackenzie, 1988: Topographic effects on the distribution of surface water and the location of ephemeral gullies. *Trans. Am. Soc. Agric. Eng.*, **31**, 1098-1107.

Namias, J., 1955: Some meteorological aspects of drought with special reference to the summers of 1952-54 over the United States. *Mon. Wea. Rev.*, **83**, 199-205.

Namias, J., 1983: Some causes of United States drought. *J. Clim. Appl. Meteor.*, **22**, 30-39.

Namias, J., 1988: The 1988 summer drought over the Great Plains: A classic example of air-sea-land interaction. *Eos Trans.*, AGU, **69**, 1067.

Niemann, K. O., M. C. R. Edgell, 1993: Preliminary analysis of spatial and temporal

distribution of soil moisture on a deforested slope. *Phy. Geog.*, **14**, 449-464.

Noilhan, J., and S. Planton, 1989: A simple parameterization of land surface processes for meteorological models. *Mon. Wea. Rev.*, **117**, 536-549.

Nyberg, L., 1996: Spatial variability of water content in the covered catchment at Gardsjon, Sweden. *Hydrol. Process.*, **10**, 89-103.

Ookouchi, Y., M. Segal, R. C. Kesslar, and R. A. Pielke, 1984: Evaluation of soil moisture effects on the general and modification of mesoscale circulations. *Mon. Wea. Rev.*, **112**, 2281-2292.

Ould Mohamed, S., P. Bertuzzi, A. Bruand, L. Raison, and L. Bruckler, 1997: Field evaluation and error analysis of soil water content measurement using the capacitance probe method. *Soil Sci. Am. J.*, **61**, 399-408.

Owe, M., E. B. Jones, and T. J. Schmugge, 1982: Soil moisture variability observed in Hand County, South Dakota. *Water Resour. Bull.*, **18**, 949-954.

Pan, H. L., and L. Mahrt, 1987: Interactions between soil hydrology and boundary-layer development. *Bound.-Layer Meteor.*, **38**, 185-202.

Paulson, C. A., 1970: the mathematical representation of wind speed and temperature profiles in the unstable atmospheric surface layer. *J. Appl. Meteor.*, **9**, 857-861.

Phene, C. J., G. J. Hoffman, and S. L. Rawlins, 1971: Measuring soil matric potential in situ by sensing heat dissipation within a porous body: 1. Theory and construction. *Soil Sci. Soc. Am. Proc.*, **35**, 27-33.

Phene, C. J., and T. A. Howell, 1984: Soil sensor control of high frequency irrigation systems. *Trans. ASAE*, **27**, 392-396.

Phene, C. J., R. L. McCormick, K. R. Davis, J. D. Pierro, and D. W. Meek, 1989: A lysimeter feedback irrigation controller system for evapotranspiration measurements and real time irrigation scheduling. *Trans. ASAE*, **32**, 477-484.

Pielke, R. A., Sr., G. E. Liston, J. L. Eastman, L. Lu, and M. Coughenour, 1999: Seasonal weather prediction as an initial value problem. *J. Geophys. Res.*, **104**, 19463-19479.

Petersen, L. W., A. Thomsen, P. Moldrup, D. H. Jacobsen, and D. E. Rolston, 1995: High resolution time-domain reflectometry: Sensitivity dependency on probe design. *Soil Sci.*, **159**, 149-154.

Rabin, R. M., S. Stadler, P. J. Wetzel, D. J. Stensrud, and M. Gregory, 1990: Observed effects of landscape variability on convective clouds. *Bull. Amer. Meteor. Soc.*, **71**, 272-280.

Razumova, L. A., 1965: Basic principles governing the organization of soil moisture observations, *Int. Assoc. Sci. Hydrol. Publ.*, **68**, 491-501.

Reid, L., 1973: The influence of slope orientation upon the soil moisture regime and its hydromorphological significance. *J. Hydrol.*, **19**, 309-321.

Reece, C. F., 1996: Evaluation of a line heat dissipation sensor for measuring soil matric potential. *Soil Sci. Soc. Am. J.*, **60**, 1022-1028.

Reynolds, S. G., 1970: The gravimetric method of soil moisture determination, I: A study of equipment, and methodological problems. *J. Hydrol.*, **11**, 258-273.

Reynolds, S. G., 1970: The gravimetric method of soil moisture determination, II: Typical required sample sizes and methods of reducing variability. *J. Hydrol.*, **11**, 274-287.

Reynolds, S. G., 1970: The gravimetric method of soil moisture determination, I: An examination of factors influencing soil moisture variability. *J. Hydrol.*, **11**, 288-300.

Robinson, M., and T. J. Dean, 1993: Measurement of near-surface soil water using a capacitance probe. *Hydrol. Proc.*, **7**, 77-86.

Robock, A., K. Y. Vinnikov, G. Srinivasan, J. K. Entin, S. E. Hollinger, N. A. Speranskaya, S. Liu, and A. Namkhai, 2000: The global soil moisture data bank. *Bull. Amer. Meteor. Soc.*, **81**, 1281-1299.

Salisbury, F. B., and C. W. Ross., 1992: *Plant Physiology*. Wadsworth Publishing Company, Belmont, 682 pp.

Segal, M., and R. W. Arritt, 1992: Non-classical mesoscale circulations caused by surface sensible heat flux gradients. *Bull. Amer. Meteor. Soc.*, **73**, 1593-1604.

Segal, M., R. W. Arritt, C. Clark, R. Rabin, and J. Brown, 1995: Scaling evaluation of the effects of surface characteristics on the potential for deep convection over uniform terrain. *Mon.y Wea. Rev.* **123**, 383-400.

Sellers, P. J., F. G. Hall, G. Asrar, D. E. Strebel, and R. E. Murphy, 1992: An overview of the First International Satellite Land Surface Climatology Project (ISLSCP) Field Experiment (FIFE). *J. Geophys. Res.*, **97**, 18345 - 18373.

Shaefer, G., 2000: Personal Communication.

Shafer, M. A., C.A. Fiebrich, D. S. Arndt, S. E. Fredrickson, T. W. Hughes, 2000: Quality assurance procedures in the Oklahoma Mesonet. *J. Atmos. Oceanic Tech.*, **17**, 474-494.

Shaw, B., and L. D. Baver, 1939: Heat conductivity as an index of soil moisture. *J. Am. Soc. Agron.*, **31**, 886-889.

Starks, P. J., 1999: A general heat dissipation sensor calibration equation and estimation of soil water content. *Soil Sci.*, **164**, 655-661.

Sun, W. Y., and Y. Ogura, 1979: Boundary layer forcing as a possible trigger to a squall-line formation. *J. Atmos. Sci.*, **36**, 235-254.

Tanner, C. B., 1960: Energy balance approach to evapotranspiation from crops. *S. Sci. Soc. of Amer. Proc.*, **24**, 1-9.

Troen, I. and L. Mahrt, 1986: A simple model of the atmospheric boundary layer: Sensitivity to surface evaporation. *Bound.-Layer Meteor.*, **37**, 129-148.

Topp, G. C., J. L. Davis, and A. P. Annan, 1980: Electromagnetic determination of soil water content: Measurements in a coaxial transmission lines. *Water Resour. Res.*, **16**, 574-582.

Topp, G. C., and J. L. Davis, 1985: Time-domain reflectometry (TDR) and its application to irrigation scheduling. In: Hillel, D. ed., *Advances in Irrigation*, Vol. 3 Academic Press, San Diego.

van Bavel, C. H. M., 1963: Neutron scattering measurements of soil moisture: Development and current status. In: *Proc. Int. Symp. Humidity Moisture*, Washington, DC, 171-184.

Wetzel, P. J., and J. T. Chang, 1987: Concerning the relationship between evaporation and soil moisture. *J. Clim. Appl. Meteorol.*, **26**, 18-27.

Whitaker, M. P. L., 1993: Small-scale spatial variability of soil moisture and hydraulic conductivity in a semi-arid rangeland soil in Arizona. M.S. Thesis, Department of Hydrology and Water Resources, The University of Arizona.

Wilson, M. F., A. Henderson-Sellers, R. E. Dickinson, and P. J. Kennedy, 1987: Sensitivity of the Biosphere-Atmosphere Transfer Scheme (BATS) to the inclusion of variable soil characteristics. *J. Clim. Appl. Meteorol.*, **26**, 341-362.

WMO 1968: Practical soil moisture problems in agriculture. *Tech. Note 97*, 69 pp.

Xu, Q., B. Zhou, S., D. Burk, and E. H. Barker, 1999: An air-soil coupled scheme for computing surface heat fluxes. *J. Appl. Meteorol.*, **38**, 211-223.

Zangvil, D., H. Portis, and P. J. Lamb, 1993: Diurnal variations in the water vapor budget components over midwestern United States in summer of 1979. *Hann. Symp. Vol., Geophys. Mono. Series*, International Geod. Geophys.

Zhang, D. L., and R. A., 1982: A high resolution model of the planetary boundary layer-sensitivity test and comparisons with SESAME-79 data. *J. Appl. Meteor.*, **21**, 1594-1609.

Zhao, W., and M. A. K. Kahil, 1993: The relationship between precipitation and temperature over the contiguous United States. *J. Clim.*, **6**, 1232-1236.

Zdunkowski, W. G., J. Paegle, and J. P. Reilly, 1975: The effect of soil moisture upon the atmospheric and soil temperature near the air-soil interface. *Arch. Meteorol. Geophys. Bioklimatol.*, Ser. AI, **24**, 245-268.

Appendix A

Soil Sampling at the Norman Mesonet Site

Between 1 June 1999 and 12 August 1999, more than 2000 discrete soil samples were collected at the Norman Mesonet site. The samples were collected at locations within a 20 m x 20 m study plot that was centered on the 229-L sensors (Fig. 3.3); the study plot enclosed the Norman Mesonet site as well as portions of the surrounding landscape. During this period, samples were collected from 5 of the 12 predetermined locations at layer depths of 0-5, 5-10, 10-20, 20-30, 30-40, 40-50, 50-60, 60-70, and 70-80 cm. The remaining 7 locations were sampled at layer depths of 0-5, 5-10, 10-20, and 20-30 cm. Each of the 12 locations were marked with a small white PVC pipe to ensure consistent sampling on future dates.

During the study period, samples were collected every 3-4 days based on weather conditions. During each site visit, samples were collected using a coring device approximately 2 centimeters in diameter. The coring process at each location involved a number of steps. Because it was impossible to sample the same exact core of soil throughout the study period, cores were collected within 20 cm of the original sampling markers. Thus, the first step was to choose a location within 20 cm of the white PVC pipe. Next, the core device was slowly inserted into the soil with great care to avoid compaction of the soil within the core. If compaction of the soil occurred, the core was ejected, replaced, and a new area was located for sampling. When compaction was not observed, the coring device was inserted to a depth of 30 cm. Upon reaching this depth, the coring device and the soil core was removed. Next, the soil core was removed and carefully divided into sections of 0-5, 5-10, 10-20, and 20-30 cm. Each discrete section was placed in a tin sample can, covered with a lid, and logged onto a form which details the location of the site, sample depth, and sample can number. To ensure that no water vapor was able to escape the can, electrical tape was attached to provide a seal between the body of the can and the lid. This procedure was repeated for each sample.

At 7 of the 12 sampling locations, the coring procedure was completed. Thus, this procedure was repeated at another sampling location. However, at 5 locations, additional

cores were collected to a depth of 80 cm. Once the 0-30 core was divided and placed into sample cans, the coring device was reinserted into the hole. Again, caution was used as pressure was placed on the coring device until it reached a depth of 60 cm. Upon reaching the 60 cm depth, the coring device was removed and the core (30 cm in length) was divided into sections of 30-40, 40-50, and 50-60 cm. As with the 0-30 cm core, the discrete sections were placed into sample cans, sealed with electrical tape, and logged. Finally, the coring device was reinserted into the sample hole to a depth of 80 cm. The final core, 20 centimeters in length, was divided into 60-70 and 70-80 cm samples, sealed with electrical tape, and logged.

Each step was repeated at each of the 12 sampling locations. On any given sampling day, approximately 3 hours elapsed between the time of the first and the last samples were collected. Once collected, the samples were transported to the laboratory for analysis. In the laboratory, each sample can was carefully weighed (without the electrical tape) and logged. This weight represented the "wet weight" of the soil sample. After weighing, the sample was placed into an oven. This procedure was repeated until all samples were weighed, logged, and placed in the oven. To ensure complete drying of the soil samples, the "batch" of samples remained in the oven for 48 hours at a temperature of 105°C.

After the allotted time, the samples were removed from the oven and weighed again. This new weight represented the "dry weight" of the soil. The amount of water contained within the soil sample was determined using Equation A.1:

$$sw = \text{wet weight} - \text{dry weight} \tag{A.1}$$

where sw is the soil water in grams. The weight of the soil in grams (sw) is determined using:

$$ws = \text{dry weight} - \text{weight of the sample can} \tag{A.2}$$

Once these values were determined, the gravimetric water content (θ_g) was determined by

forming the ratio of the soil water in grams to the weight of the soil:

$$\theta_g = \frac{sw}{ws} \tag{A.3}$$

where the units are in terms of g_{water} per g_{soil}. The volumetric water content (θ_v) of each sample was determined using:

$$\theta_v = \theta_g * \left(\frac{\rho_s}{\rho_w} \right) \tag{A.4}$$

where ρ_S is the bulk density of the soil (determined during previous soil sampling at the site) and ρ_W is the density of water. Details describing the values volumetric water content collected at the Norman site are shown in Tables A.1 through A.7.

Date	0-5 cm	5-10 cm	10-20 cm	20-30 cm	30-40 cm	40-50 cm	50-60 cm	60-70 cm	70-80 cm
6/1/99	0.283	0.221	0.225	0.377	0.362	0.367	0.378	0.343	0.362
6/4/99	0.165	0.172	0.237	0.357	0.368	0.371	0.388	0.340	0.355
6/7/99	0.194	0.145	0.215	0.343	0.333	0.334	0.352	0.328	0.356
6/11/99	0.127	0.128	0.192	0.336	0.328	0.344	0.359	0.330	0.342
6/14/99	0.191	0.193	0.236	0.341	0.352	0.349	0.363	0.319	0.341
6/18/99	0.128	0.137	0.215	0.338	0.332	0.336	0.350	0.327	0.339
6/20/99	0.274	0.174	0.222	0.351	NA	NA	NA	NA	NA
6/23/99	0.502	0.391	0.406	0.463	0.452	0.403	0.392	0.353	0.381
6/27/99	0.328	0.309	0.367	0.425	0.376	0.374	0.372	0.341	0.345
7/1/99	0.411	0.350	0.393	0.448	0.415	0.363	0.355	0.333	0.345
7/5/99	0.227	0.255	0.362	0.435	0.398	0.365	0.344	0.318	0.342
7/8/99	0.133	0.170	0.281	0.397	0.378	0.347	0.346	0.315	0.339
7/12/99	0.266	0.237	0.272	0.398	0.358	0.347	0.354	0.324	0.339
7/16/99	0.121	0.150	0.210	0.367	0.358	0.345	0.366	0.327	0.336
7/19/99	0.110	0.125	0.187	0.340	0.336	0.336	0.336	0.316	0.334
7/22/99	0.094	0.112	0.173	0.321	0.324	0.315	0.328	0.313	0.327
7/26/99	0.076	0.101	0.159	0.267	0.301	0.326	0.331	0.310	0.328
7/30/99	0.076	0.098	0.171	0.271	0.258	0.268	0.286	0.288	0.328
8/3/99	0.074	0.095	0.151	0.259	0.266	0.247	0.272	0.271	0.318
8/7/99	0.191	0.138	0.157	0.274	0.288	0.276	0.292	0.286	0.316
8/10/99	0.079	0.083	0.111	0.186	0.203	0.199	0.215	0.215	0.252

Table A.1. Mean volumetric water content of soil samples collected at the Norman Mesonet site.

Date	0-5 cm	5-10 cm	10-20 cm	20-30 cm	30-40 cm	40-50 cm	50-60 cm	60-70 cm	70-80 cm
6/1/99	0.375	0.350	0.328	0.413	0.392	0.403	0.427	0.367	0.389
6/4/99	0.206	0.228	0.299	0.402	0.410	0.396	0.417	0.354	0.381
6/7/99	0.228	0.194	0.281	0.397	0.352	0.349	0.369	0.352	0.396
6/11/99	0.171	0.154	0.307	0.365	0.380	0.413	0.420	0.387	0.388
6/14/99	0.238	0.255	0.317	0.388	0.370	0.403	0.416	0.349	0.375
6/18/99	0.154	0.172	0.279	0.388	0.363	0.358	0.371	0.357	0.382
6/20/99	0.304	0.262	0.332	0.385	NA	NA	NA	NA	NA
6/23/99	0.604	0.482	0.445	0.520	0.522	0.443	0.414	0.358	0.410
6/27/99	0.375	0.359	0.440	0.534	0.495	0.502	0.442	0.367	0.371
7/1/99	0.499	0.377	0.459	0.488	0.479	0.446	0.421	0.351	0.381
7/5/99	0.323	0.294	0.419	0.479	0.453	0.408	0.365	0.349	0.394
7/8/99	0.169	0.193	0.393	0.457	0.430	0.371	0.360	0.347	0.378
7/12/99	0.304	0.282	0.340	0.450	0.413	0.376	0.374	0.336	0.359
7/16/99	0.156	0.218	0.291	0.414	0.393	0.364	0.415	0.381	0.385
7/19/99	0.162	0.148	0.246	0.409	0.386	0.373	0.356	0.333	0.363
7/22/99	0.116	0.138	0.248	0.362	0.392	0.358	0.362	0.332	0.361
7/26/99	0.106	0.153	0.223	0.336	0.335	0.356	0.371	0.320	0.365
7/30/99	0.102	0.142	0.260	0.326	0.263	0.309	0.331	0.333	0.358
8/3/99	0.101	0.129	0.201	0.298	0.304	0.316	0.360	0.342	0.340
8/7/99	0.288	0.367	0.279	0.305	0.323	0.349	0.392	0.355	0.365
8/10/99	0.118	0.110	0.165	0.229	0.213	0.226	0.245	0.237	0.288

Table A.2. Maximum volumetric water content of soil samples collected at the Norman Mesonet site.

Date	0-5 cm	5-10 cm	10-20 cm	20-30 cm	30-40 cm	40-50 cm	50-60 cm	60-70 cm	70-80 cm
6/1/99	0.188	0.134	0.118	0.253	0.304	0.320	0.345	0.315	0.329
6/4/99	0.134	0.124	0.127	0.291	0.325	0.319	0.332	0.308	0.327
6/7/99	0.166	0.114	0.153	0.304	0.312	0.314	0.338	0.311	0.325
6/11/99	0.102	0.106	0.120	0.295	0.284	0.297	0.310	0.279	0.281
6/14/99	0.139	0.126	0.167	0.277	0.332	0.312	0.313	0.299	0.322
6/18/99	0.103	0.106	0.137	0.273	0.289	0.296	0.331	0.293	0.309
6/20/99	0.246	0.134	0.160	0.322	NA	NA	NA	NA	NA
6/23/99	0.425	0.316	0.373	0.387	0.353	0.322	0.363	0.341	0.342
6/27/99	0.281	0.279	0.296	0.375	0.299	0.307	0.336	0.316	0.327
7/1/99	0.350	0.332	0.334	0.336	0.361	0.309	0.323	0.307	0.317
7/5/99	0.180	0.205	0.276	0.415	0.367	0.335	0.322	0.292	0.304
7/8/99	0.080	0.148	0.217	0.322	0.345	0.323	0.317	0.295	0.307
7/12/99	0.225	0.189	0.169	0.351	0.291	0.302	0.316	0.313	0.316
7/16/99	0.097	0.106	0.115	0.306	0.328	0.313	0.344	0.295	0.294
7/19/99	0.033	0.100	0.118	0.277	0.304	0.314	0.294	0.277	0.292
7/22/99	0.068	0.065	0.100	0.272	0.260	0.245	0.246	0.281	0.306
7/26/99	0.052	0.070	0.094	0.098	0.264	0.290	0.309	0.299	0.295
7/30/99	0.039	0.065	0.097	0.253	0.246	0.235	0.255	0.257	0.290
8/3/99	0.049	0.072	0.098	0.166	0.231	0.145	0.181	0.226	0.285
8/7/99	0.123	0.082	0.101	0.234	0.256	0.250	0.254	0.256	0.278
8/10/99	0.060	0.050	0.079	0.116	0.181	0.174	0.194	0.197	0.219

Table A.3. Minimum volumetric water content of soil samples collected at the Norman Mesonet site.

Date	0-5 cm	5-10 cm	10-20 cm	20-30 cm	30-40 cm	40-50 cm	50-60 cm	60-70 cm	70-80 cm
6/1/99	0.187	0.216	0.210	0.160	0.088	0.083	0.081	0.053	0.061
6/4/99	0.072	0.104	0.172	0.112	0.085	0.077	0.085	0.045	0.054
6/7/99	0.062	0.079	0.128	0.093	0.040	0.034	0.031	0.042	0.071
6/11/99	0.069	0.048	0.187	0.070	0.097	0.116	0.109	0.108	0.107
6/14/99	0.099	0.129	0.150	0.111	0.038	0.092	0.103	0.050	0.053
6/18/99	0.051	0.066	0.141	0.115	0.074	0.062	0.04	0.064	0.073
6/20/99	0.058	0.128	0.172	0.063	NA	NA	NA	NA	NA
6/23/99	0.179	0.166	0.072	0.132	0.169	0.121	0.051	0.017	0.069
6/27/99	0.094	0.080	0.144	0.159	0.196	0.196	0.107	0.051	0.043
7/1/99	0.148	0.045	0.124	0.152	0.118	0.137	0.098	0.045	0.063
7/5/99	0.142	0.090	0.143	0.064	0.087	0.074	0.043	0.058	0.091
7/8/99	0.089	0.045	0.176	0.135	0.085	0.048	0.043	0.051	0.071
7/12/99	0.078	0.093	0.171	0.100	0.122	0.073	0.058	0.022	0.043
7/16/99	0.058	0.112	0.176	0.107	0.064	0.051	0.071	0.086	0.091
7/19/99	0.129	0.049	0.128	0.132	0.082	0.059	0.062	0.056	0.070
7/22/99	0.048	0.072	0.148	0.090	0.133	0.113	0.116	0.051	0.054
7/26/99	0.054	0.083	0.130	0.238	0.071	0.066	0.062	0.021	0.070
7/30/99	0.063	0.077	0.162	0.073	0.017	0.074	0.076	0.077	0.068
8/3/99	0.051	0.057	0.103	0.132	0.073	0.171	0.179	0.116	0.055
8/7/99	0.165	0.285	0.178	0.070	0.067	0.099	0.138	0.099	0.088
8/10/99	0.059	0.060	0.086	0.114	0.032	0.052	0.050	0.040	0.069

Table A.4. Range of volumetric water content of soil samples collected at the Norman Mesonet site.

Date	0-5 cm	5-10 cm	10-20 cm	20-30 cm	30-40 cm	40-50 cm	50-60 cm	60-70 cm	70-80 cm
6/1/99	0.062	0.055	0.063	0.044	0.035	0.030	0.032	0.020	0.024
6/4/99	0.025	0.026	0.058	0.038	0.034	0.033	0.033	0.018	0.022
6/7/99	0.020	0.022	0.043	0.027	0.015	0.014	0.011	0.016	0.029
6/11/99	0.021	0.020	0.055	0.024	0.040	0.048	0.041	0.039	0.042
6/14/99	0.036	0.043	0.052	0.032	0.017	0.034	0.039	0.020	0.021
6/18/99	0.017	0.021	0.041	0.038	0.033	0.027	0.015	0.023	0.030
6/20/99	0.013	0.038	0.059	0.017	NA	NA	NA	NA	NA
6/23/99	0.056	0.048	0.024	0.040	0.067	0.048	0.020	0.007	0.029
6/27/99	0.031	0.024	0.047	0.047	0.074	0.078	0.048	0.020	0.018
7/1/99	0.044	0.016	0.042	0.041	0.042	0.053	0.040	0.019	0.023
7/5/99	0.047	0.027	0.043	0.022	0.035	0.029	0.017	0.021	0.035
7/8/99	0.030	0.016	0.050	0.035	0.031	0.019	0.017	0.021	0.026
7/12/99	0.023	0.032	0.048	0.036	0.048	0.031	0.024	0.009	0.018
7/16/99	0.017	0.029	0.053	0.030	0.026	0.023	0.029	0.033	0.045
7/19/99	0.036	0.019	0.046	0.039	0.032	0.025	0.025	0.022	0.028
7/22/99	0.014	0.023	0.046	0.029	0.047	0.043	0.048	0.022	0.023
7/26/99	0.016	0.024	0.040	0.067	0.028	0.029	0.025	0.009	0.025
7/30/99	0.016	0.021	0.049	0.022	0.007	0.027	0.033	0.030	0.028
8/3/99	0.017	0.018	0.038	0.039	0.033	0.064	0.063	0.043	0.022
8/7/99	0.048	0.079	0.048	0.017	0.032	0.042	0.057	0.040	0.038
8/10/99	0.019	0.017	0.030	0.027	0.014	0.024	0.019	0.015	0.026

Table A.5. Standard deviation of volumetric water content of soil samples collected at the Norman Mesonet site.

Date	0-5 cm	5-10 cm	10-20 cm	20-30 cm	30-40 cm	40-50 cm	50-60 cm	60-70 cm	70-80 cm
6/1/99	0.00388	0.00301	0.00403	0.00196	0.00126	0.00090	0.00102	0.00038	0.00059
6/4/99	0.00061	0.00067	0.00332	0.00145	0.00114	0.00108	0.00110	0.00032	0.00049
6/7/99	0.00038	0.00049	0.00181	0.00074	0.00023	0.00020	0.00013	0.00026	0.00086
6/11/99	0.00045	0.00040	0.00307	0.00058	0.00160	0.00227	0.00169	0.00154	0.00176
6/14/99	0.00127	0.00184	0.00272	0.00100	0.00030	0.00115	0.00150	0.00040	0.00044
6/18/99	0.00029	0.00046	0.00170	0.00146	0.00109	0.00070	0.00023	0.00055	0.00089
6/20/99	0.00018	0.00147	0.00345	0.00028	NA	NA	NA	NA	NA
6/23/99	0.00318	0.00229	0.00057	0.00160	0.00450	0.00234	0.00039	0.00005	0.00083
6/27/99	0.00097	0.00059	0.00224	0.00224	0.00543	0.00615	0.00229	0.00039	0.00031
7/1/99	0.00194	0.00026	0.00177	0.00165	0.00181	0.00279	0.00158	0.00036	0.00055
7/5/99	0.00217	0.00072	0.00189	0.00050	0.00123	0.00084	0.00029	0.00043	0.00125
7/8/99	0.00089	0.00025	0.00247	0.00124	0.00097	0.00035	0.00030	0.00045	0.00066
7/12/99	0.00053	0.00101	0.00234	0.00131	0.00234	0.00096	0.00057	0.00008	0.00031
7/16/99	0.00030	0.00087	0.00277	0.00091	0.00067	0.00051	0.00082	0.00107	0.00201
7/19/99	0.00133	0.00038	0.00212	0.00155	0.00101	0.00060	0.00063	0.00050	0.00078
7/22/99	0.00020	0.00052	0.00207	0.00083	0.00225	0.00185	0.00227	0.00047	0.00052
7/26/99	0.00025	0.00056	0.00161	0.00445	0.00078	0.00083	0.00060	0.00008	0.00063
7/30/99	0.00026	0.00046	0.00239	0.00048	0.00005	0.00073	0.00106	0.00090	0.00081
8/3/99	0.00029	0.00031	0.00146	0.00155	0.00108	0.00407	0.00400	0.00184	0.00049
8/7/99	0.00229	0.00623	0.00233	0.00027	0.00100	0.00175	0.00321	0.00163	0.00142
8/10/99	0.00036	0.00030	0.00089	0.00074	0.00021	0.00056	0.00035	0.00022	0.00070

Table A.6. Sample variance of volumetric water content of soil samples collected at the Norman Mesonet site.

Date	0-5 cm	5-10 cm	10-20 cm	20-30 cm	30-40 cm	40-50 cm	50-60 cm	60-70 cm	70-80 cm
6/1/99	22.0	24.8	28.3	11.7	9.8	8.2	8.5	5.7	6.7
6/4/99	15.0	15.0	24.3	10.7	9.2	8.9	8.6	5.3	6.3
6/7/99	10.1	15.2	19.8	7.9	4.6	4.2	3.2	4.9	8.2
6/11/99	16.7	15.6	28.8	7.2	12.2	13.9	11.5	11.9	12.3
6/14/99	18.7	22.2	22.1	9.2	4.9	9.7	10.7	6.3	6.2
6/18/99	13.3	15.6	19.1	11.3	10.0	7.9	4.3	7.2	8.8
6/20/99	4.9	22.0	26.5	4.8	NA	NA	NA	NA	NA
6/23/99	11.2	12.2	5.9	8.6	14.8	12.0	5.1	1.9	7.6
6/27/99	9.5	7.9	12.9	11.1	19.6	21.0	12.9	5.8	5.1
7/1/99	10.7	4.6	10.7	9.1	10.2	14.5	11.2	5.7	6.8
7/5/99	20.6	10.5	12.0	5.1	8.8	7.9	4.9	6.5	10.3
7/8/99	22.5	9.3	17.7	8.9	8.3	5.4	5.0	6.7	7.6
7/12/99	8.7	13.4	17.8	9.1	13.5	8.9	6.7	2.7	5.2
7/16/99	14.4	19.6	25.1	8.2	7.2	6.6	7.8	10.0	13.3
7/19/99	33.2	15.5	24.7	11.6	9.4	7.3	7.5	7.1	8.4
7/22/99	15.0	20.5	26.3	9.0	14.7	13.7	14.5	7.0	7.0
7/26/99	20.7	23.3	25.3	25.0	9.3	8.8	7.4	2.9	7.7
7/30/99	21.2	21.9	28.6	8.1	2.7	10.1	11.4	10.4	8.7
8/3/99	22.9	18.5	25.3	15.2	12.3	25.8	23.2	15.8	6.9
8/7/99	25.0	57.4	30.8	6.0	11.0	15.1	19.4	14.1	11.9
8/10/99	24.2	21.0	26.8	14.6	7.1	11.9	8.7	6.9	10.5

Table A.7. Coefficient of variation of volumetric water content of soil samples collected at the Norman Mesonet site.

Appendix B

Net Radiation, Sensible Heat Flux, and Latent Heat Flux Estimated at the Norman Mesonet Site Using the Eddy Correlation System

Hourly-Averaged Estimates of Surface Energy Balance Components at the Norman, OK Mesonet Site (26 June 1999)

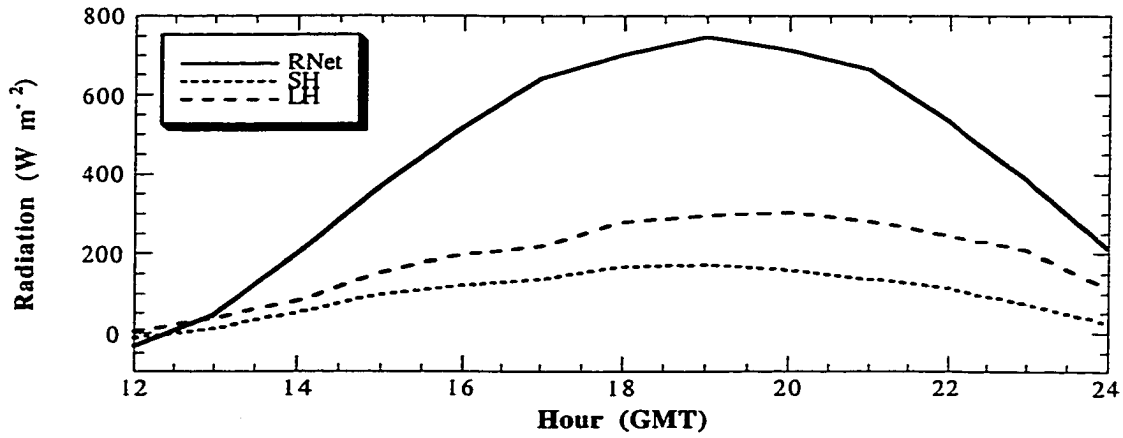

(a)

Hourly-Averaged Estimates of Surface Energy Balance Components at the Norman, OK Mesonet Site (2 July 1999)

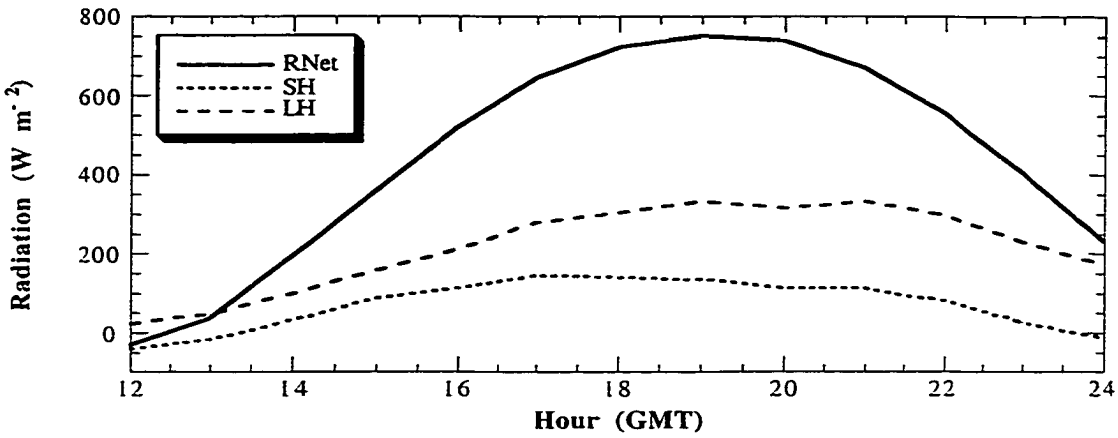

(b)

Hourly-Averaged Estimates of Surface Energy Balance Components at the Norman, OK Mesonet Site (3 July 1999)

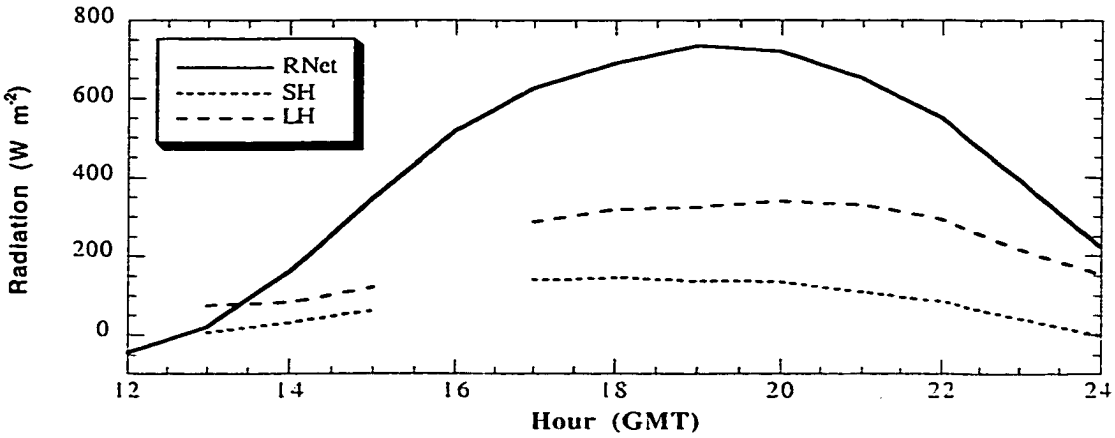

(c)

Hourly-Averaged Estimates of Surface Energy Balance Components at the Norman, OK Mesonet Site (8 July 1999)

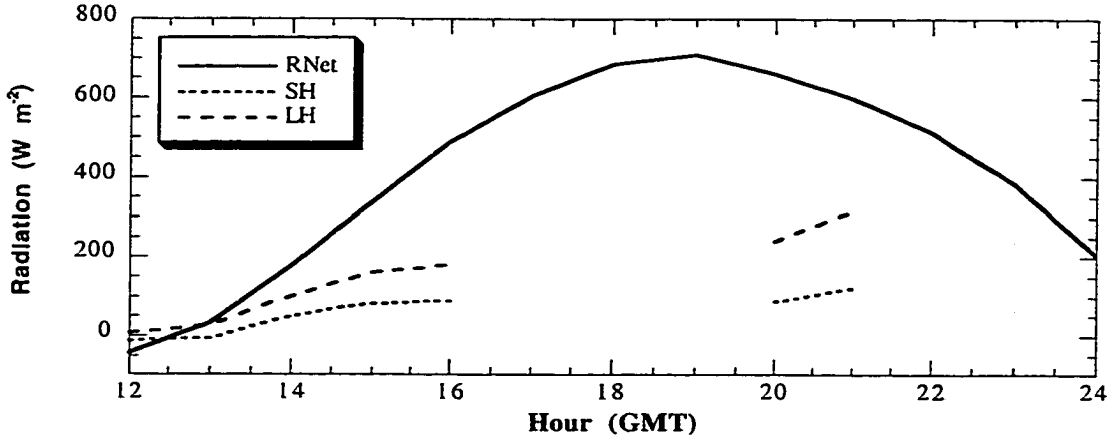

(d)

Hourly-Averaged Estimates of Surface Energy Balance Components at the Norman, OK Mesonet Site (9 July 1999)

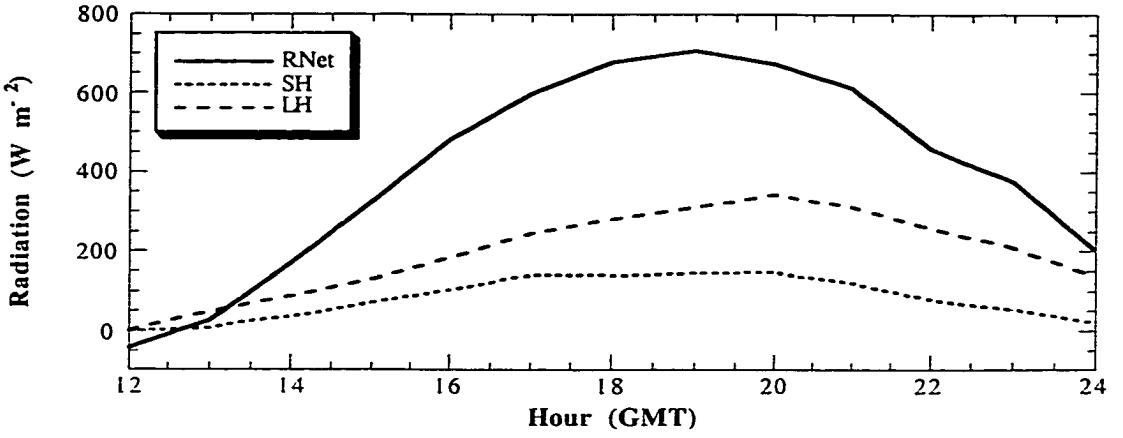

(e)

Hourly-Averaged Estimates of Surface Energy Balance Components at the Norman, OK Mesonet Site (13 July 1999)

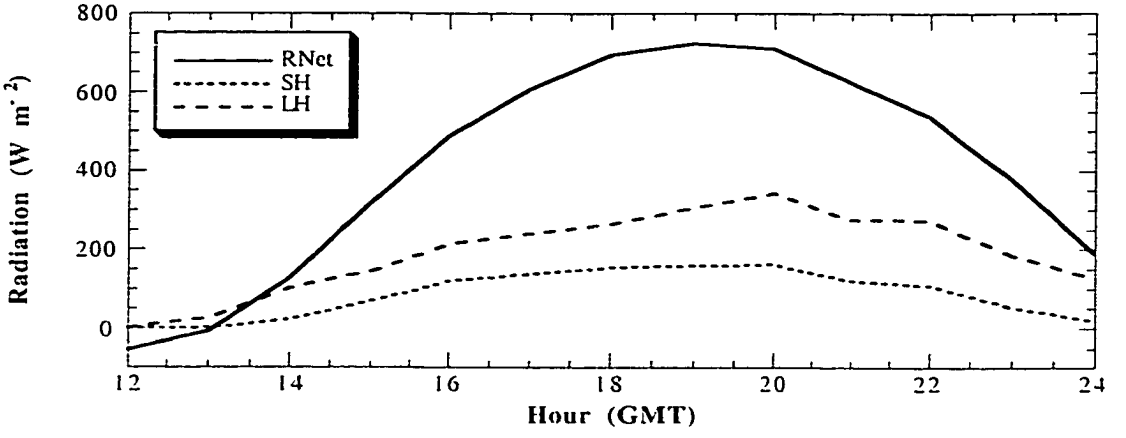

(f)

Hourly-Averaged Estimates of Surface Energy Balance Components at the Norman, OK Mesonet Site (15 July 1999)

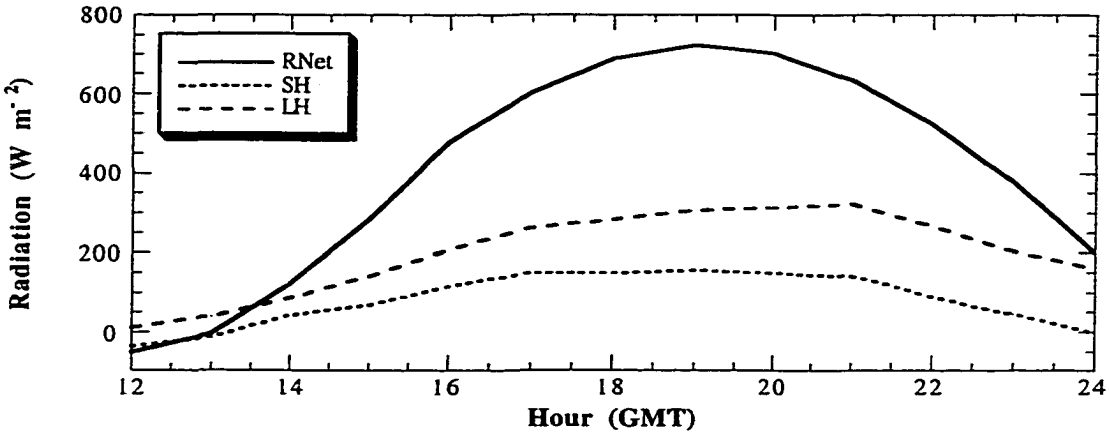

(g)

Hourly-Averaged Estimates of Surface Energy Balance Components at the Norman, OK Mesonet Site (23 July 1999)

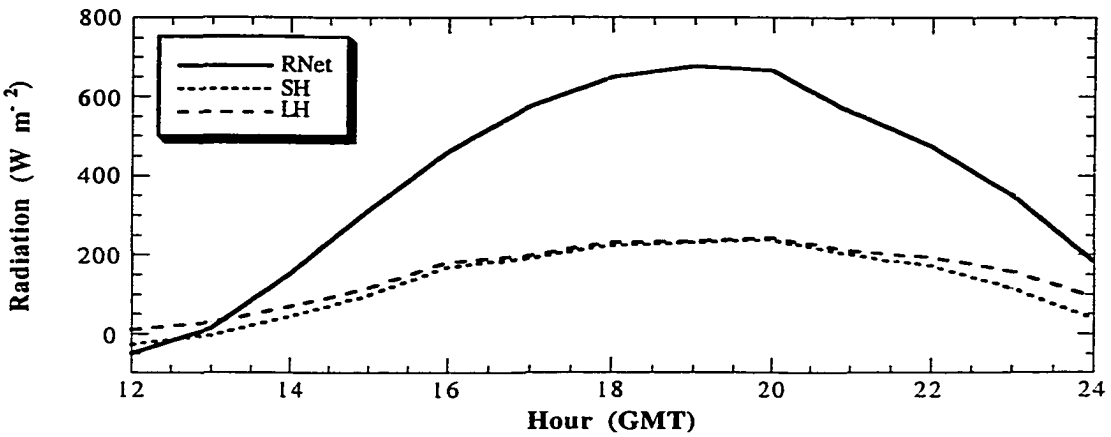

(h)

Hourly-Averaged Estimates of Surface Energy Balance Components at the Norman, OK Mesonet Site (24 July 1999)

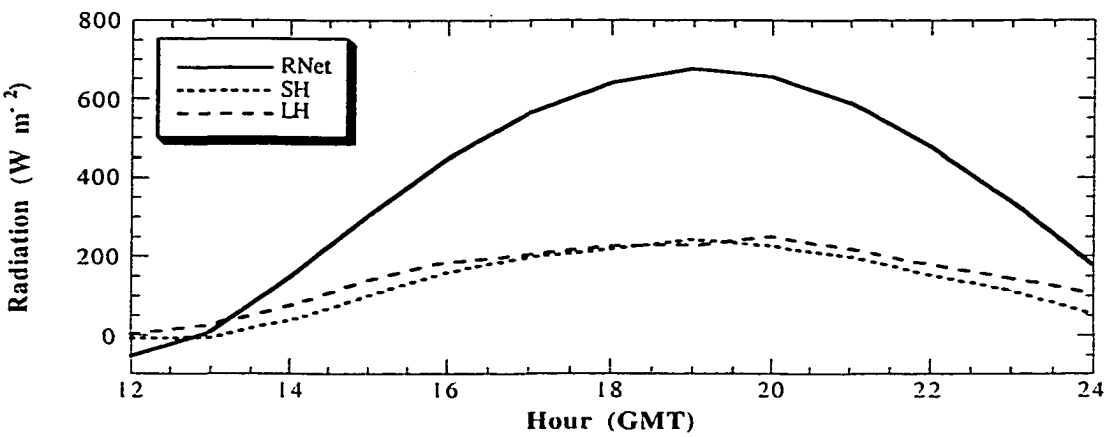

(i)

Hourly-Averaged Estimates of Surface Energy Balance Components at the Norman, OK Mesonet Site (25 July 1999)

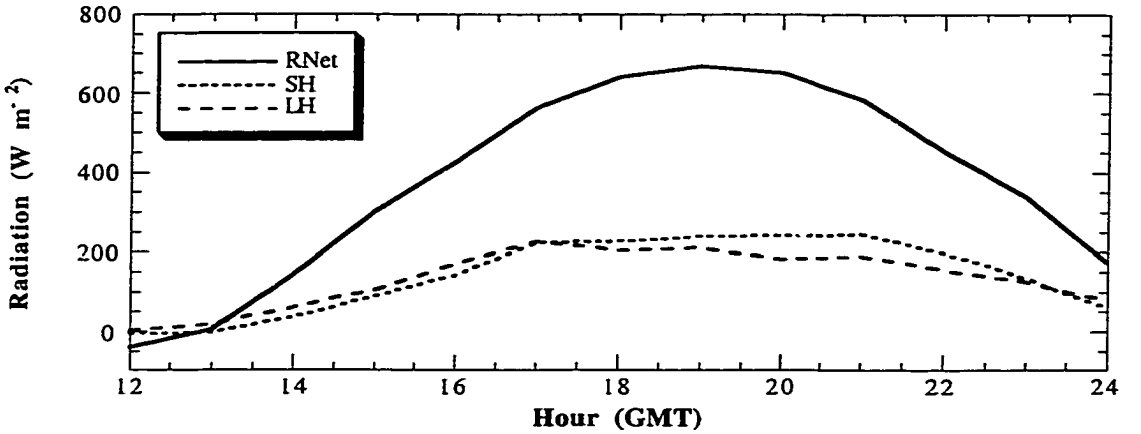

(j)

Hourly-Averaged Estimates of Surface Energy Balance Components at the Norman, OK Mesonet Site (30 July 1999)

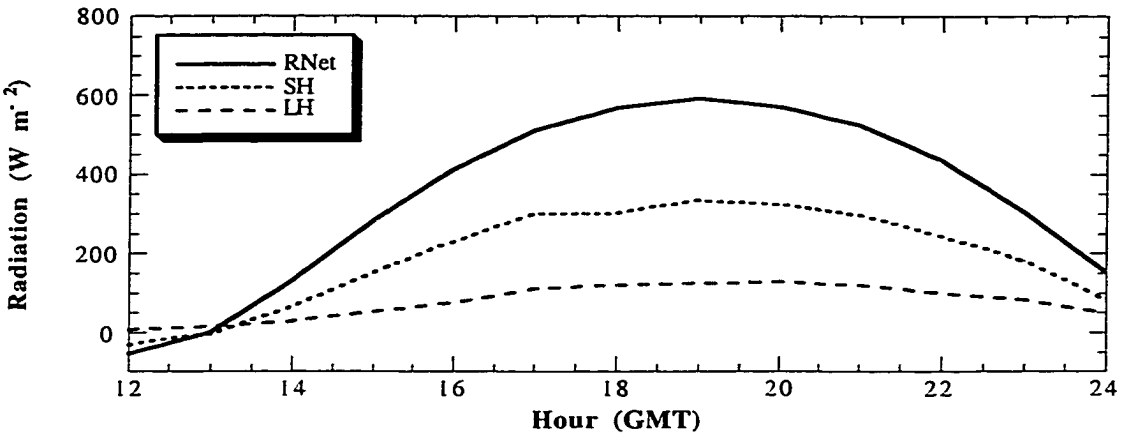

(k)

Hourly-Averaged Estimates of Surface Energy Balance Components at the Norman, OK Mesonet Site (31 July 1999)

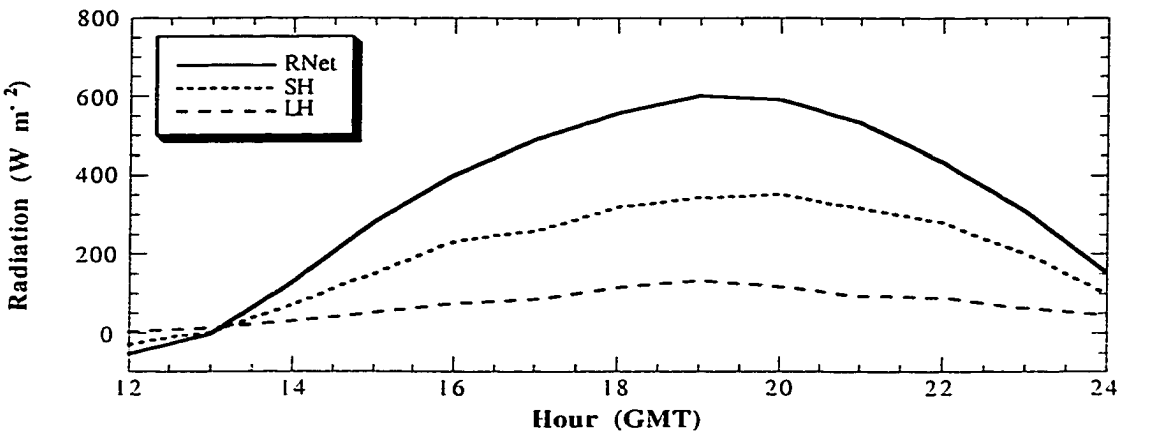

(l)

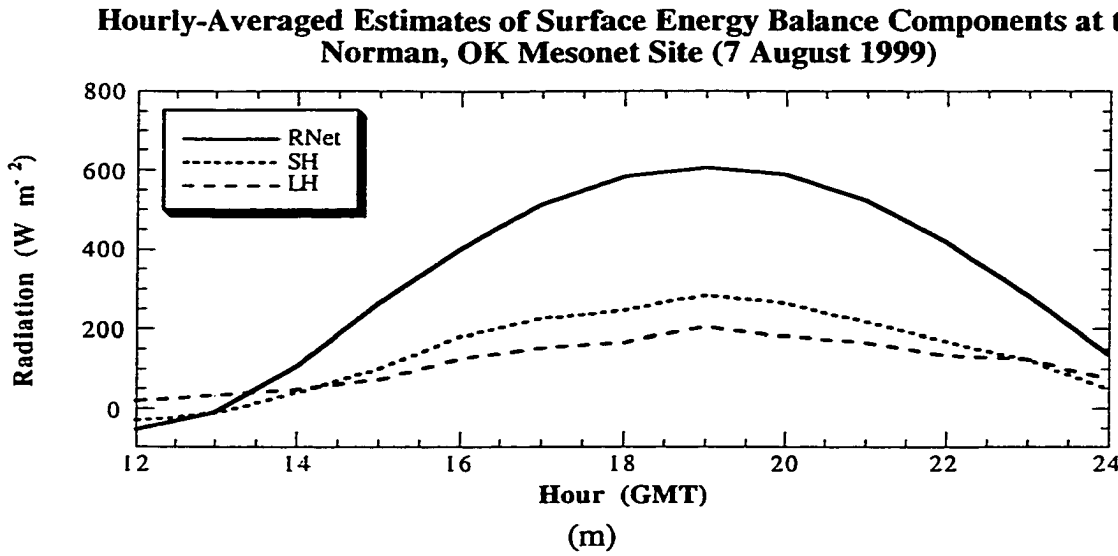

Figure B.1. Net radiation, sensible heat flux, and latent heat flux at the Norman Mesonet site computed using the eddy correlation method for the following days in 1999: (a) 26 June, (b) 2 July, (c) 3 July, (d) 8 July, (e) 9 July, (f) 13 July, (g) 15 July, (h) 23 July, (i) 24 July, (j) 25 July, (k) 30 July, (l) 31 July, and (m) 7 August.

Appendix C

Plots of Ground Heat Flux for the 13 *Ideal* Study Days

Hourly-Averaged Ground Heat Flux Estimates at the Norman, OK Mesonet Site (26 June 1999)

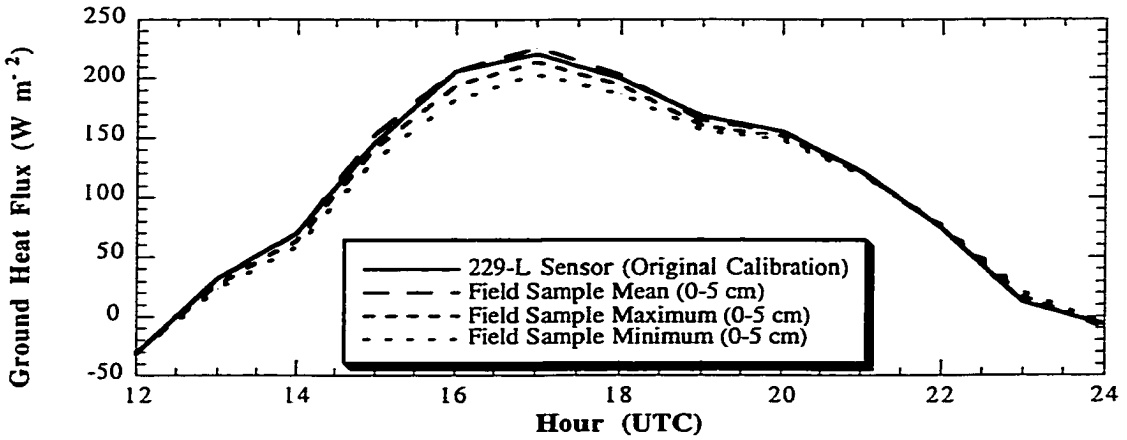

(a)

Hourly-Averaged Ground Heat Flux Estimates at the Norman, OK Mesonet Site (2 July 1999)

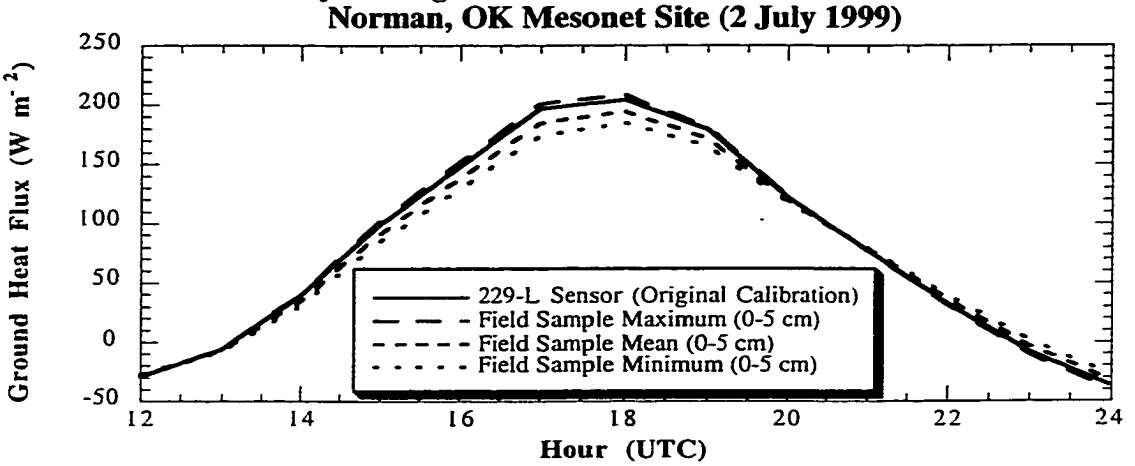

(b)

Hourly-Averaged Ground Heat Flux Estimates at the Norman, OK Mesonet Site (3 July 1999)

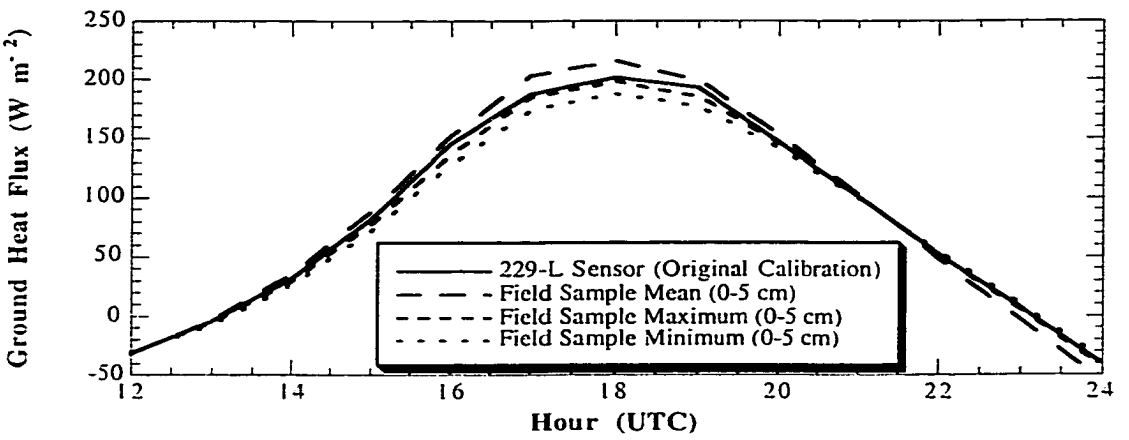

(c)

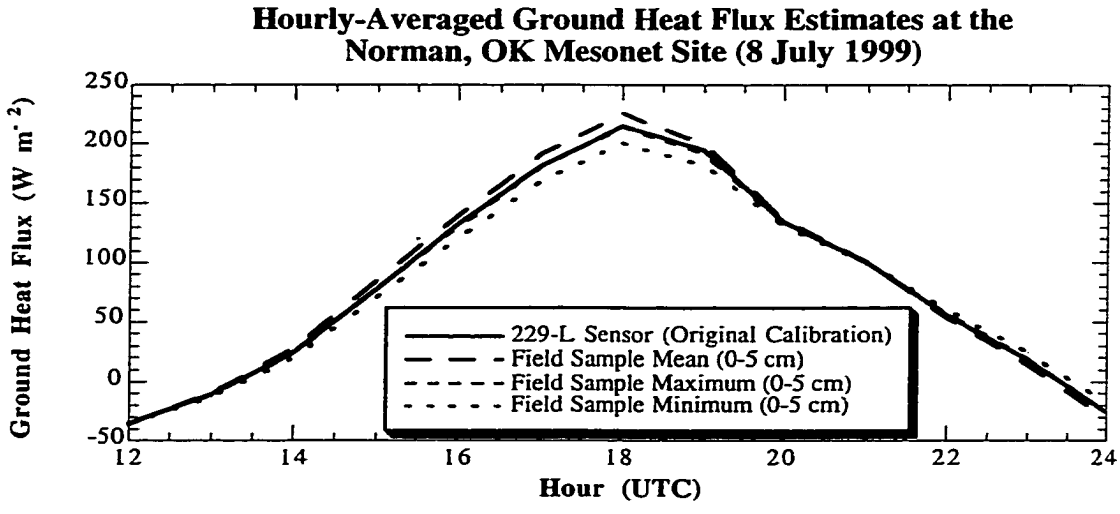
Hourly-Averaged Ground Heat Flux Estimates at the
Norman, OK Mesonet Site (8 July 1999)
Ground Heat Flux (W m-2)
250
200
150
100
50
0
-50
12
14
16
18
20
22
24
Hour (UTC)
229-L Sensor (Original Calibration)
Field Sample Mean (0-5 cm)
Field Sample Maximum (0-5 cm)
Field Sample Minimum (0-5 cm)

(d)

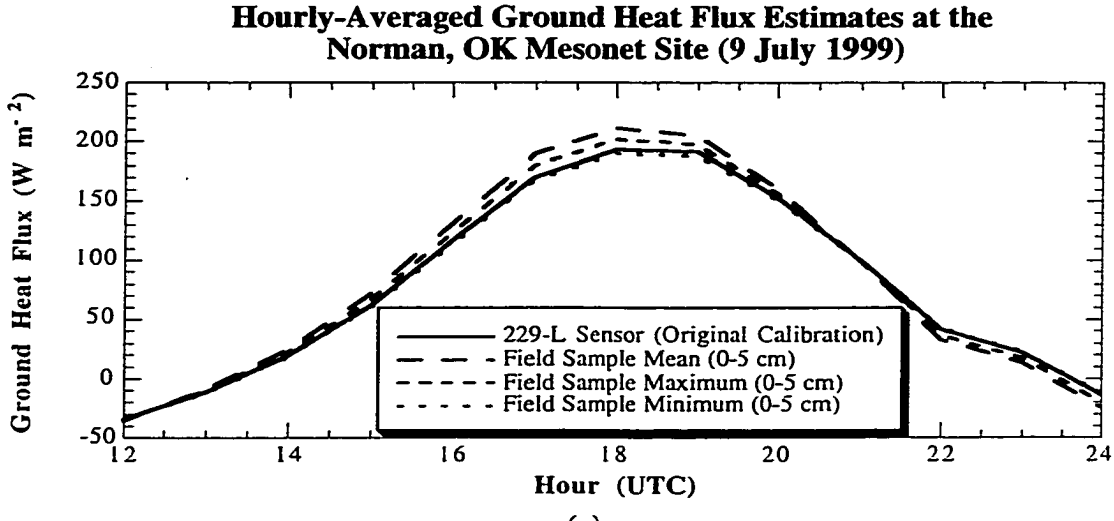
Hourly-Averaged Ground Heat Flux Estimates at the
Norman, OK Mesonet Site (9 July 1999)
Ground Heat Flux (W m-2)
250
200
150
100
50
0
-50
12
14
16
18
20
22
24
Hour (UTC)
229-L Sensor (Original Calibration)
Field Sample Mean (0-5 cm)
Field Sample Maximum (0-5 cm)
Field Sample Minimum (0-5 cm)

(e)

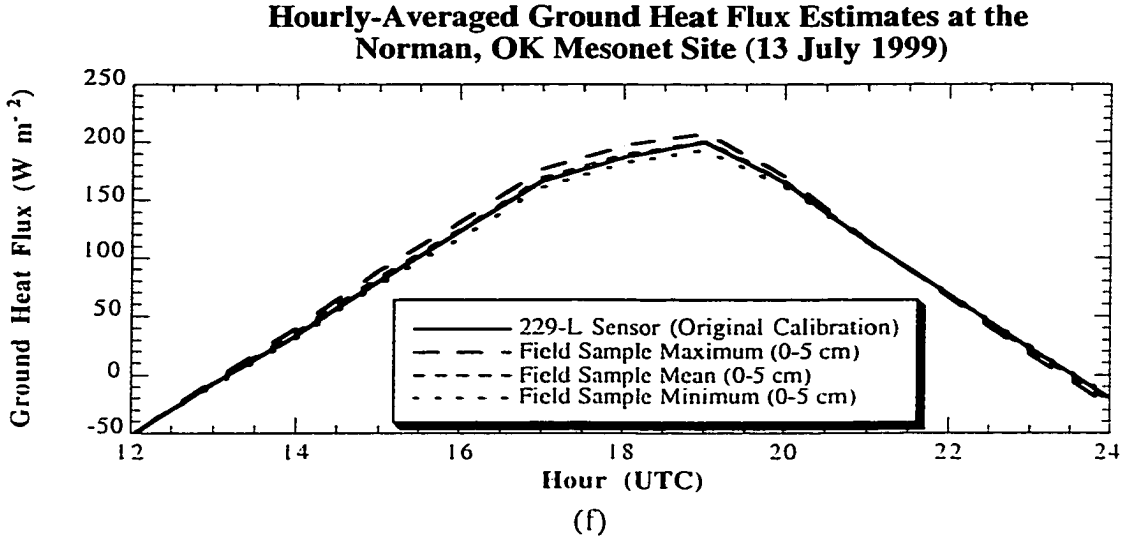
Hourly-Averaged Ground Heat Flux Estimates at the
Norman, OK Mesonet Site (13 July 1999)
Ground Heat Flux (W m-2)
250
200
150
100
50
0
-50
12
14
16
18
20
22
24
Hour (UTC)
229-L Sensor (Original Calibration)
Field Sample Maximum (0-5 cm)
Field Sample Mean (0-5 cm)
Field Sample Minimum (0-5 cm)

(f)

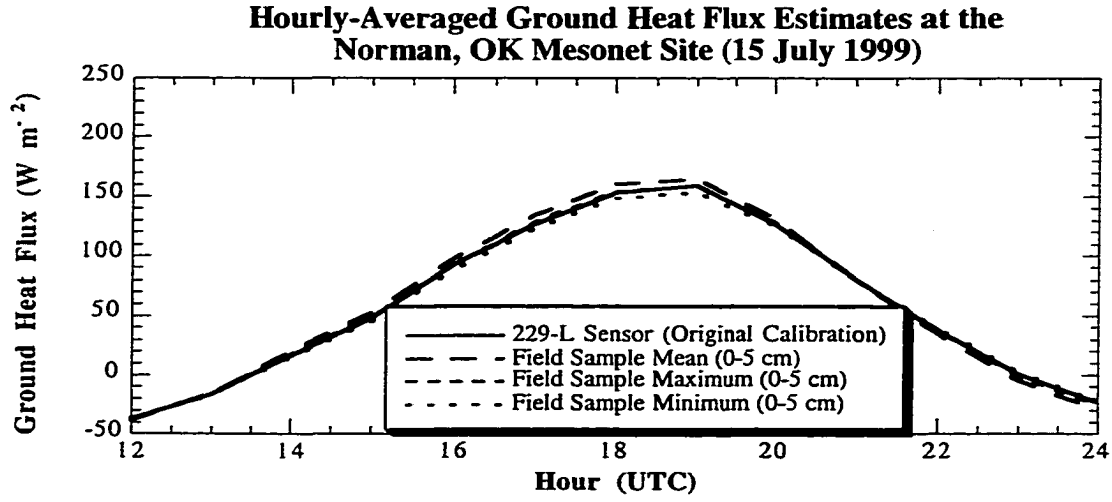
Hourly-Averaged Ground Heat Flux Estimates at the
Norman, OK Mesonet Site (15 July 1999)
Ground Heat Flux (W m-2)
250
200
150
100
50
0
-50
12
14
16
18
20
22
24
Hour (UTC)
229-L Sensor (Original Calibration)
Field Sample Mean (0-5 cm)
Field Sample Maximum (0-5 cm)
Field Sample Minimum (0-5 cm)

(g)

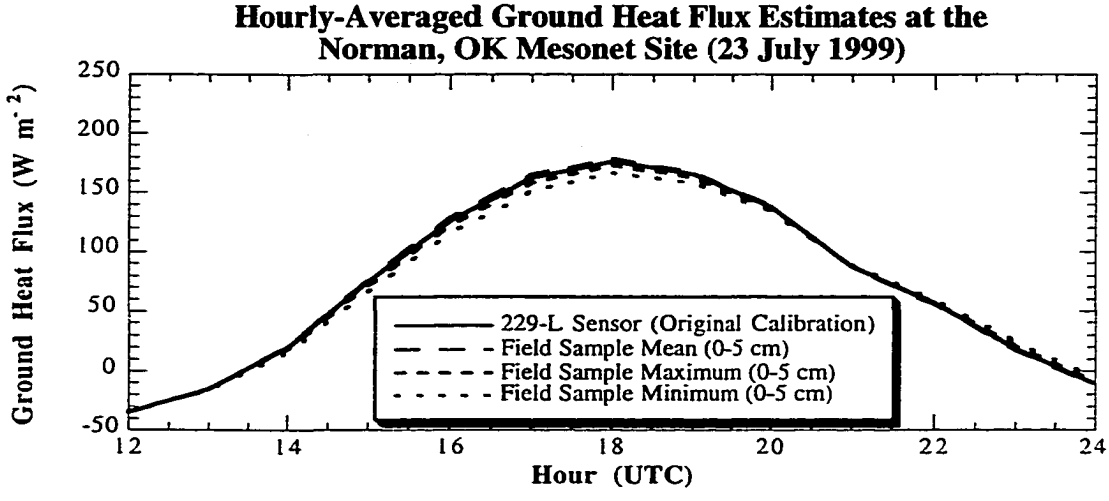
Hourly-Averaged Ground Heat Flux Estimates at the
Norman, OK Mesonet Site (23 July 1999)
Ground Heat Flux (W m-2)
250
200
150
100
50
0
-50
12
14
16
18
20
22
24
Hour (UTC)
229-L Sensor (Original Calibration)
Field Sample Mean (0-5 cm)
Field Sample Maximum (0-5 cm)
Field Sample Minimum (0-5 cm)

(h)

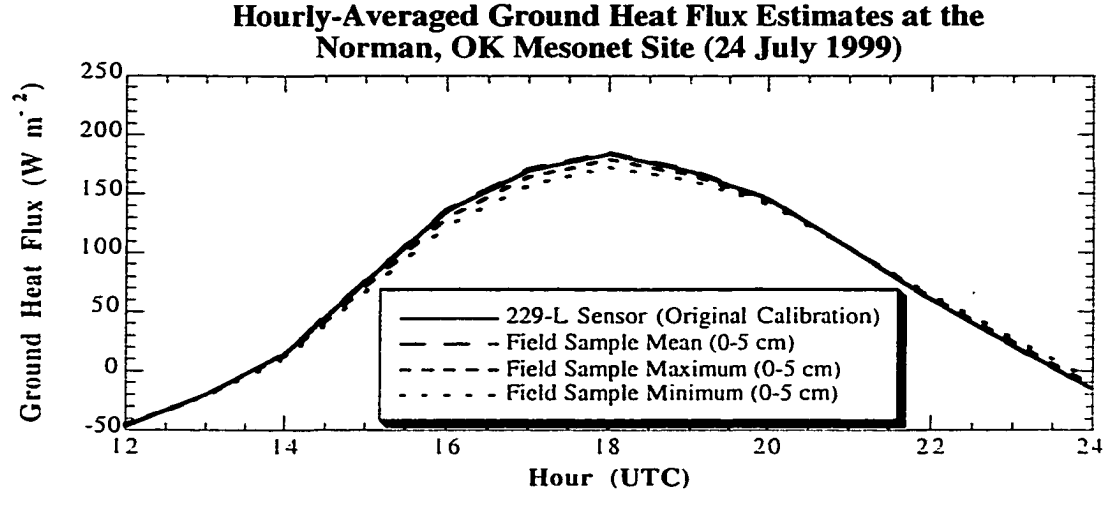
Hourly-Averaged Ground Heat Flux Estimates at the
Norman, OK Mesonet Site (24 July 1999)
Ground Heat Flux (W m-2)
250
200
150
100
50
0
-50
12
14
16
18
20
22
24
Hour (UTC)
229-L Sensor (Original Calibration)
Field Sample Mean (0-5 cm)
Field Sample Maximum (0-5 cm)
Field Sample Minimum (0-5 cm)

(i)

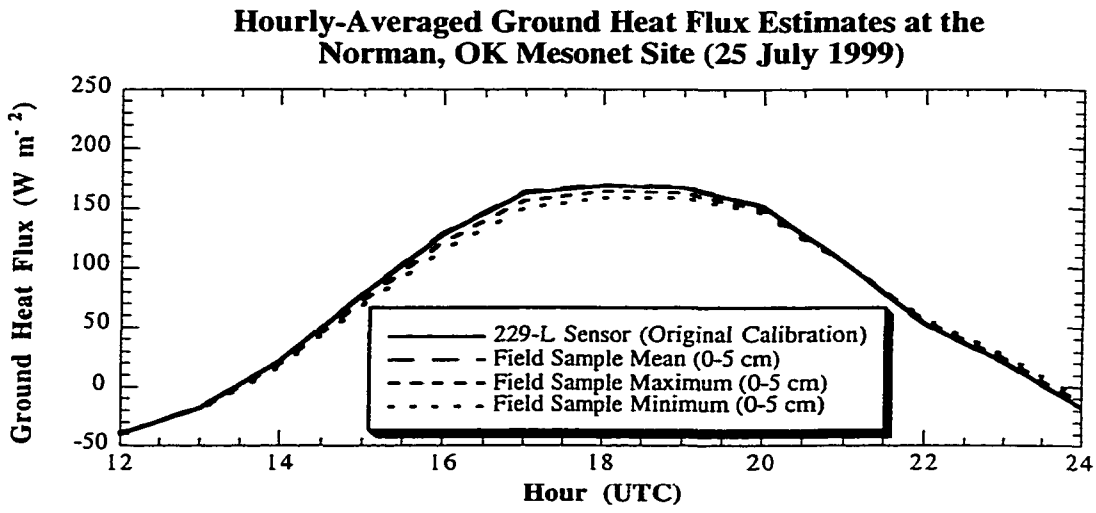
Hourly-Averaged Ground Heat Flux Estimates at the
Norman, OK Mesonet Site (25 July 1999)
Ground Heat Flux (W m-2)
250
200
150
100
50
0
-50
12
14
16
18
20
22
24
Hour (UTC)
229-L Sensor (Original Calibration)
Field Sample Mean (0-5 cm)
Field Sample Maximum (0-5 cm)
Field Sample Minimum (0-5 cm)

(j)

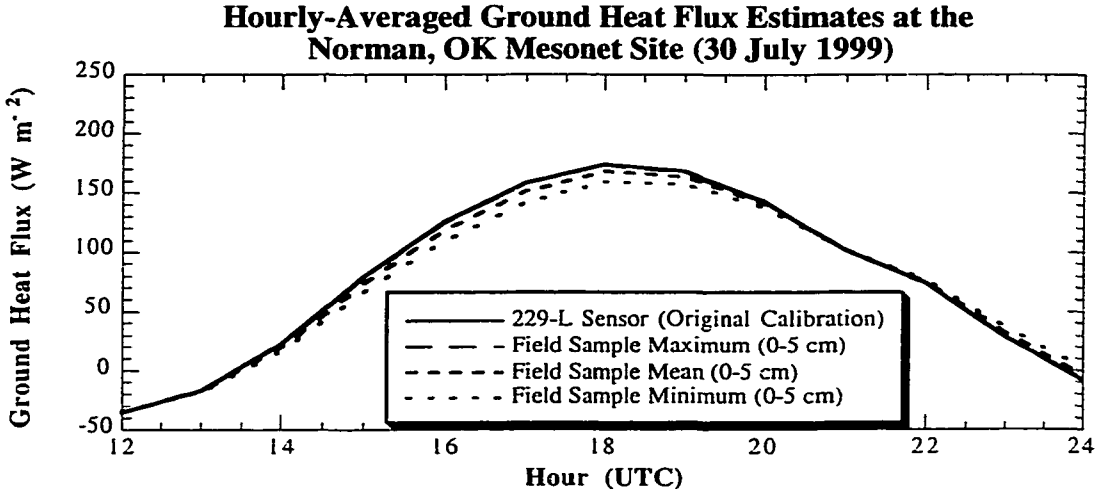
Hourly-Averaged Ground Heat Flux Estimates at the
Norman, OK Mesonet Site (30 July 1999)
Ground Heat Flux (W m-2)
250
200
150
100
50
0
-50
12
14
16
18
20
22
24
Hour (UTC)
229-L Sensor (Original Calibration)
Field Sample Maximum (0-5 cm)
Field Sample Mean (0-5 cm)
Field Sample Minimum (0-5 cm)

(k)

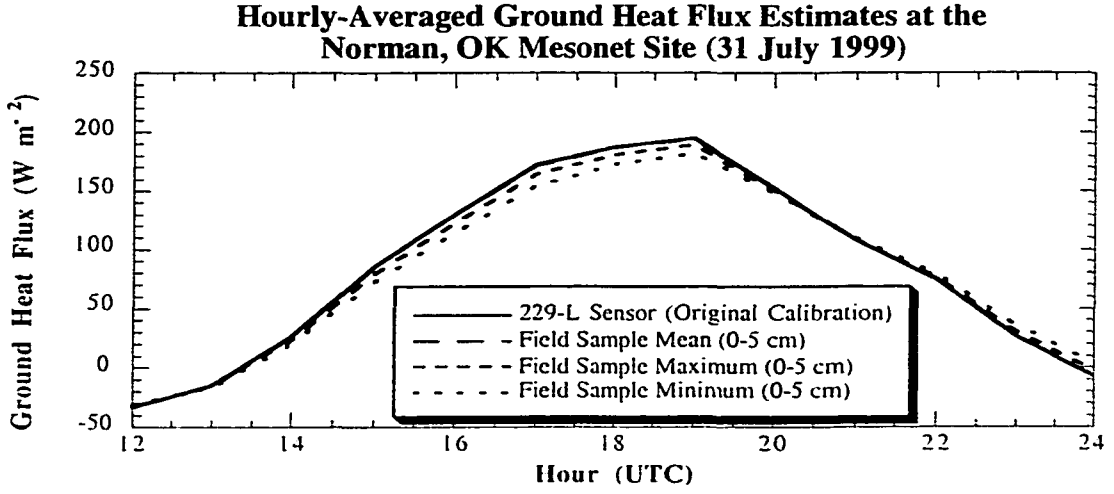
Hourly-Averaged Ground Heat Flux Estimates at the
Norman, OK Mesonet Site (31 July 1999)
Ground Heat Flux (W m-2)
250
200
150
100
50
0
-50
12
14
16
18
20
22
24
Hour (UTC)
229-L Sensor (Original Calibration)
Field Sample Mean (0-5 cm)
Field Sample Maximum (0-5 cm)
Field Sample Minimum (0-5 cm)

(l)

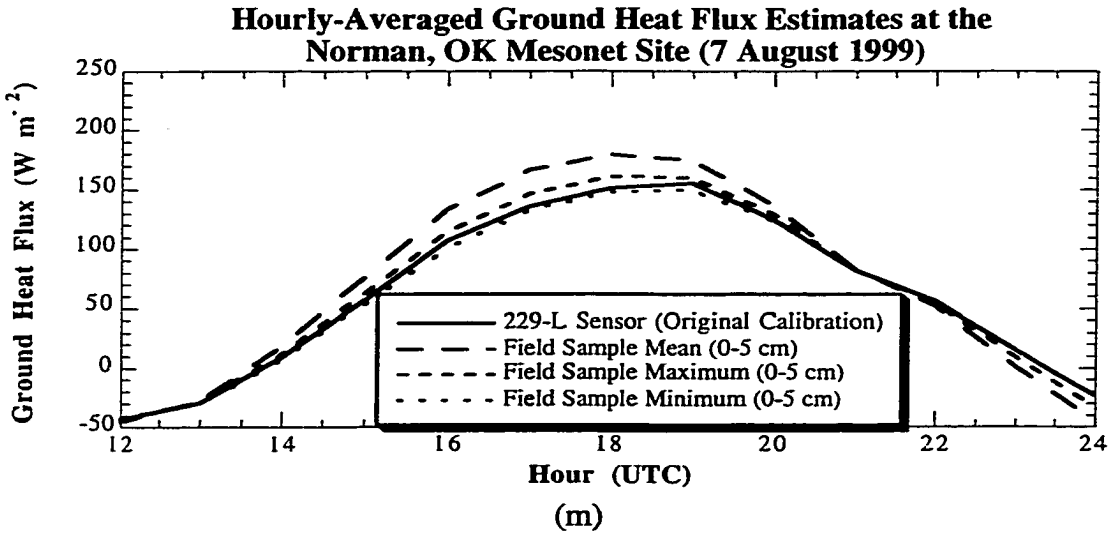

(m)

Figure C.1. Ground heat flux at the Norman Mesonet site computed using soil water content derived from data obtained via a 229-L sensor at 5 cm (original calibration). In addition, heat flux was determined using the maximum, mean, and minimum values of soil water content (0-5 cm) from field samples in 1999 on (a) 26 June, (b) 2 July, (c) 3 July, (d) 8 July, (e) 9 July, (f) 13 July, (g) 15 July, (h) 23 July, (i) 24 July, (j) 25 July, (k) 30 July, (l) 31 July, and (m) 7 August.

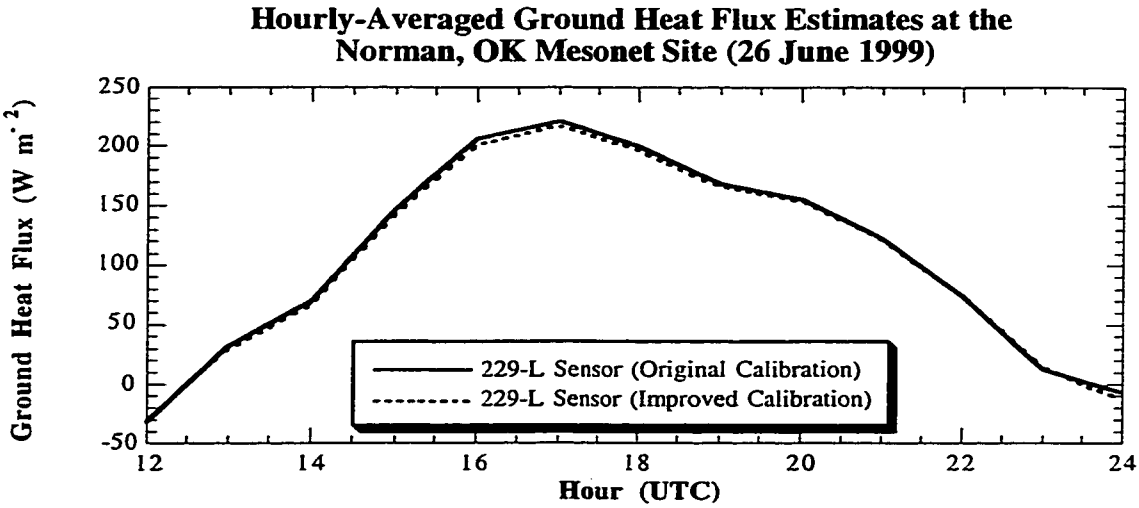
Hourly-Averaged Ground Heat Flux Estimates at the
Norman, OK Mesonet Site (26 June 1999)
Ground Heat Flux (W m-2)
250
200
150
100
50
0
-50
12
14
16
18
20
22
24
Hour (UTC)
229-L Sensor (Original Calibration)
229-L Sensor (Improved Calibration)

(a)

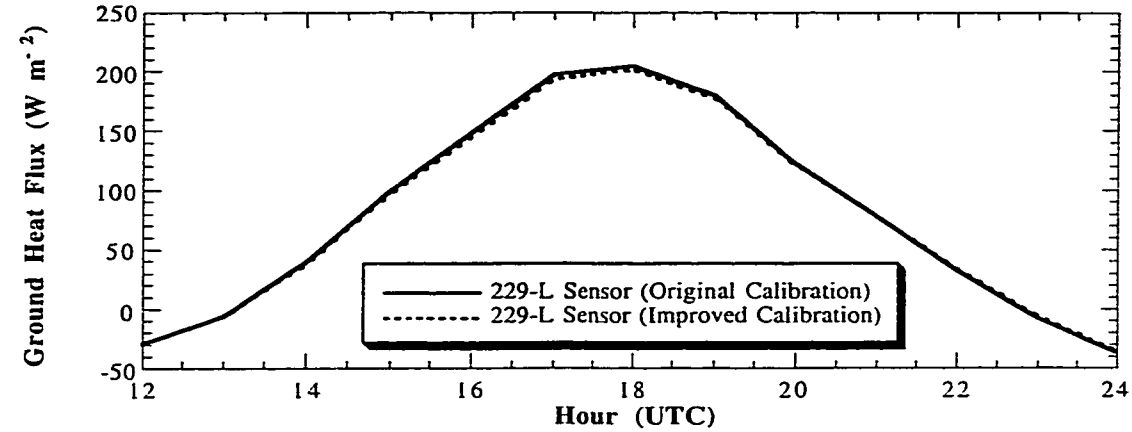
Hourly-Averaged Ground Heat Flux Estimates at the
Norman, OK Mesonet Site (2 July 1999)
Ground Heat Flux (W m-2)
250
200
150
100
50
0
-50
12
14
16
18
20
22
24
Hour (UTC)
229-L Sensor (Original Calibration)
229-L Sensor (Improved Calibration)

(b)

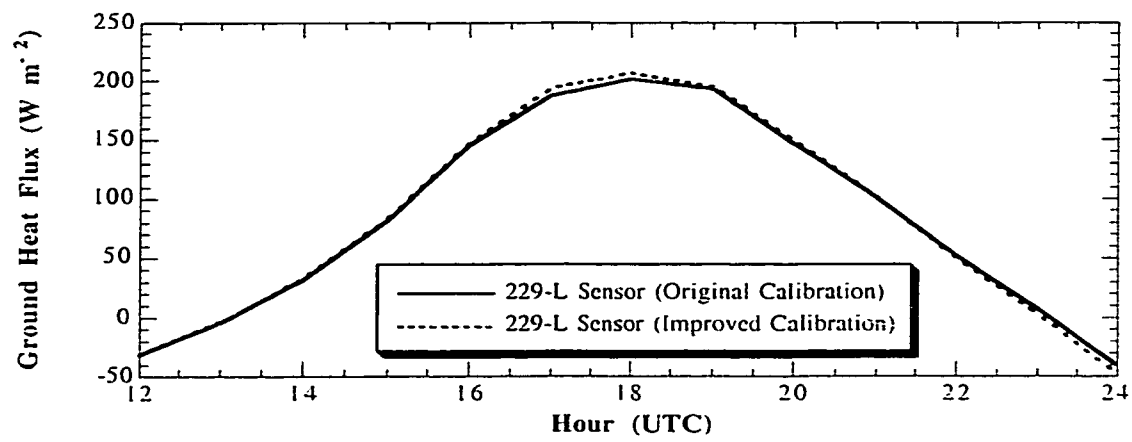
Hourly-Averaged Ground Heat Flux Estimates at the
Norman, OK Mesonet Site (3 July 1999)
Ground Heat Flux (W m-2)
250
200
150
100
50
0
-50
12
14
16
18
20
22
24
Hour (UTC)
229-L Sensor (Original Calibration)
229-L Sensor (Improved Calibration)

(c)

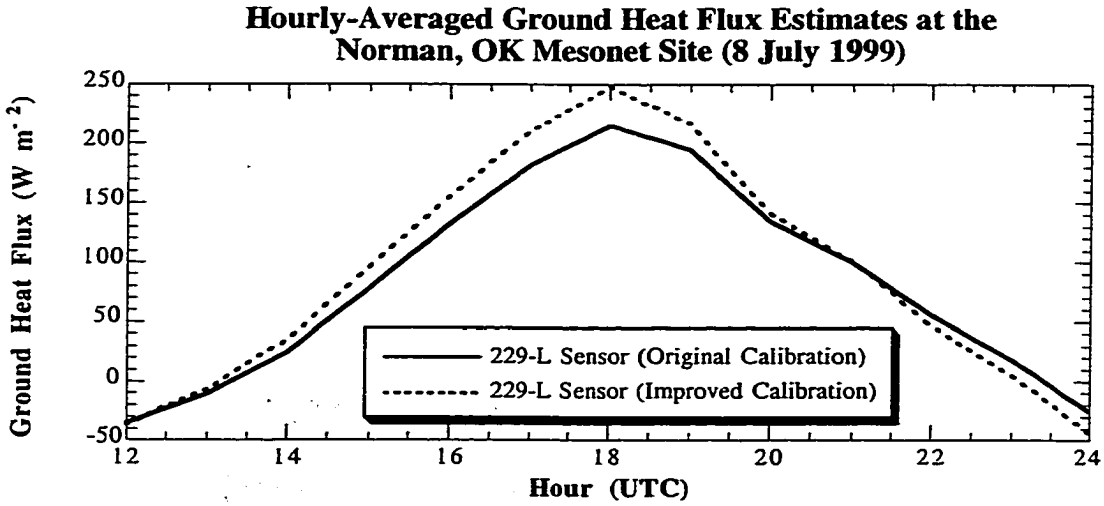
Hourly-Averaged Ground Heat Flux Estimates at the
Norman, OK Mesonet Site (8 July 1999)
Ground Heat Flux (W m-2)
250
200
150
100
50
0
-50
12
14
16
18
20
22
24
Hour (UTC)
229-L Sensor (Original Calibration)
229-L Sensor (Improved Calibration)

(d)

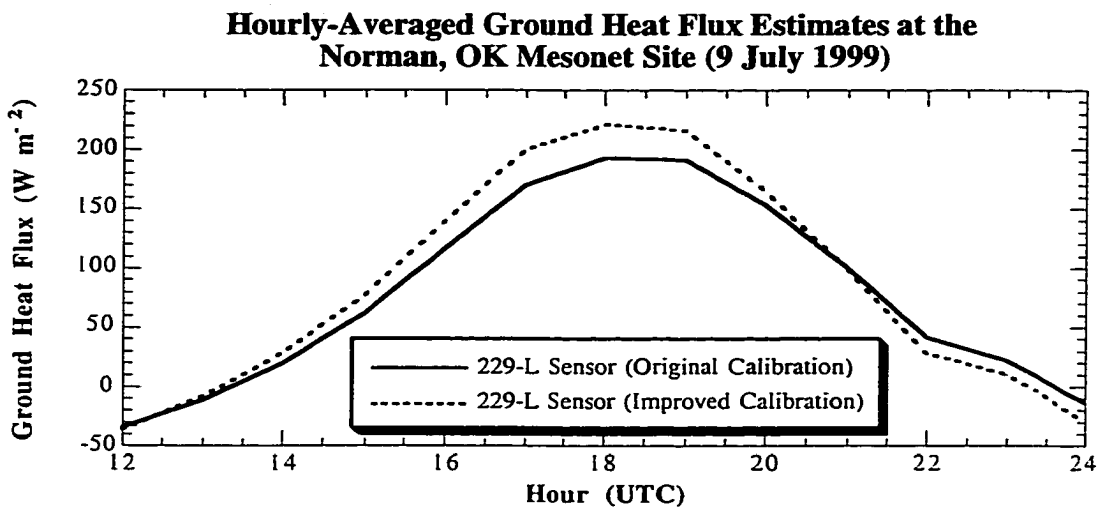
Hourly-Averaged Ground Heat Flux Estimates at the
Norman, OK Mesonet Site (9 July 1999)
Ground Heat Flux (W m-2)
250
200
150
100
50
0
-50
12
14
16
18
20
22
24
Hour (UTC)
229-L Sensor (Original Calibration)
229-L Sensor (Improved Calibration)

(e)

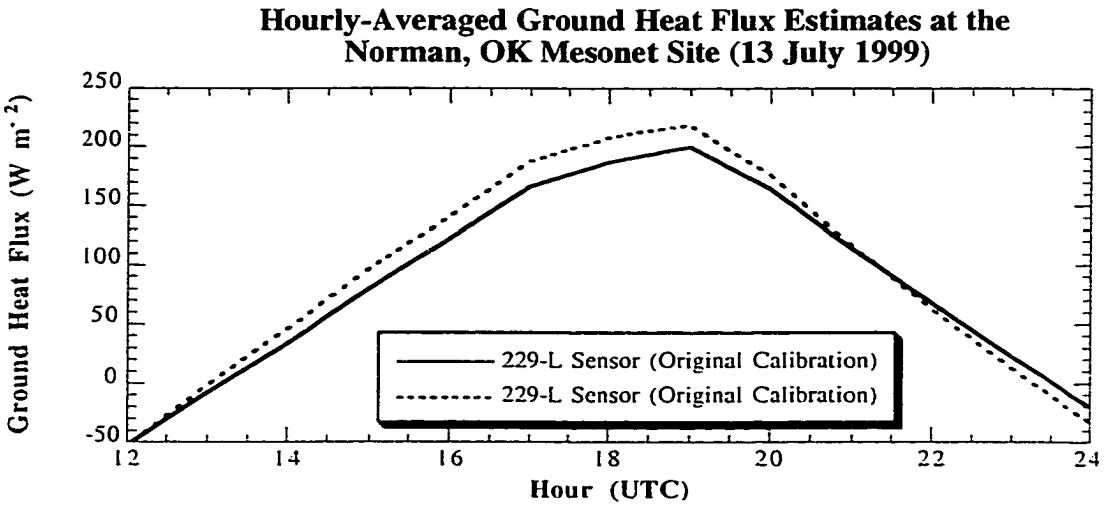
Hourly-Averaged Ground Heat Flux Estimates at the
Norman, OK Mesonet Site (13 July 1999)
Ground Heat Flux (W m-2)
250
200
150
100
50
0
-50
12
14
16
18
20
22
24
Hour (UTC)
229-L Sensor (Original Calibration)
229-L Sensor (Original Calibration)

(f)

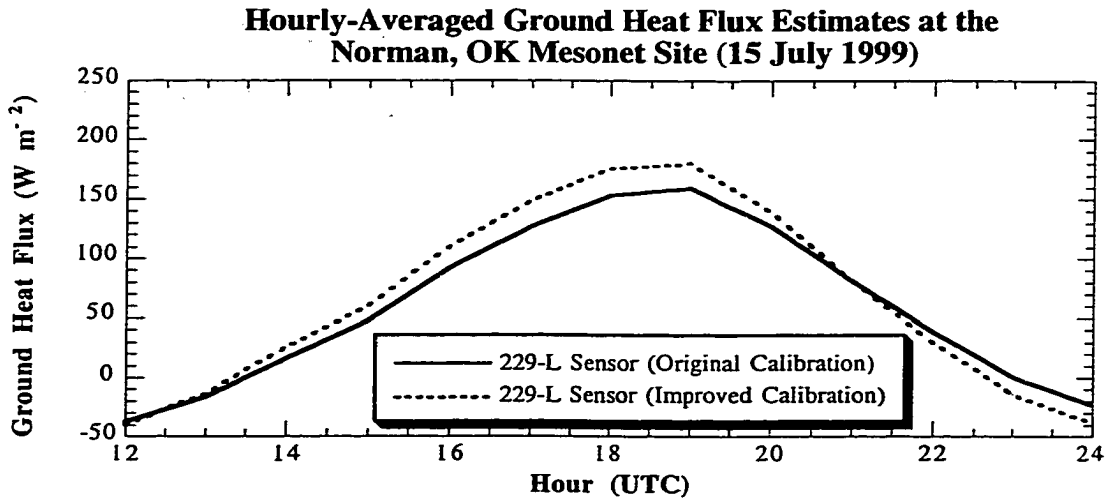
Hourly-Averaged Ground Heat Flux Estimates at the
Norman, OK Mesonet Site (15 July 1999)
Ground Heat Flux (W m-2)
250
200
150
100
50
0
-50
12
14
16
18
20
22
24
Hour (UTC)
229-L Sensor (Original Calibration)
229-L Sensor (Improved Calibration)

(g)

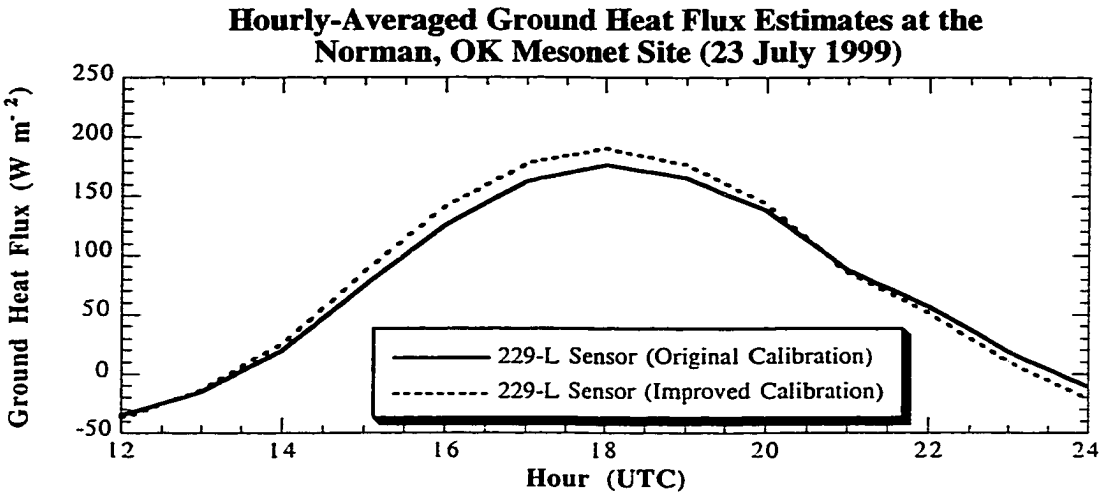
Hourly-Averaged Ground Heat Flux Estimates at the
Norman, OK Mesonet Site (23 July 1999)
Ground Heat Flux (W m-2)
250
200
150
100
50
0
-50
12
14
16
18
20
22
24
Hour (UTC)
229-L Sensor (Original Calibration)
229-L Sensor (Improved Calibration)

(h)

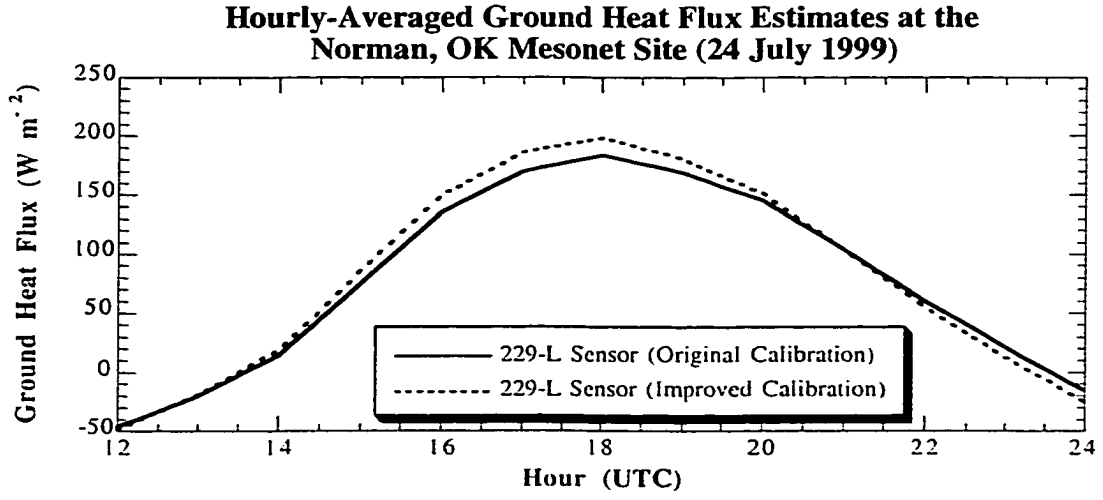
Hourly-Averaged Ground Heat Flux Estimates at the
Norman, OK Mesonet Site (24 July 1999)
Ground Heat Flux (W m-2)
250
200
150
100
50
0
-50
12
14
16
18
20
22
24
Hour (UTC)
229-L Sensor (Original Calibration)
229-L Sensor (Improved Calibration)

(i)

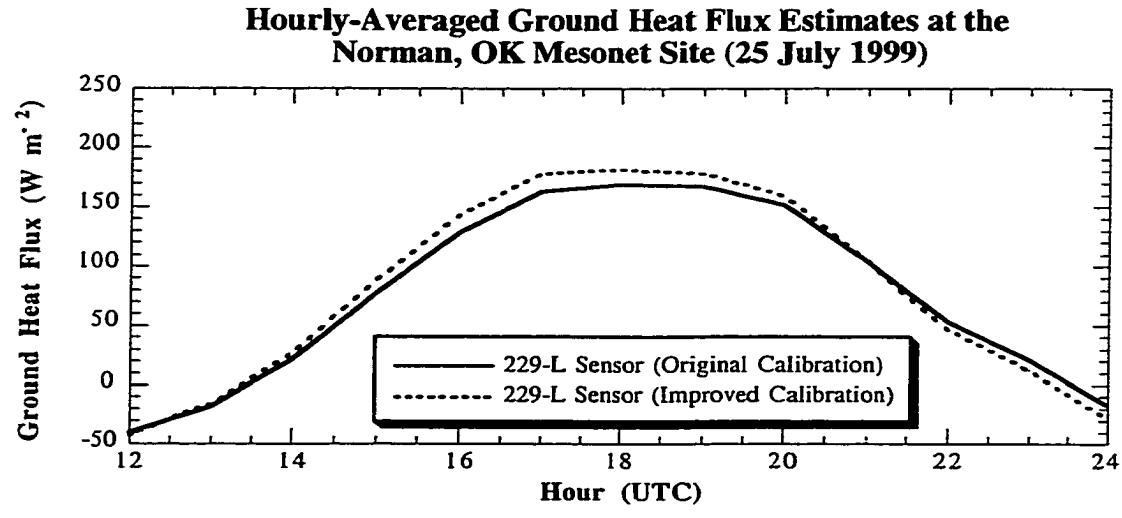
Hourly-Averaged Ground Heat Flux Estimates at the
Norman, OK Mesonet Site (25 July 1999)
Ground Heat Flux (W m-2)
250
200
150
100
50
0
-50
12
14
16
18
20
22
24
Hour (UTC)
229-L Sensor (Original Calibration)
229-L Sensor (Improved Calibration)

(j)

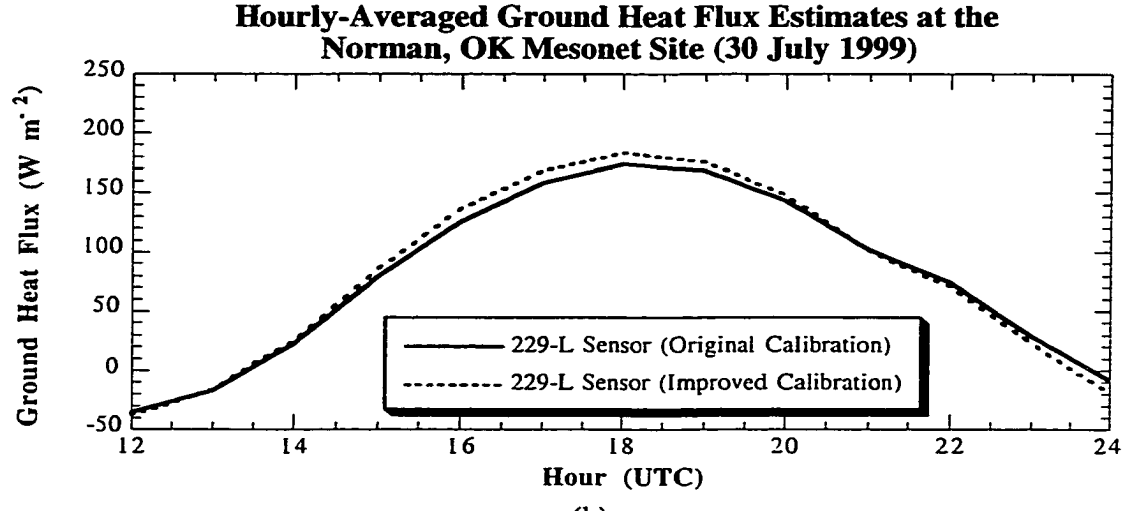
Hourly-Averaged Ground Heat Flux Estimates at the
Norman, OK Mesonet Site (30 July 1999)
Ground Heat Flux (W m-2)
250
200
150
100
50
0
-50
12
14
16
18
20
22
24
Hour (UTC)
229-L Sensor (Original Calibration)
229-L Sensor (Improved Calibration)

(k)

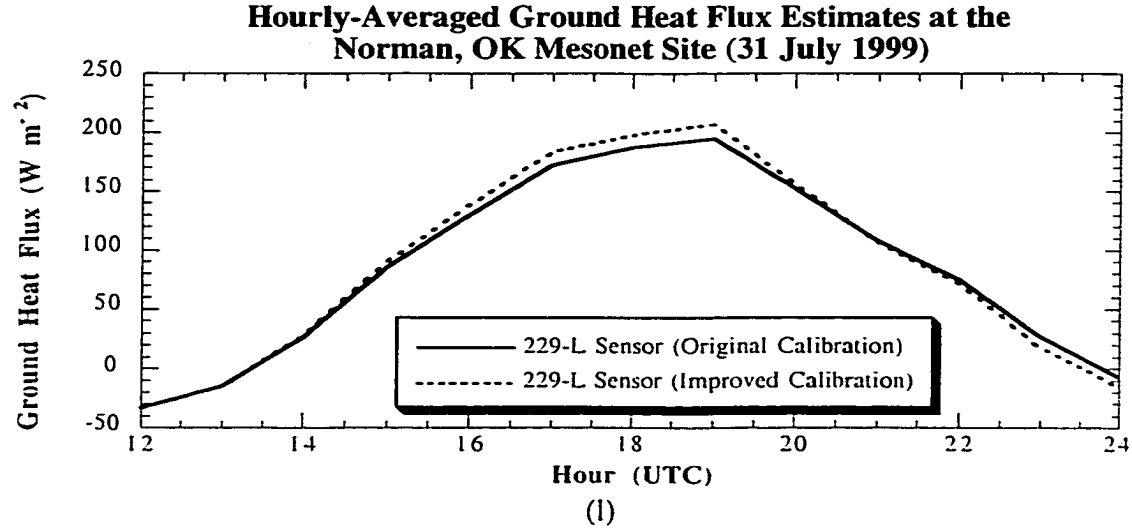
Hourly-Averaged Ground Heat Flux Estimates at the
Norman, OK Mesonet Site (31 July 1999)
Ground Heat Flux (W m-2)
250
200
150
100
50
0
-50
12
14
16
18
20
22
24
Hour (UTC)
229-L Sensor (Original Calibration)
229-L Sensor (Improved Calibration)

(l)

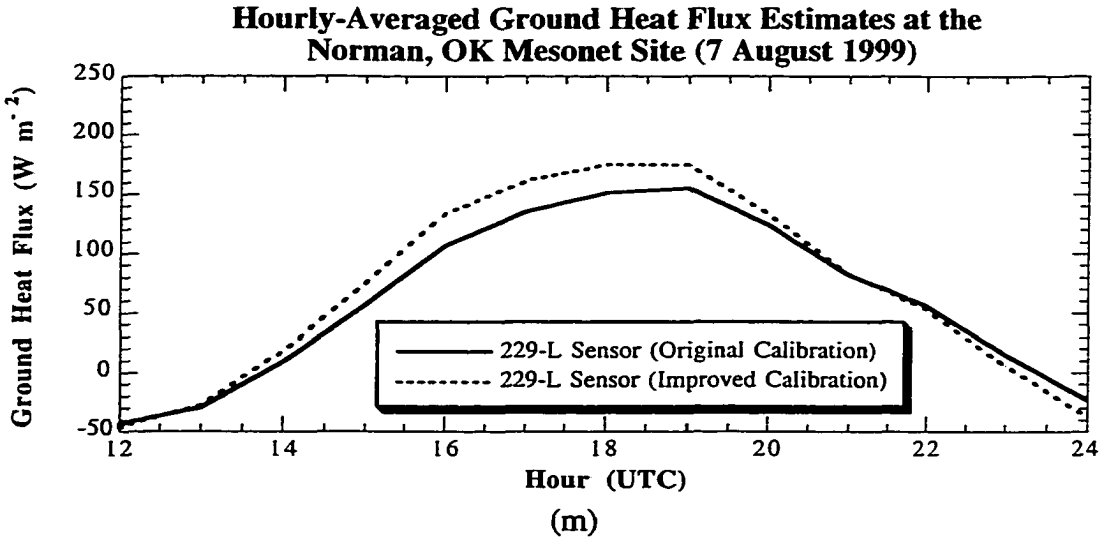

Figure C.2. Ground heat flux at the Norman Mesonet site computed using soil water content derived from data obtained via a 229-L sensor at 5 cm (original calibration and improved calibration). Plot are from (a) 26 June, (b) 2 July, (c) 3 July, (d) 8 July, (e) 9 July, (f) 13 July, (g) 15 July, (h) 23 July, (i) 24 July, (j) 25 July, (k) 30 July, (l) 31 July , and (m) 7 August.

Appendix D

Plots of Atmospheric Processes in the Planetary Boundary Layer Simulated by the OSU Model for the 13 *Ideal* Study Days

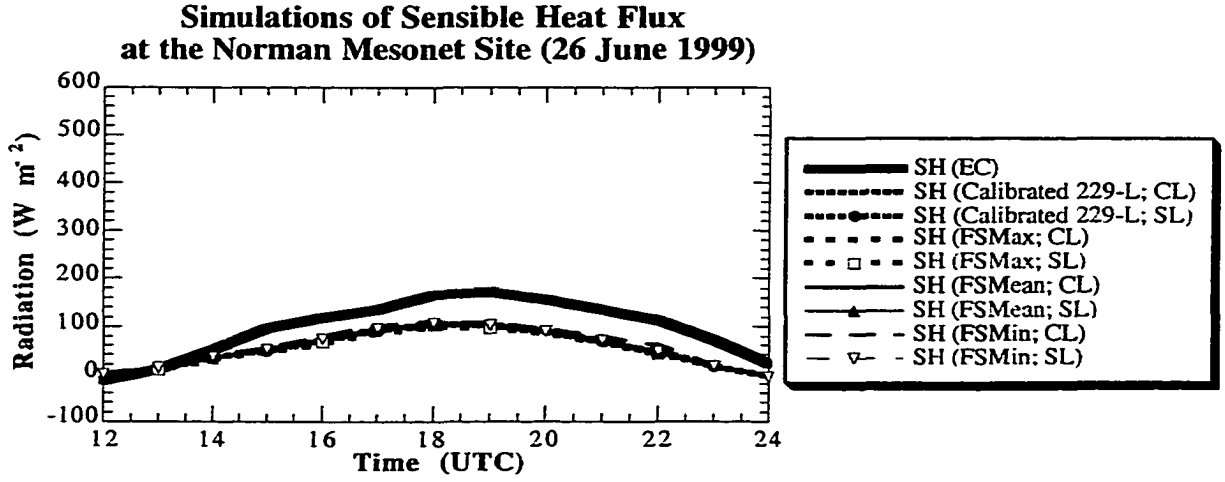

Figure D.1a. Simulations of sensible heat flux at the Norman Mesonet site on 26 June 1999 using the clay loam soil parameterization (CL) and the silt loam soil parameterization (SL). Calibrated measurements of 229-L soil water content, and soil water determined from field samples were used as input. Hourly-averaged observations from the Norman site are plotted for reference (black curve).

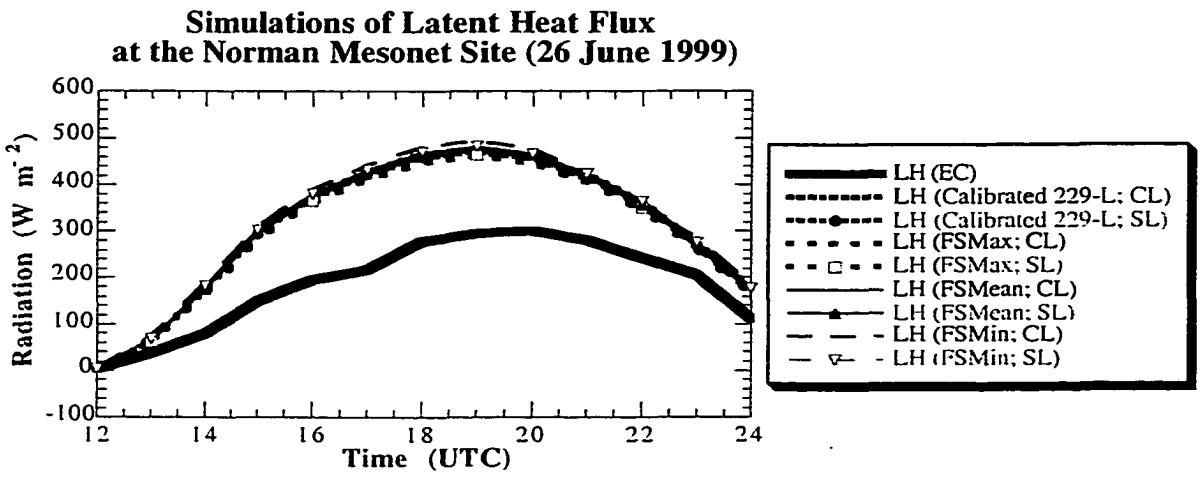

Figure D.1b. Simulations of latent heat flux at the Norman Mesonet site on 26 June 1999 using the clay loam soil parameterization (CL) and the silt loam soil parameterization (SL). Calibrated measurements of 229-L soil water content, and soil water determined from field samples were used as input. Hourly-averaged observations from the Norman site are plotted for reference (black curve).

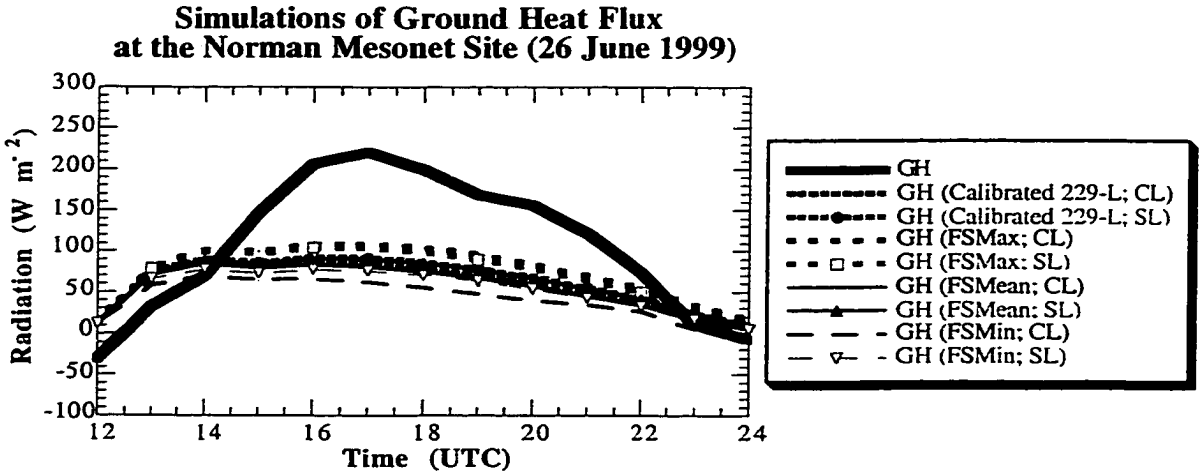

Figure D.1c. Simulations of ground heat flux at the Norman Mesonet site on 26 June 1999 using the clay loam soil parameterization (CL) and the silt loam soil parameterization (SL). Calibrated measurements of 229-L soil water content, and soil water determined from field samples were used as input. Hourly-averaged observations from the Norman site are plotted for reference (black curve).

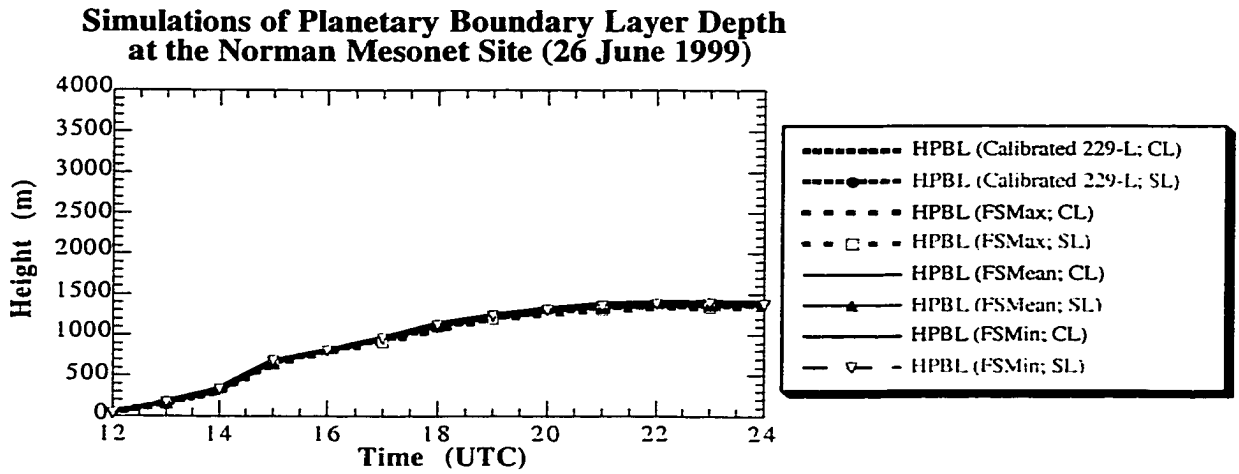

Figure D.1d. Simulations of PBL depth at the Norman Mesonet site on 26 June 1999 using the clay loam soil parameterization (CL) and the silt loam soil parameterization (SL). Calibrated measurements of 229-L soil water content, and soil water determined from field samples were used as input.

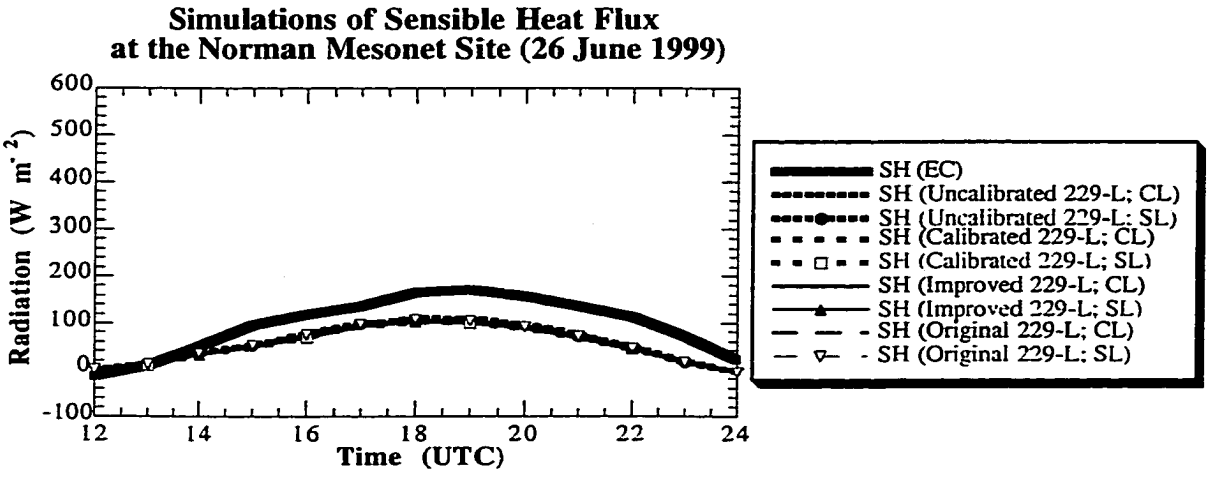

Figure D.2a. Simulations of sensible heat flux at the Norman Mesonet site on 26 June 1999 using the clay loam soil parameterization (CL) and the silt loam soil parameterization (SL). Soil water content was determined using various calibrations applied to the 229-L sensor. Hourly-averaged observations from the Norman site are plotted for reference (black curve).

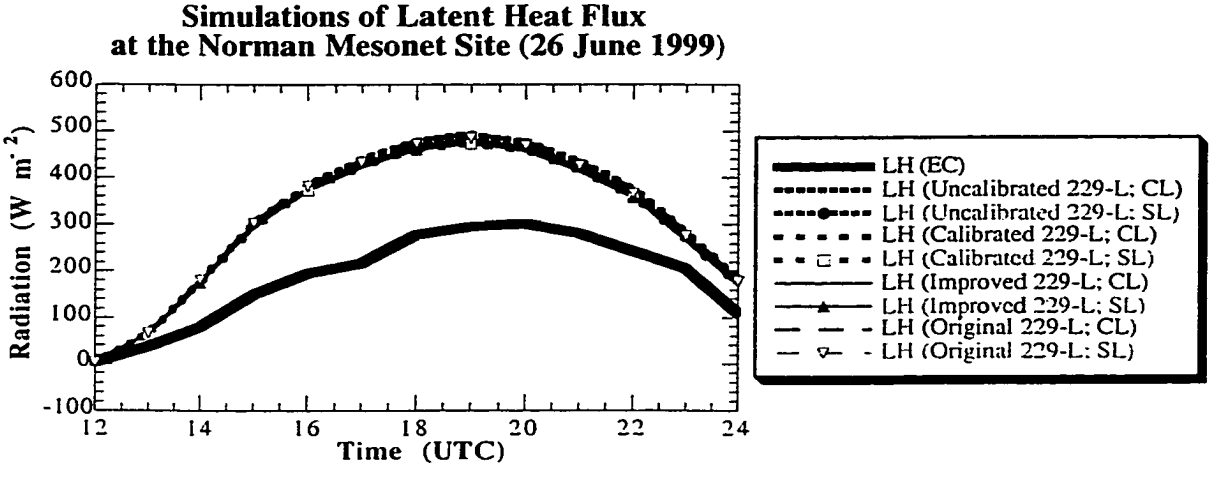

Figure D.2b. Simulations of latent heat flux at the Norman Mesonet site on 26 June 1999 using the clay loam soil parameterization (CL) and the silt loam soil parameterization (SL). Soil water content was determined using various calibrations applied to the 229-L sensor. Hourly-averaged observations from the Norman site are plotted for reference (black curve).

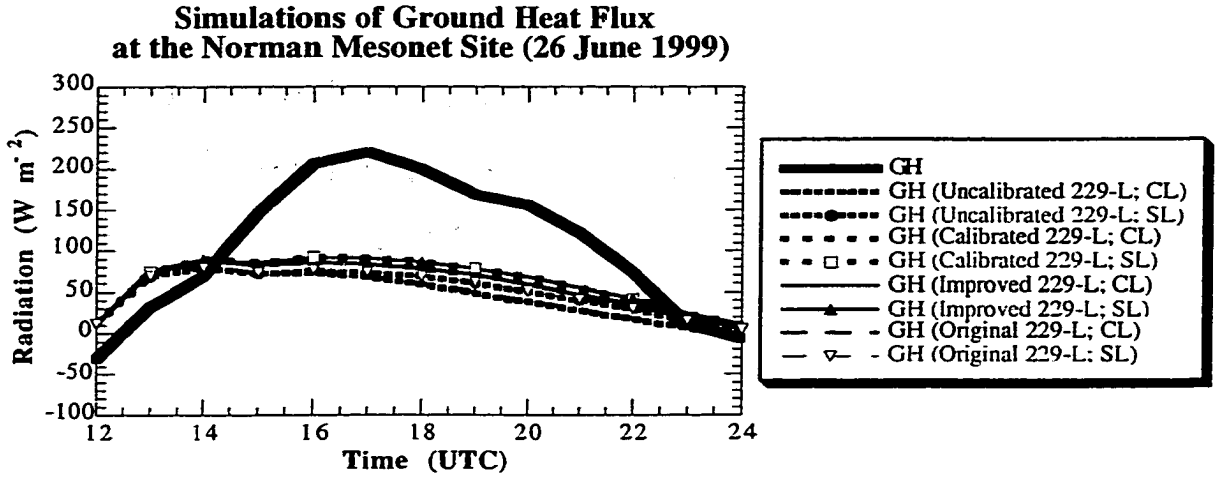

Figure D.2c. Simulations of ground heat flux at the Norman Mesonet site on 26 June 1999 using the clay loam soil parameterization (CL) and the silt loam soil parameterization (SL). Soil water content was determined using various calibrations applied to the 229-L sensor. Hourly-averaged observations from the Norman site are plotted for reference (black curve).

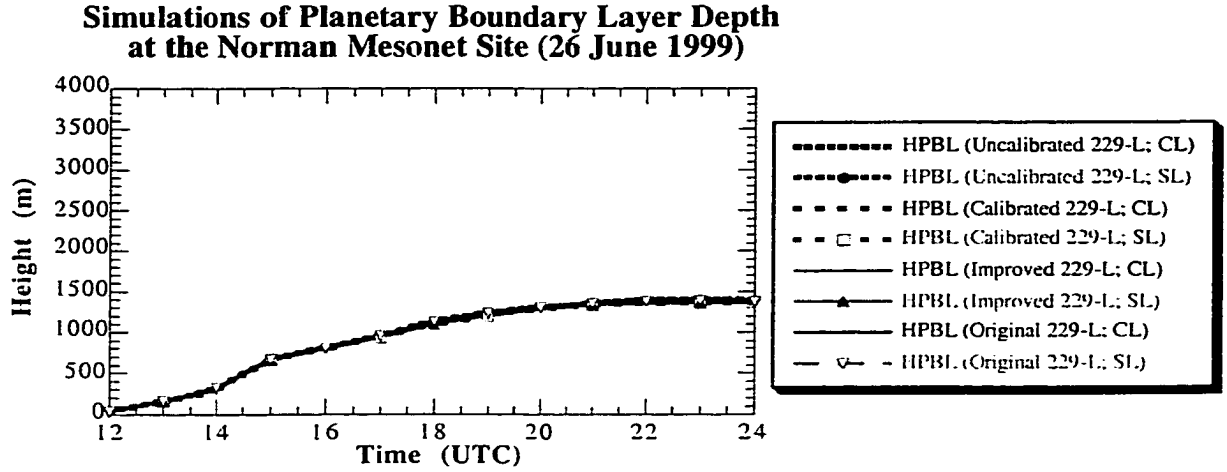

Figure D.2d. Simulations of PBL depth at the Norman Mesonet site on 26 June 1999 using the clay loam soil parameterization (CL) and the silt loam soil parameterization (SL). Soil water content was determined using various calibrations applied to the 229-L sensor.

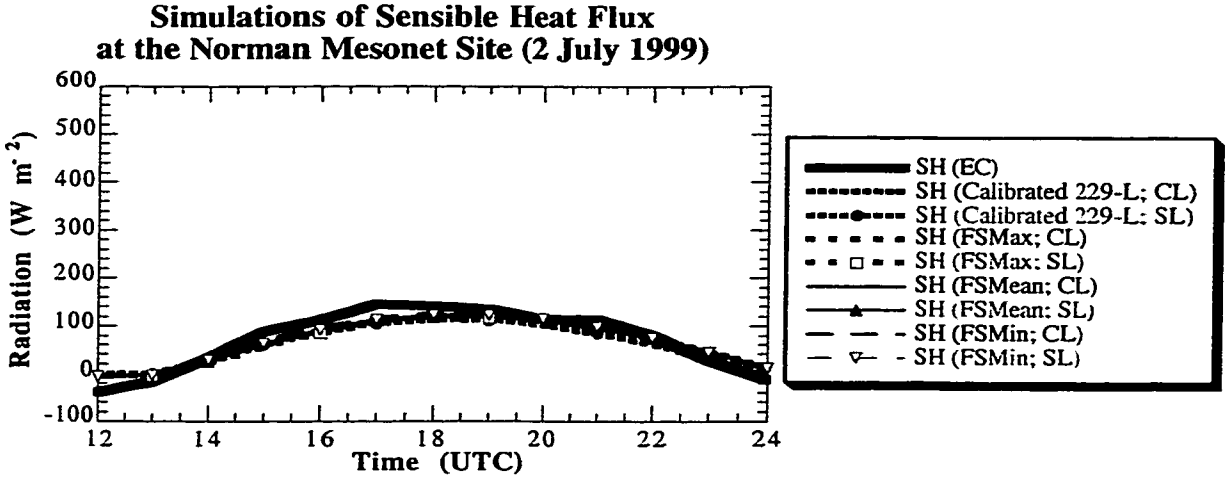

Figure D.3a. Simulations of sensible heat flux at the Norman Mesonet site on 2 July 1999 using the clay loam soil parameterization (CL) and the silt loam soil parameterization (SL). Calibrated measurements of 229-L soil water content, and soil water determined from field samples were used as input. Hourly-averaged observations from the Norman site are plotted for reference (black curve).

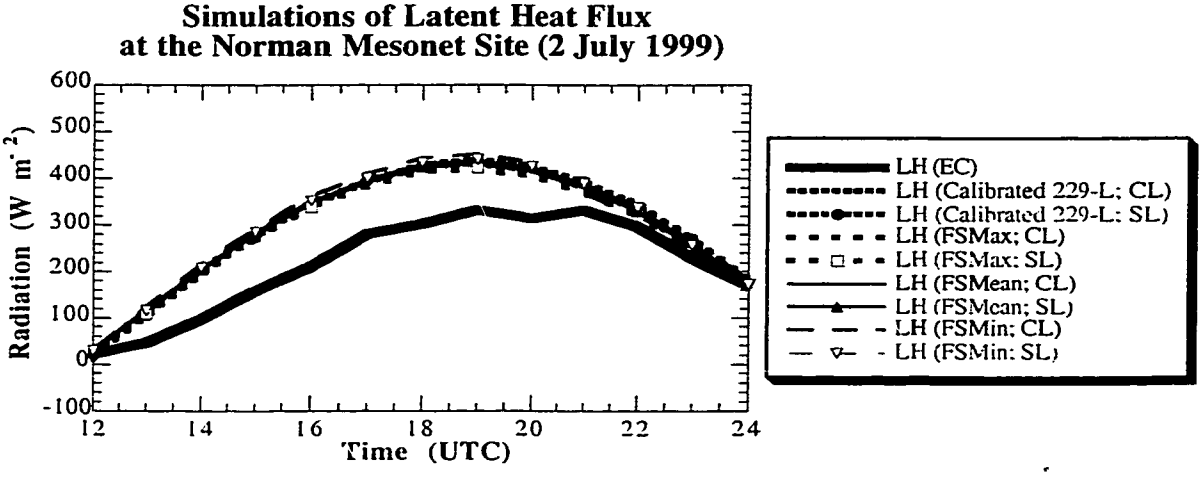

Figure D.3b. Simulations of latent heat flux at the Norman Mesonet site on 2 July 1999 using the clay loam soil parameterization (CL) and the silt loam soil parameterization (SL). Calibrated measurements of 229-L soil water content, and soil water determined from field samples were used as input. Hourly-averaged observations from the Norman site are plotted for reference (black curve).

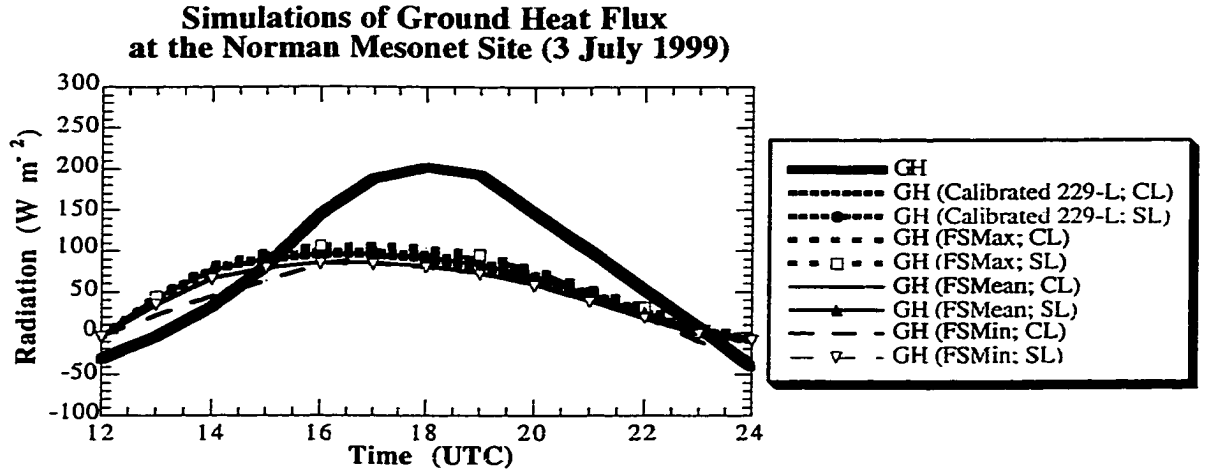

Figure D.3c. Simulations of ground heat flux at the Norman Mesonet site on 2 July 1999 using the clay loam soil parameterization (CL) and the silt loam soil parameterization (SL). Calibrated measurements of 229-L soil water content, and soil water determined from field samples were used as input. Hourly-averaged observations from the Norman site are plotted for reference (black curve).

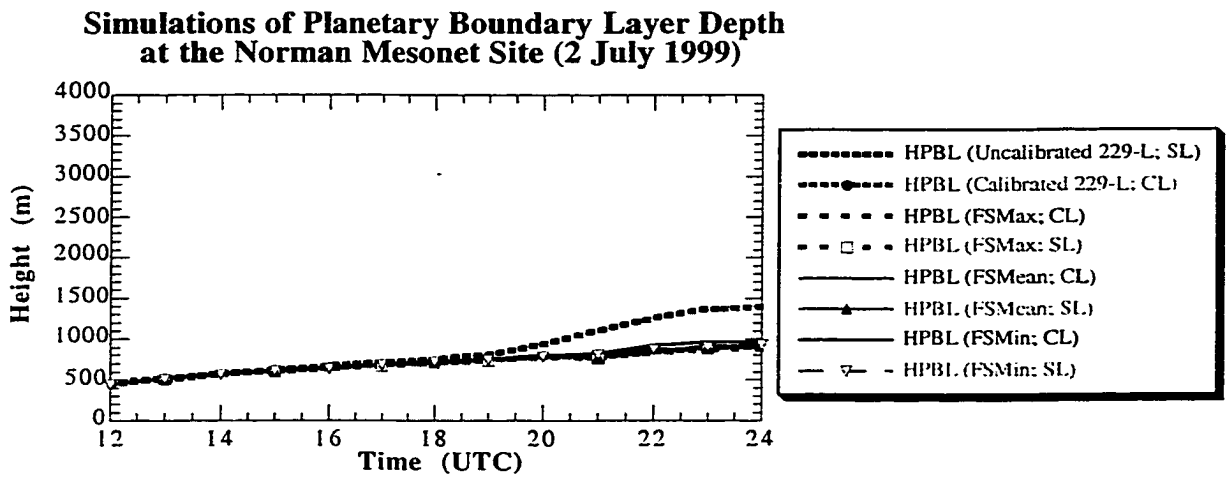

Figure D.3d. Simulations of PBL depth at the Norman Mesonet site on 2 July 1999 using the clay loam soil parameterization (CL) and the silt loam soil parameterization (SL). Calibrated measurements of 229-L soil water content, and soil water determined from field samples were used as input.

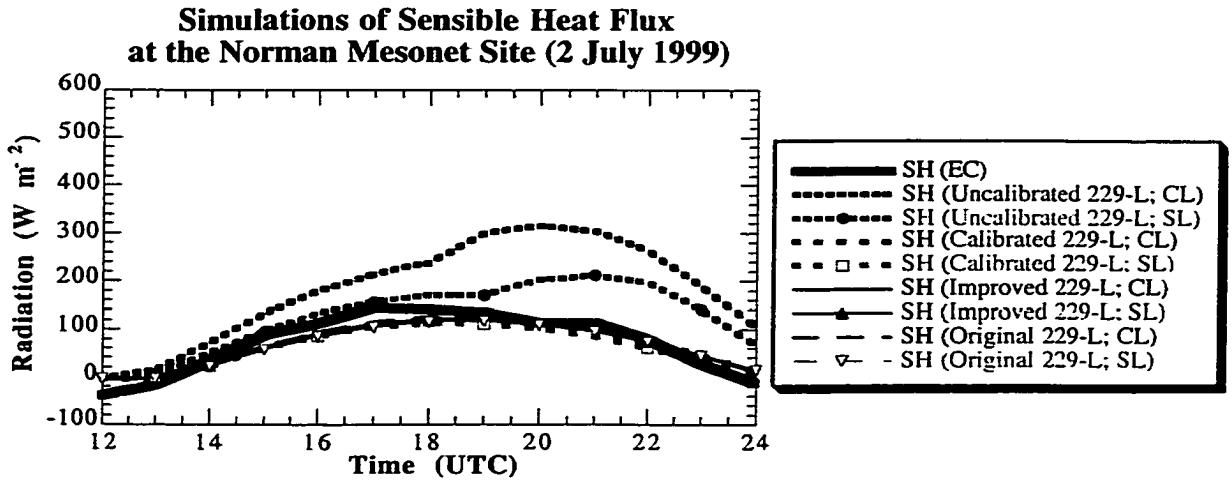

Figure D.4a. Simulations of sensible heat flux at the Norman Mesonet site on 2 July 1999 using the clay loam soil parameterization (CL) and the silt loam soil parameterization (SL). Soil water content was determined using various calibrations applied to the 229-L sensor. Hourly-averaged observations from the Norman site are plotted for reference (black curve).

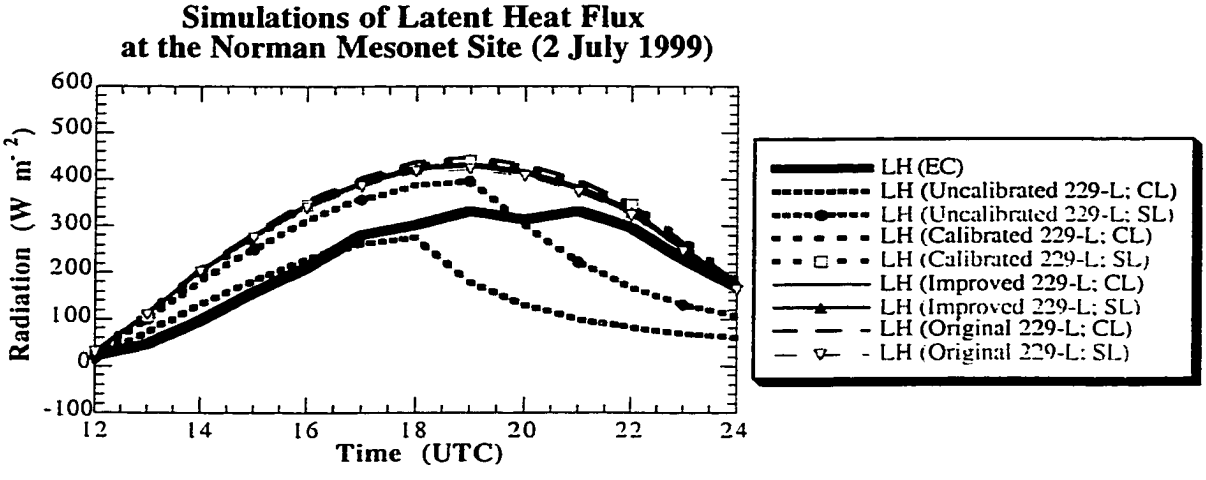

Figure D.4b. Simulations of latent heat flux at the Norman Mesonet site on 2 July 1999 using the clay loam soil parameterization (CL) and the silt loam soil parameterization (SL). Soil water content was determined using various calibrations applied to the 229-L sensor. Hourly-averaged observations from the Norman site are plotted for reference (black curve).

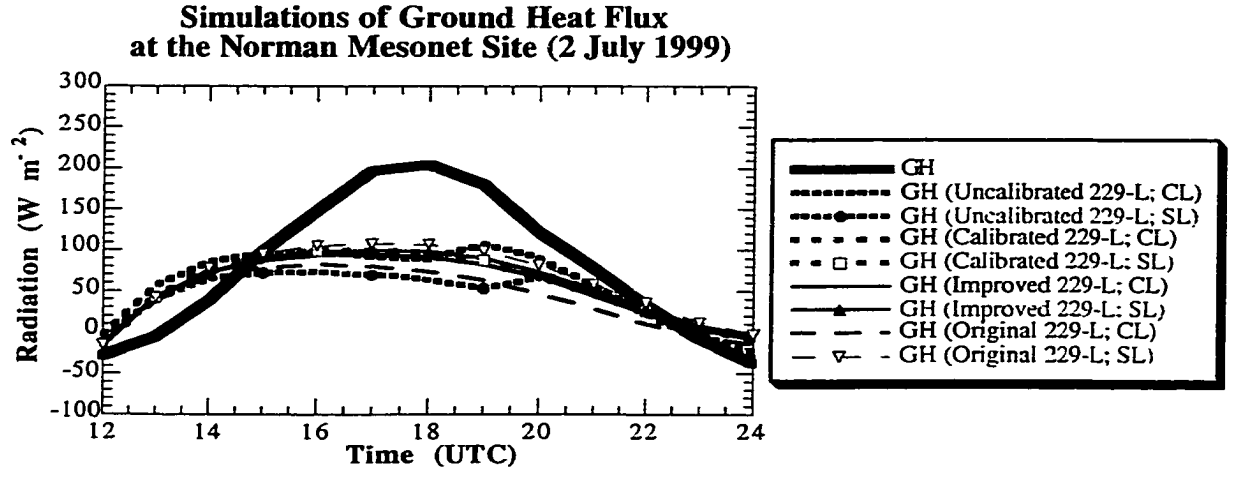

Figure D.4c. Simulations of ground heat flux at the Norman Mesonet site on 2 July 1999 using the clay loam soil parameterization (CL) and the silt loam soil parameterization (SL). Soil water content was determined using various calibrations applied to the 229-L sensor. Hourly-averaged observations from the Norman site are plotted for reference (black curve).

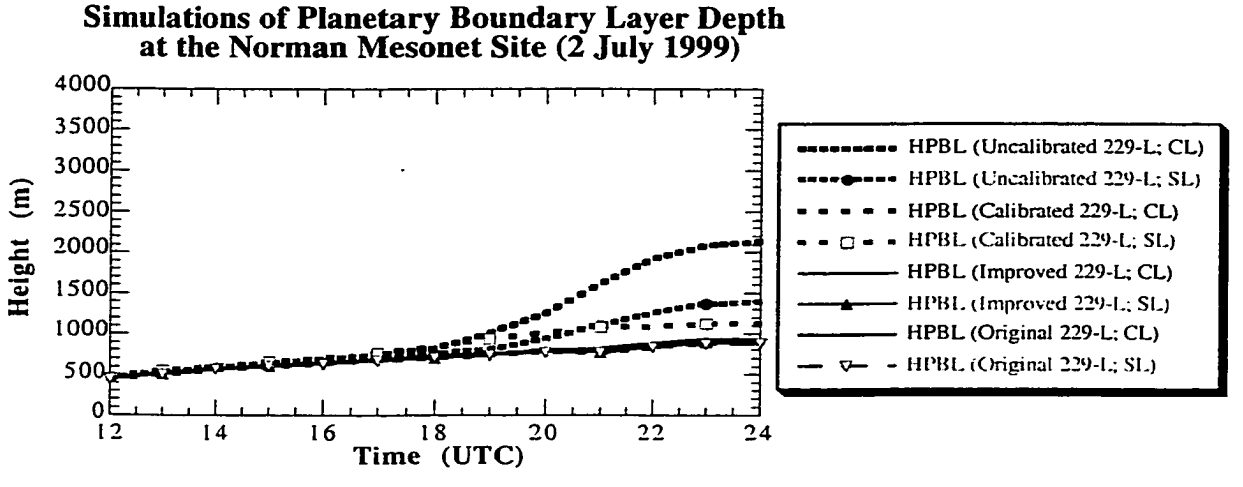

Figure D.4d. Simulations of PBL depth at the Norman Mesonet site on 2 July 1999 using the clay loam soil parameterization (CL) and the silt loam soil parameterization (SL). Soil water content was determined using various calibrations applied to the 229-L sensor.

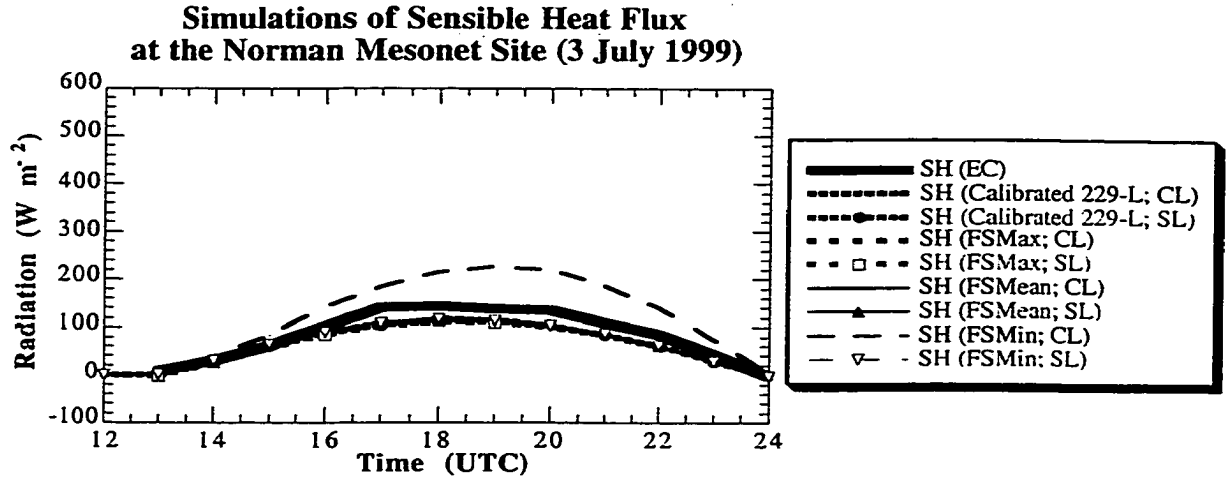

Figure D.5a. Simulations of sensible heat flux at the Norman Mesonet site on 3 July 1999 using the clay loam soil parameterization (CL) and the silt loam soil parameterization (SL). Calibrated measurements of 229-L soil water content, and soil water determined from field samples were used as input. Hourly-averaged observations from the Norman site are plotted for reference (black curve).

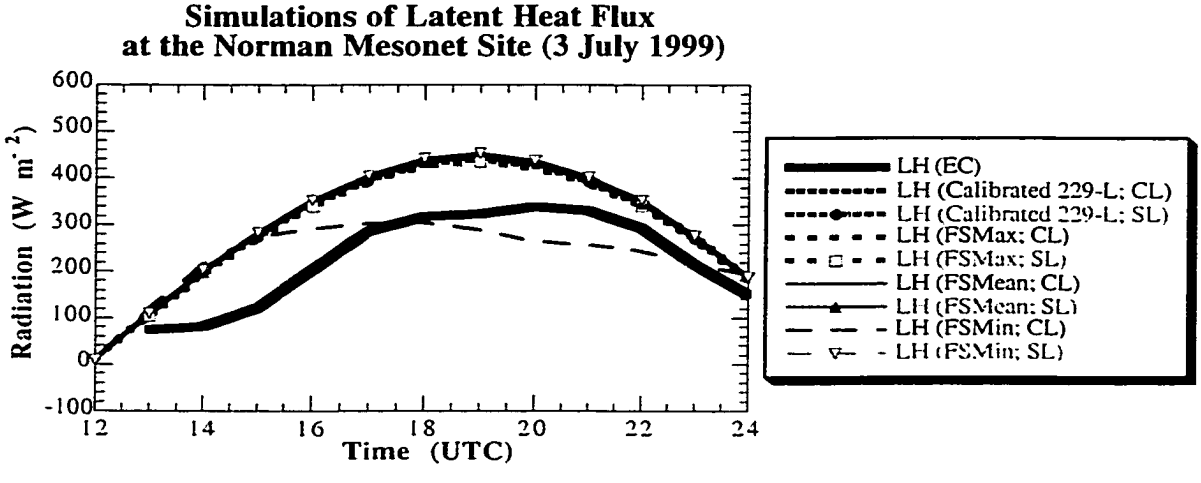

Figure D.5b. Simulations of latent heat flux at the Norman Mesonet site on 3 July 1999 using the clay loam soil parameterization (CL) and the silt loam soil parameterization (SL). Calibrated measurements of 229-L soil water content, and soil water determined from field samples were used as input. Hourly-averaged observations from the Norman site are plotted for reference (black curve).

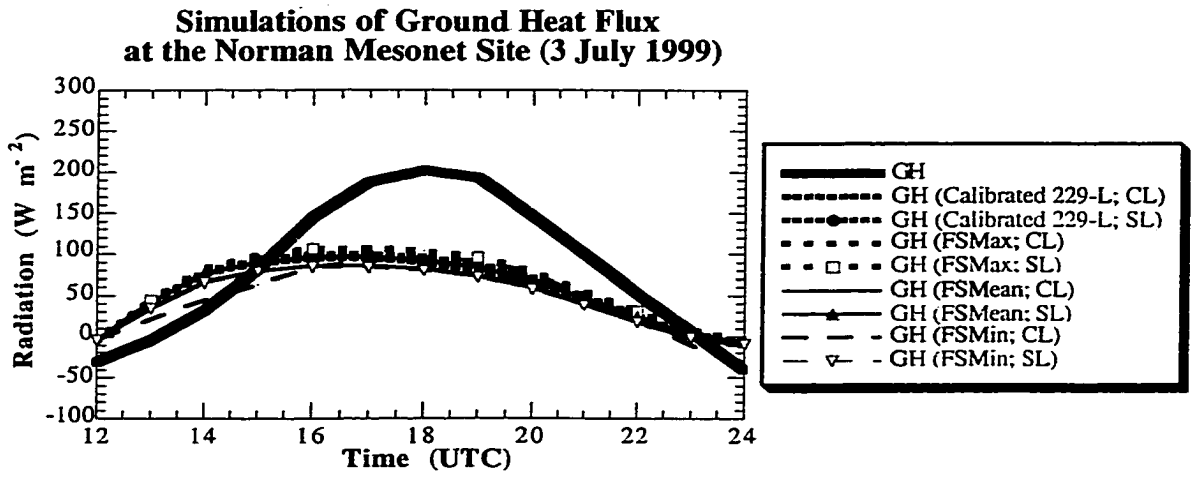

Figure D.5c. Simulations of ground heat flux at the Norman Mesonet site on 3 July 1999 using the clay loam soil parameterization (CL) and the silt loam soil parameterization (SL). Calibrated measurements of 229-L soil water content, and soil water determined from field samples were used as input. Hourly-averaged observations from the Norman site are plotted for reference (black curve).

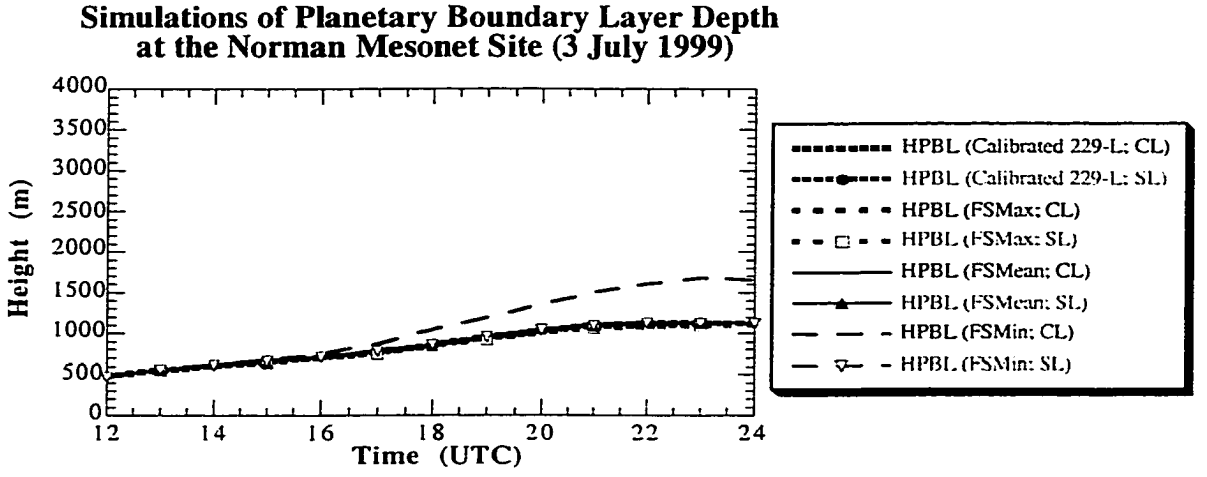

Figure D.5d. Simulations of PBL depth at the Norman Mesonet site on 3 July 1999 using the clay loam soil parameterization (CL) and the silt loam soil parameterization (SL). Calibrated measurements of 229-L soil water content, and soil water determined from field samples were used as input.

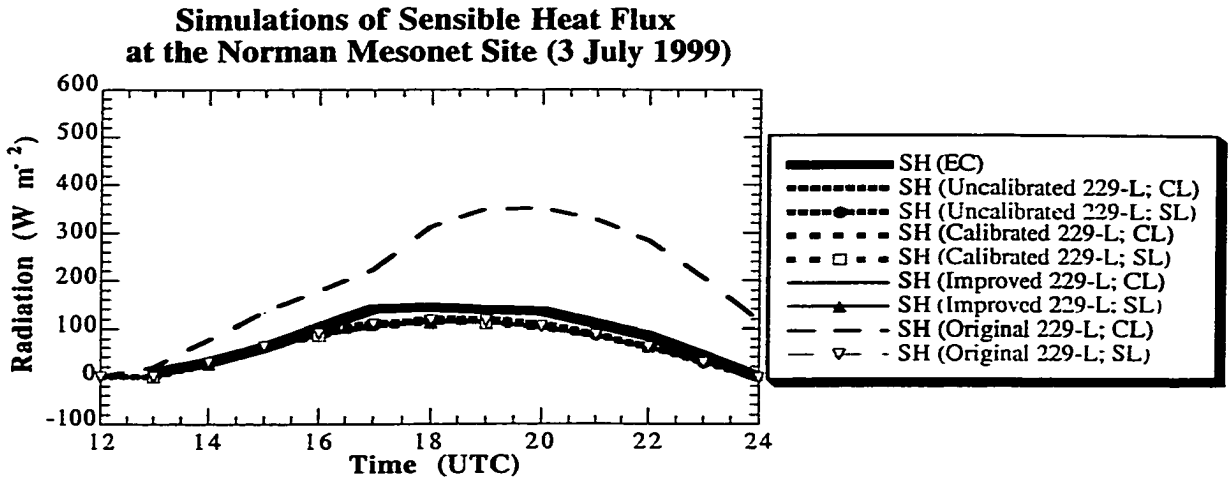

Figure D.6a. Simulations of sensible heat flux at the Norman Mesonet site on 3 July 1999 using the clay loam soil parameterization (CL) and the silt loam soil parameterization (SL). Soil water content was determined using various calibrations applied to the 229-L sensor. Hourly-averaged observations from the Norman site are plotted for reference (black curve).

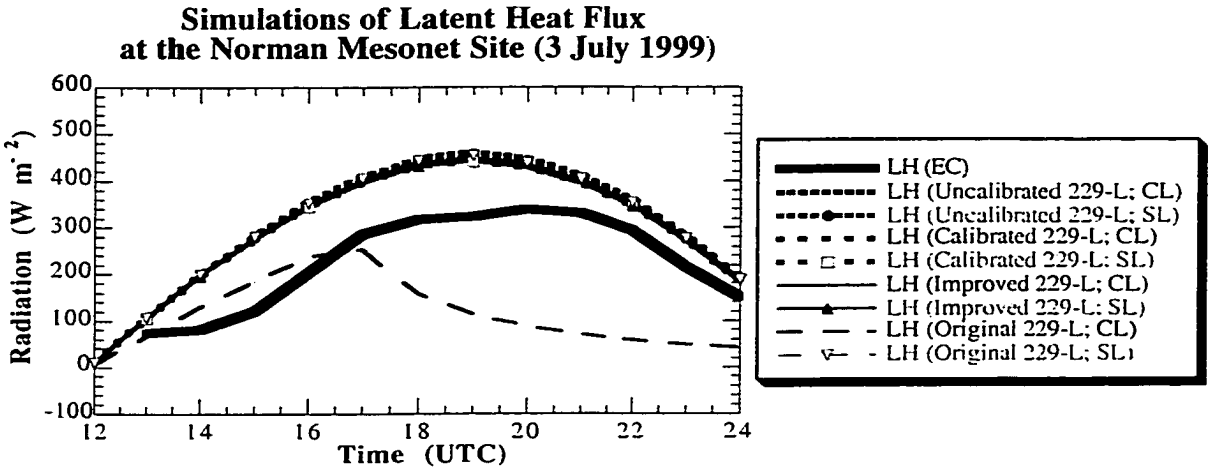

Figure D.6b. Simulations of latent heat flux at the Norman Mesonet site on 3 July 1999 using the clay loam soil parameterization (CL) and the silt loam soil parameterization (SL). Soil water content was determined using various calibrations applied to the 229-L sensor. Hourly-averaged observations from the Norman site are plotted for reference (black curve).

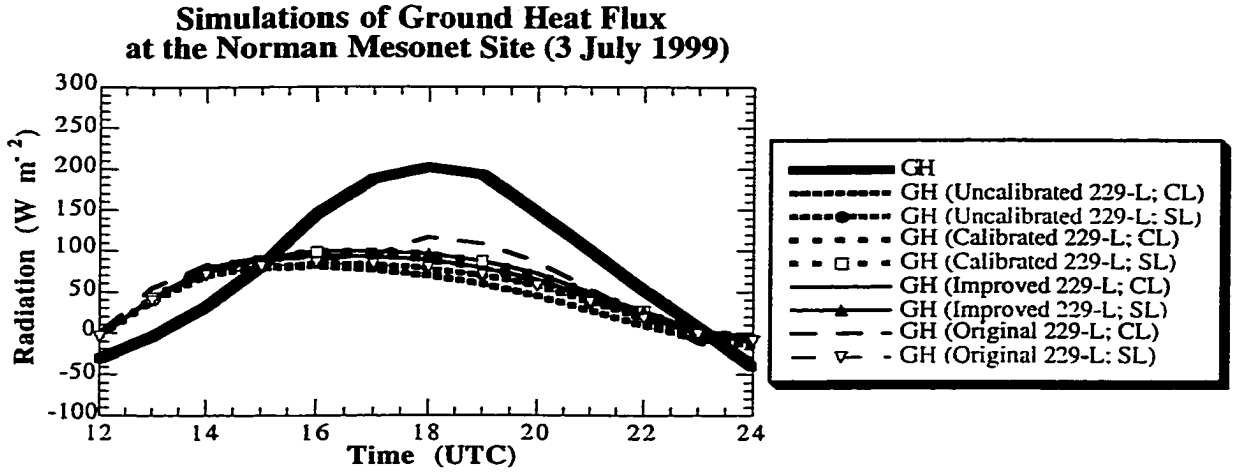

Figure D.6c. Simulations of ground heat flux at the Norman Mesonet site on 3 July 1999 using the clay loam soil parameterization (CL) and the silt loam soil parameterization (SL). Soil water content was determined using various calibrations applied to the 229-L sensor. Hourly-averaged observations from the Norman site are plotted for reference (black curve).

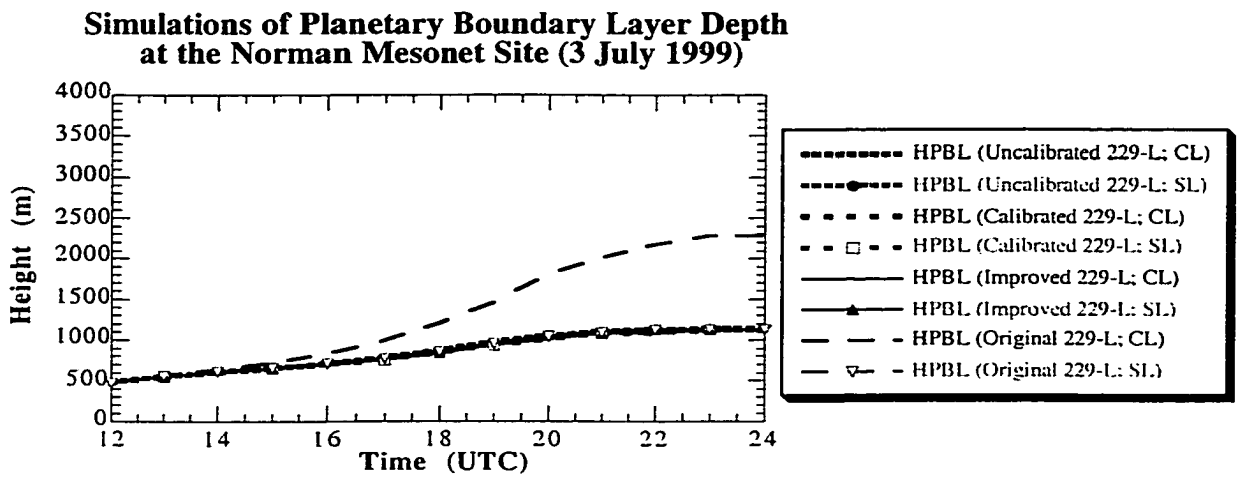

Figure D.6d. Simulations of PBL depth at the Norman Mesonet site on 3 July 1999 using the clay loam soil parameterization (CL) and the silt loam soil parameterization (SL). Soil water content was determined using various calibrations applied to the 229-L sensor.

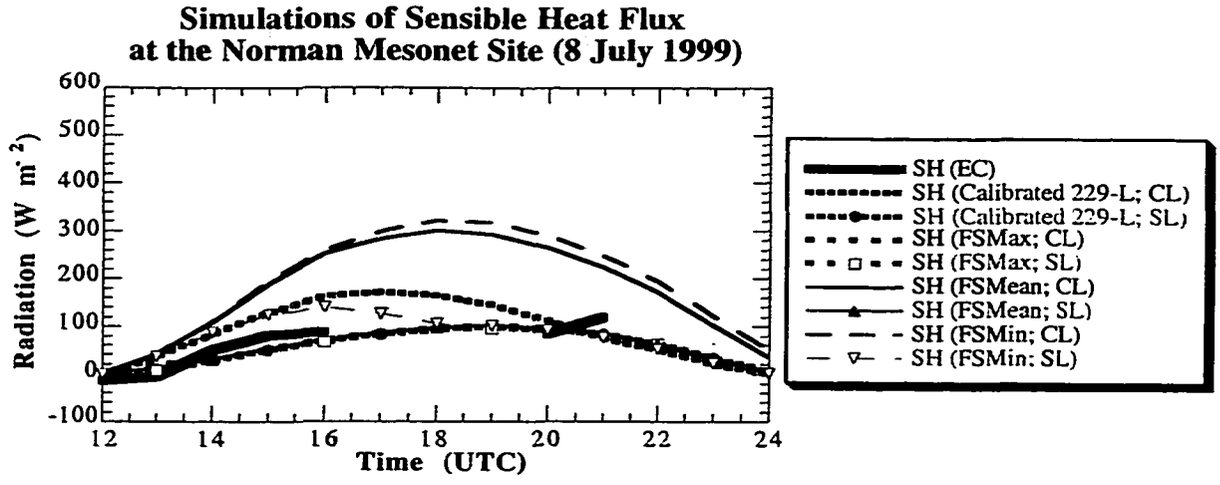

Figure D.7a. Simulations of sensible heat flux at the Norman Mesonet site on 8 July 1999 using the clay loam soil parameterization (CL) and the silt loam soil parameterization (SL). Calibrated measurements of 229-L soil water content, and soil water determined from field samples were used as input. Hourly-averaged observations from the Norman site are plotted for reference (black curve).

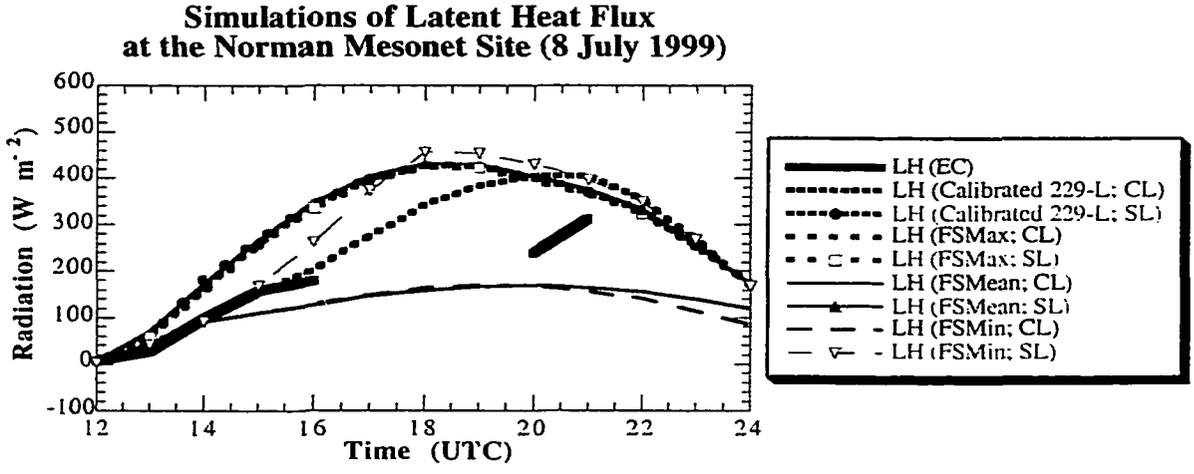

Figure D.7b. Simulations of latent heat flux at the Norman Mesonet site on 8 July 1999 using the clay loam soil parameterization (CL) and the silt loam soil parameterization (SL). Calibrated measurements of 229-L soil water content, and soil water determined from field samples were used as input. Hourly-averaged observations from the Norman site are plotted for reference (black curve).

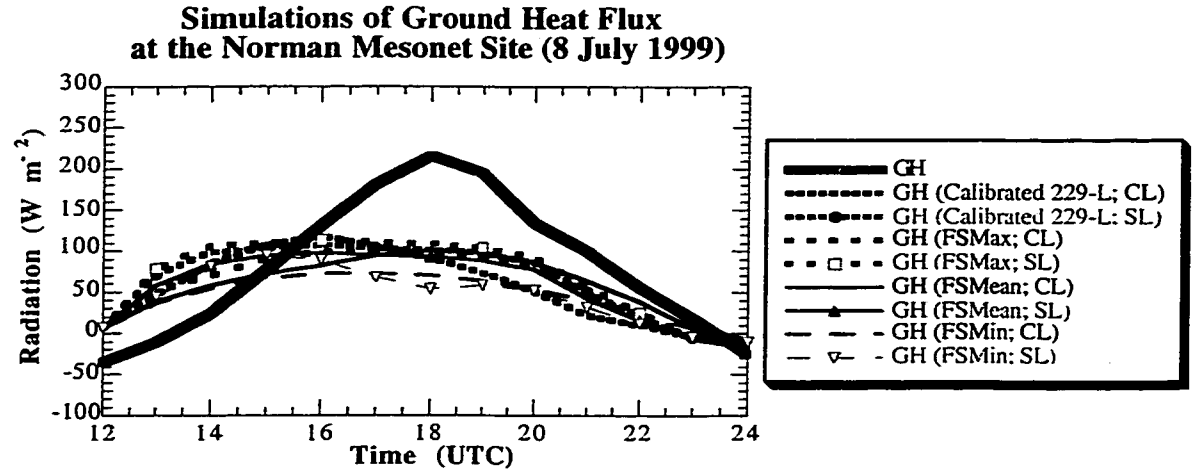

Figure D.7c. Simulations of ground heat flux at the Norman Mesonet site on 8 July 1999 using the clay loam soil parameterization (CL) and the silt loam soil parameterization (SL). Calibrated measurements of 229-L soil water content, and soil water determined from field samples were used as input. Hourly-averaged observations from the Norman site are plotted for reference (black curve).

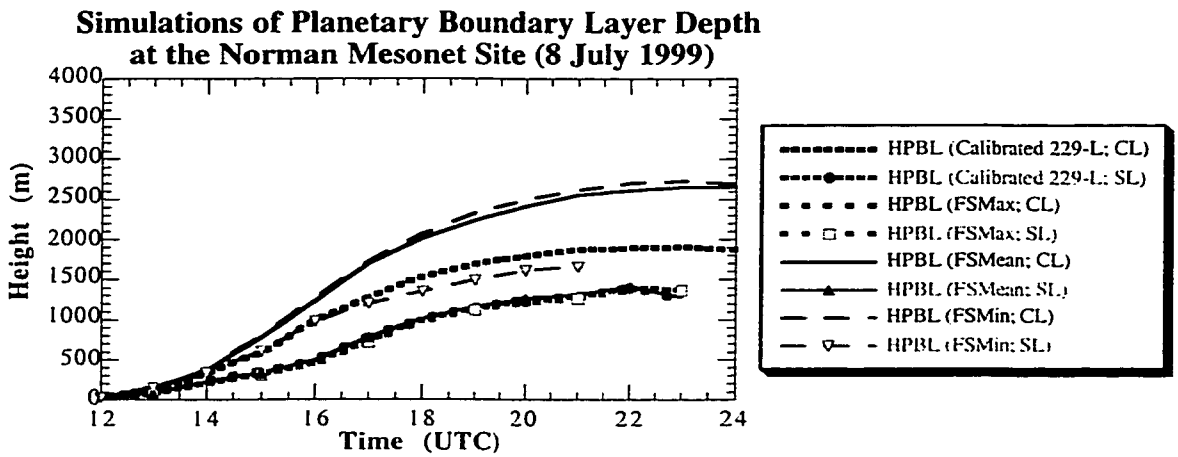

Figure D.7d. Simulations of PBL depth at the Norman Mesonet site on 8 July 1999 using the clay loam soil parameterization (CL) and the silt loam soil parameterization (SL). Calibrated measurements of 229-L soil water content, and soil water determined from field samples were used as input.

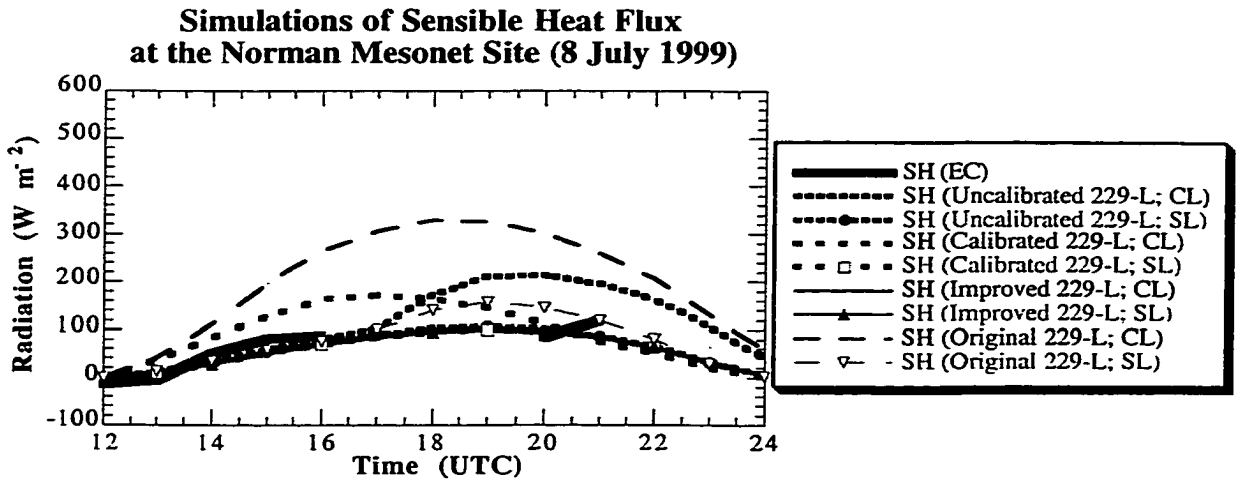

Figure D.8a. Simulations of sensible heat flux at the Norman Mesonet site on 8 July 1999 using the clay loam soil parameterization (CL) and the silt loam soil parameterization (SL). Soil water content was determined using various calibrations applied to the 229-L sensor. Hourly-averaged observations from the Norman site are plotted for reference (black curve).

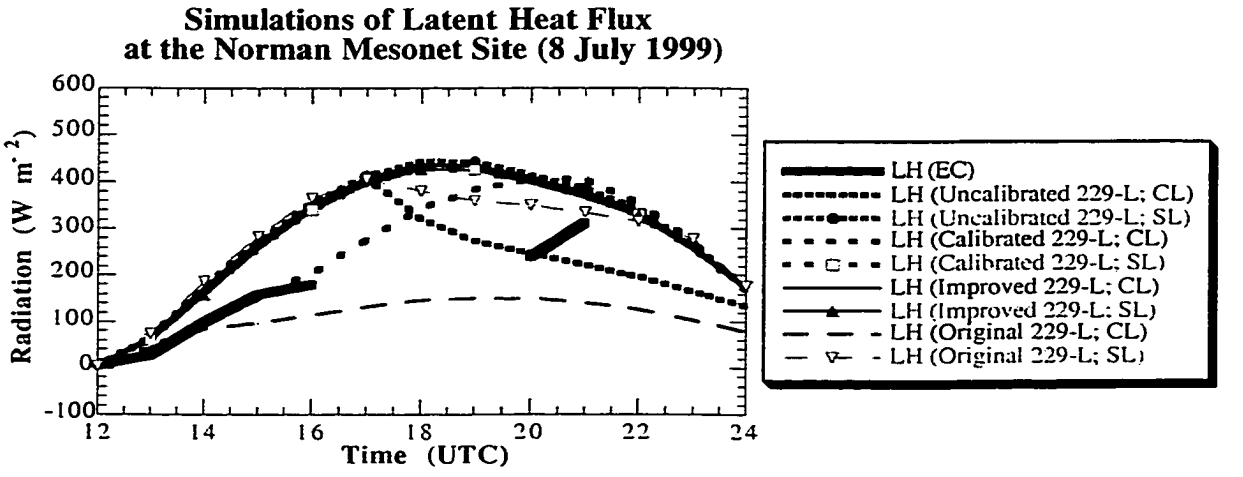

Figure D.8b. Simulations of latent heat flux at the Norman Mesonet site on 8 July 1999 using the clay loam soil parameterization (CL) and the silt loam soil parameterization (SL). Soil water content was determined using various calibrations applied to the 229-L sensor. Hourly-averaged observations from the Norman site are plotted for reference (black curve).

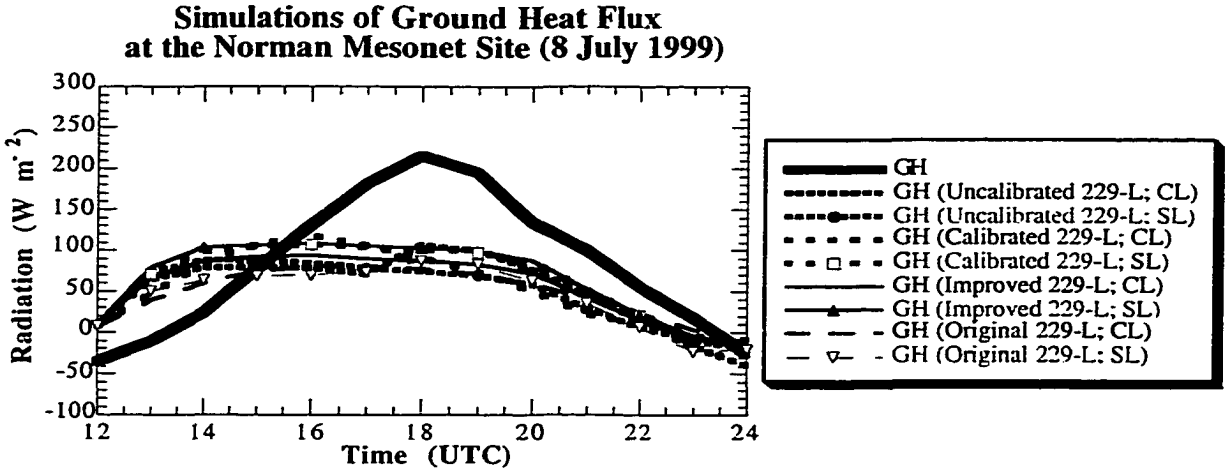

Figure D.8c. Simulations of ground heat flux at the Norman Mesonet site on 8 July 1999 using the clay loam soil parameterization (CL) and the silt loam soil parameterization (SL). Soil water content was determined using various calibrations applied to the 229-L sensor. Hourly-averaged observations from the Norman site are plotted for reference (black curve).

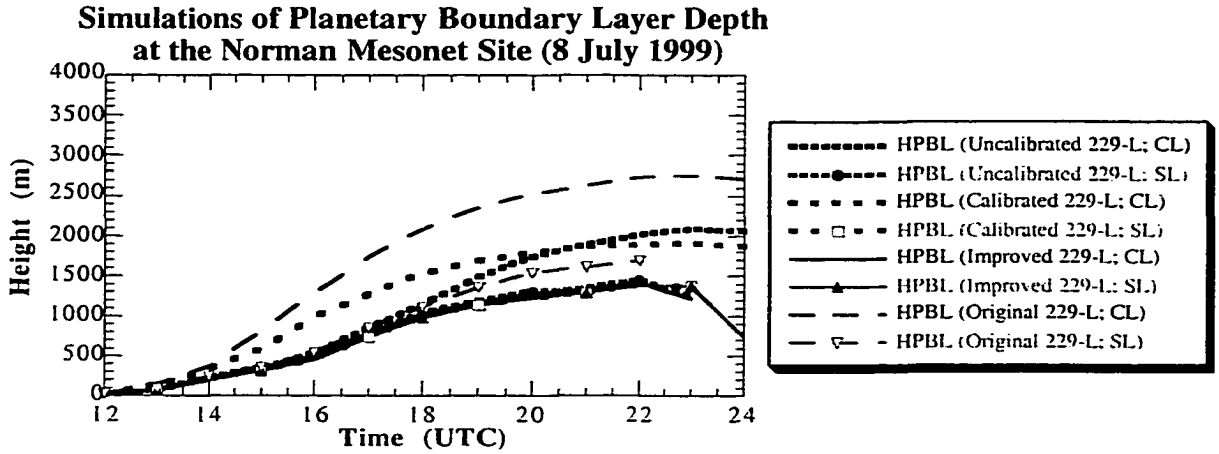

Figure D.8d. Simulations of PBL depth at the Norman Mesonet site on 8 July 1999 using the clay loam soil parameterization (CL) and the silt loam soil parameterization (SL). Soil water content was determined using various calibrations applied to the 229-L sensor. Hourly-averaged observations from the Norman site are plotted for reference (black curve).

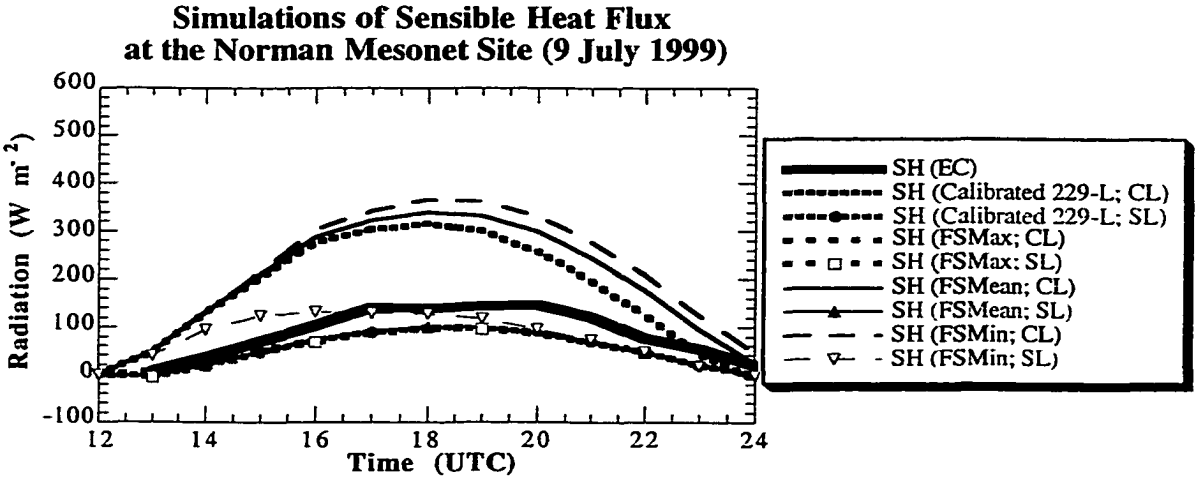

Figure D.9a. Simulations of sensible heat flux at the Norman Mesonet site on 9 July 1999 using the clay loam soil parameterization (CL) and the silt loam soil parameterization (SL). Calibrated measurements of 229-L soil water content, and soil water determined from field samples were used as input. Hourly-averaged observations from the Norman site are plotted for reference (black curve).

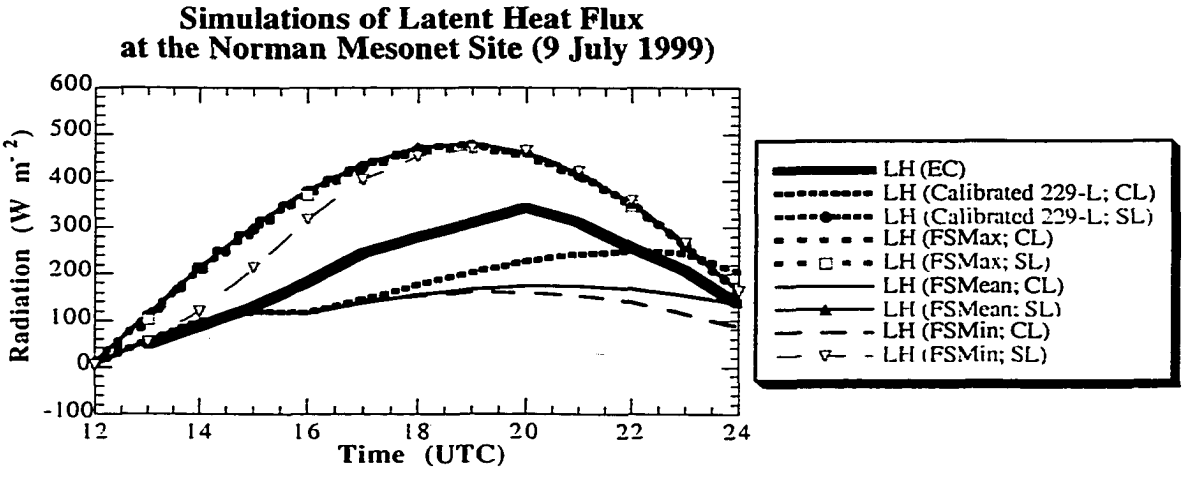

Figure D.9b. Simulations of latent heat flux at the Norman Mesonet site on 9 July 1999 using the clay loam soil parameterization (CL) and the silt loam soil parameterization (SL). Calibrated measurements of 229-L soil water content, and soil water determined from field samples were used as input. Hourly-averaged observations from the Norman site are plotted for reference (black curve).

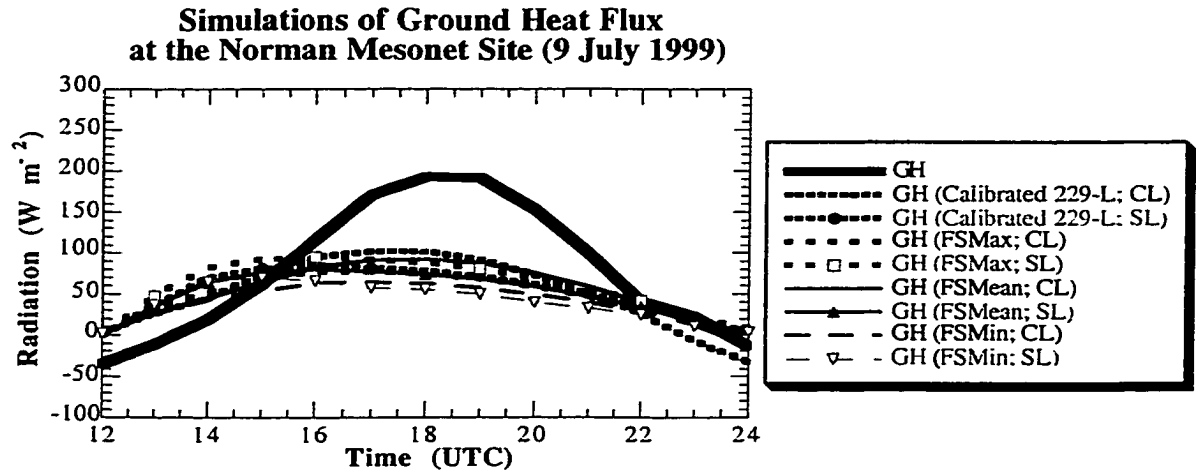

Figure D.9c. Simulations of ground heat flux at the Norman Mesonet site on 9 July 1999 using the clay loam soil parameterization (CL) and the silt loam soil parameterization (SL). Calibrated measurements of 229-L soil water content, and soil water determined from field samples were used as input. Hourly-averaged observations from the Norman site are plotted for reference (black curve).

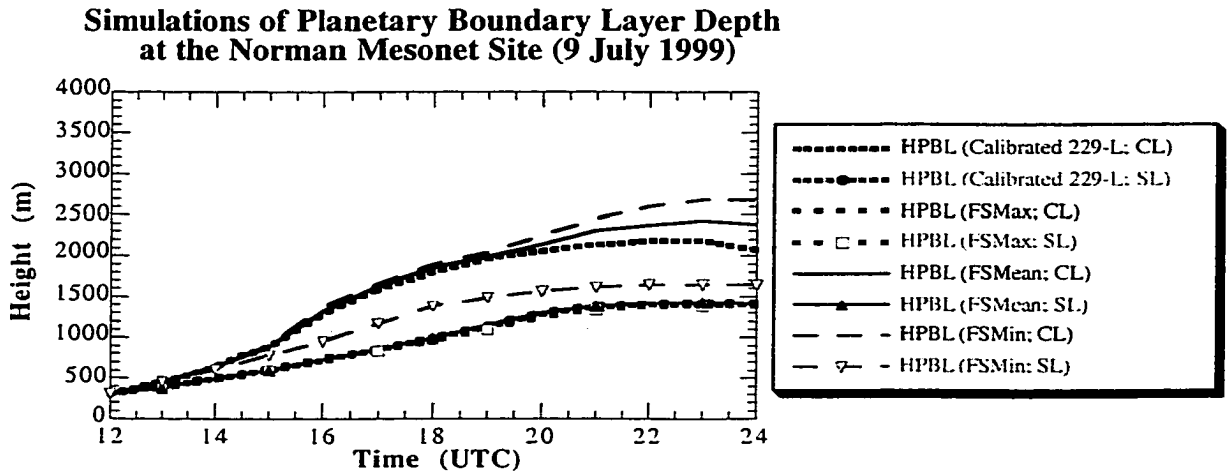

Figure D.9d. Simulations of PBL depth at the Norman Mesonet site on 9 July 1999 using the clay loam soil parameterization (CL) and the silt loam soil parameterization (SL). Calibrated measurements of 229-L soil water content, and soil water determined from field samples were used as input. Hourly-averaged observations from the Norman site are plotted for reference (black curve).

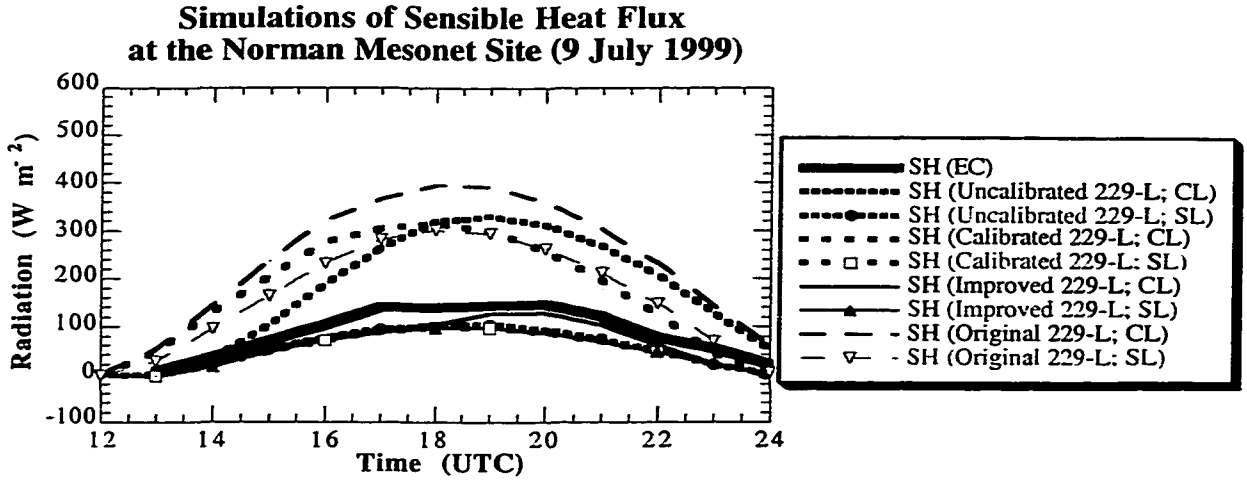

Figure D.10a. Simulations of sensible heat flux at the Norman Mesonet site on 9 July 1999 using the clay loam soil parameterization (CL) and the silt loam soil parameterization (SL). Soil water content was determined using various calibrations applied to the 229-L sensor. Hourly-averaged observations from the Norman site are plotted for reference (black curve).

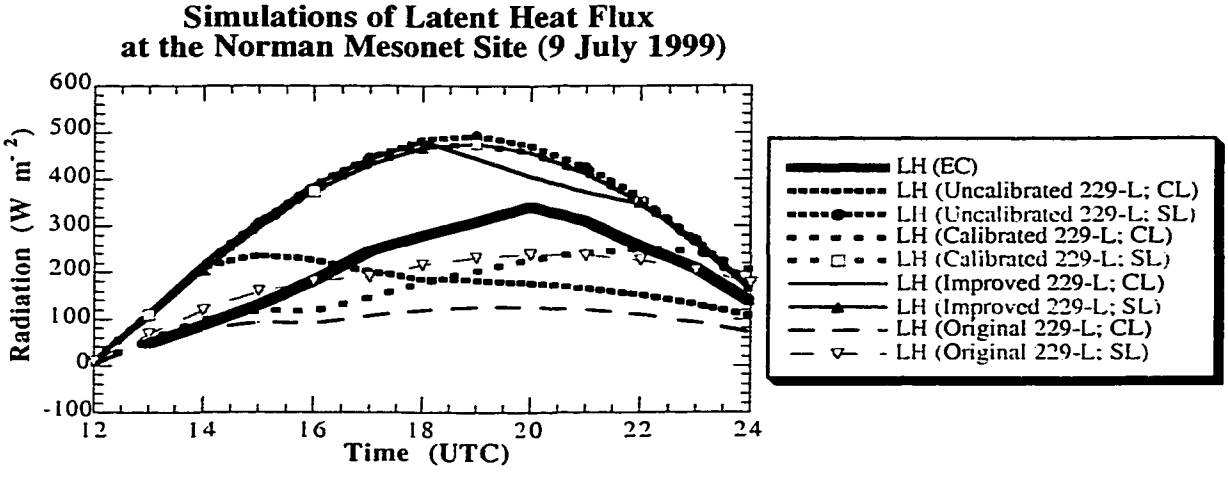

Figure D.10b. Simulations of latent heat flux at the Norman Mesonet site on 9 July 1999 using the clay loam soil parameterization (CL) and the silt loam soil parameterization (SL). Soil water content was determined using various calibrations applied to the 229-L sensor. Hourly-averaged observations from the Norman site are plotted for reference (black curve).

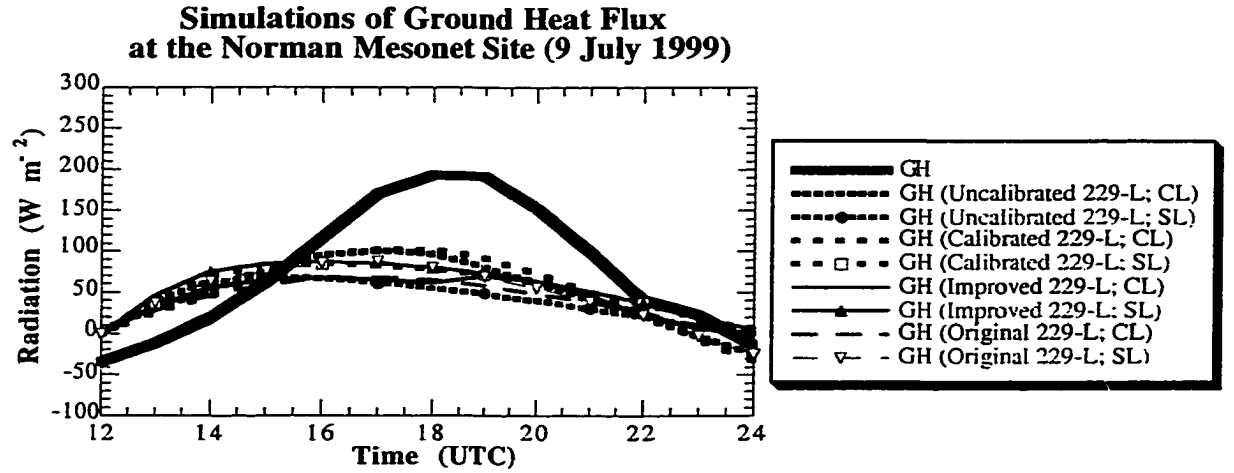

Figure D.10c. Simulations of ground heat flux at the Norman Mesonet site on 9 July 1999 using the clay loam soil parameterization (CL) and the silt loam soil parameterization (SL). Soil water content was determined using various calibrations applied to the 229-L sensor. Hourly-averaged observations from the Norman site are plotted for reference (black curve).

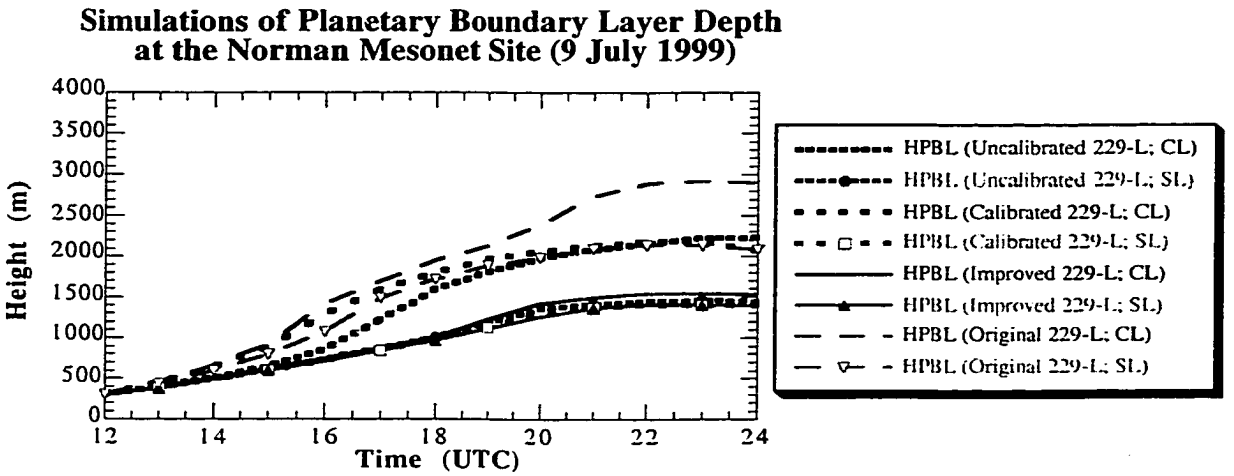

Figure D.10d. Simulations of PBL depth at the Norman Mesonet site on 9 July 1999 using the clay loam soil parameterization (CL) and the silt loam soil parameterization (SL). Soil water content was determined using various calibrations applied to the 229-L sensor.

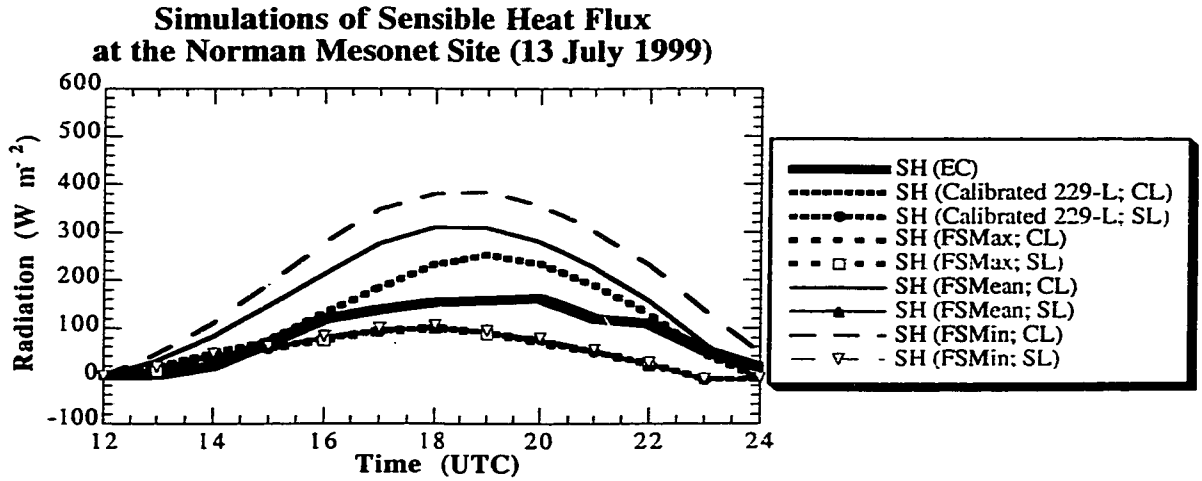

Figure D.11a. Simulations of sensible heat flux at the Norman Mesonet site on 13 July 1999 using the clay loam soil parameterization (CL) and the silt loam soil parameterization (SL). Calibrated measurements of 229-L soil water content, and soil water determined from field samples were used as input. Hourly-averaged observations from the Norman site are plotted for reference (black curve).

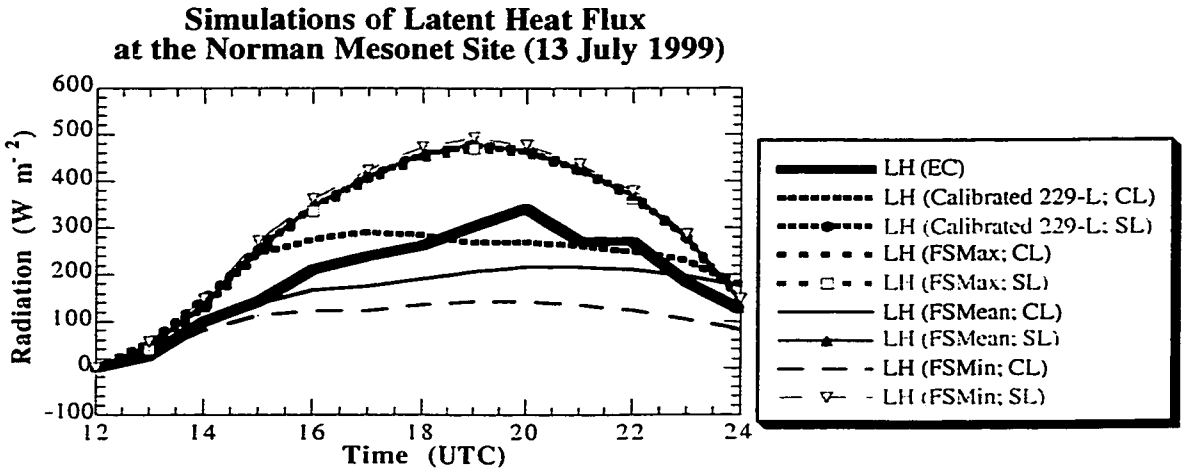

Figure D.11b. Simulations of latent heat flux at the Norman Mesonet site on 13 July 1999 using the clay loam soil parameterization (CL) and the silt loam soil parameterization (SL). Calibrated measurements of 229-L soil water content, and soil water determined from field samples were used as input. Hourly-averaged observations from the Norman site are plotted for reference (black curve).

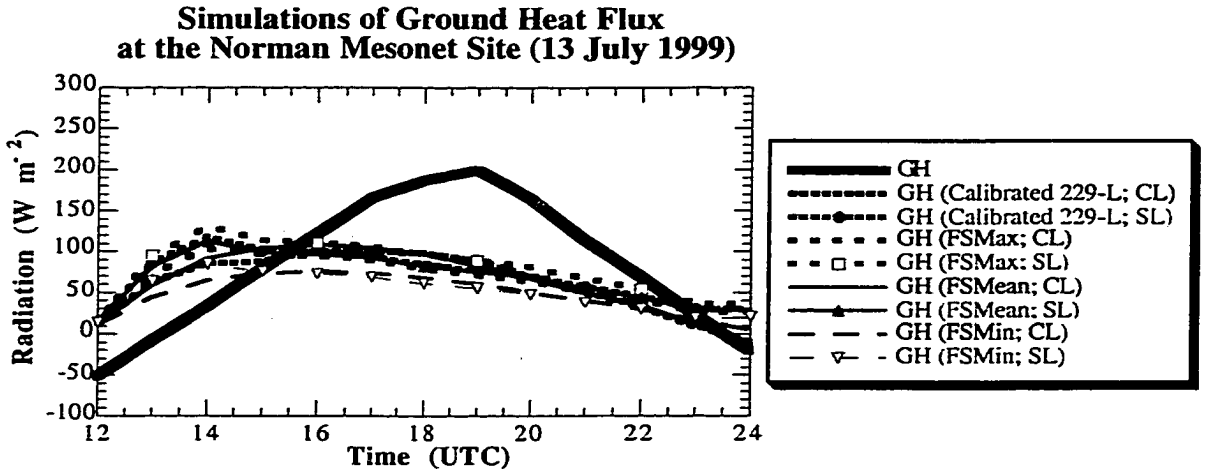

Figure D.11c. Simulations of ground heat flux at the Norman Mesonet site on 13 July 1999 using the clay loam soil parameterization (CL) and the silt loam soil parameterization (SL). Calibrated measurements of 229-L soil water content, and soil water determined from field samples were used as input. Hourly-averaged observations from the Norman site are plotted for reference (black curve).

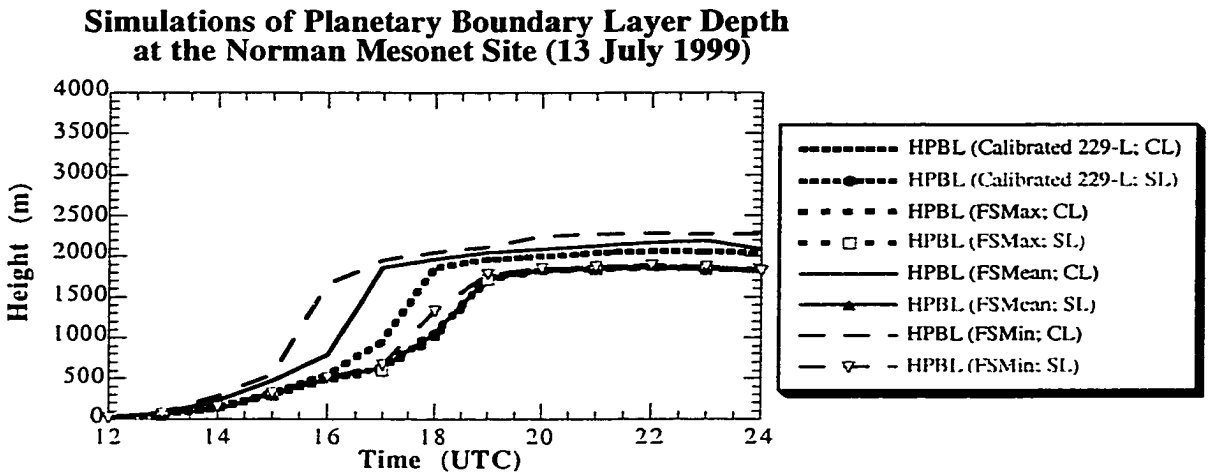

Figure D.11d. Simulations of PBL depth at the Norman Mesonet site on 13 July 1999 using the clay loam soil parameterization (CL) and the silt loam soil parameterization (SL). Calibrated measurements of 229-L soil water content, and soil water determined from field samples were used as input.

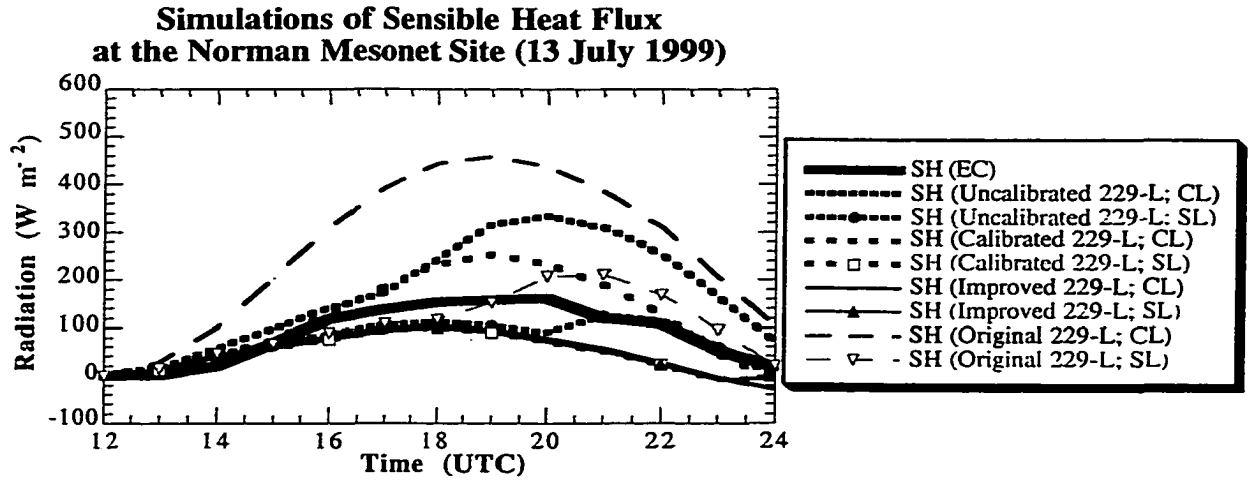

Figure D.12a. Simulations of sensible heat flux at the Norman Mesonet site on 13 July 1999 using the clay loam soil parameterization (CL) and the silt loam soil parameterization (SL). Soil water content was determined using various calibrations applied to the 229-L sensor. Hourly-averaged observations from the Norman site are plotted for reference (black curve).

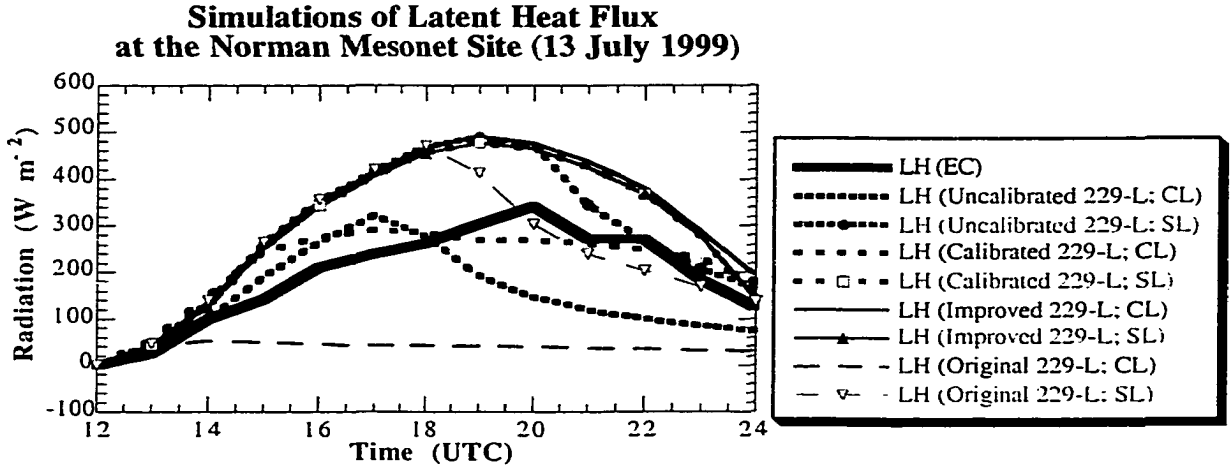

Figure D.12b. Simulations of latent heat flux at the Norman Mesonet site on 13 July 1999 using the clay loam soil parameterization (CL) and the silt loam soil parameterization (SL). Soil water content was determined using various calibrations applied to the 229-L sensor. Hourly-averaged observations from the Norman site are plotted for reference (black curve).

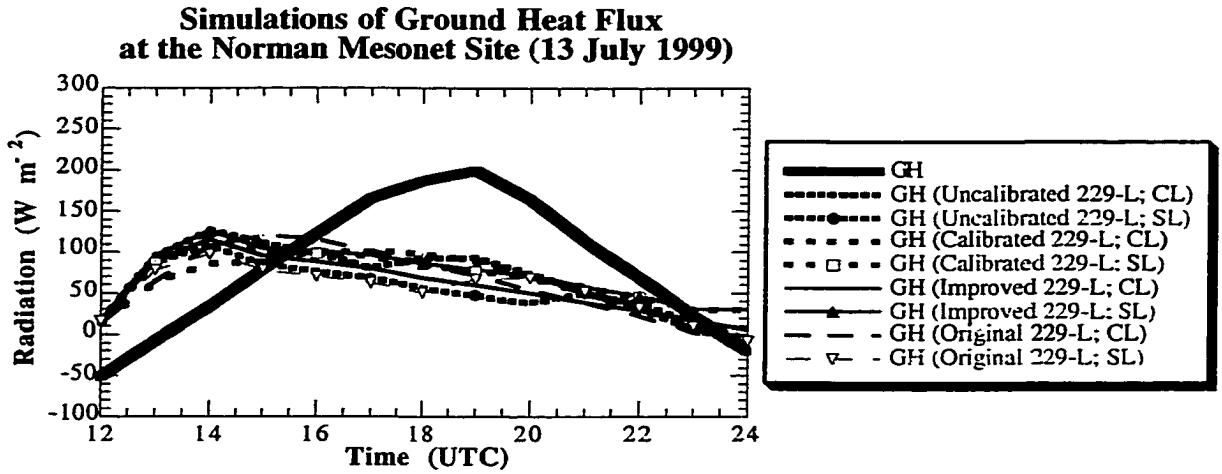

Figure D.12c. Simulations of ground heat flux at the Norman Mesonet site on 13 July 1999 using the clay loam soil parameterization (CL) and the silt loam soil parameterization (SL). Soil water content was determined using various calibrations applied to the 229-L sensor. Hourly-averaged observations from the Norman site are plotted for reference (black curve).

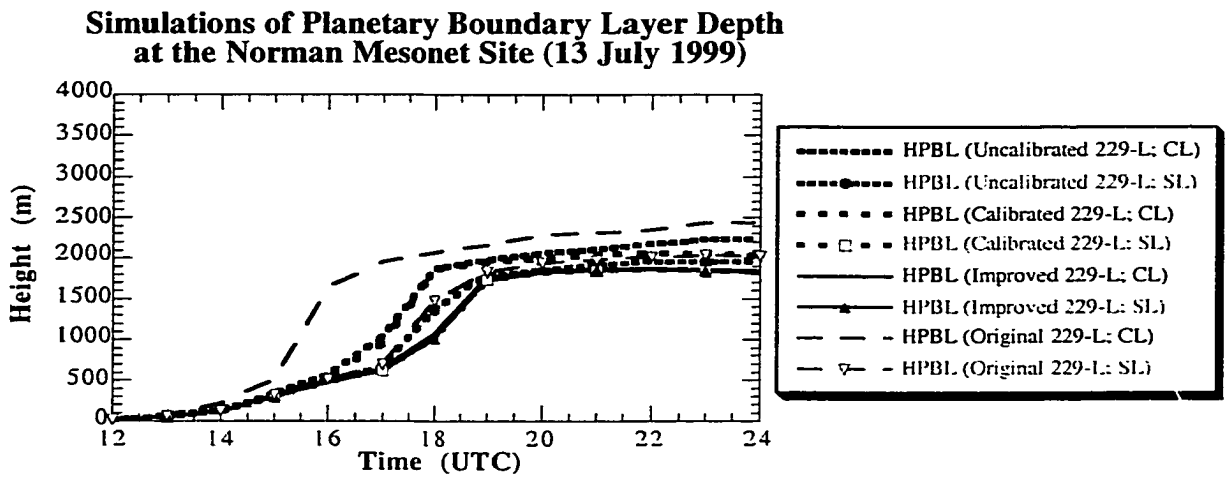

Figure D.12d. Simulations of PBL depth at the Norman Mesonet site on 13 July 1999 using the clay loam soil parameterization (CL) and the silt loam soil parameterization (SL). Soil water content was determined using various calibrations applied to the 229-L sensor.

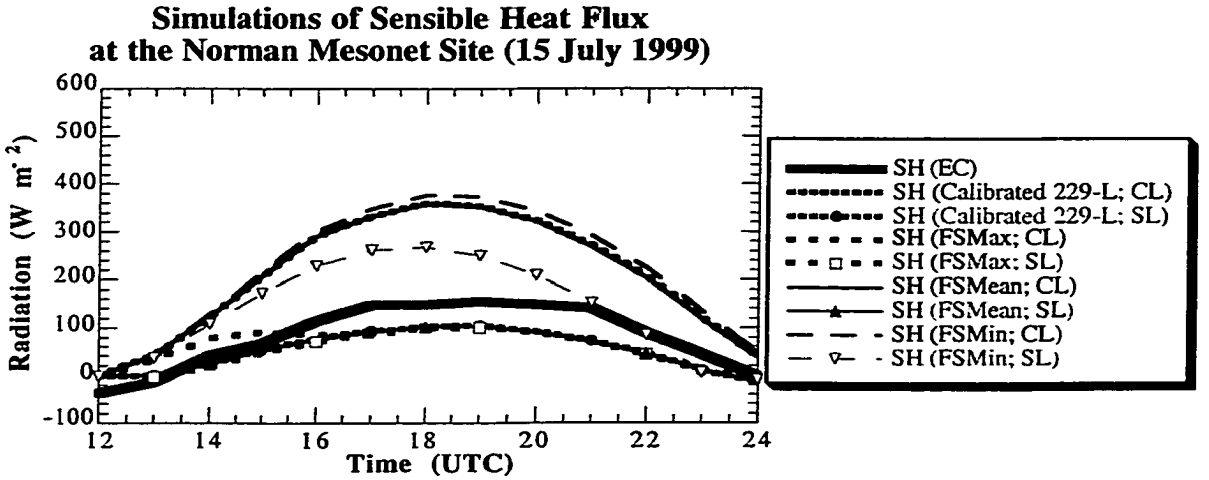

Figure D.13a. Simulations of sensible heat flux at the Norman Mesonet site on 15 July 1999 using the clay loam soil parameterization (CL) and the silt loam soil parameterization (SL). Calibrated measurements of 229-L soil water content, and soil water determined from field samples were used as input. Hourly-averaged observations from the Norman site are plotted for reference (black curve).

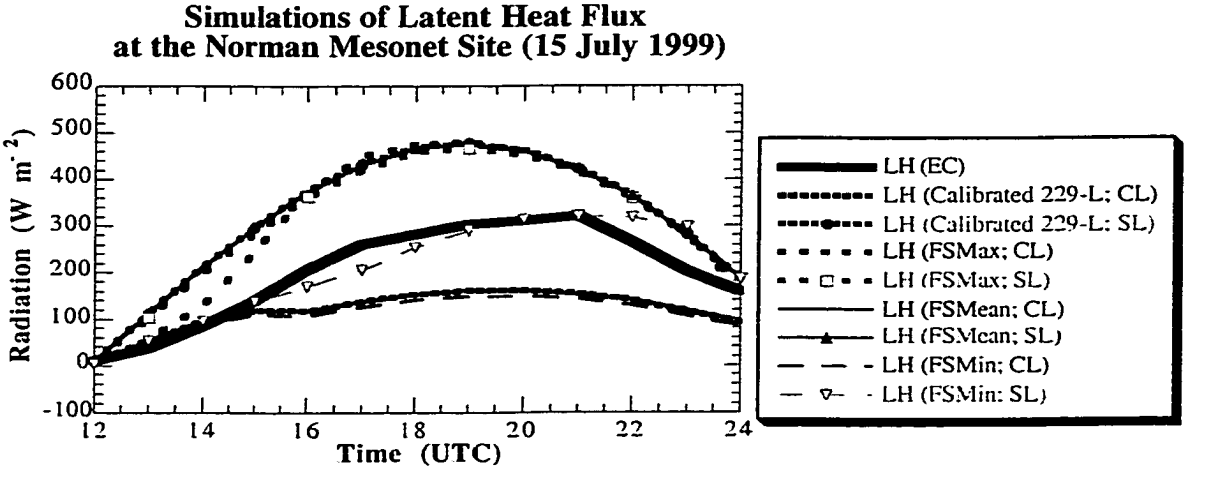

Figure D.13b. Simulations of latent heat flux at the Norman Mesonet site on 15 July 1999 using the clay loam soil parameterization (CL) and the silt loam soil parameterization (SL). Calibrated measurements of 229-L soil water content, and soil water determined from field samples were used as input. Hourly-averaged observations from the Norman site are plotted for reference (black curve).

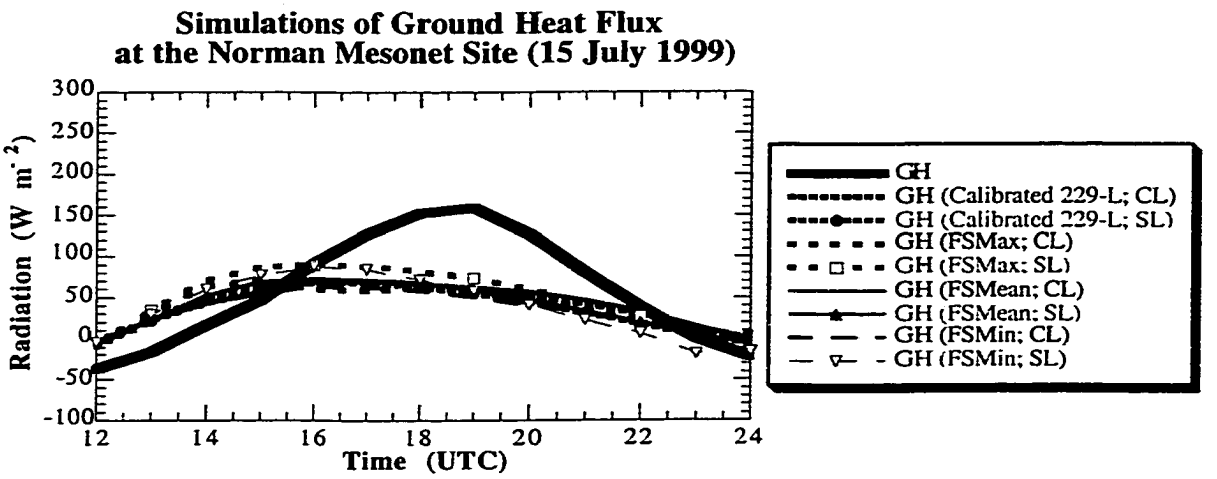

Figure D.13c. Simulations of ground heat flux at the Norman Mesonet site on 15 July 1999 using the clay loam soil parameterization (CL) and the silt loam soil parameterization (SL). Calibrated measurements of 229-L soil water content, and soil water determined from field samples were used as input. Hourly-averaged observations from the Norman site are plotted for reference (black curve).

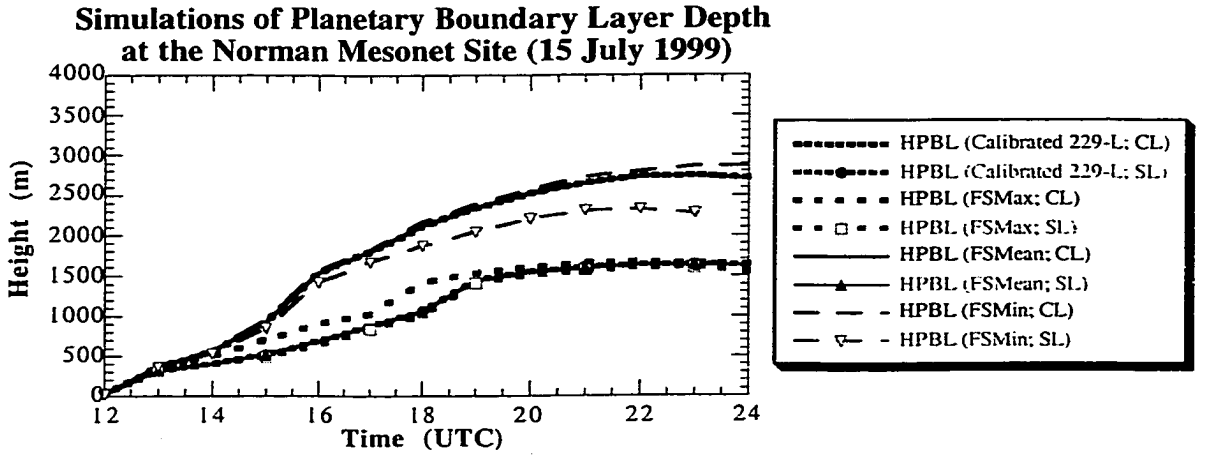

Figure D.13d. Simulations of PBL depth at the Norman Mesonet site on 15 July 1999 using the clay loam soil parameterization (CL) and the silt loam soil parameterization (SL). Calibrated measurements of 229-L soil water content, and soil water determined from field samples were used as input.

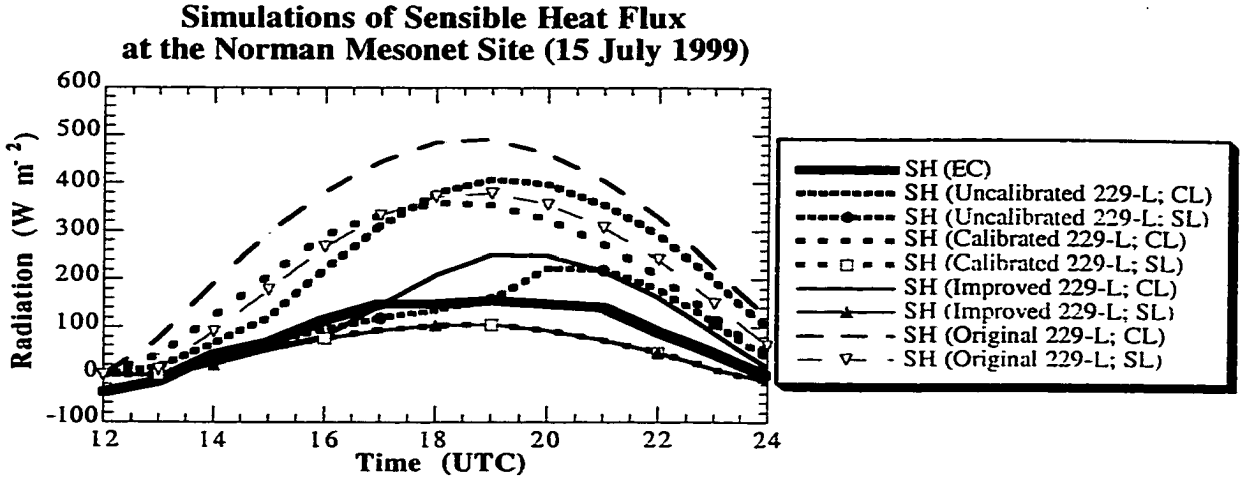

Figure D.14a. Simulations of sensible heat flux at the Norman Mesonet site on 15 July 1999 using the clay loam soil parameterization (CL) and the silt loam soil parameterization (SL). Soil water content was determined using various calibrations applied to the 229-L sensor. Hourly-averaged observations from the Norman site are plotted for reference (black curve).

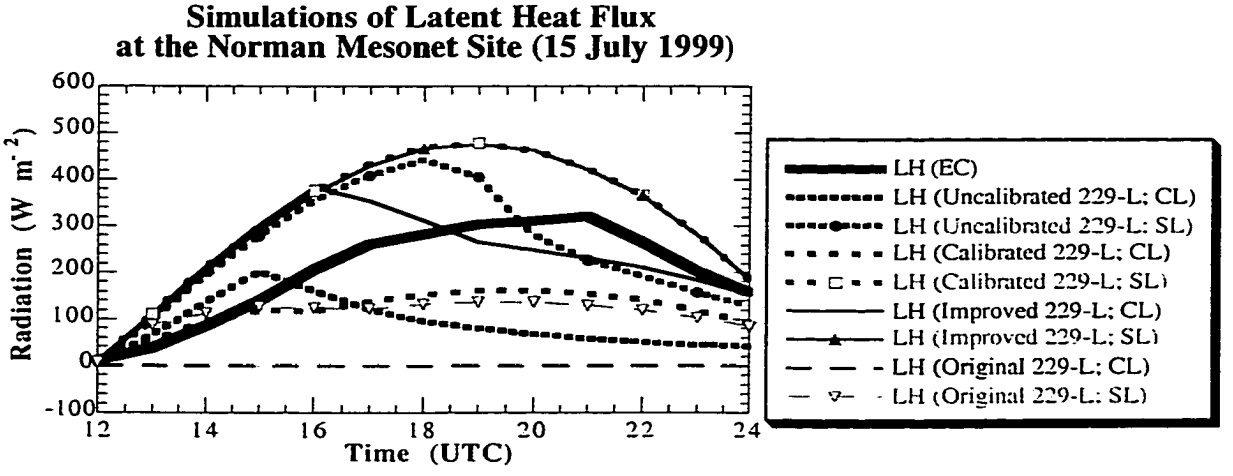

Figure D.14b. Simulations of latent heat flux at the Norman Mesonet site on 15 July 1999 using the clay loam soil parameterization (CL) and the silt loam soil parameterization (SL). Soil water content was determined using various calibrations applied to the 229-L sensor. Hourly-averaged observations from the Norman site are plotted for reference (black curve).

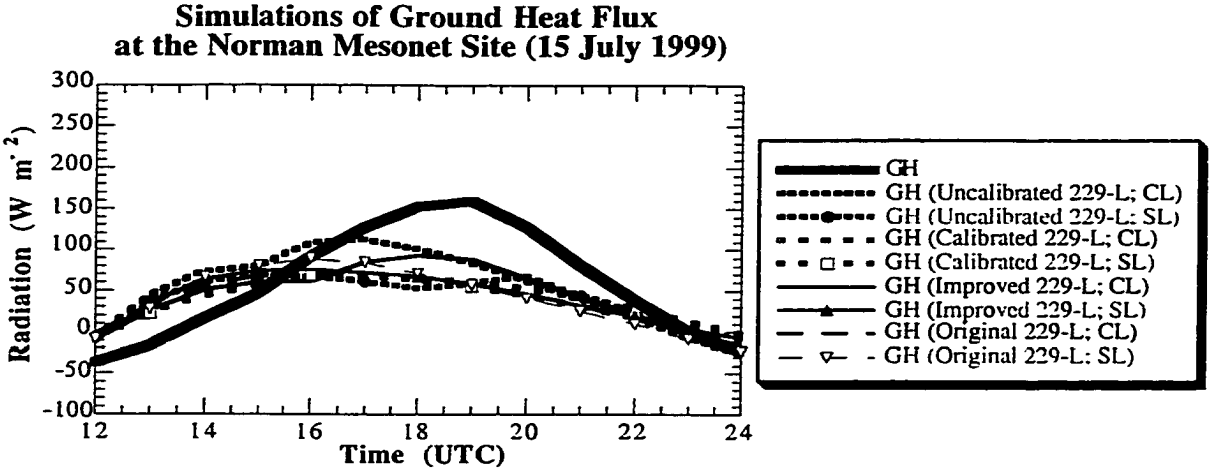

Figure D.14c. Simulations of ground heat flux at the Norman Mesonet site on 15 July 1999 using the clay loam soil parameterization (CL) and the silt loam soil parameterization (SL). Soil water content was determined using various calibrations applied to the 229-L sensor. Hourly-averaged observations from the Norman site are plotted for reference (black curve).

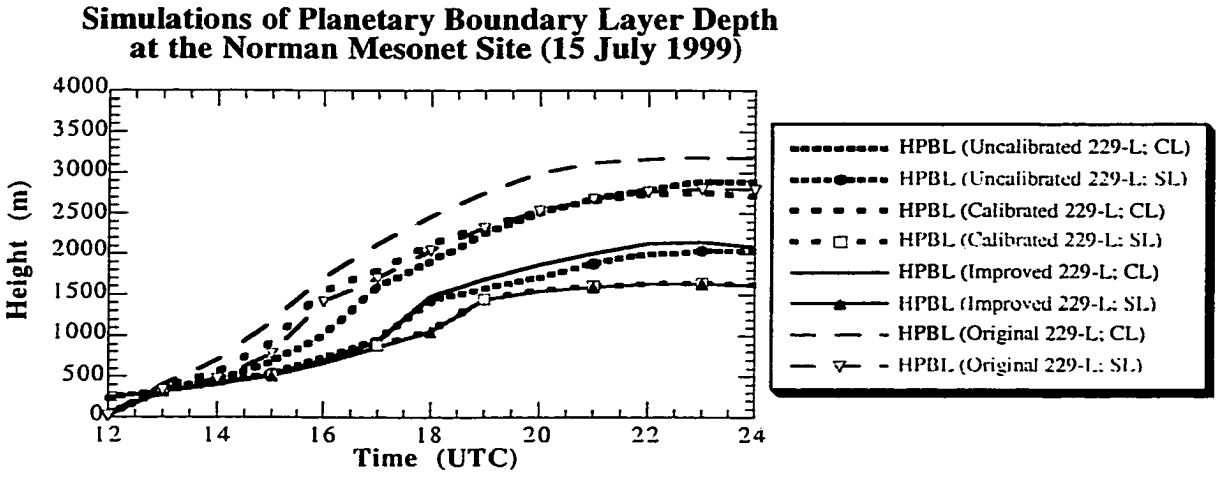

Figure D.14d. Simulations of PBL depth at the Norman Mesonet site on 15 July 1999 using the clay loam soil parameterization (CL) and the silt loam soil parameterization (SL). Soil water content was determined using various calibrations applied to the 229-L sensor.

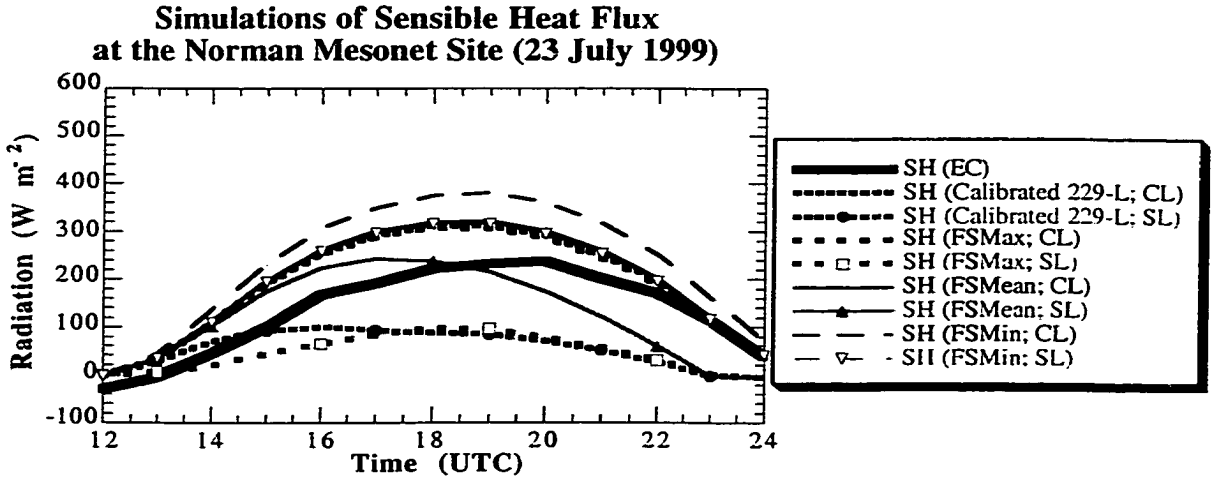

Figure D.15a. Simulations of sensible heat flux at the Norman Mesonet site on 23 July 1999 using the clay loam soil parameterization (CL) and the silt loam soil parameterization (SL). Calibrated measurements of 229-L soil water content, and soil water determined from field samples were used as input. Hourly-averaged observations from the Norman site are plotted for reference (black curve).

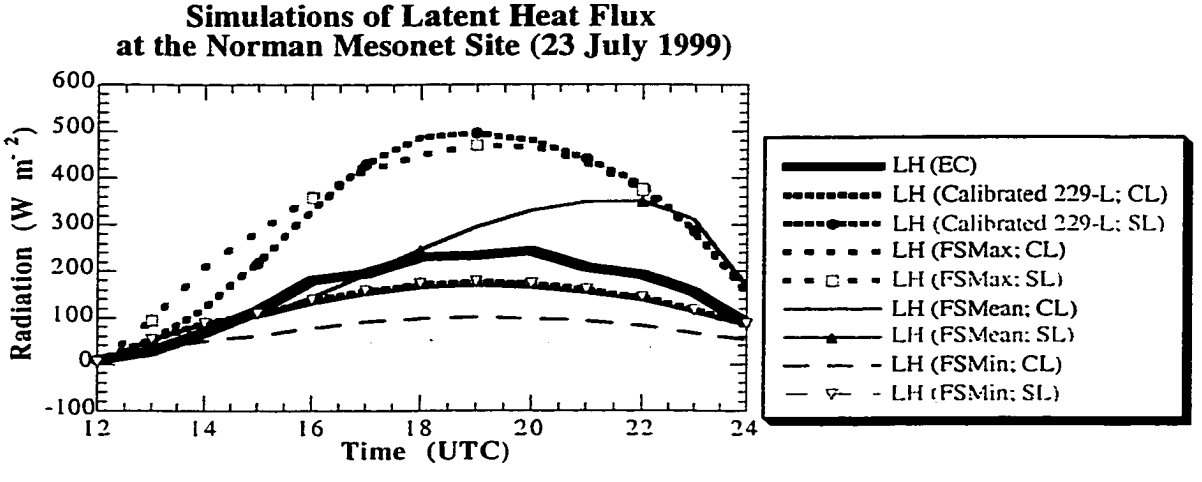

Figure D.15b. Simulations of latent heat flux at the Norman Mesonet site on 23 July 1999 using the clay loam soil parameterization (CL) and the silt loam soil parameterization (SL). Calibrated measurements of 229-L soil water content, and soil water determined from field samples were used as input. Hourly-averaged observations from the Norman site are plotted for reference (black curve).

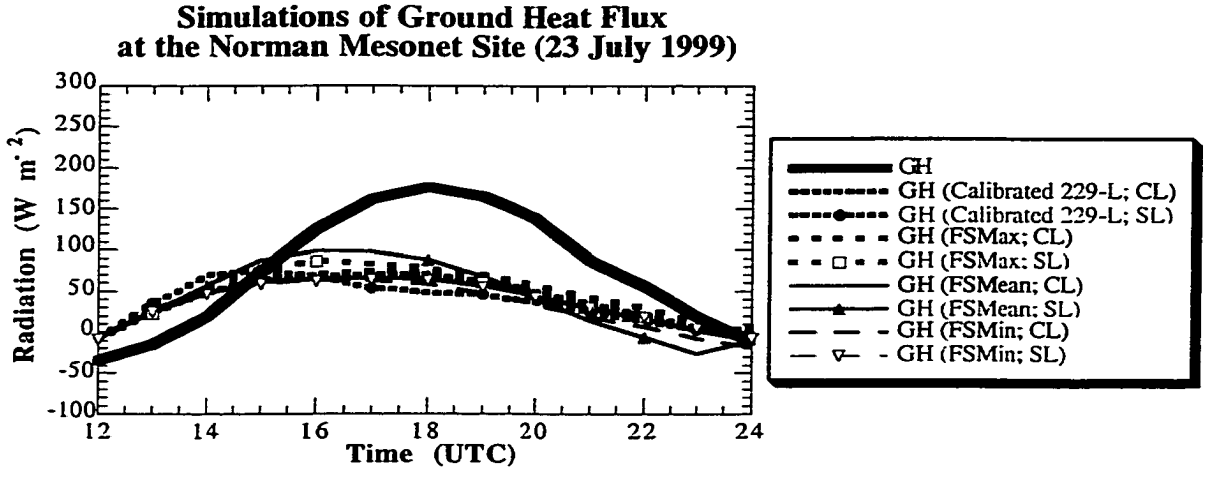

Figure D.15c. Simulations of ground heat flux at the Norman Mesonet site on 23 July 1999 using the clay loam soil parameterization (CL) and the silt loam soil parameterization (SL). Calibrated measurements of 229-L soil water content, and soil water determined from field samples were used as input. Hourly-averaged observations from the Norman site are plotted for reference (black curve).

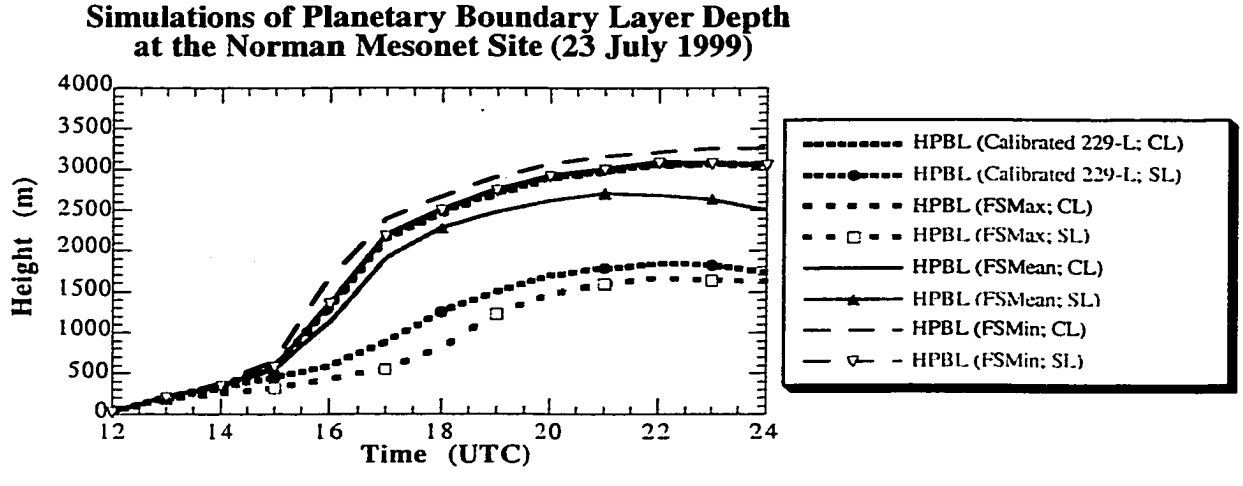

Figure D.15d. Simulations of PBL depth at the Norman Mesonet site on 23 July 1999 using the clay loam soil parameterization (CL) and the silt loam soil parameterization (SL). Calibrated measurements of 229-L soil water content, and soil water determined from field samples were used as input.

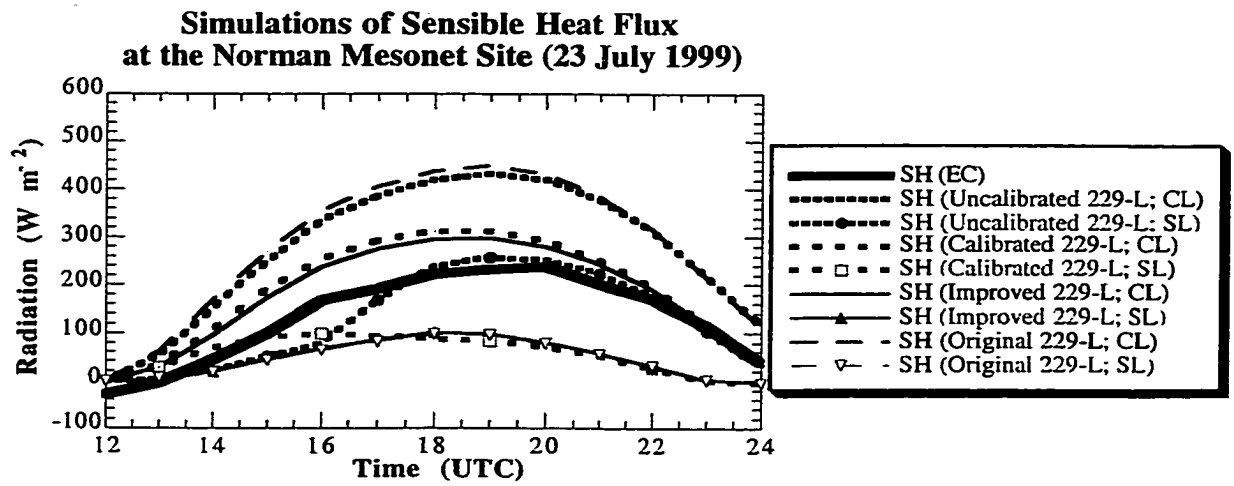

Figure D.16a. Simulations of sensible heat flux at the Norman Mesonet site on 23 July 1999 using the clay loam soil parameterization (CL) and the silt loam soil parameterization (SL). Soil water content was determined using various calibrations applied to the 229-L sensor. Hourly-averaged observations from the Norman site are plotted for reference (black curve).

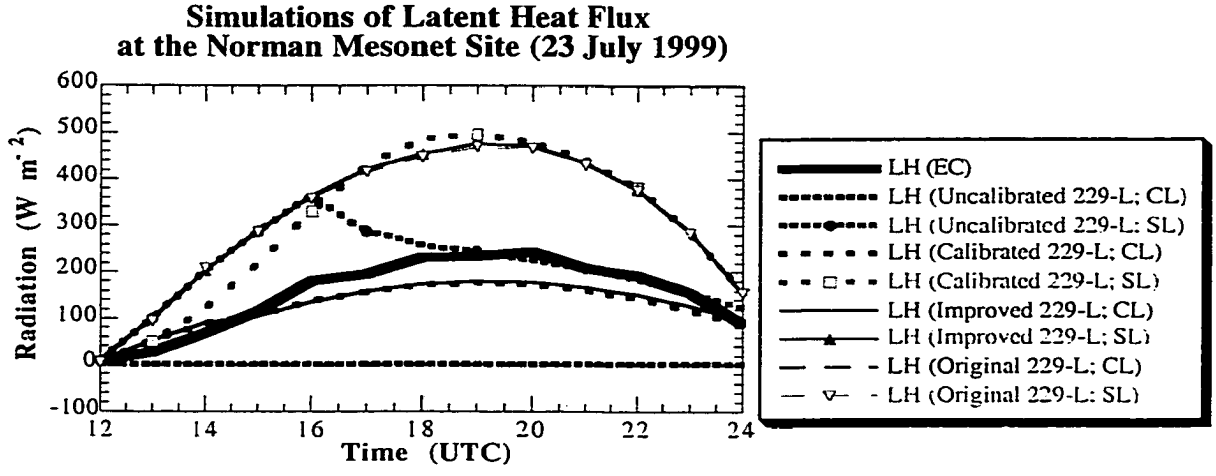

Figure D.16b. Simulations of latent heat flux at the Norman Mesonet site on 23 July 1999 using the clay loam soil parameterization (CL) and the silt loam soil parameterization (SL). Soil water content was determined using various calibrations applied to the 229-L sensor. Hourly-averaged observations from the Norman site are plotted for reference (black curve).

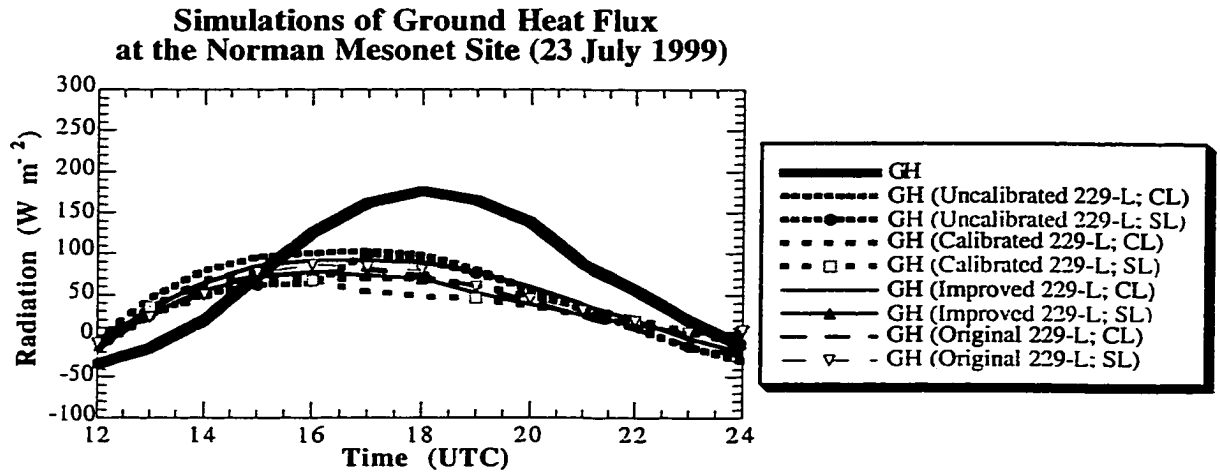

Figure D.16c. Simulations of ground heat flux at the Norman Mesonet site on 23 July 1999 using the clay loam soil parameterization (CL) and the silt loam soil parameterization (SL). Soil water content was determined using various calibrations applied to the 229-L sensor. Hourly-averaged observations from the Norman site are plotted for reference (black curve).

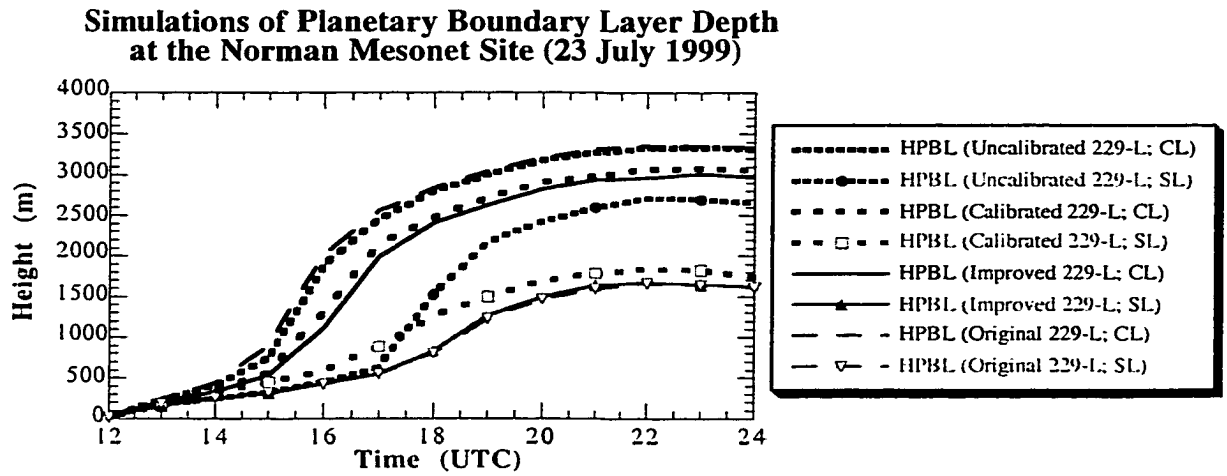

Figure D.16d. Simulations of PBL depth at the Norman Mesonet site on 23 July 1999 using the clay loam soil parameterization (CL) and the silt loam soil parameterization (SL). Soil water content was determined using various calibrations applied to the 229-L sensor.

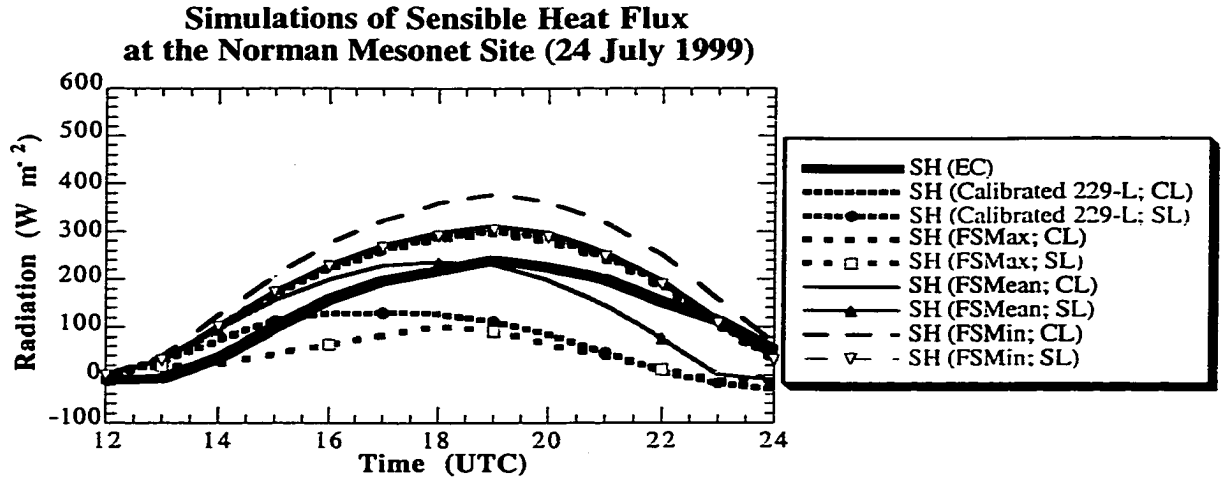

Figure D.17a. Simulations of sensible heat flux at the Norman Mesonet site on 24 July 1999 using the clay loam soil parameterization (CL) and the silt loam soil parameterization (SL). Calibrated measurements of 229-L soil water content, and soil water determined from field samples were used as input. Hourly-averaged observations from the Norman site are plotted for reference (black curve).

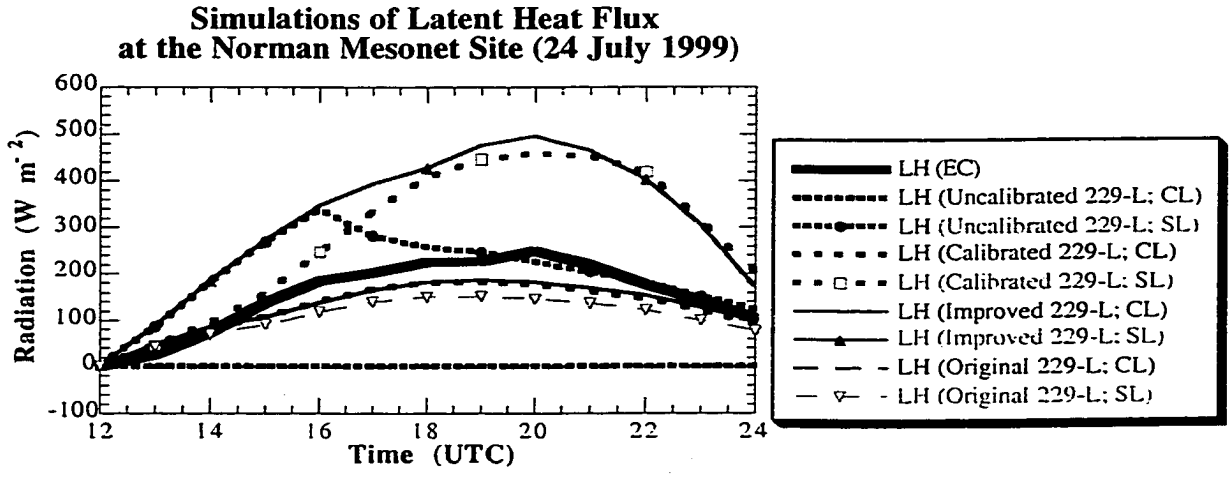

Figure D.17b. Simulations of latent heat flux at the Norman Mesonet site on 24 July 1999 using the clay loam soil parameterization (CL) and the silt loam soil parameterization (SL). Calibrated measurements of 229-L soil water content, and soil water determined from field samples were used as input. Hourly-averaged observations from the Norman site are plotted for reference (black curve).

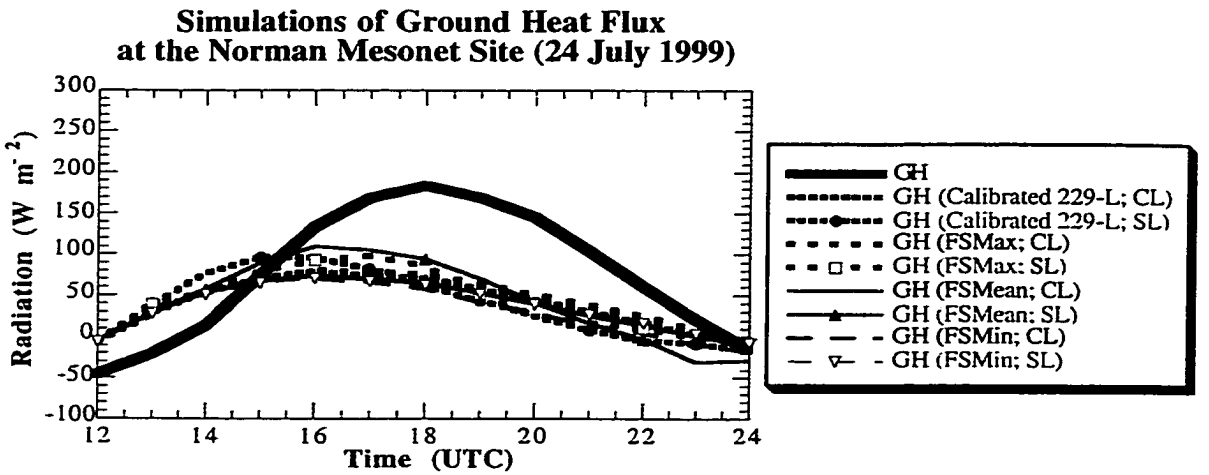

Figure D.17c. Simulations of ground heat flux at the Norman Mesonet site on 24 July 1999 using the clay loam soil parameterization (CL) and the silt loam soil parameterization (SL). Calibrated measurements of 229-L soil water content, and soil water determined from field samples were used as input. Hourly-averaged observations from the Norman site are plotted for reference (black curve).

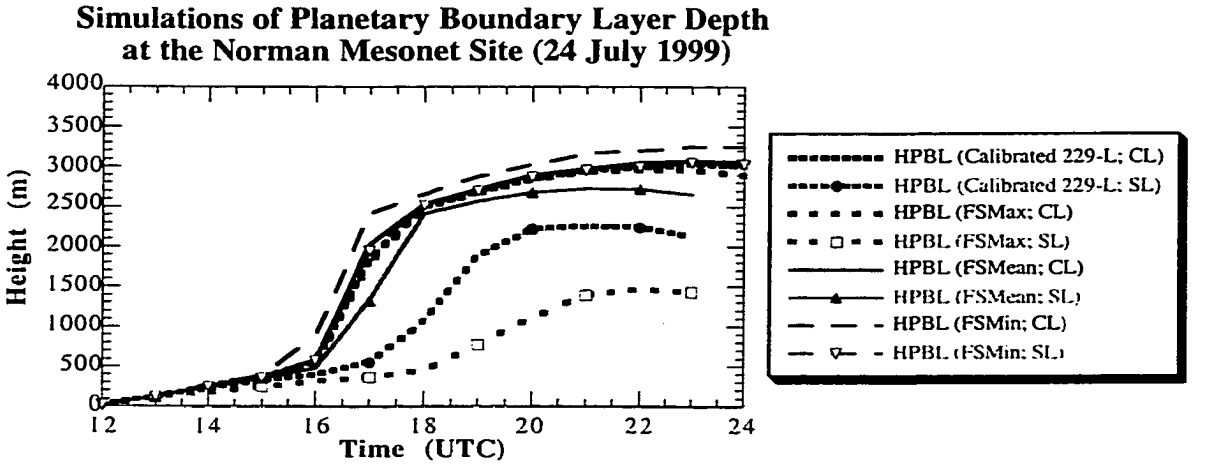

Figure D.17d. Simulations of PBL depth at the Norman Mesonet site on 24 July 1999 using the clay loam soil parameterization (CL) and the silt loam soil parameterization (SL). Calibrated measurements of 229-L soil water content, and soil water determined from field samples were used as input.

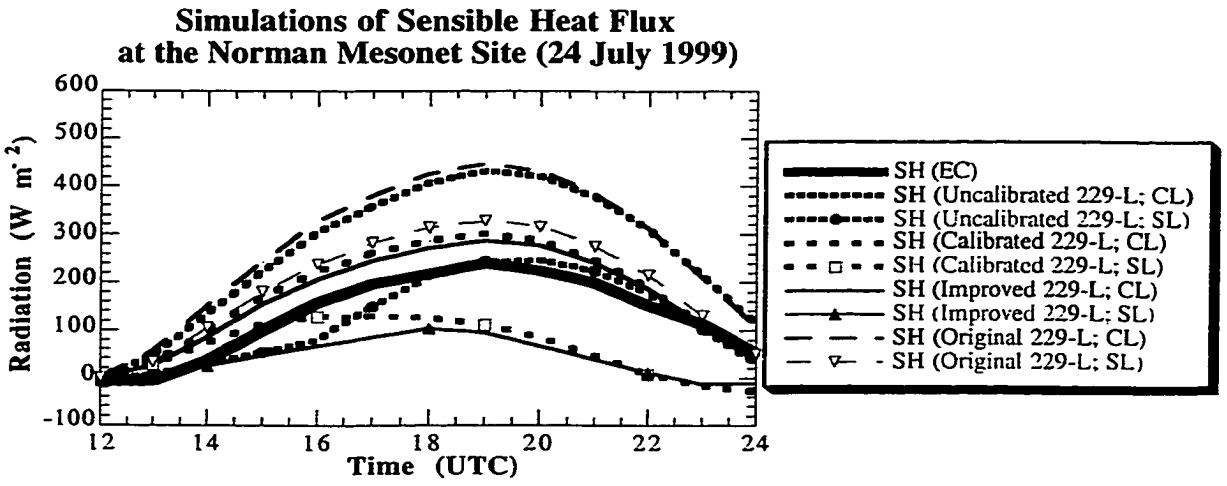

Figure D.18a. Simulations of sensible heat flux at the Norman Mesonet site on 24 July 1999 using the clay loam soil parameterization (CL) and the silt loam soil parameterization (SL). Soil water content was determined using various calibrations applied to the 229-L sensor. Hourly-averaged observations from the Norman site are plotted for reference (black curve).

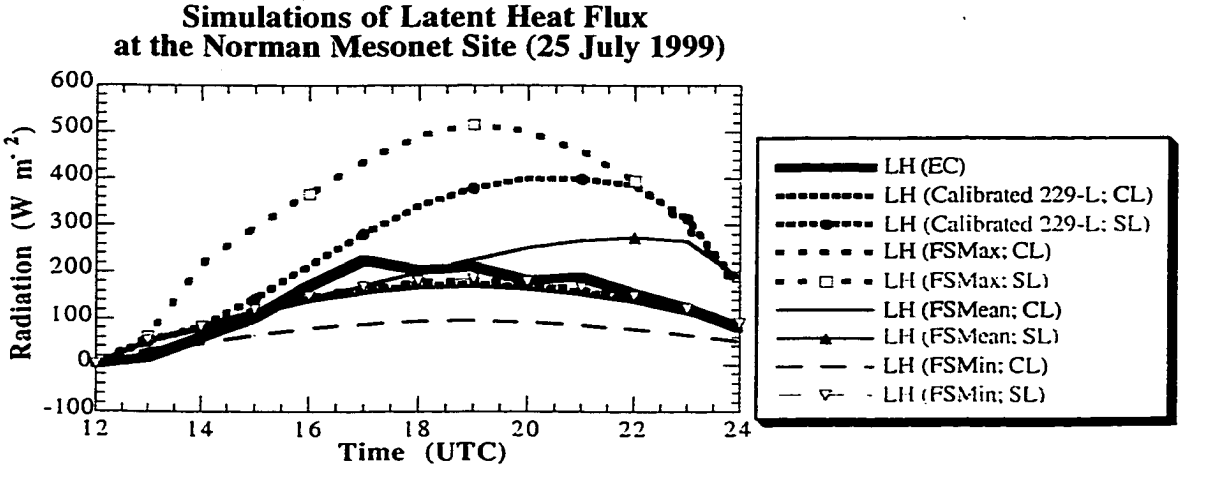

Figure D.18b. Simulations of latent heat flux at the Norman Mesonet site on 24 July 1999 using the clay loam soil parameterization (CL) and the silt loam soil parameterization (SL). Soil water content was determined using various calibrations applied to the 229-L sensor. Hourly-averaged observations from the Norman site are plotted for reference (black curve).

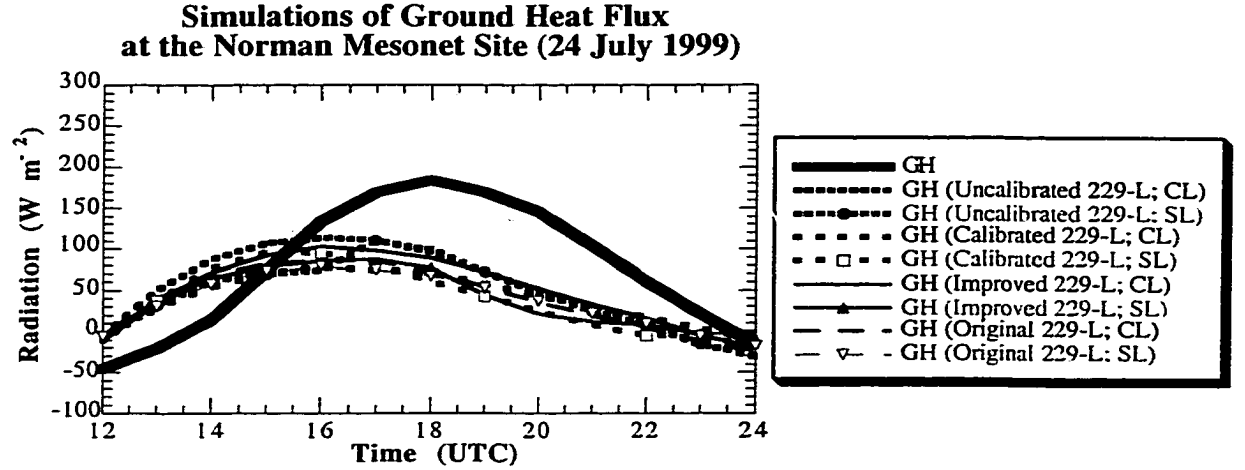

Figure D.18c. Simulations of ground heat flux at the Norman Mesonet site on 24 July 1999 using the clay loam soil parameterization (CL) and the silt loam soil parameterization (SL). Soil water content was determined using various calibrations applied to the 229-L sensor. Hourly-averaged observations from the Norman site are plotted for reference (black curve).

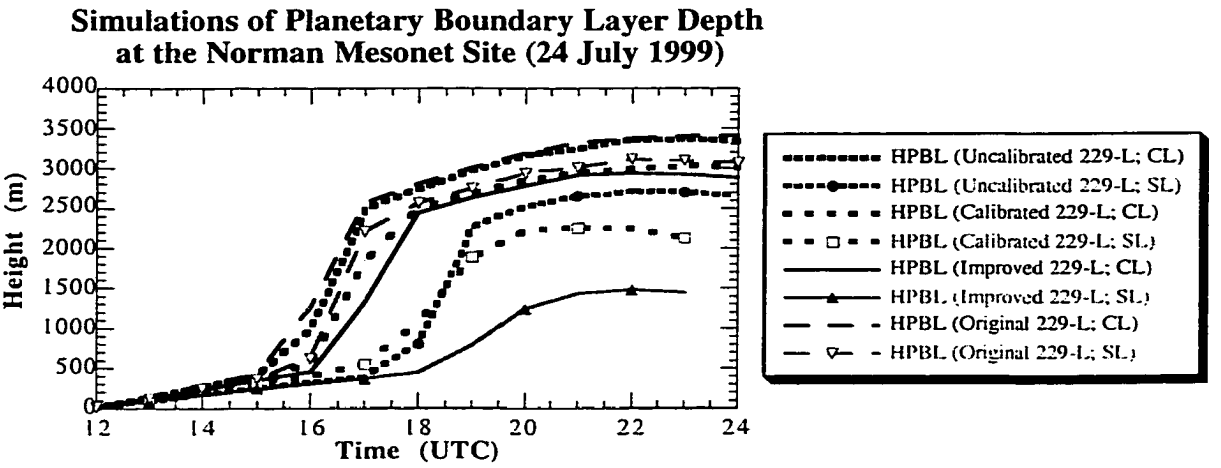

Figure D.18d. Simulations of PBL depth at the Norman Mesonet site on 24 July 1999 using the clay loam soil parameterization (CL) and the silt loam soil parameterization (SL). Soil water content was determined using various calibrations applied to the 229-L sensor.

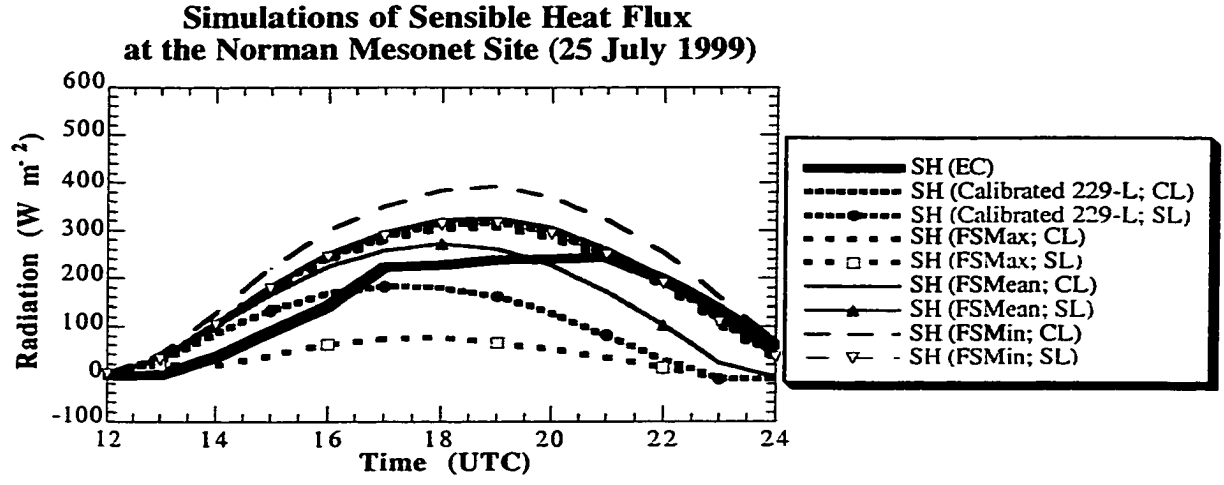

Figure D.19a. Simulations of sensible heat flux at the Norman Mesonet site on 25 July 1999 using the clay loam soil parameterization (CL) and the silt loam soil parameterization (SL). Calibrated measurements of 229-L soil water content, and soil water determined from field samples were used as input. Hourly-averaged observations from the Norman site are plotted for reference (black curve).

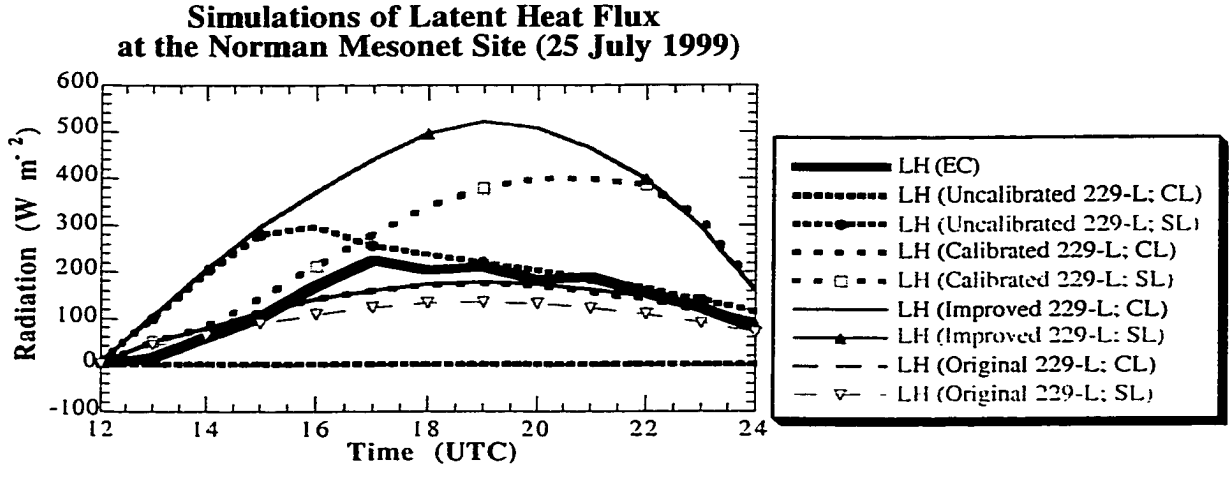

Figure D.19b. Simulations of latent heat flux at the Norman Mesonet site on 25 July 1999 using the clay loam soil parameterization (CL) and the silt loam soil parameterization (SL). Calibrated measurements of 229-L soil water content, and soil water determined from field samples were used as input. Hourly-averaged observations from the Norman site are plotted for reference (black curve).

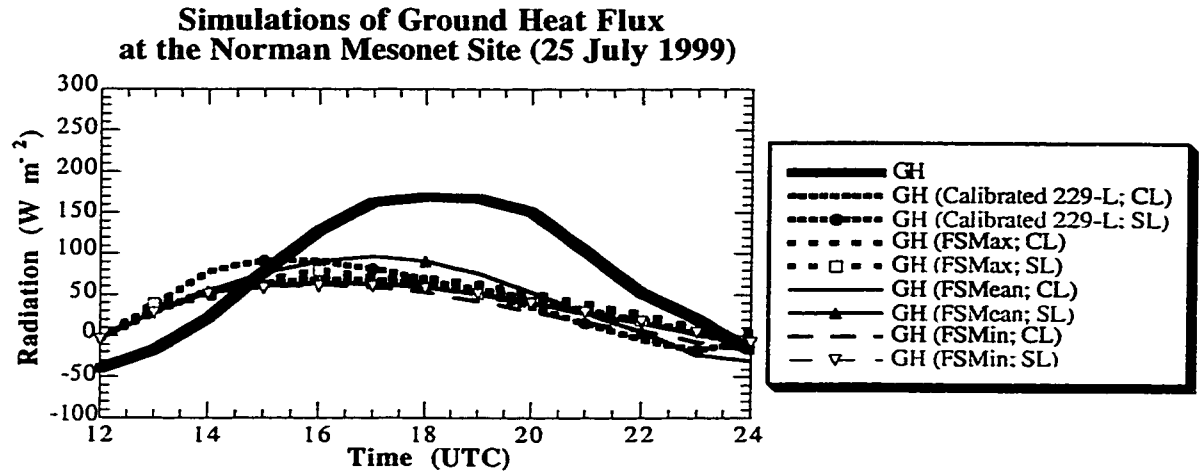

Figure D.19c. Simulations of ground heat flux at the Norman Mesonet site on 25 July 1999 using the clay loam soil parameterization (CL) and the silt loam soil parameterization (SL). Calibrated measurements of 229-L soil water content, and soil water determined from field samples were used as input. Hourly-averaged observations from the Norman site are plotted for reference (black curve).

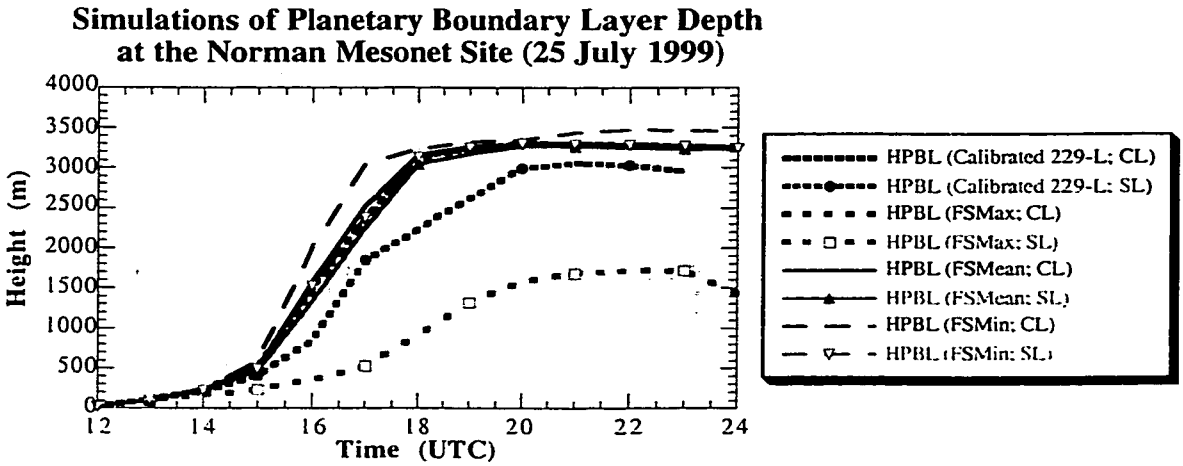

Figure D.19d. Simulations of PBL depth at the Norman Mesonet site on 25 July 1999 using the clay loam soil parameterization (CL) and the silt loam soil parameterization (SL). Calibrated measurements of 229-L soil water content, and soil water determined from field samples were used as input.

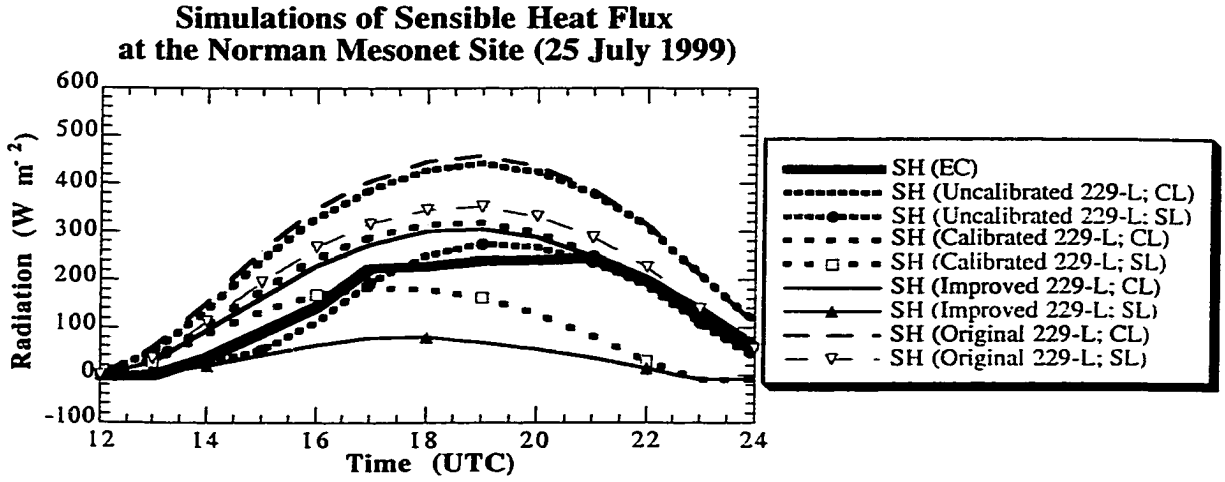

Figure D.20a. Simulations of sensible heat flux at the Norman Mesonet site on 25 July 1999 using the clay loam soil parameterization (CL) and the silt loam soil parameterization (SL). Soil water content was determined using various calibrations applied to the 229-L sensor. Hourly-averaged observations from the Norman site are plotted for reference (black curve).

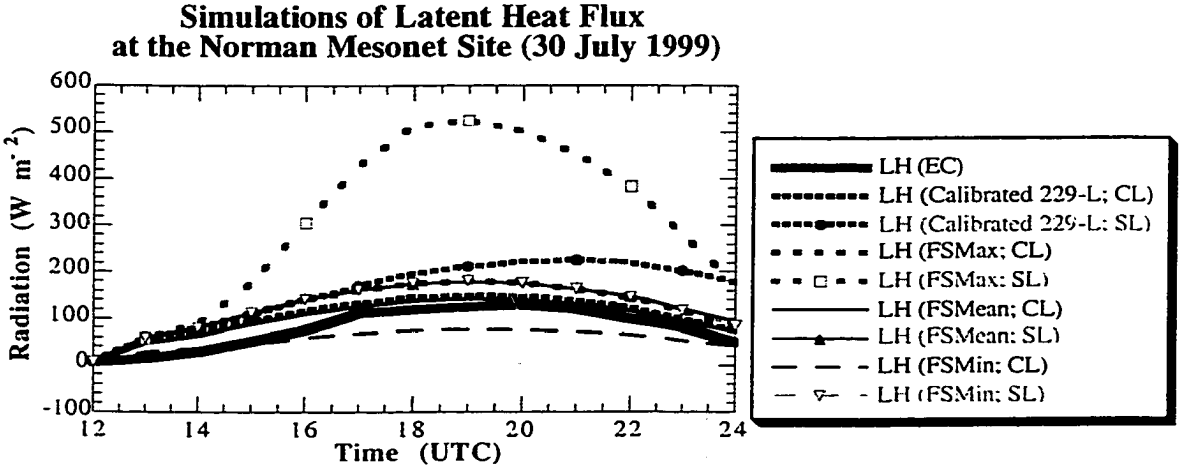

Figure D.20b. Simulations of latent heat flux at the Norman Mesonet site on 25 July 1999 using the clay loam soil parameterization (CL) and the silt loam soil parameterization (SL). Soil water content was determined using various calibrations applied to the 229-L sensor. Hourly-averaged observations from the Norman site are plotted for reference (black curve).

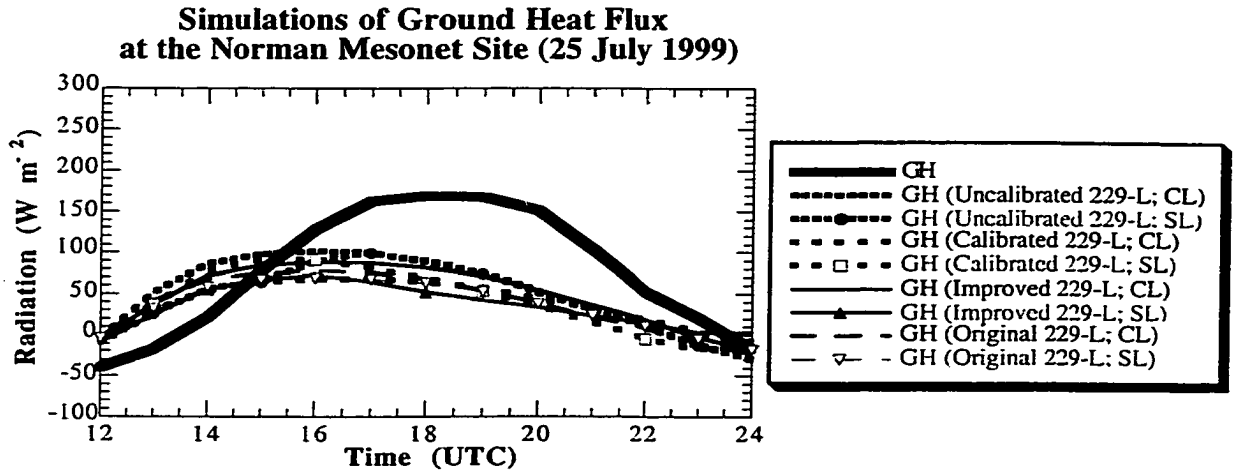

Figure D.20c. Simulations of ground heat flux at the Norman Mesonet site on 25 July 1999 using the clay loam soil parameterization (CL) and the silt loam soil parameterization (SL). Soil water content was determined using various calibrations applied to the 229-L sensor. Hourly-averaged observations from the Norman site are plotted for reference (black curve).

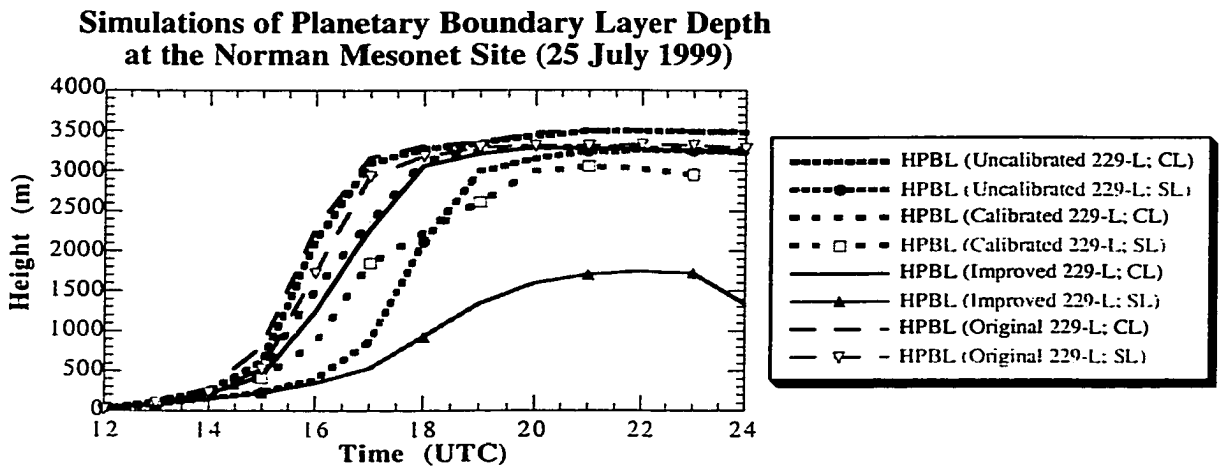

Figure D.20d. Simulations of PBL depth at the Norman Mesonet site on 25 July 1999 using the clay loam soil parameterization (CL) and the silt loam soil parameterization (SL). Soil water content was determined using various calibrations applied to the 229-L sensor.

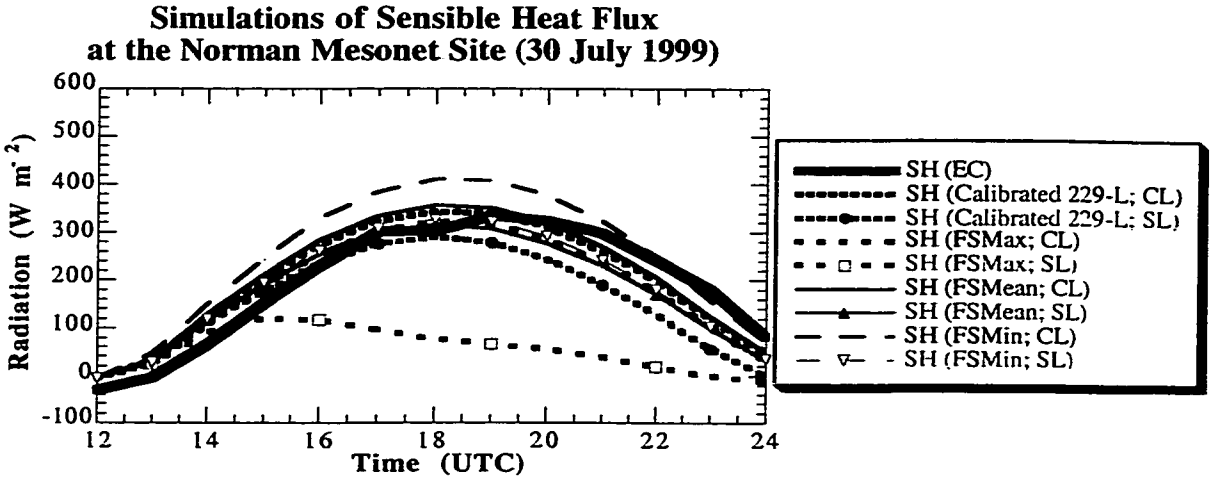

Figure D.21a. Simulations of sensible heat flux at the Norman Mesonet site on 30 July 1999 using the clay loam soil parameterization (CL) and the silt loam soil parameterization (SL). Calibrated measurements of 229-L soil water content, and soil water determined from field samples were used as input. Hourly-averaged observations from the Norman site are plotted for reference (black curve).

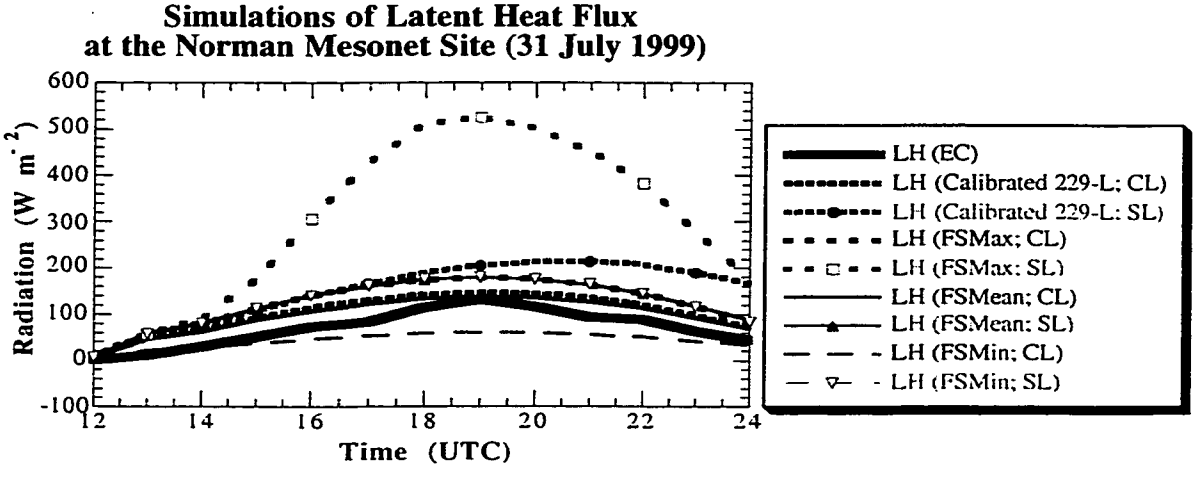

Figure D.21b. Simulations of latent heat flux at the Norman Mesonet site on 30 July 1999 using the clay loam soil parameterization (CL) and the silt loam soil parameterization (SL). Calibrated measurements of 229-L soil water content, and soil water determined from field samples were used as input. Hourly-averaged observations from the Norman site are plotted for reference (black curve).

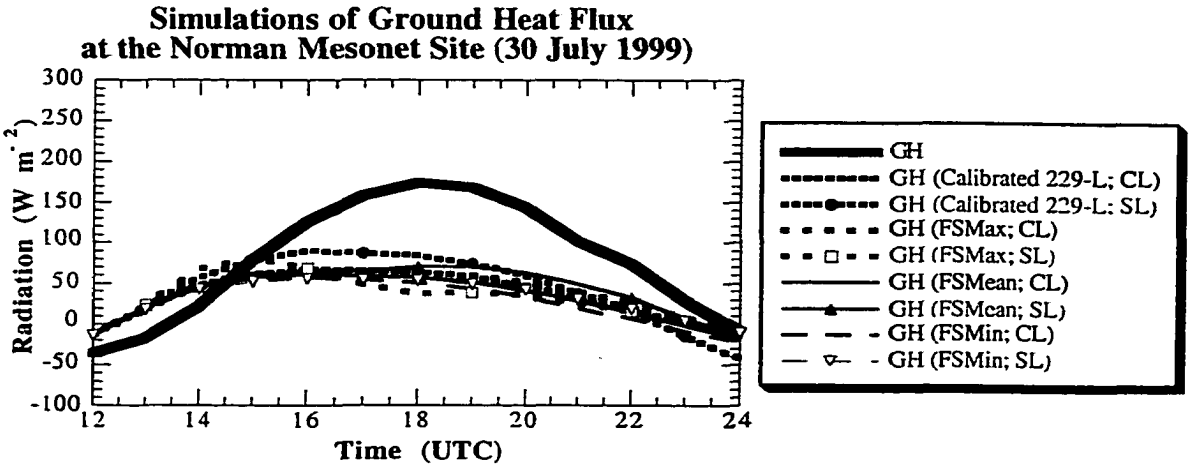

Figure D.21c. Simulations of ground heat flux at the Norman Mesonet site on 30 July 1999 using the clay loam soil parameterization (CL) and the silt loam soil parameterization (SL). Calibrated measurements of 229-L soil water content, and soil water determined from field samples were used as input. Hourly-averaged observations from the Norman site are plotted for reference (black curve).

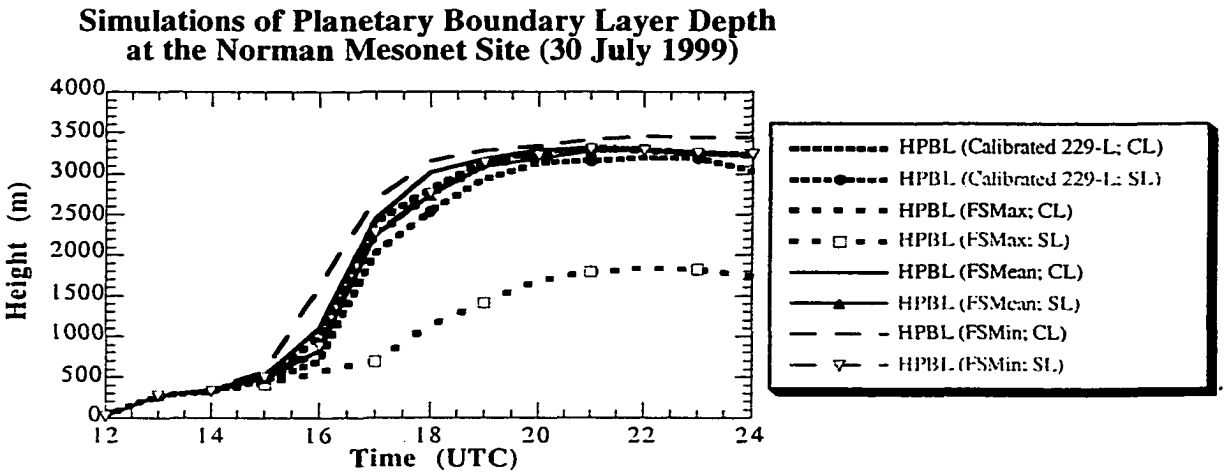

Figure D.21d. Simulations of PBL depth at the Norman Mesonet site on 30 July 1999 using the clay loam soil parameterization (CL) and the silt loam soil parameterization (SL). Calibrated measurements of 229-L soil water content, and soil water determined from field samples were used as input.

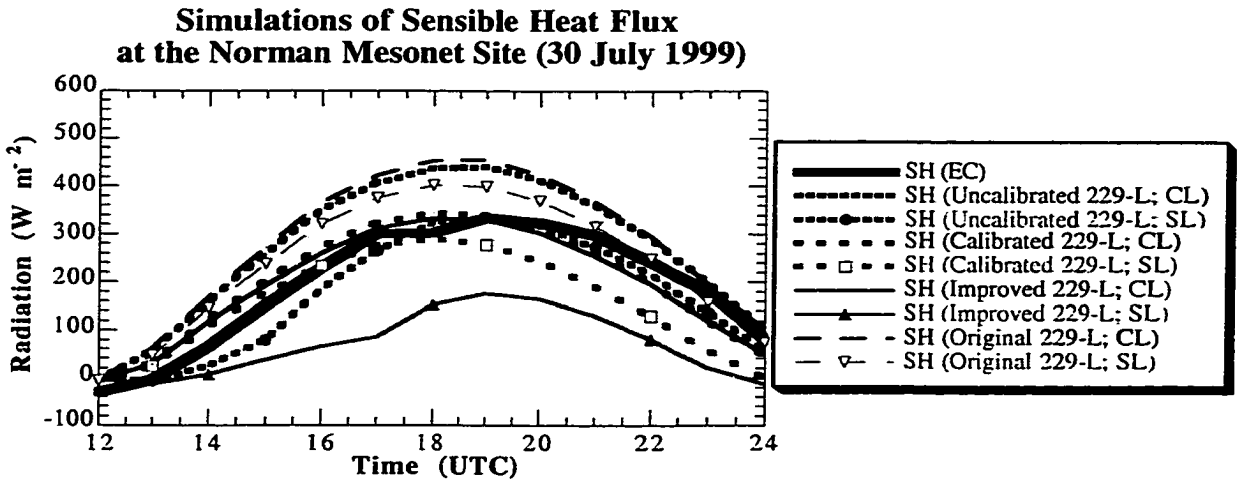

Figure D.22a. Simulations of sensible heat flux at the Norman Mesonet site on 30 July 1999 using the clay loam soil parameterization (CL) and the silt loam soil parameterization (SL). Soil water content was determined using various calibrations applied to the 229-L sensor. Hourly-averaged observations from the Norman site are plotted for reference (black curve).

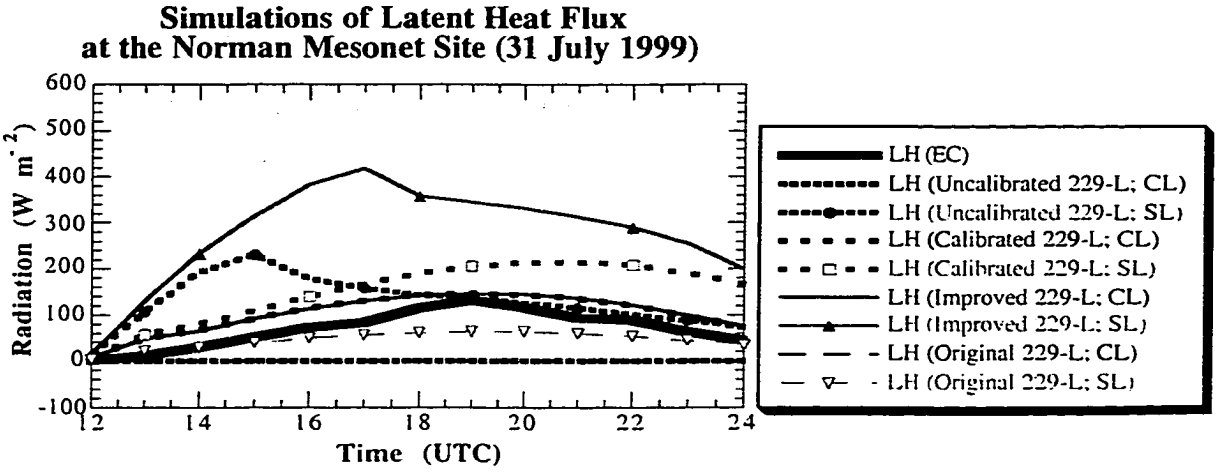

Figure D.22b. Simulations of latent heat flux at the Norman Mesonet site on 30 July 1999 using the clay loam soil parameterization (CL) and the silt loam soil parameterization (SL). Soil water content was determined using various calibrations applied to the 229-L sensor. Hourly-averaged observations from the Norman site are plotted for reference (black curve).

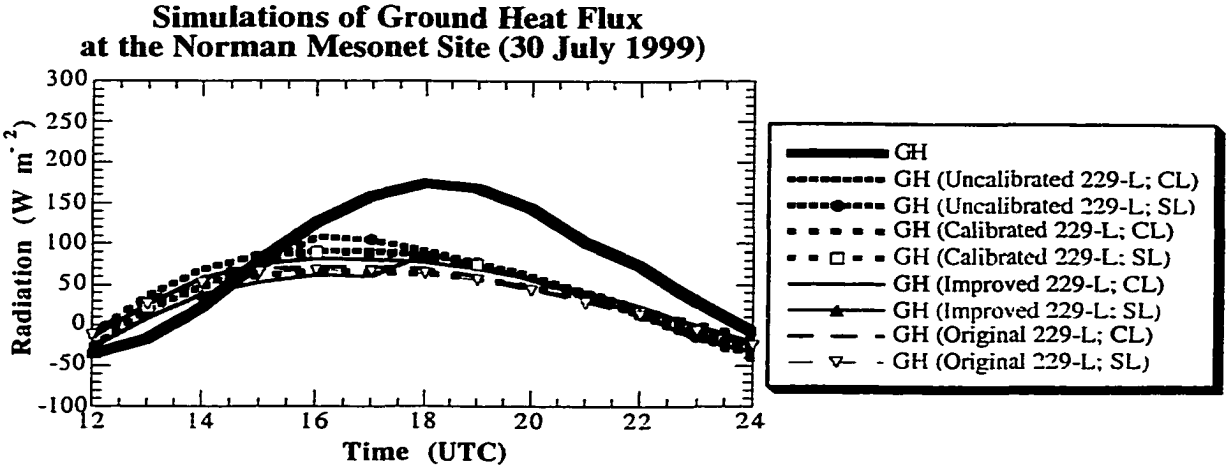

Figure D.22c. Simulations of ground heat flux at the Norman Mesonet site on 30 July 1999 using the clay loam soil parameterization (CL) and the silt loam soil parameterization (SL). Soil water content was determined using various calibrations applied to the 229-L sensor. Hourly-averaged observations from the Norman site are plotted for reference (black curve).

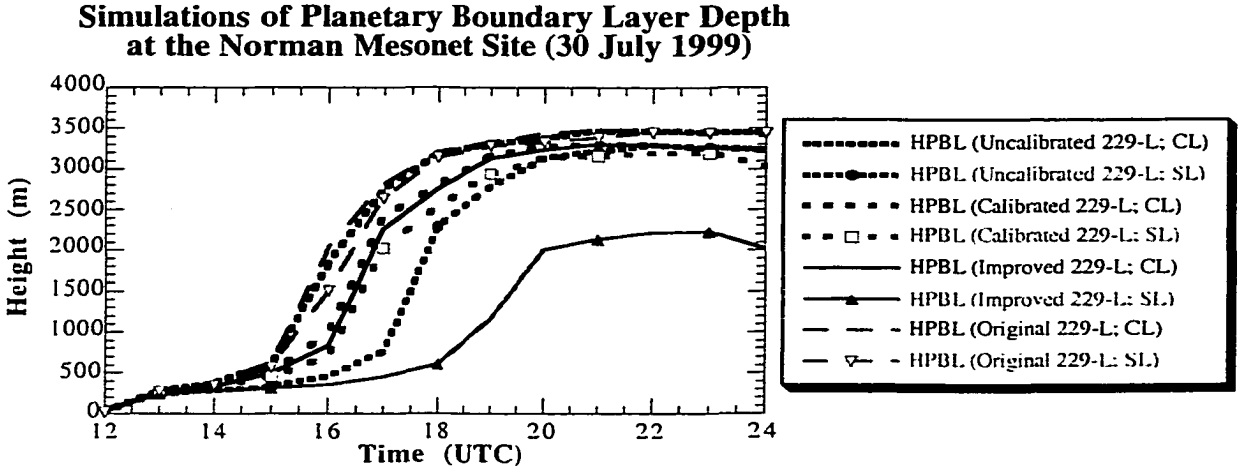

Figure D.22d. Simulations of PBL depth at the Norman Mesonet site on 30 July 1999 using the clay loam soil parameterization (CL) and the silt loam soil parameterization (SL). Soil water content was determined using various calibrations applied to the 229-L sensor.

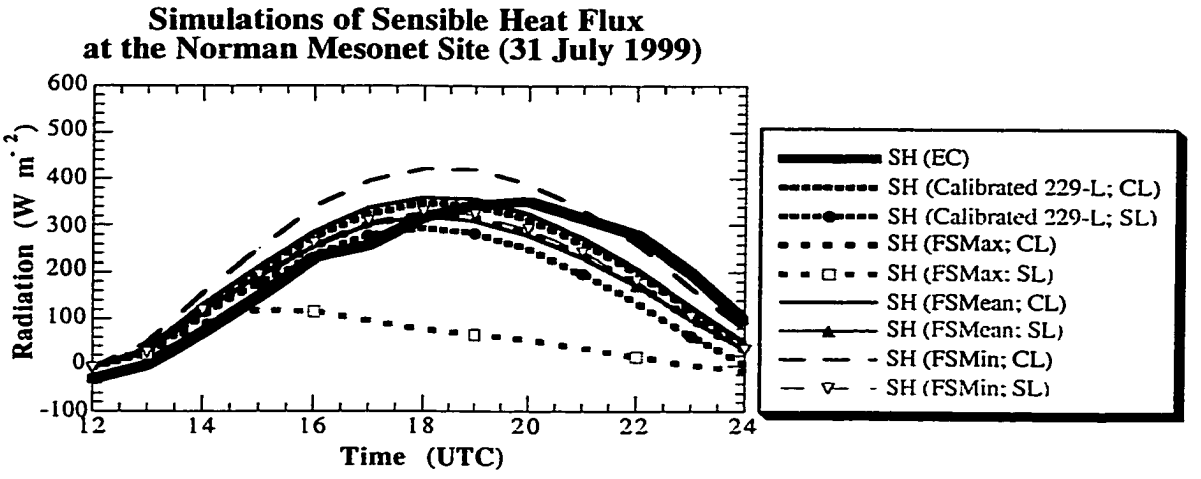

Figure D.23a. Simulations of sensible heat flux at the Norman Mesonet site on 31 July 1999 using the clay loam soil parameterization (CL) and the silt loam soil parameterization (SL). Calibrated measurements of 229-L soil water content, and soil water determined from field samples were used as input. Hourly-averaged observations from the Norman site are plotted for reference (black curve).

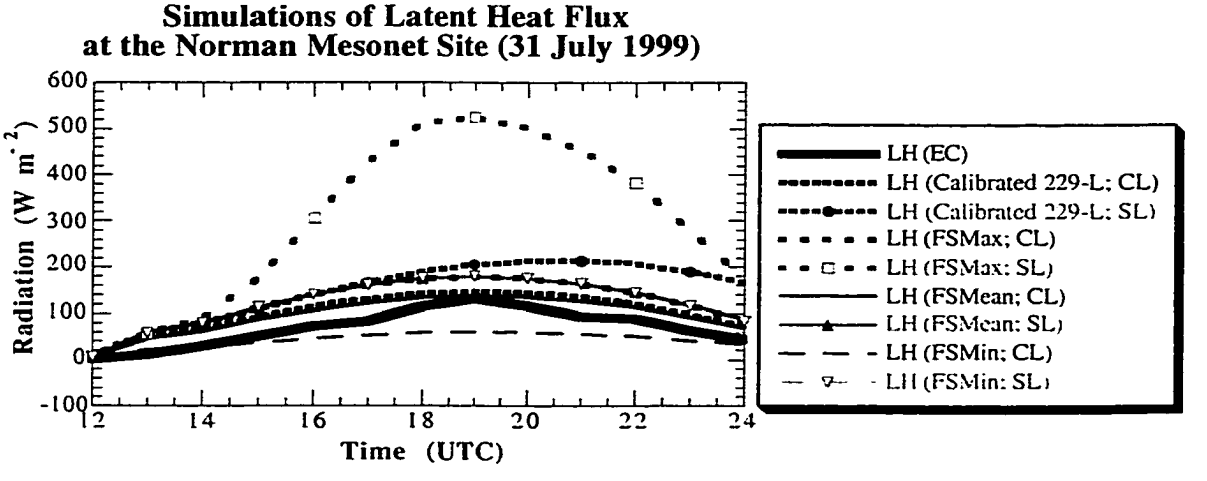

Figure D.23b. Simulations of latent heat flux at the Norman Mesonet site on 31 July 1999 using the clay loam soil parameterization (CL) and the silt loam soil parameterization (SL). Calibrated measurements of 229-L soil water content, and soil water determined from field samples were used as input. Hourly-averaged observations from the Norman site are plotted for reference (black curve).

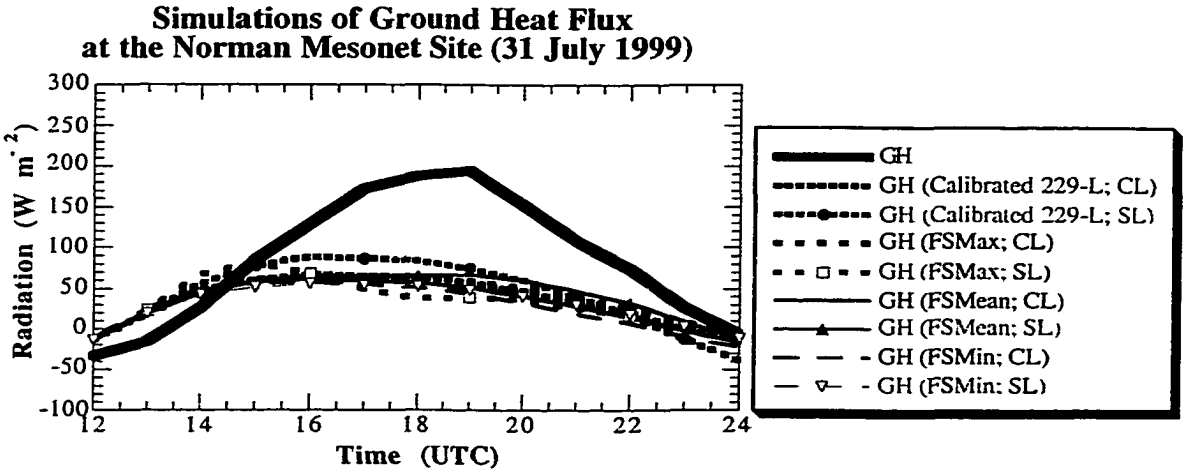

Figure D.23c. Simulations of ground heat flux at the Norman Mesonet site on 31 July 1999 using the clay loam soil parameterization (CL) and the silt loam soil parameterization (SL). Calibrated measurements of 229-L soil water content, and soil water determined from field samples were used as input. Hourly-averaged observations from the Norman site are plotted for reference (black curve).

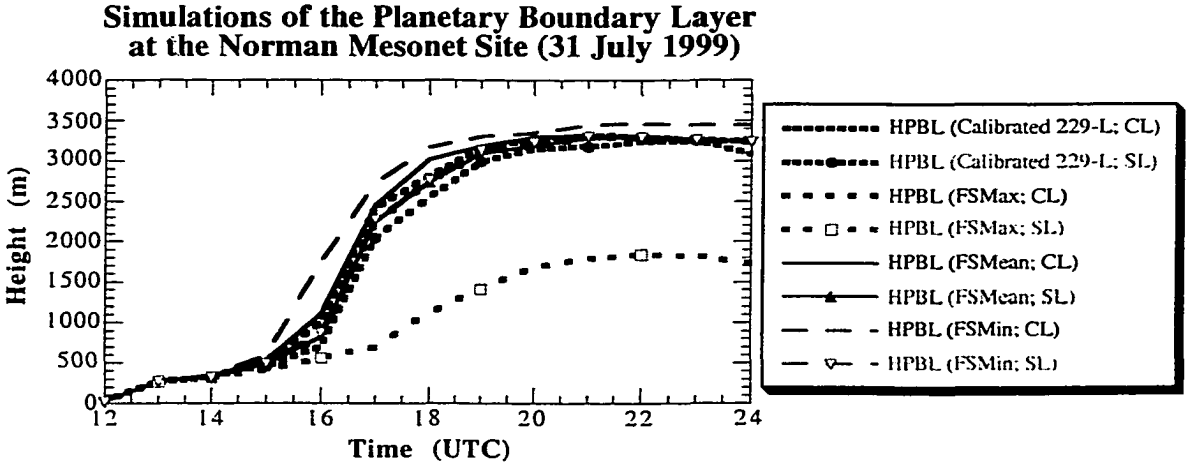

Figure D.23d. Simulations of PBL depth at the Norman Mesonet site on 31 July 1999 using the clay loam soil parameterization (CL) and the silt loam soil parameterization (SL). Calibrated measurements of 229-L soil water content, and soil water determined from field samples were used as input.

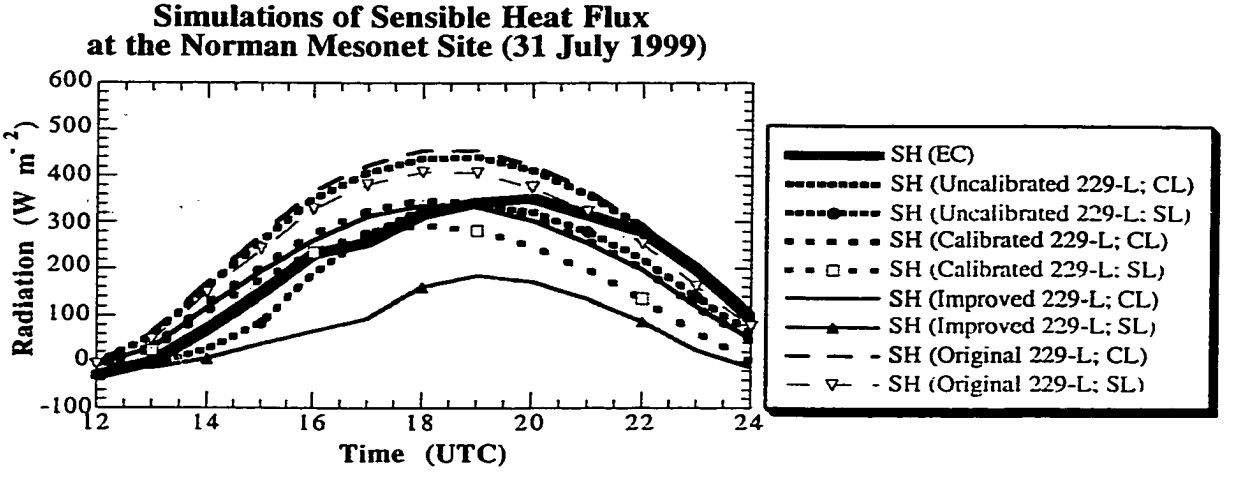

Figure D.24a. Simulations of sensible heat flux at the Norman Mesonet site on 31 July 1999 using the clay loam soil parameterization (CL) and the silt loam soil parameterization (SL). Soil water content was determined using various calibrations applied to the 229-L sensor. Hourly-averaged observations from the Norman site are plotted for reference (black curve).

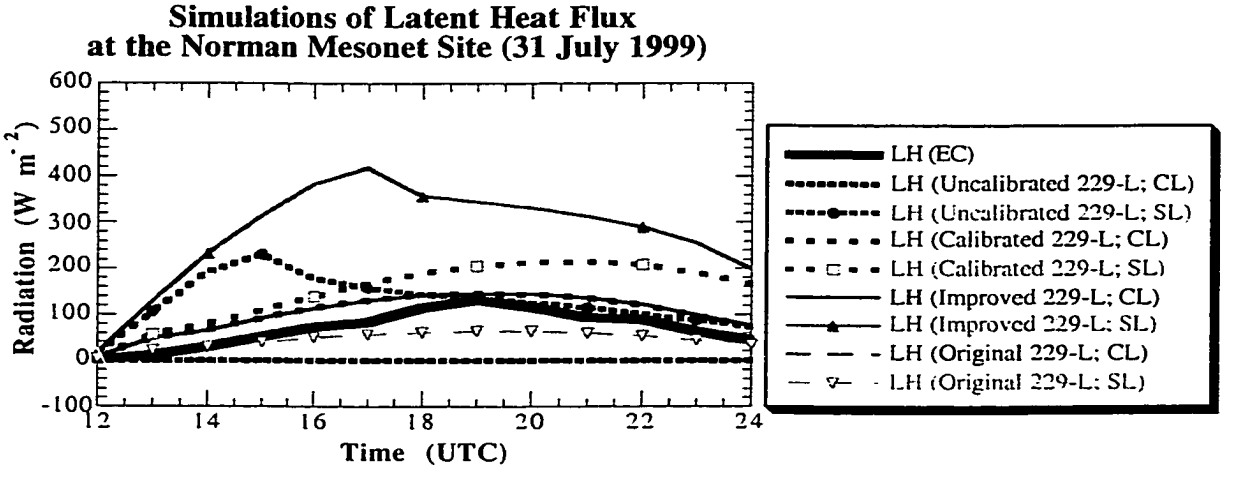

Figure D.24b. Simulations of latent heat flux at the Norman Mesonet site on 31 July 1999 using the clay loam soil parameterization (CL) and the silt loam soil parameterization (SL). Soil water content was determined using various calibrations applied to the 229-L sensor. Hourly-averaged observations from the Norman site are plotted for reference (black curve).

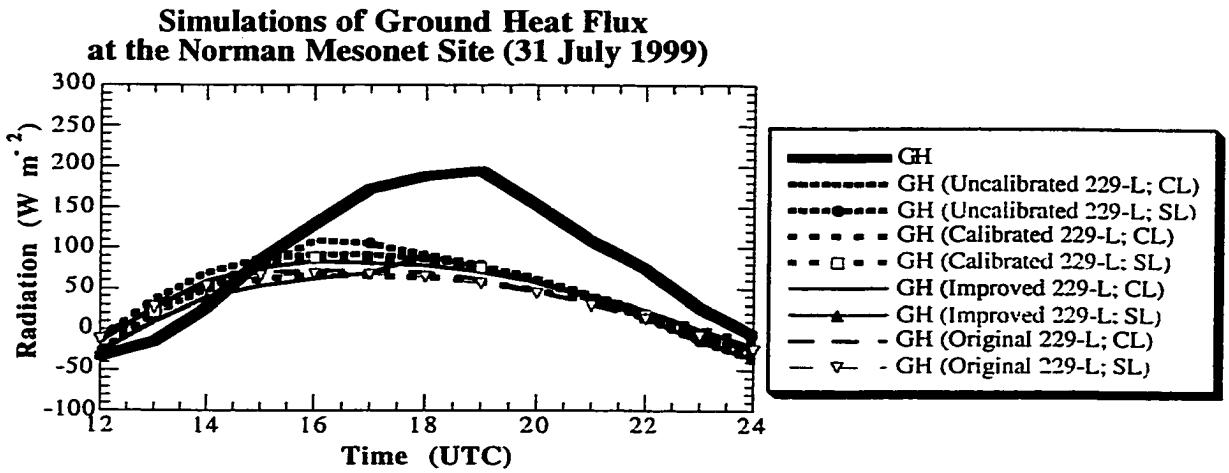

Figure D.24c. Simulations of ground heat flux at the Norman Mesonet site on 31 July 1999 using the clay loam soil parameterization (CL) and the silt loam soil parameterization (SL). Soil water content was determined using various calibrations applied to the 229-L sensor. Hourly-averaged observations from the Norman site are plotted for reference (black curve).

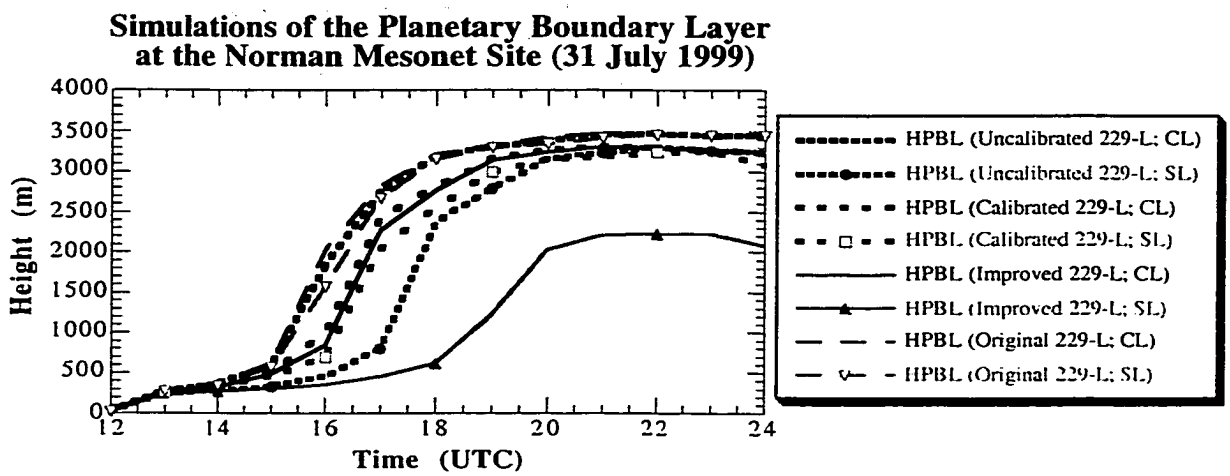

Figure D.24d. Simulations of PBL depth at the Norman Mesonet site on 31 July 1999 using the clay loam soil parameterization (CL) and the silt loam soil parameterization (SL). Soil water content was determined using various calibrations applied to the 229-L sensor.

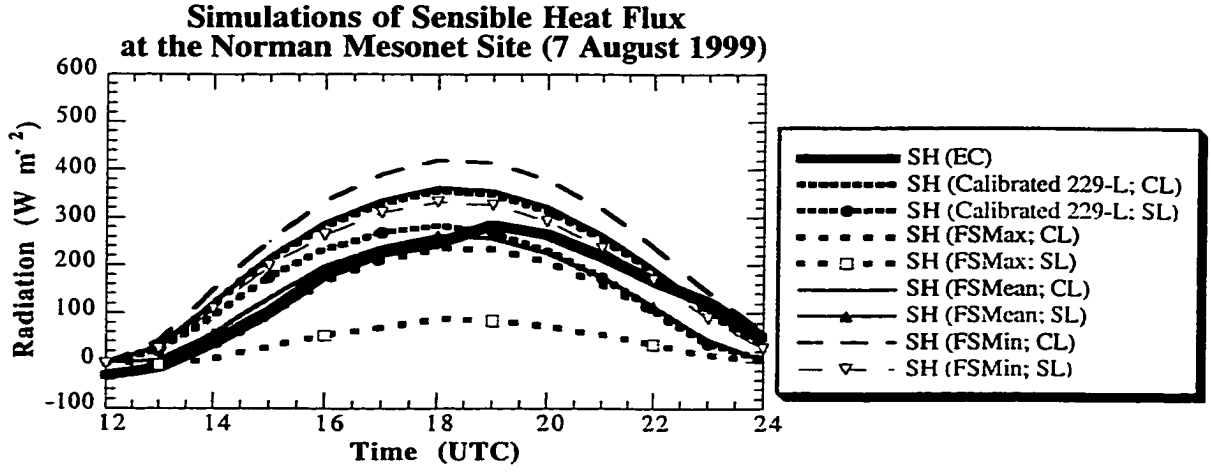

Figure D.25a. Simulations of sensible heat flux at the Norman Mesonet site on 7 August 1999 using the clay loam soil parameterization (CL) and the silt loam soil parameterization (SL). Calibrated measurements of 229-L soil water content, and soil water determined from field samples were used as input. Hourly-averaged observations from the Norman site are plotted for reference (black curve).

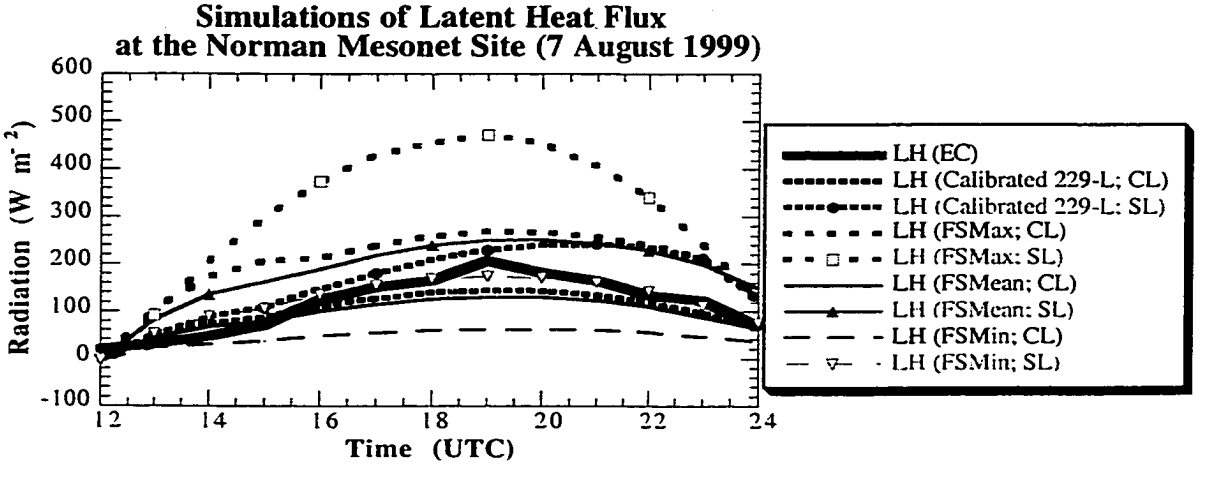

Figure D.25b. Simulations of latent heat flux at the Norman Mesonet site on 7 August 1999 using the clay loam soil parameterization (CL) and the silt loam soil parameterization (SL). Calibrated measurements of 229-L soil water content, and soil water determined from field samples were used as input. Hourly-averaged observations from the Norman site are plotted for reference (black curve).

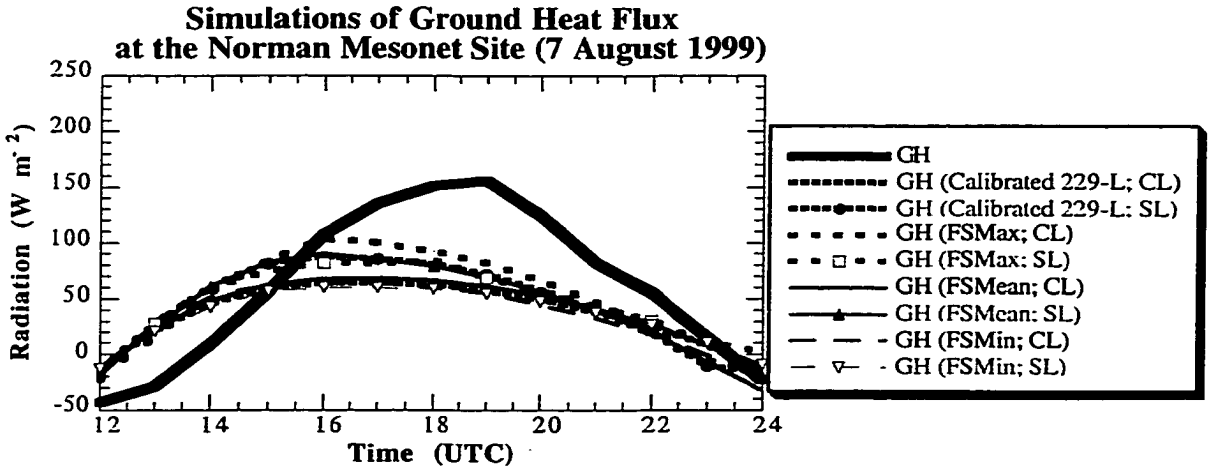

Figure D.25c. Simulations of ground heat flux at the Norman Mesonet site on 7 August 1999 using the clay loam soil parameterization (CL) and the silt loam soil parameterization (SL). Calibrated measurements of 229-L soil water content, and soil water determined from field samples were used as input. Hourly-averaged observations from the Norman site are plotted for reference (black curve).

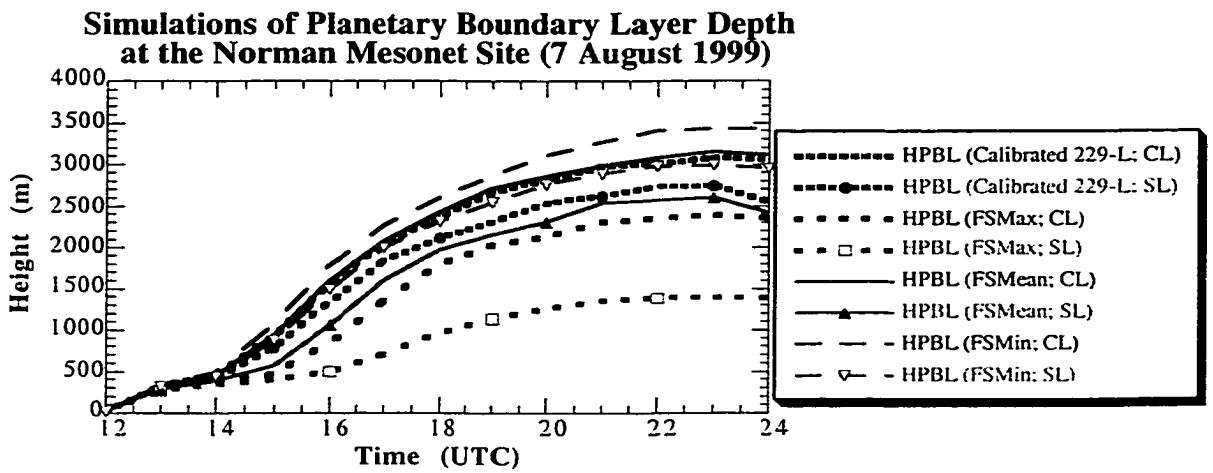

Figure D.25d. Simulations of PBL depth at the Norman Mesonet site on 7 August 1999 using the clay loam soil parameterization (CL) and the silt loam soil parameterization (SL). Calibrated measurements of 229-L soil water content, and soil water determined from field samples were used as input.

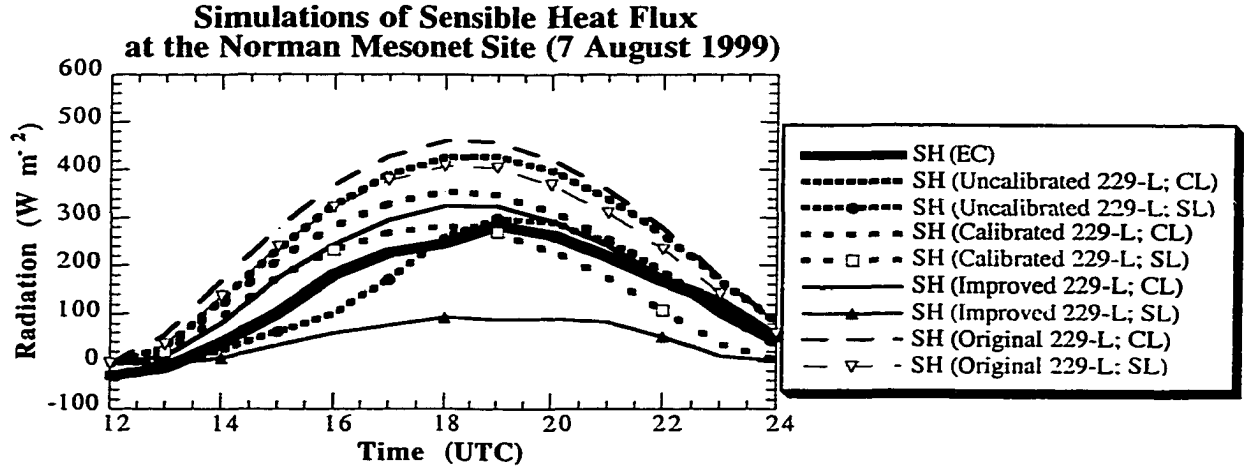

Figure D.26a. Simulations of sensible heat flux at the Norman Mesonet site on 7 August 1999 using the clay loam soil parameterization (CL) and the silt loam soil parameterization (SL). Soil water content was determined using various calibrations applied to the 229-L sensor. Hourly-averaged observations from the Norman site are plotted for reference (black curve).

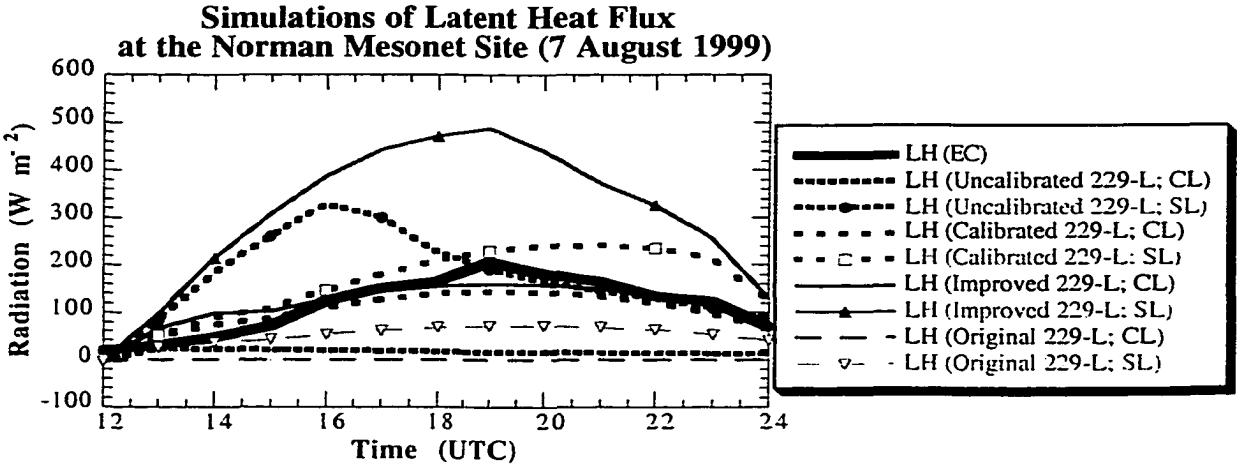

Figure D.26b. Simulations of latent heat flux at the Norman Mesonet site on 7 August 1999 using the clay loam soil parameterization (CL) and the silt loam soil parameterization (SL). Soil water content was determined using various calibrations applied to the 229-L sensor. Hourly-averaged observations from the Norman site are plotted for reference (black curve).

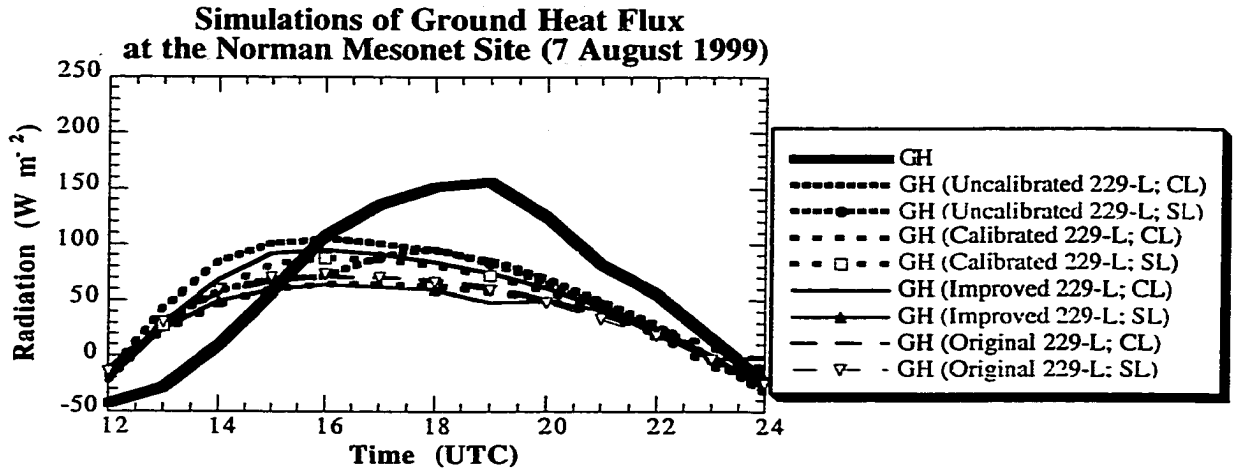

Figure D.26c. Simulations of ground heat flux at the Norman Mesonet site on 7 August 1999 using the clay loam soil parameterization (CL) and the silt loam soil parameterization (SL). Soil water content was determined using various calibrations applied to the 229-L sensor. Hourly-averaged observations from the Norman site are plotted for reference (black curve).

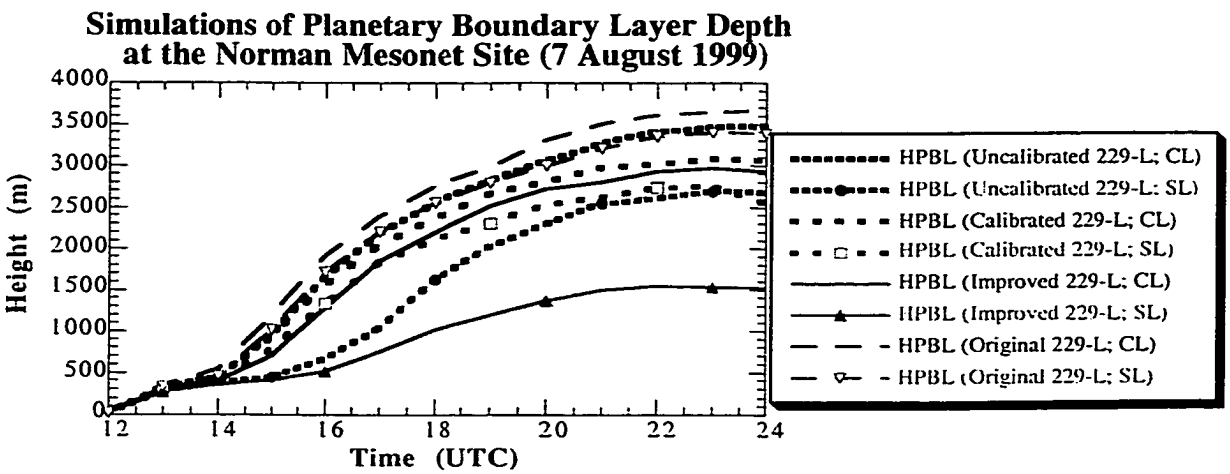

Figure D.26d. Simulations of PBL depth at the Norman Mesonet site on 7 August 1999 using the clay loam soil parameterization (CL) and the silt loam soil parameterization (SL). Soil water content was determined using various calibrations applied to the 229-L sensor.